A Novel Modal Analysis Method Based on Fuzzy Sets

This Thesis Submitted for the Degree of Doctor of Philosophy

By

Farbod Khoshnoud

Abstract

A novel method of vibration modelling is proposed in this thesis. This method involves estimating the mode shapes of a general structure and describing these shapes in terms of fuzzy membership functions. These estimations or initial guesses are based on engineering judgment or physical insight into natural mode shapes assisted by end and boundary conditions and some rules. The guessed mode shapes were referred to as Mode Shape Forms (*MSFs*). *MSFs* are approximate mode shapes, therefore there are uncertainties involve with their values where this uncertainty is expressed by fuzzy sets. The deflection or displacement magnitude of the mode shape forms are described with Zero, Medium, and Large fuzzy linguistic terms and constructed using fuzzy membership functions and rules. Fuzzy rules are introduced for each *MSF*. In that respect fuzzy membership functions provides a means of dealing with uncertainty in measured data, it gives access to a large repertoire of tools available in fuzzy reasoning field. The second stage of the process addresses the issues of updating these curves by experimental data. This involves performing experimental modal analysis. The mode shapes derived from experimental *FRFs* collect a limited number of sampling points. When the fuzzy data is updated by experimental data, the method proposes that the points of the fuzzy data correspond to the sampling points of *FRF* are to be replaced by the experimental data. Doing this creates a new fuzzy curve which is the same as the previous one, except at those points. In another word a "spiked" version of the original fuzzy curve is obtained. In the last stage of this process, neural network is used to "learn" the spiked curve. By controlling the learning process (by preventing it from overtraining), an updated fuzzy curve is generated that is the final version of the mode shape. Examples are presented to demonstrate the application of the proposed method in modelling of beams, a plate and a structure (a three beams frame).

The method is extended to evaluate the error where a wrong *MSF* is assumed for the mode shape. In this case the method finds the correct *MSF* among available guessed *MSFs*. A further extension of the method is proposed for cases where there is no guess available for a particular mode shape. In this situation the "closest" *MSF* is

selected among available *MSFs*. This *MSF* is modified by correcting the fuzzy rules that is used in constructing of the fuzzy *MSF*.

Using engineering experience (judgment), heuristic knowledge and the developed *MSF* rules in this method are the capabilities that cannot be provided with any artificial intelligent system. This provides additional advantage relative to vibration modelling approaches that have been developed until now. Therefore this method includes all aspects of an effective analysis such as mixed artificial intelligence and experimental validation, plus human interface/intelligence. Another advantage is, *MSF* rules provide a novel approach in vibration modelling where enables the method to start and operate with unknown input parameters such as unknown material properties and imprecise structure dimensions. Hence the classical computational procedures of obtaining the vibration behaviour of the system, from these inputs, are not used in this approach. As a result, this method avoids the time consuming computational procedure that exhibit in existing vibration modelling methods. However, the validation procedure, using experimental tests (modal testing) is the same acceptable procedure that is used in any other available methods which proves the accuracy of the method.

NOTATION

A	Area
$A(x)$	Fuzzy membership function of A
$B(x)$	Fuzzy membership function of B
c	Damping factor
c_c	Critical damping
$\lfloor C_q \rfloor$	Modal damping matrix
$[C_x]$	Damping matrix
D	Operator
e	Average error
E	Module of elasticity
E_i	Error
f	Shape function
F	Force
h	Transfer matrix
I	Inertia
K	Stiffness
L	Length
m	Mass
$\lfloor M_q \rfloor$	Modal mass matrix
$[M_x]$	Mass matrix
M_t	Translational inertia matrix
o_i^q	Neural network output
$\{P\}$	Mode shape or eigenvector matrix
q	Modal displacement
r	Frequency ratio
$[R]_k$	Modal constant
S	Stiffness matrix
t	time
$\{u\}_k$	Normalized mode shape

V	Volume
w_{ij}	Learning weights
$W(x, y)$	Plate deflection
x_k^q	Neural network input
$X(s)$	Laplace transformation of $x(t)$
y_i^q	Neural network target output
z_i^q	Neural network input
ζ	Damping ratio
ω_n	Natural frequency or eigenvalue
ω_d	Damped natural frequency
φ	Phase angle
λ	Amplitude ratio
η	Learning rate
ϕ	Plate aspect ratio
υ_{jk}	Learning weights
Φ_i	Mode shape or eigenvector
λ_N	Wave length
ρ	Density

SUBSCRIPTS

DOF	Degree of freedom
FFT	Fast Fourier transform
FRF	Frequency response function
L	Large
M	Medium
MDOF	Multi degree of freedom
MSF	Mode shape form
N	Negative
NL	Negative large

NLM	Negative large medium
NM	Negative medium
P	Positive
PL	Positive large
PLM	Positive large medium
PM	Positive medium
SDOF	Single degree of freedom
Z	Zero
ZNM	Zero negative medium
ZPM	Zero positive medium

Contents

Chapter 1

Introduction and structure of thesis

1.1. Introduction

The industrial revolution demanded an increase in production and required an advanced engineering technology. From early 1900 modelling of engineering systems became more and more important, and more effort was made to find more accurate and effective methods. Computers technology provided more powerful analysis tools for engineers. Using computers enabled engineers to deal with large mathematical matrices and calculations in design, analysis and modelling of systems. However as technology become more and more complex classical analysis tools (even with help of computers) becoming less effective in achieving effective and reliable solutions. For example modal analysis of a complex structure such as a whole vehicle or a helicopter may not provide reliable answer for more than first 10 modes. Even this level of success will rely on modeller's skills. Over the last 50 years, engineers and scientist looked for alternative ways of dealing with complexity and high dimensionality. As a result of this search an array of methods inspired from the nature or based on human heuristics were developed. During this period Artificial intelligence and biologically inspired algorithm (especially in optimisation such as genetic algorithms) were developed. Although success of these methods is varied, they will continue to be used as effective methods, when the alternative effective

classical methods (such as analytical approaches) are not available to deal with complexity. The outcome of complexity was not only related to solution algorithms, but parallel to those, it exposed another major problem related to modelling engineering system. This was uncertainty. Engineers, from early days of modelling were aware of this problem, however error (or uncertainty) due to identifying accurate values for parameters were not major issue for a simple component design which involved several such parameters. As dimensionality (complexity) increased uncertainty has become prominent as individual uncertainties interact with each other and propagate with analysis. It is becoming more and more obvious that to deal with this problem, effective analysis tools are needed. Classically such tools included stochastic analysis, which become the main tool in dealing with uncertainty. The thesis, here, proposes an alternative way of dealing with uncertainty by using fuzzy set theory.

Artificial intelligence methods such as neural networks were developed in 1950s. In these methods, a large volume of data can be modelled by the network. The network learns the relation between inputs and outputs data. Neural network methods include the advantages of higher degree of robustness and capability of learning. Effectiveness of neural network is due to the fact that neither a complicated programming nor rigid algorithms are required.

One of the most successful methods, in the case of vibration analysis, is modal analysis. In general this method may be classified as a system identification method. The main purpose of these methods is to obtain a mathematical description of system behaviour based on experimental observations. Experimental modal analysis method has been developed for modelling of structural vibration, and found to be a very reliable. In this case, accurate experimental measurements have to be carried out in order to obtain good results. This method is also used in verifying other modelling approaches such as Finite Element (FE) models. Various techniques have been investigated by researchers for model updating using modal analysis. Model updating is a technique to validate the model that is derived from a modelling method. Modal analysis is not the only method in model updating, other techniques are also available in updating of dynamical systems [1].

The classical modelling methods require precise data, including responses or parameters data that is obtained from the system behaviour or parameter measurements. Modelling of engineering systems involve uncertainty in parameters values of the system and errors in measurements. There are limitations in obtaining accurate data of the systems. The sources of uncertainty in the modelling of mechanical systems can be referred to as:

- Measurement error and instrumentation error involved in experiments.
- Manufacturing error where manufacturing of all machine parts involves tolerance and the exact dimensions and material property can never be produced.
- Error in operational conditions of the system such as high accelerations, resiliency, large sudden loads, severe operation and uneven heating cause changes in parameters of the system.
- Error in modelling nonlinearity. Some times some terms in equations of the behaviour of the system are neglected for sake of simplification.
- Error due to changing the characteristic of systems in their lifetime as a result of aging, creep, wear and corrosion.
- Errors, as mechanical and industrial systems may be modified during their life of operation. Each modification changes the characteristics of the structure and makes the original model of the system invalid.
- Errors, as it is difficult to measure material properties.

During the last 50 years more and more engineers have investigated the implication of modelling engineering systems with uncertainty. Engineers realized that uncertainty analysis could be used in dealing with the imprecisely defined data. In vibration problems, the response of most mechanical systems is highly sensitive to variations in the parameters of the system. Therefore, any realistic analysis requires considering the uncertainties.

One of the common approaches in uncertainty analysis includes stochastic methods [1, 2] and parallel to that, fuzzy set theory [4]. Randomness in stochastic methods has been extensively studied in literature. Stochastic analysis deals with errors in

experiments due to measurement and instrumentation errors, and the random distribution of manufacturing errors. Fuzzy approaches have been used in control and especially complex control problems. Researchers have also investigated application of fuzzy sets in modelling of the systems, which includes uncertainties in the parameters. In this respect parameters of a system such as mass, stiffness, damping, material property and geometry are considered as uncertain parameters in the equation of the motion of the system. For instance, fuzzy finite element approaches for vibration analysis of imprecisely defined systems have been developed to deal with uncertain parameters in the systems.

Therefore this thesis deals with uncertainty in the parameters and behaviour of the system where the sources of uncertainties are due to lack of information about the system, imprecise parameters, difficulties in mathematical modelling and limited number of measurements. The proposed method in this thesis deals with uncertainty in behaviour of the system directly, rather than trying to associate uncertainty of response with parameters. This approach is different from other available techniques for dealing with uncertainty proposed by other researchers. Current methods starts with uncertain system parameters, then these parameters are used in the equation of motion of the system to evaluate the system behaviour. This thesis offers a novel method and approach in dealing with uncertainty. The main advantage of the proposed method is that, it avoids complicated mathematical computations that exist in other uncertainty based methods.

1.2. Structure of the Thesis

Chapter 1, presents an overview of the thesis consist of an introduction to the proposed method and structure of the thesis. In the first section, an introduction in artificial intelligent, uncertainty in modelling and modelling of vibration behaviour of mechanical systems are presented.

Chapter 2, presents a literature survey of vibration modelling methods based on uncertainty approaches such as fuzzy sets, experimental modal analysis in model updating and intelligent systems, such as neural networks.

Chapter 3, includes background of the theories that are used in this thesis consist of modal analysis, fuzzy logic and neural networks theories.

Chapter 4, consists of a mathematical background of heuristically guessing the mode shapes or obtaining Mode Shape Forms (*MSFs*). *MSFs* are determined for mass-spring, one-dimensional bodies, two-dimensional bodies and two-dimensional structures.

Chapter 5, presents the proposed method in this thesis. The procedure of the method including constructing the guessed mode shapes by fuzzy sets, updating the fuzzy mode shape forms by experimental modal analysis and obtaining the final version of the mode shape by neural networks is presented. In this chapter, methods of calculating and reducing the errors are also introduced.

Chapter 6, presents the experimental set up in performing the procedure in the proposed method that consists of experimental modal analysis, fuzzy sets and neural networks.

Chapter 7, presents four experimental examples regarding vibration modelling of beams, plates and structures based on the proposed method. An example of reducing error is presented for one of the beam examples.

Chapter 8, presents the discussions about the proposed method, a description of the procedure of the method, the advantages and the application.

Chapter 9, presents the conclusion and future work of the thesis. The conclusion provides and overview of the proposed method and the achievements in this research.

Chapter 2

Literature Review

The research in this thesis addresses the modelling of mechanical systems, in particular, modelling the vibratory behaviour of systems using the uncertainty approach. The literature relevant to this research is presented in this chapter. The research refers to recent developments in the use of artificial intelligence (neural networks) and fuzzy reasoning in the modelling of mechanical systems. However some other relevant methods are also discussed in this chapter.

Uncertainty methods such as probabilistic methods can be used where there is a lack of information about the system [2, 3]. In vibration modelling this information can be referred to parameters such as mass, stiffness, damping, material properties, geometry or behaviour of the system.

Fuzzy sets are proved to be very efficient in dealing with systems that consist of uncertainty. This uncertainty can exist because of imprecisely defined characteristics of the system, inaccurate data and lack of information. In the dynamic analysis of structures, fuzzy sets are used to generalize the model of space structures [5, 6]. In these papers fuzzy sets are used to enhance the transient response modelling of space structures. In that respect, the finite element model of a structure is built for different system parameters. The parameters of the structures consist of material properties, geometrical parameters, initial nodal positions, velocities, accelerations, externally

applied forces and constraint parameters. Inputs of the fuzzy sets are defined based on these parameters. The behaviour of the structure such as deflection of a point on the structure, natural frequency and the mode shapes of all nodes of the model defines the output of the fuzzy system. These responses of the structure are obtained from the finite element model. The behaviour of the structure for undefined parameters can be obtained from the fuzzy model. In this method the fuzzy input is a set of structure parameter that is introduced above and the corresponding responses are fuzzy outputs. This method has been applied to the dynamic simulation of the next generation space telescope [7] and a tethered satellite system [8] and uncertainty analysis of composite materials [9]. In this method the output of the system is derived from a range of inputs, where the range of inputs corresponds to variation of the input parameters.

Another approach where parameters are considered as fuzzy is the fuzzy finite element static analysis of the structures where an optimization based scheme used for the numerical solution of the linear fuzzy equations [10]. Static analysis of foundation of the structures has been studied based on this method, where elastic modulus and Poisson's ratio of the soil are considered as uncertain parameters and introduced by fuzzy sets [11]. In this method the equation of the system is obtained by finite element methods. The parameters of the equation are considered as fuzzy parameters. Therefore the behaviour of the system is obtained for a range of variation of input parameters. The fuzzy finite element method has also been investigated in dynamic analysis of structure for the systems with imprecisely defined parameters [12]. In this method the accuracy of the method depends on the initial value of step length, where the step length gives the length for changing the parameters of the system for each finite element model calculation. The finite element model is obtained for each variation of the length. In another word, the system behaviour is obtained by a FE model for each variation of the parameters of the system. The smaller step length provides more accuracy but more computational processing. Another limitation in this method is that some numerical manipulations cannot directly be extended to fuzzy equations. This is because some mathematical operations for real numbers cannot be extended to fuzzy numbers. For example, fuzzy numbers do not perform numerical subtraction and division.

Fuzzy parameters used in FE analysis can also be used in analysis of behaviour of mathematical equation of the motion of a system that the mathematical equation includes imprecisely defined parameters. In this case, fuzzy parameters have been employed in analysis of unbalanced nonlinear rotor systems [13]. In this research, effects of fuzzy stiffness, mass and damping on the behaviour of the rotor system are studied. It is shown that uncertainties in this system will not only affect the speed and amplitude, but also the periodic characteristics of the system.

Uncertainty analysis is also used for system identification, such as identification of material properties. For instant dependency between material properties and natural frequencies of plates are modelled by fuzzy sets [14]. In this respect, the material properties are obtained correspond to the natural frequencies of plates.

Uncertain excitations are also very important in analysis of structures. As an example, analysis of plates subjected to uncertain excitations is addressed [15]. Uncertain load and initial conditions has been applied to the plate, and the behaviour of the system is studied. Mode shapes and behaviour of a point in the middle of the plate are studied. Maximum error (uncertainty) of 50% can be found in different levels of uncertain excitations relative to the deterministic model. Here, the deterministic model is the model that is obtained by analytical approaches or can be referred to the mathematical equation of motion of the system. However, in uncertainty approaches, the level of confidence is evaluated rather than calculating the error. The error value is presented here for uncertainty approaches to demonstrate the approximate error available in uncertainty analysis.

Existence of uncertainty in problems generates errors in the results, of course this is not error in normal sense, it only describes the level of uncertainty. 50% “error” can be found in literature in the problems that deals with uncertainty [15]. This error is obtained relative to deterministic models. Deterministic models are also not exact because they include unavoidable uncertain parameters. Deterministic models are referred to the models that are obtained by analytical approaches. This includes the mathematical equation of motion of the mechanical system. Therefore the error relative to a realistic model or the real behaviour of the system can be more or less than 50%. Uncertainty analysis offers a tool to deal with the modelling of mechanical

systems possessing levels of uncertainty and gives a trend, mean, range and distribution characteristics of results [3].

The models that are derived from various available methods (i.e. mathematical or FE methods) may carry errors. These errors (including parameter, discretisation and configuration errors) occur due to inappropriate modelling assumptions, uncertainties in material properties, insufficient modelling details, and incorrect boundary conditions (such as joints modelling), etc [16].

Modal analysis is a powerful experimental approach in obtaining the vibration behaviour of mechanical systems. This method is used for modelling and also updating the vibratory models that has been derived from other methods (i.e. FE model). Model updating reduces the modelling errors. The thesis presented here also deals with modal analysis for model updating. Structural modification using experimental modal analysis can be applied to update both the spatial model matrices (described by mass, stiffness and damping parameters) and modal model matrices (including natural frequencies, the corresponding mode shapes and modal damping factors) [1]. Model updating is used to expand the modal and spatial parameter matrices using different techniques and updating methods. Mode shape or eigenvector expansion is known as mode expansion. One of the recent techniques in model expansion and reduction can be referred to *System equivalent reduction expansion process (SEREP)*. This method can be used to both expand and reduce the degree of freedom of the model of the system. The method relies on the finite element or analytical model of the system. In these methods experimental measured data is called master or active degree of freedoms (*DOFs)* that represent the incomplete model. Incomplete models referred to models that the measurements have not been performed the whole geometry of the body, or where it is not possible to measure the behaviour of all the positions of a system. The unmeasured data is called inactive, deleted or slave *DOF*. The full set of data is obtained from the *FE* model where the number of *DOF* is the number of active *DOF* plus deleted *DOF* [1, 18]. However the model updating calculation is very costly in terms of computer time for models with large degrees of freedom. An example of costly and time consumption computation can be referred to modelling of a bridge, a high rise or an offshore structure [1].

The use of artificial neural network (*ANN*) is another area that the thesis studies. Identification of structural dynamics is investigated by researchers using artificial neural networks [19-22]. In these papers displacement, velocity and acceleration of an arbitrary point on a structure is stored as the input training data of neural network model. Hysteric forces of the equation of motion are obtained from experimental tests (e.g. using force gauges) and used as *ANN* output training data. The mass matrix elements are assumed to be known. A single degree of freedom equation of motion is used as the model of the system. Neural network output (hysteric force) is placed in this equation. In this stage the single degree of freedom equation of motion including the hysteric force from the neural network output is the model of the system. To test the result, an excitation is applied to the equation of the motion and also to the physical system. The response from the equation of motion is calculated numerically. The response from the physical system is also measured experimentally. These two results are compared and proved the accuracy of the method. This method has been applied to obtain the vibration behaviour of structure including nonlinearity as well as linear behaviour [23, 24]. Over 40% error can be found in neural network system identification methods [19-24]. This error is caused by the network, where there is a lack of training data or the network is predicting the behaviour out of the training data region. Fuzzy neural network has also been employed in the above problem where this approach increases the training speed of the network [25].

Although the uncertainty analysis of vibration behaviour of mechanical systems is an important issue, there is still little research in this area as the application of uncertainty analysis is applied mostly in particular applications such as modelling of civil structures [26]. Nevertheless, as we see from the literature, the research in this area includes some general weaknesses and limitations. Some of these weaknesses can be addressed as, mathematical complexity, time consuming and costly computations, dependency of the method to other methods (such as FE and mathematical approaches), large number of experimental measurements and specificity of applications (lack of generalisation). The research carried out in this thesis attempts to address some of these weaknesses and limitation.

In this thesis, the uncertainty is considered in the behaviour of structure rather than parameters of the system. Considering the uncertainty in parameters of the system and

the effect of this uncertainty in the behaviour of the system is investigated by researchers as it was mentioned above. In the proposed method in this thesis a heuristic guessing and the developed rules for guessing the mode shapes of structures are considered as uncertain behaviour of structures. The guessed mode shapes are referred to Mode Shape Forms (*MSFs*). Fuzzy sets are used to deal with uncertainty in guessing the mode shapes. Fuzzy sets are used to construct the guessed mode shapes or *MSFs*. Then experimental modal analysis is used to update the uncertain model. The updating is achieved by updating *MSFs* with experimental data. To achieve the final model, neural networks are used to fit *MSF* to experimental data in the last step. Obtaining the vibration behaviour a clamped-clamped beam is presented using the proposed method in this thesis by the author [27] and is presented in Appendix E.

2.1. Summery

A literature review in vibration modelling using uncertainty approaches, modal analysis and artificial intelligent was presented in this chapter. In this review, application of fuzzy sets in modelling of vibratory behaviour of mechanical systems was presented. In these applications fuzzy sets deal with the uncertainty in the modelling approach. Modal analysis is introduced as an effective modelling approach that also can be used in model updating. Application of artificial neural networks and fuzzy neural networks are also reviewed in modelling of vibration behaviour of structures. The proposed method in this thesis was introduced briefly as an effective method relative to available methods in vibration modelling.

Chapter 3

Background Theories

This thesis is based on a vibration modelling method that deals with uncertainty in modelling using fuzzy reasoning, modal analysis and neural networks. In this respect, fuzzy sets deal with the uncertainty in vibratory behaviour of structures. Modal analysis is used to update the fuzzy model and a neural network is used to obtain the final version of the mode shapes of the structures. Therefore in this chapter, the theory of fuzzy logic, modal analysis and neural networks are discussed.

In this research several software and experimental tools are used to implement each theory. Fuzzy toolbox of MATLAB software [28] is used for the fuzzy operation. Agilent VEE [29] software is used to obtain *FRF* and in the modal analysis procedure. Neural network toolbox of MATLAB software is used to obtain the final version of the mode shapes. The experimental procedure and application of the toolboxes is presented in Chapter 6.

3.1. Fuzzy logic theory

Fuzzy logic can be used when the exact value of a phenomenon is not available. Statements such as ‘speed is fast’ and ‘distance is long’ are some examples when there are no boundaries or exact values available. In another word, the statements are

uncertain. Fuzzy theory is one of the mathematical approaches to deal with uncertain problems where the parameters of the system are imprecise.

The idea of fuzzy reasoning originates form human decision making process. 'If … Then …' is a statement that is used in human decision making. These 'If … Then …' statements are called rules in fuzzy theory. A fuzzy system consists of inputs, outputs and fuzzy rules. A particular example is presented to understand inputs, outputs and fuzzy rules of a fuzzy system. To illustrate a fuzzy decision system let us consider a driver's decisions in controlling his/her vehicle. To control the speed of the automobile, consider following rules. 'IF the distance is LONG and the speed is LOW, THEN increase gas'. In this rule, the distance is the first input, the speed is the second input and the gas is the output. The statement 'IF the distance is LONG and the speed is LOW, THEN increase gas', is the fuzzy rule. Fuzzy rules relate the inputs to outputs. After introducing the inputs, outputs and rules of the fuzzy system, then these input, output and rules have to be introduced in a mathematical way. The following sections give the mathematical background to fuzzy systems.

3.1.1 Fuzzy Sets

Fuzzy sets are the inputs and outputs in a fuzzy system. The fuzzy sets are introduced below.

For a set x, a *Fuzzy Subset A*, refers to an interval [0, 1] that for each set of x there is a corresponding function that varies between 0 and 1. A Fuzzy subset can simply be called a *Fuzzy set*. Function $A(x)$ is called *membership function* of subset A.

An example of a fuzzy membership function is illustrated in Figure 3-1 where the vertical axis shows the subset A and the horizontal axis the set x.

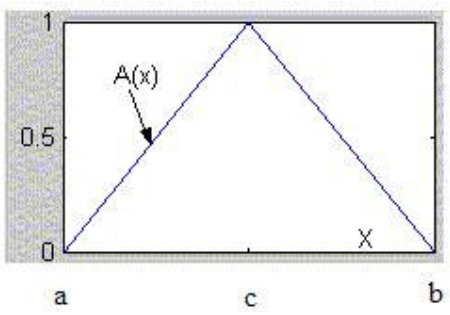

Figure 3-1. A fuzzy membership function (A triangle function).

3.1.2. Membership Functions

There are various representations of fuzzy membership functions. *Triangles and trapezoids* functions are the most popular membership functions in engineering applications. These functions are linear [30]. The triangle membership function can be presented by equation (3-1).

$$A(x)=\begin{cases}\alpha\left(\dfrac{x-a}{c-a}\right) & if \quad a\le x\le c\\ \alpha\left(\dfrac{x-b}{c-b}\right) & if \quad c\le x\le b\\ 0 & otherwise\end{cases} \tag{3-1}$$

Where point (c,α) is the high point and points $(a,0)$ and $(b,0)$ are the end points of the triangle.

The trapezoid membership function can be presented by equation (3-2).

$$B(x)=\begin{cases}\alpha\left(\dfrac{x-a}{c-a}\right) & if \quad a\le x\le c\\ \alpha & if \quad c\le x\le d\\ \alpha\left(\dfrac{x-b}{d-b}\right) & if \quad d\le x\le b\\ 0 & otherwise\end{cases} \tag{3-2}$$

Where points (c,α) and (d,α) are the high point and points $(a,0)$ and $(b,0)$ are the end points of the trapezoid.

Other membership functions are available such as Gaussian, Cauchy function, Cauchy and Sigmoidal functions [30].

3.1.3. Fuzzy inputs-outputs and fuzzy rules

Fuzzy membership functions are used to construct the fuzzy inputs and outputs. Figure 3-2 illustrates an example of input or output membership functions. Triangle membership functions are used in this example. A_1, A_2, A_3, A_4, A_5 and A_6 are 6 membership functions in Figure 3-2. Fuzzy membership functions are used to introduce fuzzy linguistic terms such as low, high, medium, small, etc. In this respect, each fuzzy linguistic term is introduced by a membership function. For example, in Figure 3-2, A_2 can be LOW or any other fuzzy linguistic term. Each membership function includes a region of an input or output. For example the region of A_3 in Figure 3-2, includes x_2 to x_4. x is the input or output value.

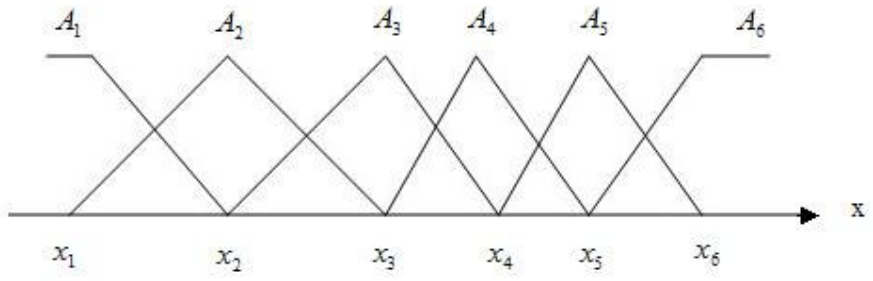

Figure 3-2. Membership functions.

Fuzzy rules are used to relate the fuzzy inputs to the fuzzy outputs. These rules are defined based on 'If … Then …' statements. In each statement the inputs and output membership functions are placed as below in the rule statements.

'If input 1 is A_1, input 2 is B_1, …, Then output is Y_1'

where A_1 is an input 1 membership function, B_1 is an input 2 membership function and so on. Y_1 is an output membership function. Other rules are introduced with the same format. The following section describes the method of obtaining the output value from inputs and fuzzy rules.

3.1.4. Obtaining the output from inputs

The following example is presented to understand the method of obtaining the output from inputs in fuzzy theory. Assume the fuzzy system consist of two inputs as in Figure 3-3. In this example, the output has to be obtained from these two inputs. The input values are X1 and F1.

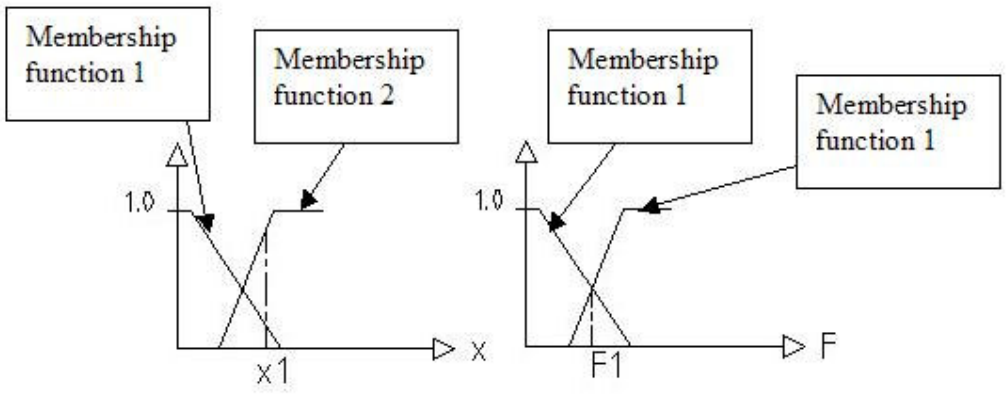

Figure 3-3. Two inputs.

The corresponding values of each input (X1 and F1) on the vertical axis is illustrated in Figure 3-4.

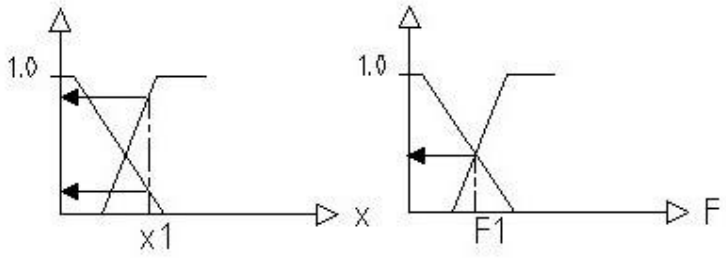

Figure 3-4. Corresponding value of each input on the vertical axis.

The method of obtaining the output from inputs is presented below. Mamdani method [28] is used here to obtain the output from inputs. This method is one of the most popular methods in engineering application that is used in MATLAB software [28]. Following procedure is used to obtain the output based on this method.

First, all combinations of the membership functions from one input with the membership functions from the other input are considered as in Figure 3-5. In this figure membership functions, 1 and 2 of each input is considered with membership functions, 1 and 2 of the other input.

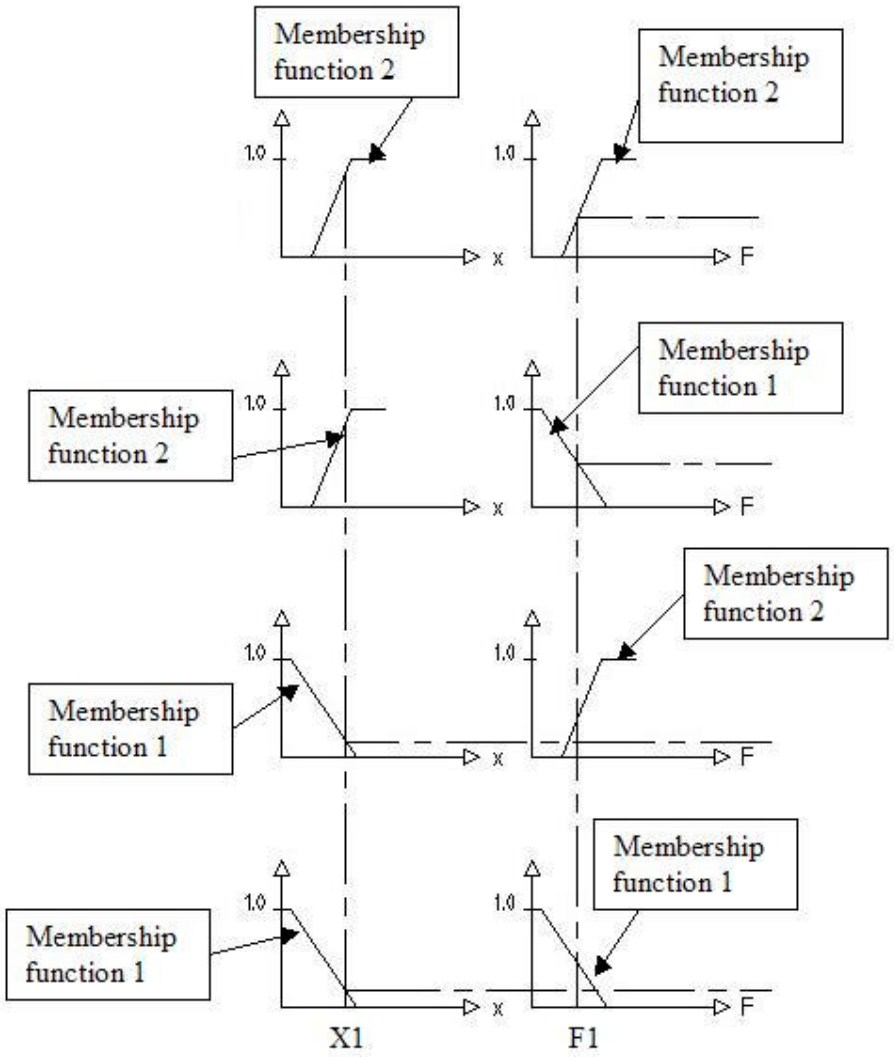

Figure 3-5. All combinations of input values.

In the second stage, for each combination, the minimum value of input on the vertical axis is considered. For example for combination 1 in Figure 3-7, the minimum value is the value from input 1. This is illustrated in Figure 3-6.

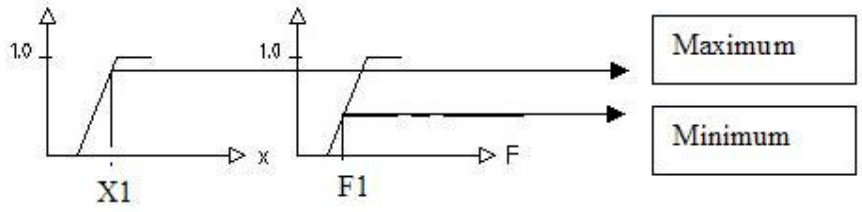

Figure 3-6. The minimum value between membership function 2 in input 1 and membership function 2 in input 2

In the last stage, an area of output membership function is obtained. In this respect, the corresponding output membership function of each combination is obtained from the fuzzy rules and Mamdani method. In this specific example the fuzzy rules are as below.

Rule 1: If input 1 is membership function 2 and input 2 is membership function 2, then the output is the membership function 1.

Rule 2: If input 1 is membership function 2 and input 2 is membership function 1, then the output is the membership function 2.

Rule 3: If input 1 is membership function 1 and input 2 is membership function 2, then the output is the membership function 3.

Rule 4: If input 1 is membership function 1 and input 2 is membership function 1, then the output is the membership function 4.

These rules are illustrated in Figure 3-7. The output area is obtained in each rule based on Mamdani method.

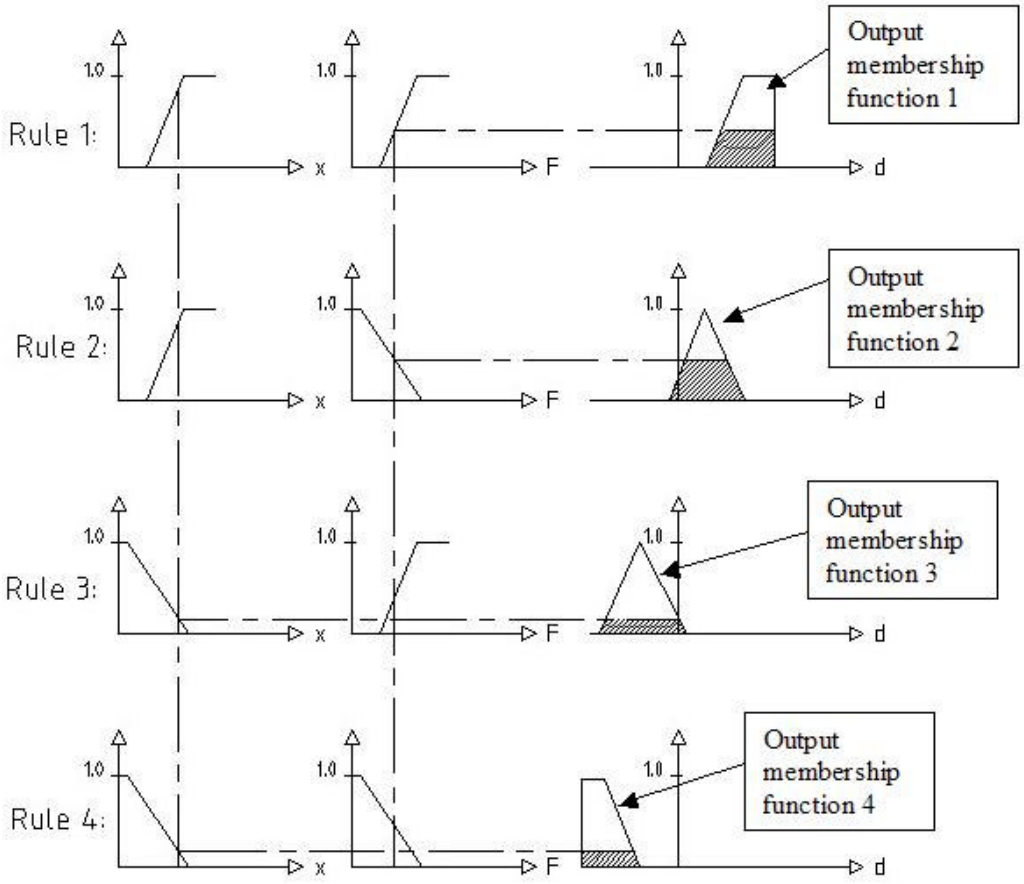

Figure 3-7. Obtaining the output from inputs using mamdani method

Based on Mamdani method the output area is obtained by adding all four areas in **Figure 3-7**. The combination of output areas for the particular input is presented in Figure 3-8.

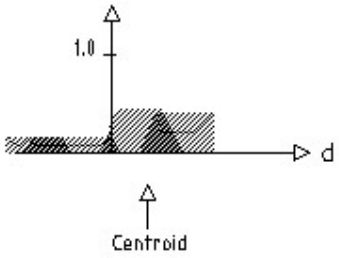

Figure 3-8. Output areas from the particular inputs.

In this stage, by applying a defuzzification method, the output magnitude can be derived from the area shown in Figure 3-8.

3.1.5. Defuzzification

Defuzzification gives the output values from output areas. The output areas was explained in the previous section (Figure 3-8). Different defuzzification methods are available in literature such as centre of area, high-centre of area, max criterion, first of maxima and middle of maxima methods. Centre of area method is the most popular method and is used in this thesis. There are other names that are used for this method such as centre of gravity or centroid method. In this method the centre of area under the Fuzzy output curve is the output value. The centre of area can be obtained by equation (3-3).

$$z_0 = \frac{\int_a^b zC(z)dz}{\int_a^b C(z)dz} \tag{3-3}$$

Where C is the Fuzzy set and a and b are the interval of C. The centre of area can be presented by equation (3-4) if the area is discrete.

$$z_0 = \frac{\sum_{j=1}^{n} z_j C(z_j)}{\sum_{j=1}^{n} C(z_j)} \tag{3-4}$$

3.2. Theory of modal analysis

Modal analysis is used in the procedure of the proposed method in this thesis. Agilent VEE [29] software is used to drive the frequency response functions (*FRFs*). The theory of obtaining *FRF* is described in the following section.

3.2.1. Fundamental review of theory of vibration

In modal analysis multi degree of freedom systems are considered as several *SDOF* systems. *SDOF* vibration fundamentals are presented here.

a) Single degree of freedom forced vibration equation of motion

Force excitation equation of motion can be presented as [31-33].

$$m\ddot{x} + c\dot{x} + kx = F_0 \sin(\omega t) \qquad (3\text{-}5)$$

In force excitation situation the system oscillates at the same frequency ω of the external force, but with a time or phase delay. The solution of the equation can be presented as below.

$$x(t) = X \sin(\omega t + \phi)$$

Where X (amplitude) and ϕ (phase angle) has to be determined.

Another expression of harmonic force with complex notation can be expressed as

$$F(t) = F_0 e^{j\alpha} e^{j\omega t}$$

Then the corresponding harmonic response to the above force would be as below.

$$x(t) = Xe^{j(\omega t+\phi)}$$

By substituting this solution in equation (3-5), the equation of motion will be as below.

$$\left(k-\omega^2 m+j\omega c\right)Xe^{j\phi}e^{j\omega t}=F(t)=F_0e^{j\alpha}e^{j\omega t} \qquad (3\text{-}6)$$

b) Frequency response function and Phase of harmonic vibration

Frequency response function (*FRF*) is defined by dividing *X* (amplitude) by excitation force. From equation (3-6), *FRF* would be as below.

$$\left|\Phi(\omega)\right|=\left|\frac{X}{F_0}\right|=\frac{1}{k}\frac{1}{\sqrt{\left(1-r^2\right)^2+\left(2\zeta r\right)^2}}$$

Where phase of harmonic vibration is

$$\phi=\tan^{-1}\frac{-2\zeta r}{1-r^2}+\alpha \qquad (3\text{-}7)$$

r is called frequency ratio and defined as $r=\omega/\omega_n$.

Damping ratio is a parameter that is used in vibration analysis and is defined as $\zeta=\frac{c}{c_c}$ or $\zeta=\frac{c}{2\sqrt{km}}$.

In most metal structures the damping ratio is $\zeta<0.05$ or even less.

Natural frequency of the single degree of freedom system can be introduced as $\omega_n=\sqrt{\frac{k}{m}}$.

Damped natural frequency is defined by the following equation $\omega_d=\omega_n\sqrt{1-\zeta^2}$.

3.2.2. Analytical modal analysis

In this section, the theoretical modal analysis is described. A multi degree of freedom (*MDOF*) mass spring and damper system is considered to derive uncoupled equations of motion. These equations are used in obtaining the parameters required for modal analysis.

a) Multi degree of freedom equation of motion

The equation of motions of the mass-spring-damper system is [17, 34]

$$[M_x]\{\ddot{x}\}+[C_x]\{\dot{x}\}+[K_x]\{x\}=\{F\} \tag{3-8}$$

The mass, stiffness, and damping matrixes would be

$$[M_x]=\begin{bmatrix} m_1 & & & 0 \\ & m_2 & & \\ & & \ddots & \\ 0 & & & m_n \end{bmatrix},\ [K_x]=\begin{bmatrix} k_{11} & k_{12} & \cdots & \\ k_{21} & \ddots & & \\ \vdots & & \ddots & \\ & & & k_{nn} \end{bmatrix}$$

$$[C_x]=\begin{bmatrix} C_{11} & C_{12} & \cdots & \\ C_{21} & \ddots & & \\ \vdots & & \ddots & \\ & & & C_{nn} \end{bmatrix}$$

Displacement vector $\{x\}$ and force vector $\{F\}$ are $\{x\}=\begin{Bmatrix} x_1(t) \\ x_2(t) \\ \vdots \\ x_n(t) \end{Bmatrix}$ and $\{F\}=\begin{Bmatrix} F_1(t) \\ F_2(t) \\ \vdots \\ F_n(t) \end{Bmatrix}$.

b) Undamped free vibration

The transfer function will be introduced in the next section based on undamped vibration. Undamped equation of motion of a system is introduced here that is used in developing the multi degree of freedom transfer function. The Undamped equation of motion is [17, 34].

$$[M_x]\{\ddot{x}\}+[K_x]\{x\}=\{0\} \tag{3-9}$$

The general solution is $\{x(t)\}=\{X\}\sin(\omega t+\psi)$. Where $\{X\}$ and ψ are constants and ω is the natural frequency of the system. Derivative of the above equation gives the acceleration as below.

$$\{\ddot{x}\}=-\omega^2\{X\}\sin(\omega t+\psi)$$

Then equation (3-9) becomes

$$\left([K_x]-\omega^2[M_x]\right)\{x(t)\}=\{0\} \tag{3-10}$$

Then first matrix must be zero. If the first matrix is equal to zero then its determinant has to be zero or $\left|[K_x]-\omega^2[M_x]\right|=\{0\}$.

c) *MDOF* undamped equation of motion in modal coordinate (space)

The general solution of a *MDOF* undamped vibration has the following form.

$$\begin{Bmatrix} x_1(t) \\ x_2(t) \\ \vdots \\ x_m(t) \end{Bmatrix}_1 = \begin{Bmatrix} X_1 \\ X_2 \\ \vdots \\ X_m \end{Bmatrix}_1 \sin(\omega_{n1}t)+\begin{Bmatrix} X_1 \\ X_2 \\ \vdots \\ X_m \end{Bmatrix}_2 \sin(\omega_{n2}t)+\cdots+\begin{Bmatrix} X_1 \\ X_2 \\ \vdots \\ X_m \end{Bmatrix}_m \sin(\omega_{nm}t)$$

$\left(\frac{X_t}{X_s}\right)_i = \lambda_{tsi}$, where $i = 1, 2, \cdots, m$ is the natural frequency number. Therefore we have the following relationship.

$$X_{si} = \frac{X_{ti}}{\lambda_{tsi}} = Q_{tsi} \text{ or } X_{ti} = \lambda_{tsi} Q_{tsi}.$$

Therefore the general solution of a *MDOF* undamped vibration has can be expressed as the following form.

$$\begin{Bmatrix} x_1(t) \\ x_2(t) \\ \vdots \\ x_m(t) \end{Bmatrix} = \begin{bmatrix} \lambda_{1s1} & \lambda_{1s2} & \cdots & \lambda_{1sm} \\ \lambda_{2s1} & \lambda_{2s2} & \cdots & \lambda_{2sm} \\ \vdots & \vdots & \ddots & \vdots \\ \lambda_{ms1} & \lambda_{ms2} & \cdots & \lambda_{msm} \end{bmatrix} \begin{Bmatrix} Q_{1s1} \sin(\omega_{n1} t + \psi_1) \\ Q_{2s2} \sin(\omega_{n2} t + \psi_2) \\ \vdots \\ Q_{msm} \sin(\omega_{n2} t + \psi_2) \end{Bmatrix}$$

Or

$$\{x(t)\} = [\{P\}_1 \quad \{P\}_2 \quad \cdots \quad \{P\}_m] \begin{Bmatrix} q_1(t) \\ q_2(t) \\ \vdots \\ q_m(t) \end{Bmatrix} = [P]\{q(t)\} \qquad (3\text{-}11)$$

Where $\{P\}_i = \{\lambda_{1s1} \quad \lambda_{2s1} \quad \cdots \quad \lambda_{ms1}\}^T$ is the i^{th} mode shape. q_1 is the modal displacement contributed by the first mode. Equation (3-11) is called the equation of motion in modal coordinate.

d) Orthogonality of the modes relative to mass, stiffness and damping matrixes

The principal of orthogonality is used in the next section to obtain the transfer function. The modes are orthogonal to each other (Appendix A) therefore the following relations can be expressed.

$\{P\}_1^T [M_x]\{P\}_2 = 0$, $\{P\}_1^T [M_x]\{P\}_1 = m_{q1}$ and

$$\begin{cases} [M_q] = [P]^T [M_x][P] \\ [K_q] = [P]^T [K_x][P] \end{cases} \tag{3-12}$$

In this case, the modal mass ($[M_q]$) and modal stiffness ($[K_q]$) matrixes are diagonal. The system might have proportional damping as below.

$$[C_x] = \alpha_1 [M_x] + \alpha_2 [K_x]$$

Where α_1 and α_2 are constants from the experiment. In this condition, the following relation is valid.

$$[C_q] = [P]^T [C_x][P]$$

e) Equation of motions in modal space (uncoupled equations)

By multiplying the modal matrixes to equation (3-8) and using equation (3-12), then the equation of motion in modal space will be as below.

$$\begin{bmatrix} m_{q1} & & & 0 \\ & m_{q2} & & \\ & & \ddots & \\ 0 & & & m_{qm} \end{bmatrix} \begin{Bmatrix} \ddot{q}_1(t) \\ \ddot{q}_2(t) \\ \vdots \\ \ddot{q}_m(t) \end{Bmatrix} + \begin{bmatrix} c_{q1} & & & 0 \\ & c_{q2} & & \\ & & \ddots & \\ 0 & & & c_{qm} \end{bmatrix} \begin{Bmatrix} \dot{q}_1(t) \\ \dot{q}_2(t) \\ \vdots \\ \dot{q}_2(t) \end{Bmatrix} +$$

$$\begin{bmatrix} k_{q1} & & & 0 \\ & k_{q2} & & \\ & & \ddots & \\ 0 & & & k_{qm} \end{bmatrix} \begin{Bmatrix} q_1(t) \\ q_2(t) \\ \vdots \\ q_m(t) \end{Bmatrix} = \begin{Bmatrix} 0 \\ 0 \\ \vdots \\ 0 \end{Bmatrix}$$

Or

$$[M_q]\{\ddot{q}\} + [C_q]\{\dot{q}\} + [K_q]\{q\} = \{0\}$$

The equations of motion in modal space are uncoupled or each mass in the system behaves like single degree of freedom mass-spring-damper system. For example, from the above equation for q_1, the equation of motion would be as below.

$$m_{q1}\ddot{q}_1 + c_{q1}\dot{q}_1 + k_{q1}q_1 = 0$$

This equation has the same solution of a single degree of freedom system as below.

$$q_1(t) = Q_1 e^{-\zeta\omega_{n1}t}\sin\left(\omega_{n1}\sqrt{1-\zeta^2}t + \psi_1\right)$$

Where $\zeta_1 = \frac{c_{q1}}{\left(2\sqrt{k_{q1}m_{q1}}\right)}$ and Q_1 can be obtained from initial conditions.

f) Transferring the modal coordinate to local coordinate

After uncoupling and solving the equations of motion, then it is required to transfer the displacement in modal coordinate (q) to the displacement in local coordinate (x). For an *m DOF* system, the relationship between q and x can be expressed as below.

$$\{x(t)\} = [\{P\}_1 \quad \{P\}_2 \quad \cdots \quad \{P\}_m]\begin{Bmatrix} q_1(t) \\ q_2(t) \\ \vdots \\ q_m(t) \end{Bmatrix} = [P]\{q(t)\}$$

By multiplying both sides of the equation (3-14) to $[P]^T$ and substituting $x(t)$ by the following equation,

$$\{x(t)\} = [P]\{q\} \qquad (3\text{-}13)$$

The equation of motion will have the following form.

$$[M_q]\{\ddot{q}\} + [C_q]\{\dot{q}\} + [K_q]\{q\} = \{R\}$$

Where $\{R\} = [P]^T \{F\}$ (3-14)

For the *m DOF* system, the equations of motion for the i^{th} mode will have the following form.

$$m_{qi}\ddot{q}_i + c_{qi}\dot{q}_i + k_{qi}q_i = R_i$$

As mentioned before these equations are uncoupled differential equations as the equations are introduced in modal coordinate. These equations can be solved like the *SDOF* equation of motion.

For each mode *k*, the absolute value of displacement divided by force will be (displacement and force are expressed in modal coordinate)

$$\left|\Phi_{q,k}(\omega)\right| = \left|\frac{q_k}{R_k}\right| = \frac{1}{k_{qk}} \frac{1}{\sqrt{\left(1 - r_k^2\right)^2 + \left(2\zeta_k r_k\right)^2}}$$

Where $r_k = \dfrac{\omega}{\omega_{nk}}$.

Therefore matrix form of the equation in modal space is expressed as below.

$$\begin{Bmatrix} q_1(t) \\ q_2(t) \\ \vdots \\ q_m(t) \end{Bmatrix} = \begin{bmatrix} \Phi_{q1} & & & 0 \\ & \Phi_{q2} & & \\ & & \ddots & \\ 0 & & & \Phi_{qm} \end{bmatrix} \begin{Bmatrix} R_1 \\ R_2 \\ \vdots \\ R_m \end{Bmatrix}$$

Or can be expressed as below.

$$\{q\} = [\Phi_q]\{R\} \quad (3\text{-}15)$$

From equations (3-13), (3-14) and (3-15), the displacement in the local coordinate can be derived as below.

$$\{x\} = [P][\Phi_q][P]^T \{F\}$$

The above equation in indices form, have the following form.

$$\{x\} = \left(\sum_{k=1}^{n} \{P\}_k \{P\}_k^T \Phi_{q,k} \right) \{F\}$$

Where $\{P\}_k$ is the k^{th} eigenvector (of mode k).

If the force applies to mass number one with force function $F_1 \sin(\omega_t)$ then the force matrix will be as below.

$$\{F\} = \{F_1 \sin(\omega_t) \quad 0 \quad \cdots \quad 0\}$$

g) Transfer function

Transfer function can be obtained by dividing the displacement (response) by the excitation force. In the following section, the transfer function of the single degree of freedom is introduced first and then the transfer function of the multi degree of freedom is obtained. The equation of motion for a single degree of freedom system (*SDOF*) can be expressed as below.

$$m\ddot{x} + c\dot{x} + kx = F(t)$$

The above equation in frequency domain has the following form if $x = X \sin(\omega t + \varphi)$ and $\omega_n^2 = \frac{k}{m}$.

$$\left(\omega_n^2 - \omega^2 + 2j\zeta\omega_n\omega\right)X = F/m \qquad (3\text{-}16)$$

By applying Laplace transform to the *MDOF* equation of motion then the equation will be as below.

$$\left([M]s^2+[C]s+[K]\right)\{X(s)\}=\{F(s)\}$$

The equation can be presented in the following form.

$$\left([M]s^2+[C]s+[K]\right)=[B(s)]$$

Where $[B(s)]\{X(s)\}=\{F(s)\}$.

Then the transfer function that is the division of displacement by excitation force would be as below.

$$[H(s)]=\frac{\{X(s)\}}{\{F(s)\}}=\frac{adj[B(s)]}{\left|[B(s)]\right|}$$

$\left|[B(s)]\right|$ is called the characteristic equation. The solution of $\left|[B(s)]\right|=0$ gives the eigenvalues of the system. For a *mDOF* system, the transfer function would be as below.

$$[H(s)]=\begin{bmatrix} h_{11}(s) & h_{12}(s) & \cdots & \\ h_{21}(s) & h_{22}(s) & & \\ \vdots & & \ddots & \\ & & & h_{mm}(s) \end{bmatrix}$$

The elements of the matrix are as below.

$$h_{11}(s)=\left[\frac{\alpha_{11,1}+\beta_{11,1}s}{s^2+2\zeta_1\omega_{n,1}s+\omega_{n,1}^2}\right]_{\mathrm{mod}\,e1}+\left[\frac{\alpha_{11,2}+\beta_{11,2}s}{s^2+2\zeta_2\omega_{n,2}s+\omega_{n,2}^2}\right]_{\mathrm{mod}\,e2}+\cdots+\left[\frac{\alpha_{11,m}+\beta_{11,m}s}{s^2+2\zeta_m\omega_{n,m}s+\omega_{n,m}^2}\right]_{\mathrm{mod}\,em} \quad (3\text{-}17)$$

Or in indices form, the *h* parameter would be

$$h_{il}(s) = \sum_{k=1}^{n} \frac{\alpha_{il,k} + \beta_{il,k} s}{s^2 + 2\zeta_k \omega_{n,k} s + \omega_{n,k}^2} \tag{3-18}$$

The transfer function matrix can be introduced as the following equation .

$$[H(s)] = \sum_{k=1}^{n} \frac{[R]_k}{s^2 + 2\zeta_k \omega_{n,k} s + \omega_{n,k}^2} \tag{3-19}$$

In this equation $[R]_k = [\alpha + \beta s]_k$.

h) Mode shape matrix of MDOF systems

From section (f) the displacement in local coordinates can be expressed as [34]

$$\{x\} = \left(\sum_{k=1}^{n} \{P\}_k \{P\}_k^T \Phi_{q,k} \right) \{F\}$$

Thus

$$[H(s)] = \frac{\{x\}}{\{F\}} = \sum_{k=1}^{n} \{P\}_k \{P\}_k^T \Phi_{q,k} \tag{3-20}$$

Where $\{P\}_k$ is the eigenvector.

From section (f) for mode *k* we have $m_{qk}\ddot{q}_k + c_{qk}\dot{q}_k + k_{qk}q_k = R_k$ and the following equation.

$$\Phi_{q,k}(\omega)=\frac{q_k}{R_k}=\frac{1}{m_{qk}s^2+c_{qk}s+k_{qk}}\rightarrow\times\left(\frac{1}{m_{qk}/m_{qk}}\right)\rightarrow,\ c/m=2\zeta\omega_n$$
$$\Rightarrow\Phi_{q,k}(\omega)=\frac{1}{m_{qk}}\frac{1}{s^2+2\zeta\omega_{nk}s+\omega_{nk}^2} \quad (3\text{-}21)$$

From (3-20) and (3-21), two transfer functions can be equal to each other as below.

$$[H(s)]=\sum_{k=1}^{n}\frac{\{P\}_k\{P\}_k^T}{m_{qk}}\frac{1}{s^2+2\zeta_k\omega_{nk}s+\omega_{nk}^2}=\sum_{k=1}^{n}\frac{[R]_k}{s^2+2\zeta_k\omega_{nk}s+\omega_{nk}^2}$$

Or from Equation (3-16) the equation will have the following form.

$$[H]=\sum_{k=1}^{n}\frac{[R]_k}{\omega_{nk}^2-\omega^2+2j\zeta_k\omega\omega_{nk}} \quad (3\text{-}22)$$

The modal mass, for mode *k*, from equation (3-12) is as bellow.

$$m_{q,k}=\{P\}_k^T[M_x]\{P\}_k$$

$\{P\}_k$ is the eigenvector (mode shape) and,

$$\left(\{P\}_k^T\{P\}_k\right)/m_{qk}\equiv\{u\}_k\{u\}_k^T=[R]_k \quad (3\text{-}23)$$

In this equation $\{u\}_k$ is the normalized mode shape ($\{u\}_k=\{P\}_k/\sqrt{m_{qk}}$) or the mode shapes normalized relative to mass.

$$\{u\}_k^T[M_x]\{u\}_k=1$$

Matrix $[R]_k$ for a particular mode *k* can be expressed in the following form.

$$[R]_k = \begin{bmatrix} u_1u_1 & u_1u_2 & \dots & u_1u_l & \dots & u_1u_n \\ u_2u_1 & u_2u_2 & \dots & u_2u_l & \dots & u_2u_n \\ \vdots & \vdots & \vdots & \vdots & \vdots & \\ u_lu_1 & u_lu_1 & \dots & u_lu_l & \cdots & u_lu_n \\ \vdots & \vdots & \vdots & \vdots & \vdots & \\ u_nu_1 & u_nu_2 & \dots & u_nu_l & \dots & u_nu_n \end{bmatrix}_k$$

Column l from matrix R is equal to column l from matrix u as below.

$$\begin{Bmatrix} R_{1l} \\ R_{2l} \\ \vdots \\ R_{ll} \\ \vdots \\ R_{nl} \end{Bmatrix}_k = \begin{Bmatrix} u_1u_l \\ u_2u_l \\ \vdots \\ u_lu_l \\ \vdots \\ u_nu_l \end{Bmatrix}_k$$

This matrix can also be expressed as below.

$$\begin{cases} u_{lk} = \dfrac{R_{ll,k}}{u_{l,k}} \Rightarrow u_{lk} = \sqrt{R_{ll,k}} \\ u_{1k} = \dfrac{R_{1l,k}}{u_{l,k}} \\ u_{2k} = \dfrac{R_{2l,k}}{u_{l,k}} \\ \vdots = \vdots \\ u_{nk} = \dfrac{R_{nl,k}}{u_{l,k}} \end{cases} \tag{3-24}$$

For $\omega_n = \omega_{nk}$, from Equations (3-22) and (3-24) the following relation is valid.

$$u_{ik}u_{lk} = |h_{il}|_k \zeta_k \omega_{nk}^2 \tag{3-25}$$

The **modal matrix** of the system consists of mode shapes of the system is stated as below.

$$[U] = [\{u\}_1 \quad \{u\}_2 \quad \cdots \quad \{u\}_n]$$

3.3. Theory of Neural Networks

The theory of neural networks is presented in this section. Artificial neural network is a mathematical model of biological neural networks.

In this section the mathematical presentation of this method is described. In neural network, there is a set of inputs and outputs data. The task of neural network includes simulation of these input-output data. In another word neural network is a tool to find mathematical relationship between sets of input-outputs. In fact neural network is a multi dimensional interpolation method. The mathematical approach is presented below. The inputs and outputs of the neural network can be related to each other by the following equation [30]:

$$y_i = f_i\left(\sum_{j=1}^{n} w_{ij} x_j\right)$$

In this equation, y_i is the output, for $i = 1,\ldots,m$, and x_j is the input for $j = 1,\ldots,n$. In this case the system is a multi-input-multi-output system that each set of input and output data consist of *n* inputs and *m* outputs. Neural network task includes obtaining the coefficient w_{ij}. w_{ij} called ***weight***. Function f_i can be selected arbitrary. The most popular function in engineering applications is referred to ***sigmoid function*** and is expressed as below.

$$f(x) = \frac{1}{1+e^{-x}}$$

Neural networks consist of an input layer (containing input data), an output layer (containing output data) and middle layers that consist of the mathematical relation of input and output layers. Middle layers are called hidden layers. If there is only one hidden layer in the network then the network is called single layer neural network or ***perceptron***. Neural network uses the available input-output data to obtain w_{ij}. The

method for deriving w_{ij} from available input-output data is called learning algorithm. Different learning algorithms are available for multi layer and single layer networks. In this section ***delta rule algorithm*** is introduced for single layer and ***backpropagation algorithm*** for multi layer algorithm as the most popular methods in engineering applications. The data used in obtaining the neural network parameters (weights) is called ***training data***. Training data are the input-output data sets as below.

$$T = \left(x_j^q, y_i^q\right)$$

Where $i = 1,\ldots,m$ is the input numbers of each set, $j = 1,\ldots,n$ is the output numbers of each set of data and $q = 1,\ldots,N$ is the number of input-output sets of available data.

a) The delta rule

Obtaining the weights is the aim of learning algorithm. At the first stage, arbitrary values are considered for weights. The difference between available output data (y_i^q), also known as target, and output of the neural network determines the error. Minimizing this error is the algorithm task. The weight values are obtained by minimizing the error. The summation of the errors is introduced as [30].

$$E = \sum_{q=1}^{N} E^q$$

In this equation, E^q is as below.

$$E^q = \frac{1}{2}\sum_{i=1}^{m}\left(y_i^q - o_i^q\right)^2 \qquad (3\text{-}26)$$

Where o_i^q is the output of the neural network that is calculated by the weights. y_i^q is the available output data from the real system. y_i^q is called target. Network task is to derive o_i^q as close as y_i^q by changing the weights values. i is the number of outputs

and q is the number of training data set. As mentioned before, o_i^q value can be calculated by the network weights by the following equation.

$$o_i^q = f_i\left(\sum_{j=0}^{n} w_{ij} x_j\right) \tag{3-27}$$

Where x_j is the input for $j = 1,\ldots,n$ and j is the number of inputs in each training data set. From equations (3-26) and (3-27), it can be seen that the error is a function of w_{ij}. To investigate the variation of error respect to w_{ij}, the gradient of E has to be calculated. This leads to obtaining the optimised value of weights. The following equation can be used to update the weight values.

$$w_{jk} \rightarrow w_{jk} + \Delta w_{jk} \tag{3-28}$$

Where

$$\Delta w_{jk} = -\eta \frac{\partial E}{\partial w_{ij}}$$

In this equation $\eta > 0$ is a constant value and can be chosen arbitrary. η is called ***learning rate***. The derivative of error respect to w_{ij} can be calculated as bellow.

$$\frac{\partial E}{\partial w_{ij}} = \sum_{q=1}^{N} \frac{\partial E^q}{\partial w_{ij}}$$

From the above equation and equation (3-26):

$$\frac{\partial E^q}{\partial w_{ij}} = \frac{\partial}{\partial w_{ij}}\left(\frac{1}{2}\sum_{i=1}^{m}\left(y_i^q - o_i^q\right)^2\right)$$
$$= \left(y_1^q - o_1^q\right)\frac{\partial}{\partial w_{ij}}\left(y_1^q - o_1^q\right) + \left(y_2^q - o_2^q\right)\frac{\partial}{\partial w_{ij}}\left(y_2^q - o_2^q\right) + \cdots + \left(y_m^q - o_m^q\right)\frac{\partial}{\partial w_{ij}}\left(y_m^q - o_m^q\right)$$

As y is a constant data, then $\frac{\partial y_i^q}{\partial w_{ij}} = 0$ and from (3-27)

$$\frac{\partial E^q}{\partial w_{ij}} = -\left(y_1^q - o_1^q\right)\frac{\partial}{\partial w_{ij}} f_1\left(\sum_{j=0}^{n} w_{1j}x_j\right) - \left(y_2^q - o_2^q\right)\frac{\partial}{\partial w_{ij}} f_2\left(\sum_{j=0}^{n} w_{2j}x_j\right) - \cdots -$$

$$\left(y_m^q - o_m^q\right)\frac{\partial}{\partial w_{ij}} f_m\left(\sum_{j=0}^{n} w_{mj}x_j\right)$$

(3-29)

Where $\frac{\partial}{\partial w_{ij}} f_1\left(\sum_{j=0}^{n} w_{1j}x_j\right) = 0$ if $i \neq 1$, but $\frac{\partial}{\partial w_{1j}} f_1\left(\sum_{j=0}^{n} w_{1j}x_j\right) \neq 0$ as w_{ij} is a constant value. The same relation is valid for $i = 2,\ldots,m$ .Then equation (3-29) will be as below.

$$\frac{\partial E^q}{\partial w_{ij}} = -\left(y_i^q - o_i^q\right)\frac{\partial}{\partial w_{ij}} f_i\left(\sum_{j=0}^{n} w_{ij}x_j\right) \qquad (3\text{-}30)$$

To simplify this equation the following equation can be introduced.

$$S = \sum_{j=0}^{n} w_{ij}x_j$$

By chain derivative respect to *S* in equation (3-30) will be in the following form.

$$\frac{\partial E^q}{\partial w_{ij}} = -\left(y_i^q - o_i^q\right)\frac{\partial S}{\partial w_{ij}}\frac{\partial}{\partial S} f_i\left(\sum_{j=0}^{n} w_{ij}x_j\right)$$

By changing indices the equation can be presented in the following forms

$$\frac{\partial E^q}{\partial w_{ji}} = -\left(y_j^q - o_j^q\right)\frac{\partial S}{\partial w_{ji}}\frac{\partial}{\partial S} f_j\left(\sum_{i=0}^{n} w_{ji}x_i\right)$$

$$\frac{\partial E^q}{\partial w_{jk}} = -\left(y_j^q - o_j^q\right)\frac{\partial S}{\partial w_{jk}}\frac{\partial}{\partial S} f_j\left(\sum_{i=0}^{n} w_{ji}x_i\right) \qquad (3\text{-}31)$$

Where

$$\frac{\partial S}{\partial w_{jk}} = \frac{\partial}{\partial w_{jk}} \sum_{j=1}^{n} w_{ji} x_i = \delta_{jj} \delta_{ki} x_i = x_k$$

And

$$\frac{\partial}{\partial S} f_j(S) = f_j'$$

Then equation (3-31) will be in the following form.

$$\frac{\partial E^q}{\partial w_{jk}} = x_k^q \left(o_j^q - y_j^q\right) f_j' \left(\sum_{i=0}^{n} w_{ji} x_i^q\right) = \delta_j^q . x_k^q \qquad (3\text{-}32)$$

Where

$$\delta_j^q = \left(y_j^q - o_j^q\right) f_j' \left(\sum_{i=0}^{n} w_{ji} x_i^q\right)$$

Equations (3-28) and (3-32) can be used to update the weights.

b) The backpropagation algorithm

This learning algorithm is designed for multi layer networks. The principal of this method is based on the delta rule algorithm. The relation for a two layer network consists of a hidden layer and an output layer is presented below. In this method the weights can be updated by the following relations [30].

$$\begin{aligned} \Delta \upsilon_{ji} &= -\eta \sum_{j=1}^{N} \frac{\partial E^q}{\partial \upsilon_{ji}} \\ &= \sum_{j=1}^{N} \left(-\eta \delta_j^q z_i^q\right) \end{aligned} \qquad (3\text{-}33)$$

Where υ_{ji} is the weight between outputs o_j^q and z_i^q, and z_i^q is the net input of the output layer (the behaves like inputs in delta rule). z_i^q is also the output of the hidden layer. Weights can relate z_i^q to the inputs, x_k^q, by the following equation.

$$z_i^q = f_i\left(\sum_{k=0}^{n} w_{ik} x_k^q\right)$$

δ_j^q in equation (3-33) can be presented as below.

$$\delta_j^q = \left(o_j^q - y_j^q\right) f_k'\left(\sum_{k=1}^{m} \upsilon_{jk} z_k^q\right)$$

The same equation in delta rule can be used to update the weights between the inputs and the hidden layer as below.

$$\Delta w_{ik} = -\eta \sum_{i=1}^{N} \frac{\partial E^q}{\partial w_{ik}} \qquad (3\text{-}34)$$

It has been investigated that the following equation can be used to update these weights [30].

$$\frac{\partial E^q}{\partial w_{ik}} = \frac{\partial E^q}{\partial z_i^q} \frac{\partial z_i^q}{\partial w_{ik}}$$

Equations (3-33) and (3-34) can be used to update the weights in this algorithm. After minimizing the weights by the presented method then the network is trained and is ready to use.

3.3.1. Neural fuzzy systems

Combination of fuzzy and neural networks is possible in two ways. The first method is referred to as fuzzy-neural systems and the second one to neural-fuzzy. In this project the application of ***neural fuzzy*** method is used that is a combination of fuzzy

systems and neural networks. In this method, the training data of a real system is available. A fuzzy system consists of membership functions and the rules, are built based on this training data. Then this fuzzy system can be used as a network model. The most popular method in engineering application that is used in MATLAB software is called adaptive neural network fuzzy inference systems [30]. The training algorithm is known as neuro-fuzzy inference systems or adaptive network fuzzy inference systems (ANFIS). This method is presented below. The available training data set can be assumed as below.

$$\{(x^1, y^1), \ldots, (x^k, y^k)\}$$

For a single input and single output training data, fuzzy rules can be presented as below.

$$R_i : If\ x\ is\ A_i\ \ then\ y = z_i$$

Where A_i are fuzzy membership functions and z_i are real numbers and both are desired. z_i is called ***consequent parameters***. Fuzzy membership functions A_i can be a sigmoid function as below.

$$A_i(x) = \frac{1}{1 + e^{b_i(x - a_i)}}$$

a_i and b_i are the parameter of the membership function A_i . These parameters are called ***premise parameters*** and are desired. The fuzzy output can be presented by the centre of gravity defuzzification method that mentioned before as below.

$$O(x) = \frac{\sum_{i=1}^{n} A_i(x) z_i}{\sum_{i=1}^{n} A_i(x)}$$

The training set can be used to learn the premise parameter (a_i and b_i) and consequent parameters (z_i). The error can be calculated by the following equation.

$$E^k = E^k(a_i, b_i, z_i) = \frac{1}{2}\left(O^k(a_i, b_i, z_i) - y^k\right)^2$$

The algorithm that the parameters can be calculated based on the error function is as below.

$$z_i(t+1) = z_i(t) - \eta \frac{\partial E^k}{\partial z_i} = z_i(t) - \eta\left(O^k - y^k\right) \frac{A_i(x)}{\sum_{i=1}^{n} A_i(x)}$$

$$a_i(t+1) = a_i(t) - \eta \frac{\partial E^k}{\partial a_i}$$

$$b_i(t+1) = b_i(t) - \eta \frac{\partial E^k}{\partial b_i}$$

$\eta > 0$ is the learning rate.

3.4. Conclusion

The theory of fuzzy logic, modal analysis and neural networks are presented in this chapter. Some of these theories have been used in the proposed method in this thesis such as in modal analysis mode shape extraction. Although MATLAB software is used to perform fuzzy logic and neural network procedure, it is very important to understand the theory of these concepts as it helps for understanding the proposed method.

Chapter 4

Estimating Mode Shapes

In this chapter, vibration behaviour or mode shapes of mechanical systems are investigated. The aim is to obtain a general rule of estimating an approximate mode shape for structures. In this section, first, the mode shapes of mass spring systems are studied. In this study the mode shapes of two and multi mass-spring systems are investigated. Then the problem of one-dimensional elastic bodies is explored and again, the mode shapes are studied. In the end, the study is expanded to mode shapes of structures.

This section presents a background of guessing the mode shapes of different mechanical systems. It is argued that guessing is possible heuristically, that is based on the experiments and observations of vibration behaviour of structures. Some rules are also developed in this chapter in order to guess the mode shapes. However there is no claim that guessing is always possible. In this respect, two methods are introduced for two cases where the guessing is not possible or the guess is wrong (These methods are explained in Chapter 5). The *Mode Shape Form* (*MSF*) term is proposed here to describe an approximate mode shape. This chapter studies mode shapes of various mechanical systems and attempt to derive rules relating to mode shapes. Guessed mode shape, approximate mode shape and the mode shape form (*MSF*) are used in this thesis where all represent the same meaning.

4.1. Two Degrees of freedom mass-spring systems

In this section the mode shapes of two-degree of freedom (*2DOF*) mass and spring systems are investigated. The aim is to show that the approximate mode shape or *MSF* of a two degree of freedom mass and spring system always obeys a rule, regardless of magnitudes of masses and springs stiffness. This rule describes the direction of motion of the masses for the first and the second natural frequency.

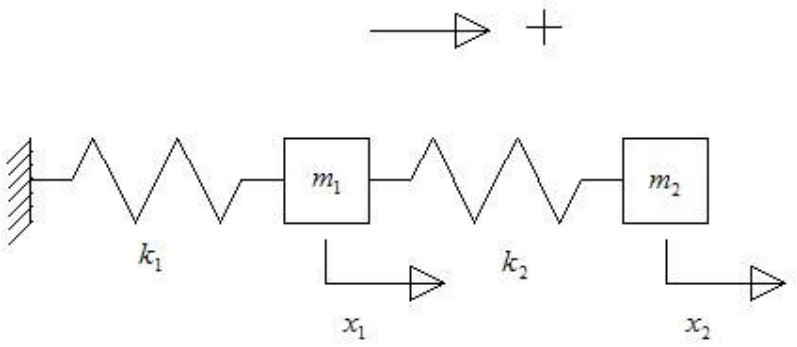

Figure 4-1. Two degree of freedom mass and spring system.

Figure 4-1 demonstrates a two-degree of freedom mass-spring system. The free body diagram of the system is presented in Figure 4-2.

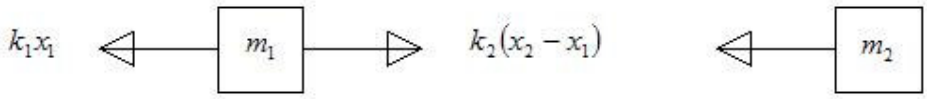

Figure 4-2. Free body diagram.

If $x_2 > x_1$, from Figure 4-2, the Newton equation of motion can be presented as below.

$$\begin{cases} -k_2(x_2-x_1)=m_2\ddot{x}_2 \\ k_2(x_2-x_1)-k_1x_1=m_1\ddot{x}_1 \end{cases} \tag{4-1}$$

If $x = X\sin\omega t$ then $\ddot{x} = -X\omega^2 \sin\omega t$ and by substituting these equations in (4-1) then the equation will have the following form.

$$\begin{cases} \left(-k_2 + m_2\omega^2\right)X_2 = -k_2 X_1 \\ k_2 X_2 + \left(-k_2 - k_1 + m_1\omega^2\right)X_1 = 0 \end{cases}$$

The above equations can be expressed as below.

$$\frac{X_2}{X_1} = \frac{-k_2}{-k_2 + m_2\omega^2} \tag{4-2}$$

And

$$\frac{X_2}{X_1} = \frac{-k_2 - k_1 + m_1\omega^2}{-k_2} \tag{4-3}$$

The procedure proposed here is different than classical solution of eigenvalues and eigenvectors. In the method developed here, approximate mode shapes (in terms of direction of motion of the masses) are assumed and feasible frequencies satisfying mode shape equations are investigated.

The objective is to obtain the *MSFs* from Equations (4-2) and (4-3). *MSFs* give the direction of motion of the masses relative to each other. There is one *MSF* for each natural frequency of the system. In obtaining *MSFs,* it is not required to know the magnitude of natural frequencies. The only information required for *MSFs* is, if the *MSF* belongs to the first natural frequency or the second natural frequency for *2DOF* systems. For a *2DOF* system there are two natural frequencies and two mode shapes.
In eigenvector problems, displacement of one of masses can be considered to have the value of one and then the displacement of the other masses are calculated relative to this mass. Therefore it is possible to assume $X_1 = 1$. However in the process of obtaining *MSFs* presented in this chapter, it is sufficient to have $X_1 \rangle 0$. The same *MSF* have to be obtained from both Equation (4-2) and Equation (4-3) for each natural frequency. If the *MSF* from Equation (4-2) is different from Equation (4-3) then the *MSF* is not acceptable. The reason is, each natural frequency can only exhibit one mode shape.

Two symbols, $\rightarrow\oplus$ and $\leftarrow$ are used to show the displacement of a mass in the positive direction and the negative direction respectively. In another word $X \rightarrow \oplus$ and $X \leftarrow$ are equivalent to $X \rangle 0$ and $X \langle 0$ respectively.

For $X_1 \rangle 0$:

i) To have $\frac{X_2}{X_1} \rangle 0$, or $X_1 \rightarrow \oplus$ and $X_2 \rightarrow \oplus$ for consistency

From Equation (4-2) the natural frequency must be **smaller** than $\sqrt{\frac{k_2}{m_2}}$ and from Equation (4-3) **smaller** than $\sqrt{\frac{k_1 + k_2}{m_1}}$.

ii) To have $\frac{X_2}{X_1} \langle 0$, or $X_1 \rightarrow \oplus$ and $X_2 \leftarrow$

From Equation (4-2) the natural frequency must be **larger** than $\sqrt{\frac{k_2}{m_2}}$ and from Equation (4-3) the natural frequency must be **larger** than $\sqrt{\frac{k_1 + k_2}{m_1}}$.

Now it is required to know which *MSF* is the first and which one is the second. In this respect, the *MSF* for the smallest natural frequency is the first *MSF* and the *MSF* for the larger natural frequency is the second *MSF*. Therefore the results can be expressed as below.

- From section (i), the first *MSF* is

$X_1 \rightarrow \oplus$ and $X_2 \rightarrow \oplus$

- From section (ii), the second *MSF* is

$X_1 \rightarrow \oplus$ and $X_2 \leftarrow$

Therefore the conclusion of this section is the rule in obtaining the *MSFs* for the first and the second natural frequency of *2DOF* (degree of freedom) mass-spring systems as below.

The *MSF* for the first natural frequency (The first *MSF*): ***the motion of two masses follow the same direction of motion.***

The *MSF* for the second natural frequency (The second *MSF*): ***the displacements of the masses are in the opposite directions relative to each other.***

4.2. Three Degrees of freedom mass-spring system

The objective of this section is to obtain *MSF* rules for the *3DOF* mass-spring systems. The same procedure that applied to *2DOF* system is applied here. A *3DOF* mass-spring system is presented in Figure 4-3.

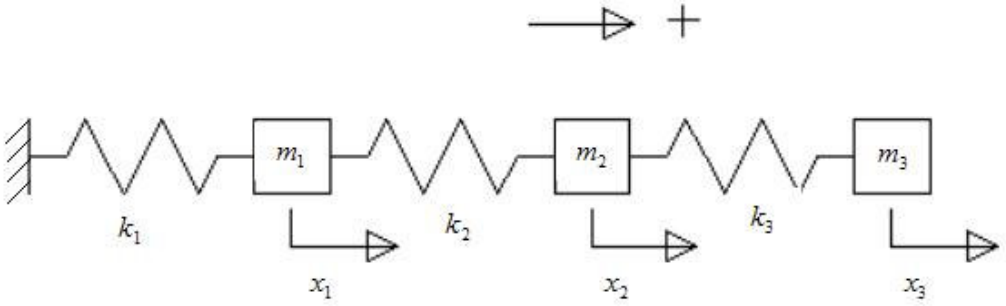

Figure 4-3. 3DOF mass-spring system

If $x_3 > x_2 > x_1$ then the free body diagram will be

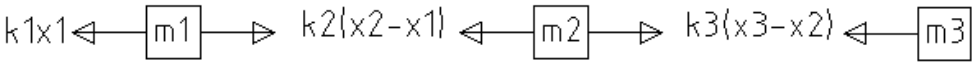

Figure 4-4. 3DOF free body diagram of the mass-spring system

The equation of motions can be obtained as

$$\begin{cases} k_2(x_2 - x_1) - k_1 x_1 = m_1 \ddot{x}_1 \\ k_3(x_3 - x_2) - k_2(x_2 - x_1) = m_2 \ddot{x}_2 \\ -k_3(x_3 - x_2) = m_3 \ddot{x}_3 \end{cases} \quad (4\text{-}4)$$

If $x_1 = X_1 \sin \omega t$ then $\ddot{x}_1 = -X_1 \omega^2 \sin \omega t$ and by substituting these equations in (4-4) then the equations can be expressed as below.

$$k_2 X_2 + \left(-k_2 - k_1 + m_1 \omega^2\right) X_1 = 0 \qquad (4\text{-}5)$$

$$k_3 X_3 + \left(-k_3 - k_2 + m_2 \omega^2\right) X_2 + k_2 X_1 = 0 \qquad (4\text{-}6)$$

$$k_3 X_2 + \left(-k_3 + m_3 \omega^2\right) X_3 = 0 \qquad (4\text{-}7)$$

From equation (4-5):

$$\frac{X_2}{X_1} = \frac{k_2 + k_1 - m_1 \omega^2}{k_2} \qquad (4\text{-}8)$$

From equation (4-7):

$$\frac{X_2}{X_3} = \frac{k_3 - m_3 \omega^2}{k_3} \qquad (4\text{-}9)$$

Where ω, k and m are positive parameters. Again the same procedure as described above for 2 mass system is followed. The procedure starts with assuming a mode shape.

If $X_1 = 1$.

i) To have $X_1 \rightarrow \oplus \;\; X_2 \rightarrow \oplus \;\; X_3 \rightarrow \oplus$

From Equation (4-8) the natural frequency must be **smaller** than $\sqrt{\frac{k_2 + k_1}{m_1}}$ and

from Equation (4-9) the natural frequency must be **smaller** than $\sqrt{\frac{k_3}{m_3}}$.

ii) To have $X_1 \rightarrow \oplus \;\; X_2 \rightarrow \oplus \;\; X_3 \leftarrow$

From Equation (4-8) the natural frequency must be **smaller** than $\sqrt{\frac{k_2 + k_1}{m_1}}$ and

from Equation (4-9) the natural frequency must be **larger** than $\sqrt{\frac{k_3}{m_3}}$.

iii) To have $X_1 \leftarrow \; X_2 \rightarrow \oplus \; X_3 \rightarrow \oplus$

From Equation (4-8) the natural frequency must be **larger** than $\sqrt{\frac{k_2 + k_1}{m_1}}$ and from Equation (4-9) the natural frequency must be **smaller** than $\sqrt{\frac{k_3}{m_3}}$.

iv) To have $X_1 \rightarrow \oplus \; X_2 \leftarrow \; X_3 \rightarrow \oplus$

From Equation (4-8) the natural frequency must be **larger** than $\sqrt{\frac{k_2 + k_1}{m_1}}$ and from Equation (4-9) the natural frequency must be **larger** than $\sqrt{\frac{k_3}{m_3}}$.

Now the *MSFs* from sections (i), (ii), (iii) and (iv) has to be investigated in an order to understand which *MSF* is the first, second or third. As this is a *3DOF* system then we have three *MSFs*. Each *MSF* is exhibited in a natural frequency. From sections (i), (ii), (iii) and (iv), for each *MSF* there is an indication of magnitude of a natural frequency which shows if the natural frequency is smaller or larger than certain values ($\sqrt{\frac{k_2 + k_1}{m_1}}$ and $\sqrt{\frac{k_3}{m_3}}$). The objective is, to locate the natural frequencies corresponding to these *MSFs*.

From section (i) the natural frequency must be smaller than $\sqrt{\frac{k_2 + k_1}{m_1}}$ and $\sqrt{\frac{k_3}{m_3}}$.

From section (ii) the natural frequency must be smaller than $\sqrt{\frac{k_2 + k_1}{m_1}}$ and larger than $\sqrt{\frac{k_3}{m_3}}$.

From section (iii) the natural frequency must be larger than $\sqrt{\frac{k_2+k_1}{m_1}}$ and smaller than $\sqrt{\frac{k_3}{m_3}}$.

From section (iv) the natural frequency must be larger than $\sqrt{\frac{k_2+k_1}{m_1}}$ and larger than $\sqrt{\frac{k_3}{m_3}}$.

By comparing the above statements, (i) is the smallest natural frequency, (ii) or (iii) is the middle natural frequency and (iv) is the largest natural frequency. In a particular system, either section (ii) or section (iii) is true. This depend on either $\sqrt{\frac{k_2+k_1}{m_1}} \rangle \sqrt{\frac{k_3}{m_3}}$ or $\sqrt{\frac{k_2+k_1}{m_1}} \langle \sqrt{\frac{k_3}{m_3}}$. If $\sqrt{\frac{k_2+k_1}{m_1}} \rangle \sqrt{\frac{k_3}{m_3}}$, then section (ii) is true and if $\sqrt{\frac{k_2+k_1}{m_1}} \langle \sqrt{\frac{k_3}{m_3}}$, then section (iii) is true.

The outcomes of this section are some rules for guessing the *MSFs* for a *3DOF* mass-spring system. These rules are as below.

The *MSF* for the first natural frequency (The first *MSF*): ***the motion of the three masses follow the same direction of motion.***

The *MSF* for the second natural frequency (The second *MSF*): ***the motion of the two neighbour masses (neighbours, 1-2 or 2-3) follow the same direction of motion and the displacements of the third mass is in the opposite directions relative to the other two masses.***

The *MSF* for the third natural frequency (The third *MSF*): ***the motion of masses 1 and 3 follow the same direction and the displacements of mass2 (the middle mass) is in the opposite directions relative to 1 and 3.***

The following rule is proposed to guess the n^{th} *MSF* of a *m* degree of freedom mass-spring system.

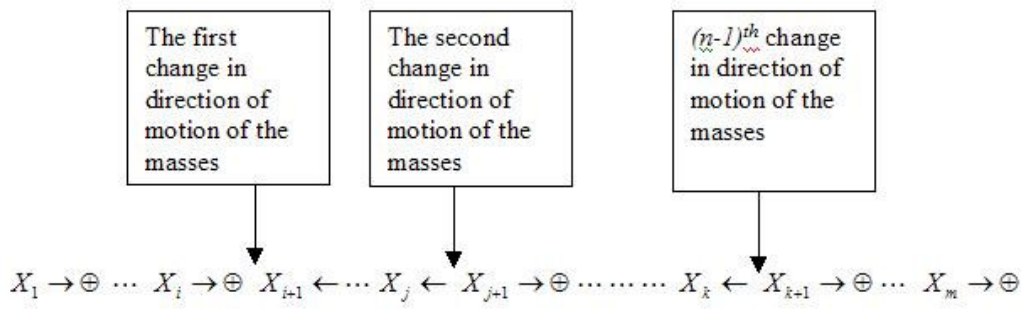

Therefore the rule for the n^{th} *MSF* of a *m* degree of freedom mass-spring system is, ***there are n-1 places on the MSF where the direction of motion of the masses changes.***

Based on this rule mode shapes for a four mass system can be proposed as follow.

The first *MSF*:

$X_1 \rightarrow \oplus\ \ X_2 \rightarrow \oplus\ \ X_3 \rightarrow \oplus\ \ X_4 \rightarrow \oplus$

The second *MSF*:

$X_1 \rightarrow \oplus\ \ X_2 \rightarrow \oplus\ \ X_3 \rightarrow \oplus\ \ X_4 \leftarrow$

or

$X_1 \rightarrow \oplus\ \ X_2 \rightarrow \oplus\ \ X_3 \leftarrow\ \ X_4 \leftarrow$

or

$X_1 \rightarrow \oplus\ \ X_2 \leftarrow\ \ X_3 \leftarrow\ \ X_4 \leftarrow$

The third *MSF*:

$X_1 \rightarrow \oplus\ \ X_2 \leftarrow\ \ X_3 \rightarrow \oplus\ \ X_4 \rightarrow \oplus$

or

$X_1 \rightarrow \oplus\ \ X_2 \rightarrow \oplus\ \ X_3 \leftarrow\ \ X_4 \rightarrow \oplus$

or

$X_1 \rightarrow \oplus\ \ X_2 \leftarrow\ \ X_3 \leftarrow\ \ X_4 \rightarrow \oplus$

The forth *MSF*:

$X_1 \rightarrow \oplus \;\; X_2 \leftarrow \;\; X_3 \rightarrow \oplus \;\; X_4 \leftarrow$

In order to use rules obtained above, these need to be further generalised by exploring various combination or nodal (mass) neighbourhood. The study will enable an understanding of 2 dimensional structures to be built.

Another *3DOF* mass spring system is illustrated in Figure 4-5. In this example, mass 1 and mass 3 are connected. This structure has some similarity to a triangular element in finite element modelling where three nodes are connected to each other.

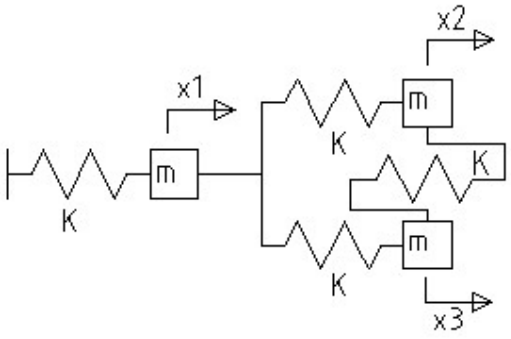

Figure 4-5. A *3DOF* mass-spring system

The equations of motion of this system are as below.

$$\left(3k - m\omega^2\right)X_1 - kX_2 - kX_3 = 0$$
$$-kX_1 + \left(2k - m\omega^2\right)X_2 - kX_3 = 0$$
$$-kX_2 - kX_1 + \left(2k - m\omega^2\right)X_3 = 0$$

These equations can also be expressed as below.

$$\frac{X_1}{X_2} = \frac{2k - m\omega^2}{4k - m\omega^2}$$
$$\frac{X_1}{X_3} = \frac{3k - m\omega^2}{4k - m\omega^2}$$
$$\frac{X_1}{X_3} = \frac{-k^2 - \left(2k - m\omega^2\right)^2}{3k^2 - mk\omega^2}$$

The *MSFs* can be obtained using the same approach as above. The only difference is, the *MSFs* are presented with the same configuration of masses as in Figure 4-5. These *MSFs* are presented below.

i) $X_1 \rightarrow \oplus \quad \begin{matrix} X_2 \rightarrow \oplus \\ X_3 \rightarrow \oplus \end{matrix}$ then $\omega^2 < \frac{k}{m}$

ii) $X_1 = 0 \quad \begin{matrix} X_2 \leftarrow \\ X_3 \rightarrow \oplus \end{matrix}$ then $\omega^2 = \frac{3k}{m}$

iii) $X_1 \rightarrow \oplus \quad \begin{matrix} X_2 \leftarrow \\ X_3 \leftarrow \end{matrix}$ then $\frac{3k}{m} < \omega^2 < \frac{4k}{m}$

In section (ii) equal sign is used. The reason is that, this is the only condition that satisfies all three equations of motion. The rules are as below.

The first *MSF* is the same *MSF* rule for *mDOF* system that stated above (three masses follow the same direction of motion). For the second and third *MSFs* we have:
For this mass-spring system, it is not possible to have 2 changes in the direction of motion of the masses relative to each other. This can be seen by looking at the above *MSFs*. Therefore in the second and third *MSFs* rule, direction of motion of two masses are the same, and the third mass direction is in the opposite direction. In this case another rule is introduced to obtain the second and third *MSFs*. In a smaller natural frequency, the mass with the smaller number of spring connection has the opposite direction of the motion to the other masses (the rule for case (ii)). In a larger natural frequency, the mass with the larger number of spring connection has the opposite direction of the motion to the other masses (the rule for case (iii)).

In the above example, in the second natural frequency, the direction of motion of masses 2 and 3 are in opposite direction relative to each other. In the third natural frequency, the direction of motion of mass 1 is in opposite direction relative to 2 and 3. The reason is that, there are 3 of spring connections for mass1 but mass 2 and 3 has two spring connection each. Therefore mass number 1 with 3 spring connection has the opposite direction of motion relative to the masses 2 and 3 in a higher natural

frequency mode (the third natural frequency). This rule can be applied for the systems where the number of spring connections for each mass is different with equal mass and stiffness values.

4.3. 4DOF mass-spring system

The objective in this section is to obtain the *MSF* for mass-spring systems with more than one spring connection for each mass. A 4DOF mass-spring system is illustrated in Figure 4-6.

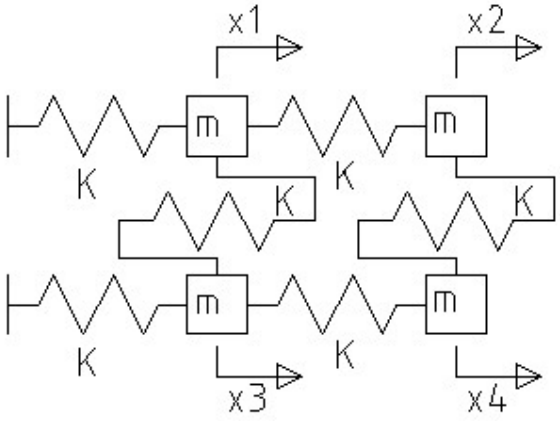

Figure 4-6. A 4DOF mass-spring system

The *MSFs* are presented with the same configuration of masses as in Figure 4-6. Using the same approach for the *3DOF* mass-spring system in Figure 4-5 then the *MSFs* can be expressed as below.

i) $\begin{matrix} X_1 \rightarrow \oplus & X_2 \rightarrow \oplus \\ X_3 \rightarrow \oplus & X_4 \rightarrow \oplus \end{matrix}$ then $\omega^2 \langle \frac{2k}{m}$

ii) $\begin{matrix} X_1 \rightarrow \oplus & X_2 \rightarrow \oplus \\ X_3 \leftarrow & X_4 \leftarrow \end{matrix}$ then $\frac{2k}{m} \langle \omega^2 \langle \frac{5k}{2m}$

iii) $\begin{matrix} X_1 \leftarrow & X_2 \rightarrow \oplus \\ X_3 \leftarrow & X_4 \rightarrow \oplus \end{matrix}$ then $\frac{5k}{2m} \langle \omega^2 \langle \frac{\left(\sqrt{2}+3\right)k}{m}$

iv) $\begin{matrix} X_1 \leftarrow & X_2 \rightarrow \oplus \\ X_3 \rightarrow \oplus & X_4 \leftarrow \end{matrix}$ then $\omega^2 \rangle \frac{\left(\sqrt{2}+3\right)k}{m}$

Therefore the *MSF* rules for the above system can be expressed as below. The rule for the first *MSF* is the same rule as before where all the masses follow the same direction of motion. In order to understand the motion, the system is seen as collection of 2 mass systems. In this respect, the directions of motion of neighbour masses are the subject of interest, rather than motion of individual masses. For example, in the *MSF* in section (iii), the direction of motion of neighbour masses 1 and 3 is in opposite direction relative to neighbour masses 2 and 4. Therefore there is only one change in the direction of motion of the masses. The rule for this example is as below. There is less change in direction of motion of the neighbour masses in lower natural frequencies and more change in direction of motion of the masses in higher natural frequencies. In this example, zero change in direction of motion of masses in the first natural frequency, one change in the second and third natural frequency and 4 changes in the forth natural frequency.

For the mass arrangement in Figure 4-6, it is not possible to have 3 changes in the direction of motion of the masses. Therefore we do not have this option in the above *MSFs*. In this example the second and the third *MSFs* obey the same rule. In another word, no rule is obtained to identify the difference between the second and the third *MSFs* in this example.

4.4. One-dimensional elastic bodies

In this section the objective is to obtain a general rule for *MSFs* of one-dimensional elastic bodies in lateral vibration. A clamped-free beam with two degrees of freedom (D1 and D2) is considered in lateral vibration. The following approach is used to obtain the first and second *MSFs* in this example. The beam is illustrated in Figure 4-7.

The equation of motion of the beam is given by [35]. The elemental mass and stiffness matrices are presented in the Appendix C.

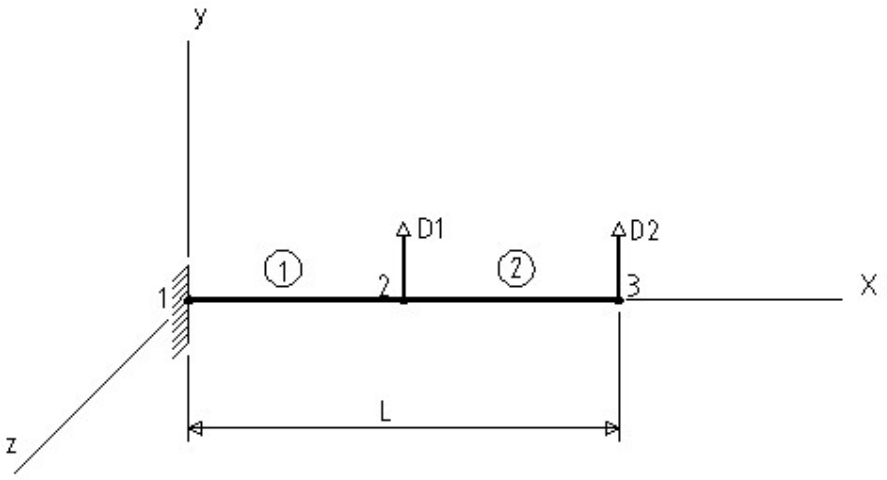

Figure 4-7. A *2DOF* clamped-free beam.

The structural stiffness matrix can be obtained by the following equation.

$$S = \sum_{i=1}^{n_e} K_i = K_1 + K_2$$

Where S is the structural stiffness matrix, n_e is the number of the elements and K_i is the stiffness matrix of the elements of the structure. The stiffness matrix can be expressed by the following relation.

$$S = a\begin{bmatrix} 0 & 0 & 0 \\ 0 & 6 & 0 \\ 0 & 0 & 0 \end{bmatrix} + a\begin{bmatrix} 0 & 0 & 0 \\ 0 & 6 & -6 \\ 0 & -6 & 6 \end{bmatrix} = a\begin{bmatrix} 0 & 0 & 0 \\ 0 & 12 & -6 \\ 0 & -6 & 6 \end{bmatrix}$$

In this relation $a = \dfrac{2EI}{L^3}$. The structural mass matrix can be obtained by the following equation.

$$M = \sum_{i=1}^{n_e} M_i = M_1 + M_2$$

Where M is the structural mass matrix, n_e is the number of the elements and M_i is the mass matrix of the elements of the structure. This equation can be obtained as below.

$$M = b\begin{bmatrix}0 & 0 & 0\\ 0 & 156 & 0\\ 0 & 0 & 0\end{bmatrix} + b\begin{bmatrix}0 & 0 & 0\\ 0 & 156 & 54\\ 0 & 54 & 156\end{bmatrix} = b\begin{bmatrix}0 & 0 & 0\\ 0 & 312 & 54\\ 0 & 54 & 156\end{bmatrix}$$

In this relation $b = \dfrac{\rho A_r L}{420}$.

Free vibration equation of motion of the structure can be expressed as below.

$$\left(S - \omega_i^2 M\right)\Phi_i = 0$$

Where $i = 1, 2, \ldots, n$, and n is the number of degrees of freedom. Φ_i is a vector of nodal amplitude or the mode shape for the i^{th} mode of vibration. ω_i is the angular frequency of mode i. The equation of motion can be obtained by substituting the mass and stiffness matrices in this equation as below.

$$\left(a\begin{bmatrix}0 & 0 & 0\\ 0 & 12 & -6\\ 0 & -6 & 6\end{bmatrix} - b\omega_i^2\begin{bmatrix}0 & 0 & 0\\ 0 & 312 & 54\\ 0 & 54 & 156\end{bmatrix}\right)\begin{Bmatrix}\Phi_1\\ \Phi_2\\ \Phi_3\end{Bmatrix} = \begin{Bmatrix}0\\ 0\\ 0\end{Bmatrix}$$

Then

$$\begin{bmatrix}0 & 0 & 0\\ 0 & 12a - 312b\omega_i^2 & -6a - 54b\omega_i^2\\ 0 & -6a - 54b\omega_i^2 & 6a - 156b\omega_i^2\end{bmatrix}\begin{Bmatrix}\Phi_1\\ \Phi_2\\ \Phi_3\end{Bmatrix} = \begin{Bmatrix}0\\ 0\\ 0\end{Bmatrix}$$

The equations of motion can be derived from the above matrix as below.

$$\left(12a - 312b\omega_i^2\right)\Phi_2 - \left(6a + 54b\omega_i^2\right)\Phi_3 = 0 \qquad (4\text{-}10)$$

Then

$$\frac{\Phi_2}{\Phi_3} = \frac{6a + 54b\omega_i^2}{12a - 312b\omega_i^2} \qquad (4\text{-}11)$$

And

$$\left(-6a-54b\omega_i^2\right)\Phi_2+\left(6a-156b\omega_i^2\right)\Phi_3=0$$

Then

$$\frac{\Phi_2}{\Phi_3}=\frac{6a-156b\omega_i^2}{6a+54b\omega_i^2} \tag{4-12}$$

$\frac{\Phi_2}{\Phi_3}=\frac{6a+54b\omega_i^2}{12a-312b\omega_i^2}$ and if $\Phi_2=+1$ then:

i) To have $\Phi_2\to\oplus$ $\Phi_3\to\oplus$ then from Equations (4-11) and (4-12),

$$\omega_i^2\langle\frac{12a}{312b}=\frac{a}{26b}.$$

This is the first *MSF* of the beam. In this *MSF* all the points on beam (in this example, 2 points on the beam) follow the same direction of motion. This is a general rule of *MSF* for beams as proved above. This *MSF* is valid for any value of the parameters of the system. These parameters consist of *E*, *I*, A_r, *L* and ρ. This result is illustrated in Figure 4-8.

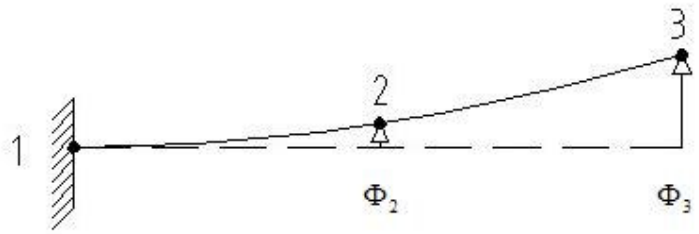

Figure 4-8. The first mode shape form.

The conclusion of this section for the first *MSF* is as below.

All the points on the body follow the same direction of motion in the first MSF.

This rule for the first *MSF* is the same as the rule for mass spring systems.

ii) To have $\Phi_2 \rightarrow \oplus \quad \Phi_3 \leftarrow$ then from equations (4-11) and (4-12),

$$\omega_i^2 \rangle \frac{12a}{312b} = \frac{a}{26b}.$$

This is the second *MSF* of the beam. In this *MSF*, the direction of motion of point 2 on the beam is opposite of direction of motion of point 3 (Figure 4-9). This is a general rule of the second *MSF* for any value of the beam parameter such as *a* and *b*. This result is illustrated in Figure 4-9.

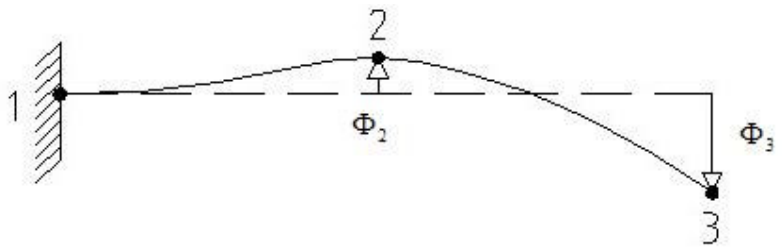

Figure 4-9. The second mode shape form.

The rule for the second *MSF* of a beam is as below.

The displacement of the nodes on the beam is in the opposite direction of motion relative to each other.

This rule for the second *MSF* is the similar to the rule for mass spring systems.

In describing the mode shape of this continuous system its boundary conditions need to be stated. In this case the beam is clamped and at this point, the deflection as well as its slope are zero.

By looking at the similarity between the mass-spring and beam problems then the following rule is proposed to guess the n^{th} *MSF* of a *m* degree of freedom beam.

There are n-1 places on the MSF where the direction of motion of the nodes on the beam changes.

4.5. Two-dimensional elastic bodies

In this section the objective is to obtain a general rule for *MSFs* of two-dimensional elastic bodies in lateral vibration. The equation of motion of the plate in Figure 4-10 is as below [38-40].

$$\frac{\partial^4 W(x,y)}{\partial x^4}+2\frac{\partial^4 W(x,y)}{\partial x^2\partial y^2}+\frac{\partial^4 W(x,y)}{\partial y^4}=\frac{q(x,y)}{D}$$

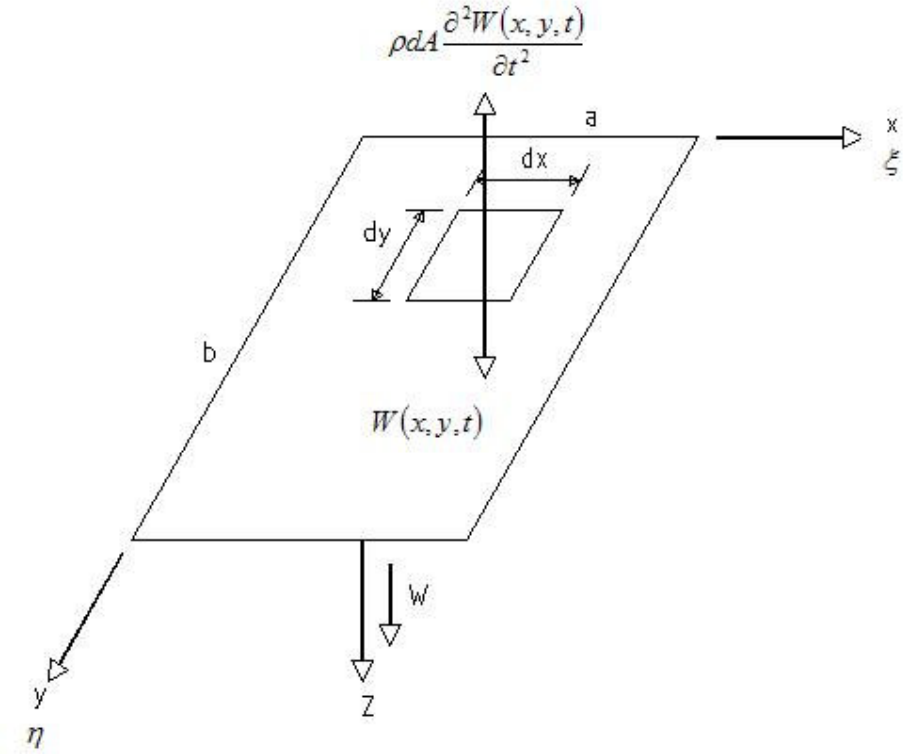

Figure 4-10. A rectangular plate and an element of the plate

Where $q(x,y)$ is the applied static force and W is the displacement (deflection) of the plate.

Free vibration equation of motion of the plate is as below.

$$\frac{\partial^4 W(x,y,t)}{\partial x^4}+2\frac{\partial^4 W(x,y,t)}{\partial x^2\partial y^2}+\frac{\partial^4 W(x,y,t)}{\partial y^4}+\frac{\rho}{D}\frac{\partial^4 W(x,y,t)}{\partial t^2}=0 \qquad (4\text{-}13)$$

Where the last term is the inertial force.

Free vibration of rectangular plates with simple support along all edges is given as below (Appendix B).

$$W(\xi,\eta) = A_{m,n}\sin(n\pi\eta)\sin(m\pi\xi)$$

Where $A_{m,n}$ is the amplitude coefficient and m and n are positive integers. In this equation for $m=1$, $n=1$, $0\le\xi\le1$ and $0\le\eta\le1$, then $W(\xi,\eta)\ge0$. Therefore in the first *MSF*, the displacement of all the points on the plate is in the positive direction. In another word all points follow the same direction of motion (same rule as the beam and mass-spring examples). The first *MSF* of a rectangular plate with simple support along all edges is illustrated in Figure 4-11.

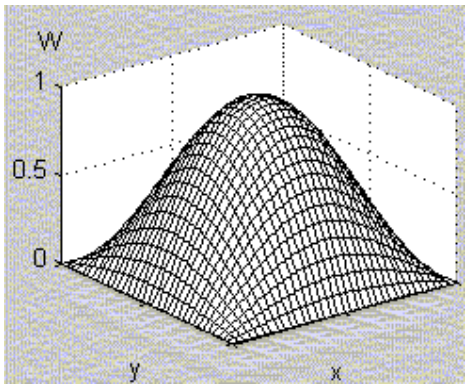

Figure 4-11. *MSFs* of a simple support plate along all edges.

m and n identify the number of waves in a particular mode shape. m and n can be obtained from the following equation [38].

$$\lambda^2 = (m\pi)^2 + \frac{(n\pi)^2}{\Phi^2}$$

where $\Phi = \frac{b}{a}$. λ is obtained by giving various *m* and *n* values to the above equation. *m* and *n* represent the number of waves in *x* and *y* directions respectively. Smaller value of λ for a particular *m* and *n* values corresponds to the lower natural frequency. Therefore value of λ identifies that a mode shape with a particular *m* and *n* is a higher or lower mode.

Therefore a rule is introduced for plate mode shapes as below.

The rule for the n^{th} *MSF* is, ***there are n-1 places on the MSF where the direction of motion of the particles changes.***

However this rule may not be correct in all cases but still can be applied because the *MSF* will be corrected by the method of correcting fuzzy *MSFs* that is presented in chapter 5.

In describing the mode shape of this continuous system its boundary conditions need to be stated. In this case the plate is simply supported along all edges and the deflection is zero.

4.6. Structural Frame Vibrations

In this section the objective is to obtain a general rule for *MSFs* of the structural lateral vibration. The following approach is used to obtain the first and second *MSFs* of a 3-beam structure (Figure 4-12) with 3 degrees of freedom (D1, D2 and D3).
Then the system of equation can be expressed as below (Appendix C).

$$\left[2L^2a_1 + 2L^2a_2 - \omega_i^2\left(4L^2c_1 + 4L^2c_2\right)\right]\Phi_6 + \left[L^2a_2 + \omega_i^2\left(3L^2c_2\right)\right]\Phi_9 = 0 \qquad (4\text{-}14)$$

$$\left[b_2a_2 + 6a_3 - \omega_i^2\left(d_2c_2 + 156c_3\right)\right]\Phi_7 + \left[3La_3 - \omega_i^2\left(22Lc_3\right)\right]\Phi_9 = 0 \qquad (4\text{-}15)$$

$$\left[L^2a_2+\omega_i^2\left(3L^2c_2\right)\right]\Phi_6+\left[3La_3-\omega_i^2\left(22Lc_3\right)\right]\Phi_7+\left[2L^2a_2+2L^2a_3-\omega_i^2\left(4L^2c_2+4L^2c_3\right)\right]\Phi_9=0$$

Where $a=\dfrac{2EI}{L^3}$, $c=\dfrac{\rho A_r L}{420}$ and $d=\dfrac{\dfrac{\rho A_r L}{6}}{\dfrac{\rho AL}{420}}=70$.

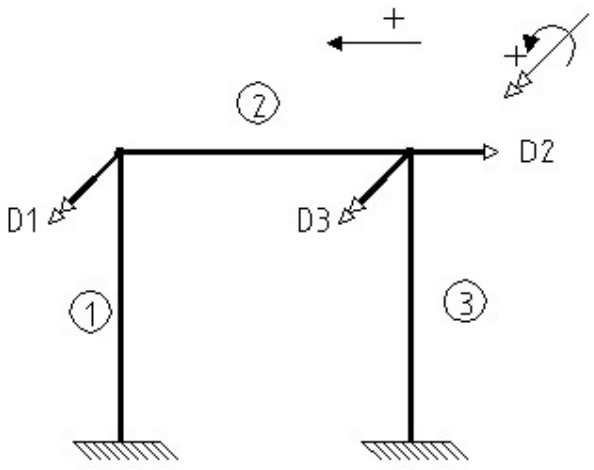

Figure 4-12. A 3-beam structure.

From Equation (4-14), the following relation can be obtained.

$$\frac{\Phi_6}{\Phi_9}=\frac{L^2a_2+\omega_i^2\left(3L^2c_2\right)}{-2L^2a_1-2L^2a_2+\omega_i^2\left(4L^2c_1+4L^2c_2\right)} \tag{4-16}$$

From Equation (4-15), the following equation can be obtained.

$$\frac{\Phi_7}{\Phi_9}=\frac{-3La_3+\omega_i^2\left(22Lc_3\right)}{b_2a_2+6a_3-\omega_i^2\left(d_2c_2+156c_3\right)} \tag{4-17}$$

From Equations (4-16) and (4-17), the *MSFs* of the system can be obtained as below.

If $\Phi_9=-1$ then:

i) For $\Phi_6 \rightarrow \oplus \quad \Phi_7 \rightarrow \oplus \quad \Phi_9 \leftarrow$ then from Equation (4-16),

$\omega_i^2 \langle \frac{2L^2a_1 + 2L^2a_2}{4L^2c_1 + 4L^2c_2} = \frac{a_1 + a_2}{2(c_1 + c_2)}$ and from Equation (4-17), $\omega_i^2 \langle \frac{3La_3}{22Lc_3}$

and $\omega_i^2 \langle \frac{b_2a_2 + 6a_3}{d_2c_2 + 156c_3}$.

It is important to be noted that parameters of the structure are all grater than zero or $a_1, a_2, a_3, c_1, c_2, c_3 \succ 0$. The results are illustrated in Figure 4-13.

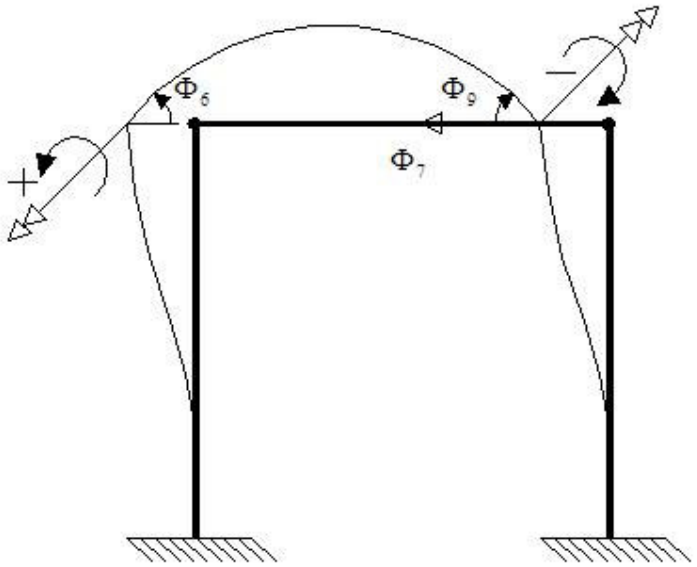

Figure 4-13. The first *MSF* for the first natural frequency.

Therefore the first *MSF* of the above system for the first natural frequency is as below. All the points of the structure follow the same direction (locally) of motion. This rule also can be expressed for each beam individually as below.

In the first MSF all the points of each beam, follow the same direction of motion.

In order to continue the procedure to find the second *MSF*, we need to know which one of $\frac{a_1 + a_2}{2(c_1 + c_2)}$, $\frac{3La_3}{22Lc_3}$ or $\frac{b_2a_2 + 6a_3}{d_2c_2 + 156c_3}$ is larger or smaller than the other ones. This gives the second region of frequency for the second mode shape. In this case the

objective is to obtain the *MSF* for the second region of ω_i^2, where ω_i^2 is greater than one of these three expressions ($\frac{a_1+a_2}{2(c_1+c_2)}$, $\frac{3La_3}{22Lc_3}$ and $\frac{b_2a_2+6a_3}{d_2c_2+156c_3}$) and smaller than the other two. These regions of ω_i^2 is similar to the *3DOF* mass-spring problem where we separated each frequency region.

For example assume $\frac{a_1+a_2}{2(c_1+c_2)} \rangle \frac{3La_3}{22Lc_3}$ and $\frac{b_2a_2+6a_3}{d_2c_2+156c_3}$, in this case the second *MSF* can be obtained as below.

ii) For $\Phi_6 \rightarrow \oplus \quad \Phi_7 \leftarrow \quad \Phi_9 \rightarrow \oplus$ then from Equation (4-16)

$\omega_i^2 \rangle \frac{a_1+a_2}{2(c_1+c_2)}$ and from Equation (4-19), $\omega_i^2 \langle \frac{3La_3}{22Lc_3}$ and

$\omega_i^2 \langle \frac{b_2a_2+6a_3}{d_2c_2+156c_3}$.

The results are illustrated in Figure 4-14. This is the second *MSF* of this system. In this *MSF* we have:

a) The elements of a beam follow the same direction of motion. For example beams 1 and 3 in Figure 4-14.

Or

b) The displacement of the points of a part of the beam is in the same direction of motion and the displacement of the other part of the body is in the opposite direction of motion. For example, beam 2 in Figure 4-14.

The conclusion of this section is as below. In the first *MSF* all points of each beam follow the same direction of motion. This *MSF* for each beam is the same *MSF* for one-dimensional elastic bodies the explained in section 4.3.

The second natural frequency of a structure depends on the relative value of the parameters (such as *E*, *I*, A_r, *L* and ρ) of the beams in the structure. In this example parameters are $\frac{a_1+a_2}{2(c_1+c_2)}$, $\frac{3La_3}{22Lc_3}$ and $\frac{b_2a_2+6a_3}{d_2c_2+156c_3}$. In the above example by knowing which one of the parameters are larger or smaller than the other, then the second *MSF* can be obtained. Sometimes these relative values can be found by looking

at the structure and observing it. For example the cross section area of a beam 1 (A_{r1}) is larger than the cross section area of a beam 2 (A_{r2}). This relative value can be found by looking at the structure. In the second *MSF*, displacement of the particles of each beam is either in the same direction of motion (beam 1 and 3 in this example), or is in two opposite direction of motion (beam 2).

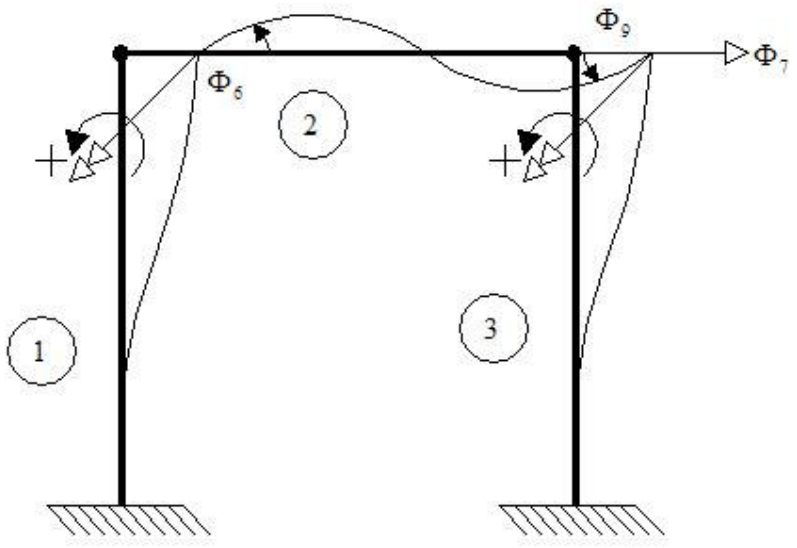

Figure 4-14. The second *MSF* of the structure.

4.7. Conclusion

A general rule is introduced in guessing the *MSFs* of mechanical systems as below.

The rule for *the* n^{th} *MSF* of a mechanical system is, ***there are n-1 places on the MSF where the directions of motion of the masses or the direction of deflections on an elastic body change.***

The mass-spring system rule in this thesis is not used in the following chapters in practical and experimental examples. However as we see it helps for better understanding of the mode shape rules for continuous systems. This is because each continuous system can be modelled as a discrete (mass-spring) system and therefore the

rules of mass-spring systems help in obtaining and understanding the rules for continuous systems.

As discussed above there are additional rules for each particular system. These rules are summarized below.

- Additional rule for 2 dimensional mass-spring with equal mass and stiffness distribution:

A mass with less number of spring connections has the opposite direction of motion relative to other masses in the lower natural frequency (Figure 4-15).

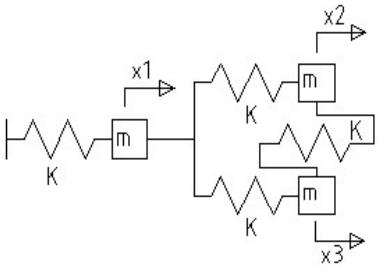

The Second *MSF*

$X_1 = 0 \quad X_2 \leftarrow \; X_3 \rightarrow \oplus$

The Third *MSF*

$X_1 \rightarrow \oplus \quad X_2 \leftarrow \; X_3 \leftarrow$

Figure 4-15. Two dimensional three *DOF* mass-spring system

- Additional rule for Elastic bodies:

Typical boundary conditions rules that is used for the mode shapes of elastic bodies can be used here for *MSFs.*

- Additional rule for structures:

For n^{th} *MSF* of 2 dimensional structures, there are maximum n-1 places for each beam where the direction of motion of the particles on the beam changes (Figure 4-16).

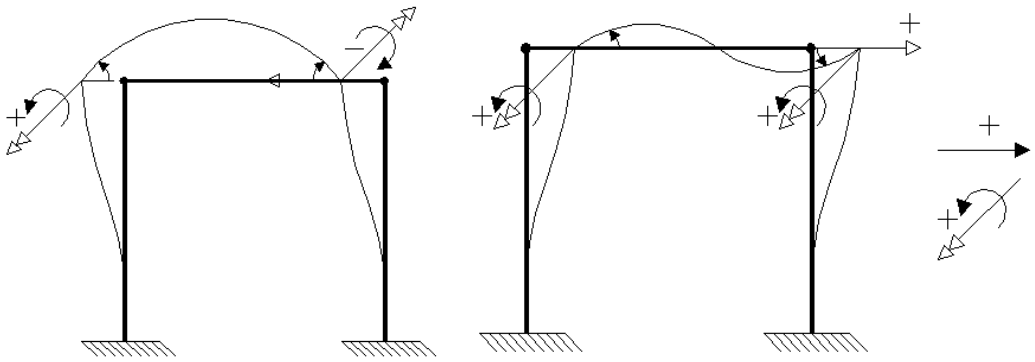

Figure 4-16. *MSFs* for 2 dimensional structures.

- Additional rule for 2D mass-spring systems and 2D bodies:

Sometimes it is not possible to have *n*-1 places where the direction of masses changes because of configuration of the system. In this case *n*-2 or *n* number is exhibited (Figure 4-17)

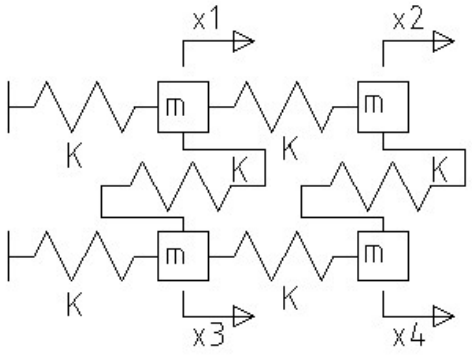

The Forth *MSF*

$X_1 \leftarrow \quad X_2 \rightarrow \oplus$

$X_3 \rightarrow \oplus \quad X_4 \leftarrow$

Figure 4-17. Two dimensional four degree of freedom mass-spring system.

Note:

The *MSF* rules may not be true for any situation. In this case the rule is still used. In this respect the *MSF* can be corrected by the method that will be discussed in Chapter 5.

Chapter 5

Modal Analysis Method Based on Fuzzy Sets

In this section, the proposed method for describing modal shapes of a general vibrating system by using fuzzy linguistics will be described. The details of the method will appear under different headings. The method attempts to identify the mode shapes of a general structure subjected to excitations. The main premise of the method is the assumptions that a number of modes, especially those at lower frequencies, could be guessed (in that respect the method resembles, early energy methods). The rational of such proposition lies in the fact that these initial guessed shapes can be updated by observations. The advantage of the method over the standard modal analysis is that it provides a "head start" in constructing the mode geometry and also provides a method which deals with limited sampling points and uncertainty, inherently present in experimental data.

The main steps of the method are as follows:

- Guessing the mode shapes of the system based on engineer experience, common sense and the mode shape rules in chapter 4 and constructing the guessed mode shapes using fuzzy membership functions.
- Modification of the fuzzy mode shapes using experimental modal analysis

- Obtaining the mode shape curves from updated fuzzy mode shapes using fuzzy neural network.
- Obtaining the error and creating a mode shape where, a) the guess mode shape is wrong, and where b) there is no guess available.

5.1. Constructing the mode shape forms using fuzzy membership functions

The guessed mode shape is called *MSF* (Mode Shape Form). Guessing the mode shapes was presented in chapter 4. These mode shapes are approximate mode shapes. Corresponding *MSFs* can be constructed using fuzzy linguistic terms such as Large, Medium and zero. The construction of *MSFs* based on fuzzy systems is introduced below.

Fuzzy inputs are divided to geometry and a frequency inputs. Geometry inputs are used to define the geometry of the system. One membership function is introduced for each section of the system where a deflection has to be referred to it. In another word if n membership functions are defined for a one-dimensional elastic body then the body deflections can be introduced by n number of deflection along the length of the body. In some cases other inputs may be introduced. For example, if a structure consists of several beams, then an input is introduced to identify each beam in the structure. Then the geometry input describes the geometry of each beam. Frequency inputs identify the natural frequency of the system. The natural frequencies are determined experimentally from *FRF* signals.

A sample of position membership functions is presented in Figure 5-1. In this figure each membership function belongs to a position on the body. For example the membership function between 0 and 0.05 (the first triangle) belongs to the 0 and 0.05 length of the body or the first mass in a mass-spring system. For two and three-dimensional bodies two and three position membership functions are presented respectively. In this membership function the lengths of the bodies are normalized to one.

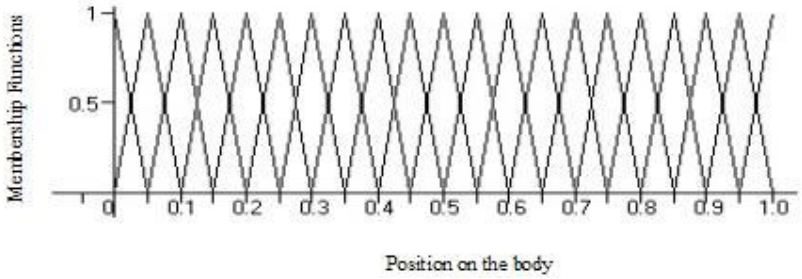

Figure 5-1. Geometry input fuzzy membership function.

The other input is natural frequencies. The magnitudes of the natural frequencies are obtained by experimental modal analysis. The sample of natural frequency membership functions is presented in Figure 5-2. In this figure the natural frequencies of interest are up to 4th natural frequency. The frequency magnitudes can be normalized to one as in this figure.

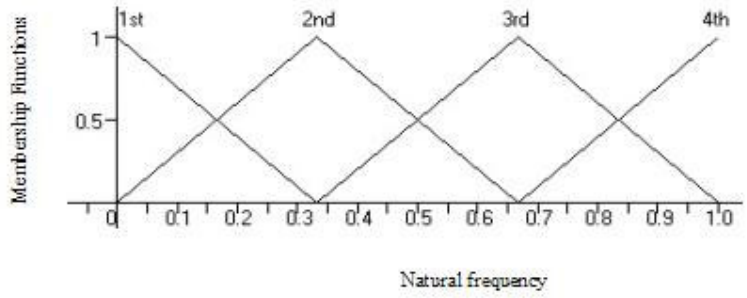

Figure 5-2. Natural frequency membership functions.

Fuzzy output membership function includes deflection of an elastic body or displacement of masses. A sample of output membership function is presented in Figure 5-3. In this figure, deflections of an elastic body or displacement of masses are presented by fuzzy linguistic terms. These terms include *NL, NM, Z, PM, PL*. In this respect, *Z* is Zero, *PM* is Positive Medium, *PL* is Positive Large, *NM* is Negative Medium and *NL* is Negative Large.

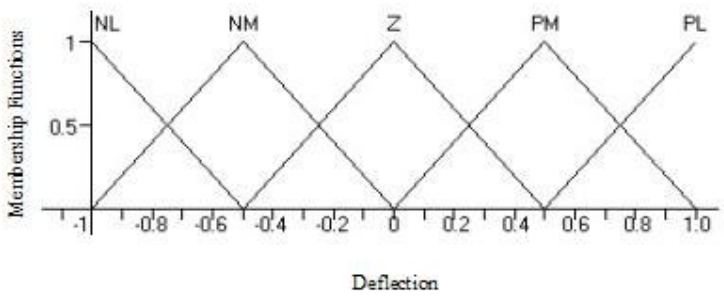

Figure 5-3. Output membership functions.

Fuzzy rules introduce the relation between inputs and the output. For each natural frequency the fuzzy rules describe the deflection of the mechanical system for the geometry of the system. For instance, assume that the second *MSF* of a clamped-clamped beam is guessed as in Figure 5-4. This *MSF* can be guessed based on the rules in chapter 4 or can be guessed by engineering experience.

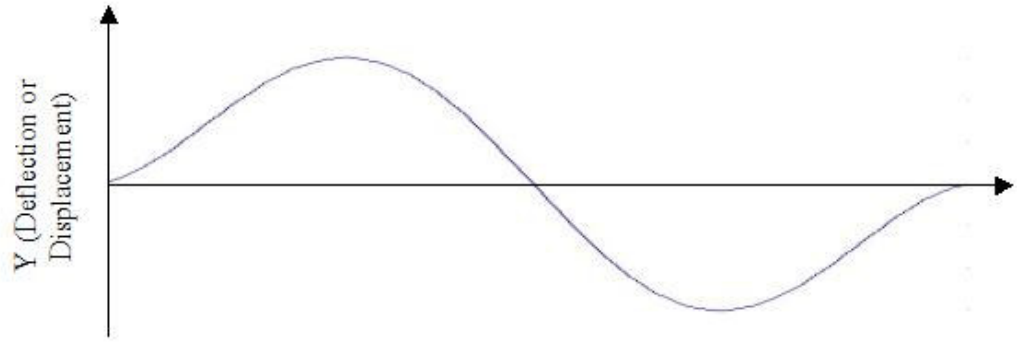

Figure 5-4. A *MSF* of a clamped-clamped beam.

Then fuzzy rules have to be introduced to construct this *MSF*. The rules are introduced as below. The first input (X) is the position, the second input (F) is the natural frequency and the output (Y) is the deflection.

Rule 1: If X=X1 and F=2, then Y=Zero *(Z)*.

Rule 2: If X=X2 and F=2, then Y=Positive Medium (*PM)*.

Rule 3: If X=X3 and F=2, then Y=Positive Large (*PL)*.

Rule 4: If X=X4 and F=2, then Y=Positive Medium (*PM)*.

Rule 5: If X=X5 and F=2, then Y=Zero (*Z)*.

Rule 6: If X=X6 and F=2, then Y=Negative Medium (*NM)*.

Rule 7: If X=X7 and F=2, then Y=Negative Large (*NL)*.

Rule 8: If X=X8 and F=2, then Y=Negative Medium (*NM)*.

Rule 9: If X=X9 and F=2, then Y=Zero (*Z)*.

Figure 5-5 illustrates the fuzzy rules.

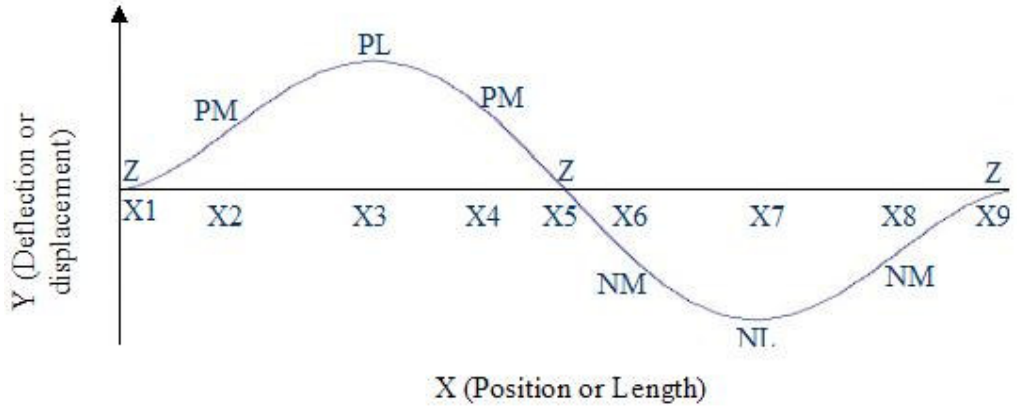

Figure 5-5. Fuzzy rules to define a *MSF*.

In this figure *Z* is Zero, *PM* is Positive Medium, *PL* is Positive Large, *NM* is Negative Medium and *NL* is Negative Large. Negative or positive appear if the deflection is less than or more than zero respectively.

Introducing the deflection magnitudes by fuzzy linguistic terms is arbitrary. In this respect, any fuzzy term that demonstrates an approximate mode shape can be used. For example, other terms can be added to generate the *MSF* in Figure 5-5 such as *NS* and *PS* (negative small and positive small). In this case, these terms can introduce more information about the deflection between Medium (*M*) and zero (*Z*) magnitudes. Some of the membership functions can be deleted too. For example Medium (*NM* and *PM*) term can be cancelled in the output. The only difference that happens by introducing more or less membership functions is, to have more or less information about deflections. The most important membership functions are the *PL* and *NL* membership functions, which obtain the maximum and minimums of the mode shapes. It is necessary to have *PL* and *NL* membership functions. Also, the membership functions that represent the boundaries of the system are necessary. For example, in Figure 5-5, it is necessary to have two *Z* for the boundaries and *PL* and *NL* to illustrate the outline of the mode shape. The mode shape with only necessary deflection terms is illustrated in Figure 5-6.

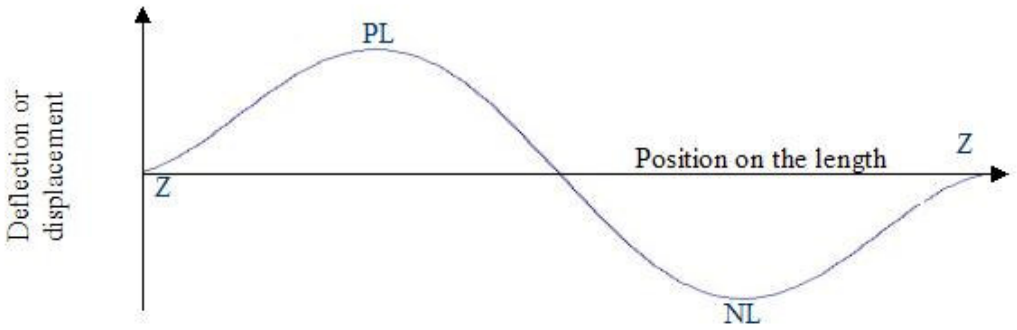

Figure 5-6. Necessary fuzzy deflections.

The membership functions presented above and the complete rules for the whole input and output, creates the Mode Shape Forms (*MSFs*) that are presented in Figure 5-7.

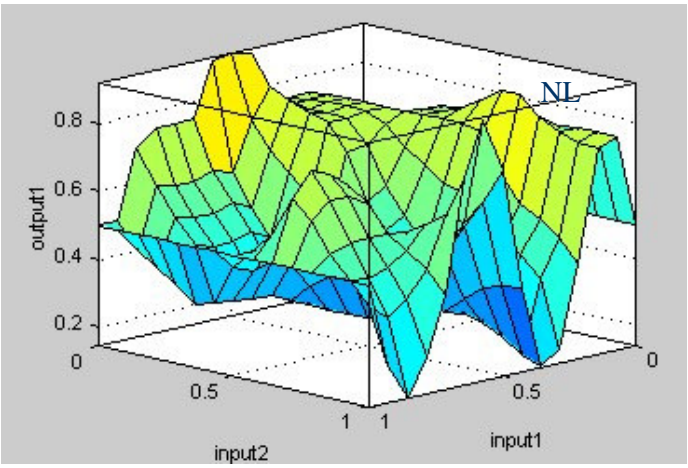

Figure 5-7. A sample of *MSFs* from the sample fuzzy membership functions and the corresponding rules.

From Figure 5-7 the *MSFs* can be extracted by selecting the desired natural frequency from input 2 for all the point from input one (position). For example, the second *MSF* of the above example is presented in Figure 5-8.

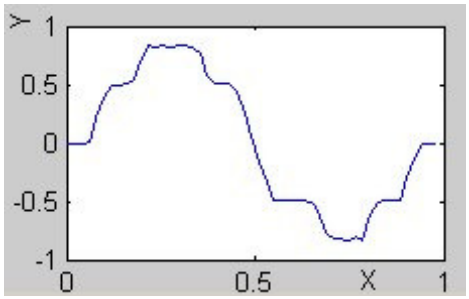

Figure 5-8. Fuzzy second *MSF*, obtained form fuzzy output membership functions.

The fuzzy *MSF* depends on the number of the membership functions and the type of function that is used for membership. The fuzzy *MSF* in Figure 5-8 is the second *MSF* of a clamped-clamped beam. This *MSF* is obtained using various position membership functions. The result of these fuzzy *MSFs* is presented to be compared with the fuzzy *MSF* in Figure 5-8. The results are illustrated in Figure 5-9.

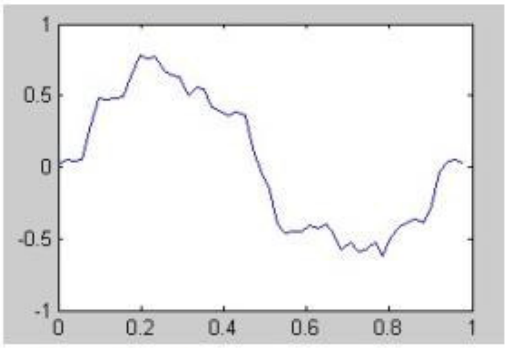

a) 20 membership functions with Gaussian function.

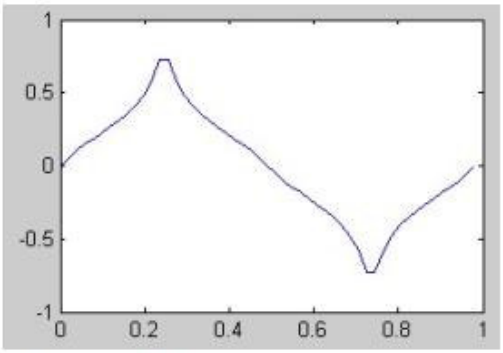

b) 5 membership functions with triangle function.

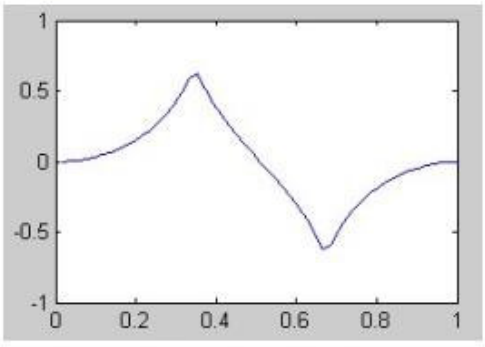

c) 4 membership functions with triangle function.

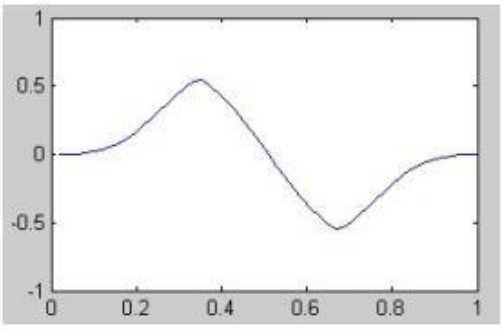

d) 4 membership functions with Gaussian function.

Figure 5-9. Constructing a fuzzy *MSF* using various position membership functions. The vertical axis is the deflection and the horizontal axis is position on the beam.

The number of position membership functions of the fuzzy *MSF* in Figure 5-8 is 21 membership functions and triangle membership functions are used in this example.

The fuzzy *MSFs* obtained in this section have to be updated. This is because *MSF* represent an initial guess and need to be related to experimental results and updated accordingly. Experimental modal analysis is used to update these *MSFs* that is explained in the next section.

5.2. Updating the fuzzy mode shape forms using experimental modal analysis

The objective of updating, is to find an interpolated curve between the measured data, which is described only by few points, and fuzzy representation of the mode shape, which is described by a large number of points. This updates the initial "guess" fuzzy mode profile or fuzzy *MSFs*.

Experimental modal analysis is employed to model the system. The procedure of the modal analysis for a multi degree of freedom modelling requires the use of instrumented hammer, accelerometer, data acquisition card, and modal analysis software. The outcome of modal analysis is a discrete model. In this practice the degree of freedom of the model depends on the number of points at which vibration is measured. The experimental procedure is explained for a beam as an example (Figure 5-10). For example, in order to find a four-degree of freedom model of the beam, the beam is divided to 5 equal segments (Figure 5-10). An accelerometer is attached to the beam to receive the oscillation signals. An instrumented hammer is used to excite the beam. The accelerometer is placed in each of four selected positions. The instrumented hammer is used to excite the beam at each of the four selected points. Fast Fourier transforms of hammer excitation and accelerometer signals are obtained. *FRF* values are obtained by dividing the accelerometer signals by the corresponding signals from the hammer.

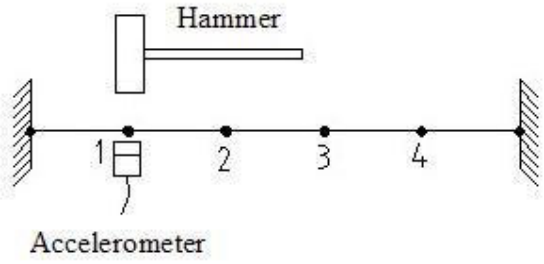

Figure 5-10. Experimental modal analysis using an instrumented hammer.

An example of an element of a *FRF* matrix is illustrated in Figure 5-11. In this figure there are 6 peaks regarding 6 different natural frequencies. In this figure $|h|_i$ $i = 1,\ldots,6$, is the *FRF* magnitude corresponding to each natural frequency. $|h|$ is the peak value on the vertical axis. In this example, $|h_{11}|$ shows that the hammer excitation at position 1 and the accelerometer is located at position 1.

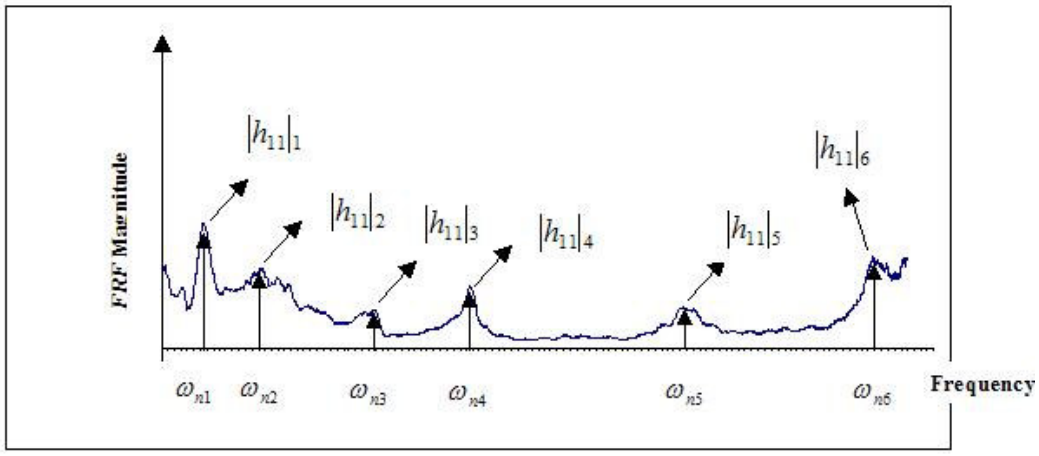

Figure 5-11. An element of a *FRF* matrix.

Peak-picking method is used to extract the mode shapes from *FRF* results. Second mode shape of a four-degree of freedom clamped-clamped beam is obtained here to explain the procedure of extracting the mode shapes from *FRFs*. To determine this mode shape, $|h_{11}|_2$, $|h_{12}|_2$, $|h_{13}|_2$ and $|h_{14}|_2$ are obtained from 4 different *FRF* curves. In another word corresponding $|h|$ value for $\omega_n = \omega_{n2}$ is obtained from 4 different *FRF* curves (each *FRF* curve is an element of *FRF* matrix). Eigenvectors can be

obtained using the following relation. The following equation is valid for $\omega_n = \omega_{nk}$ and from Chapter 3, Equations (3-25).

$$u_{ik}u_{lk} = |h_{il}|_k \zeta_k \omega_{nk}^2$$

Where $\omega_n = \omega_{nk}$ is the natural frequency, u is the deflection and ζ_k can be obtained as below.

$$\zeta_k = \frac{\left(\omega_a^2 - \omega_b^2\right)}{\omega_{nk}^2} \approx \frac{\Delta\omega}{\omega_{nk}}$$

Figure 5-12 illustrates the method that is used to extract the modal parameters (u and ζ_k) from *FRF* peaks.

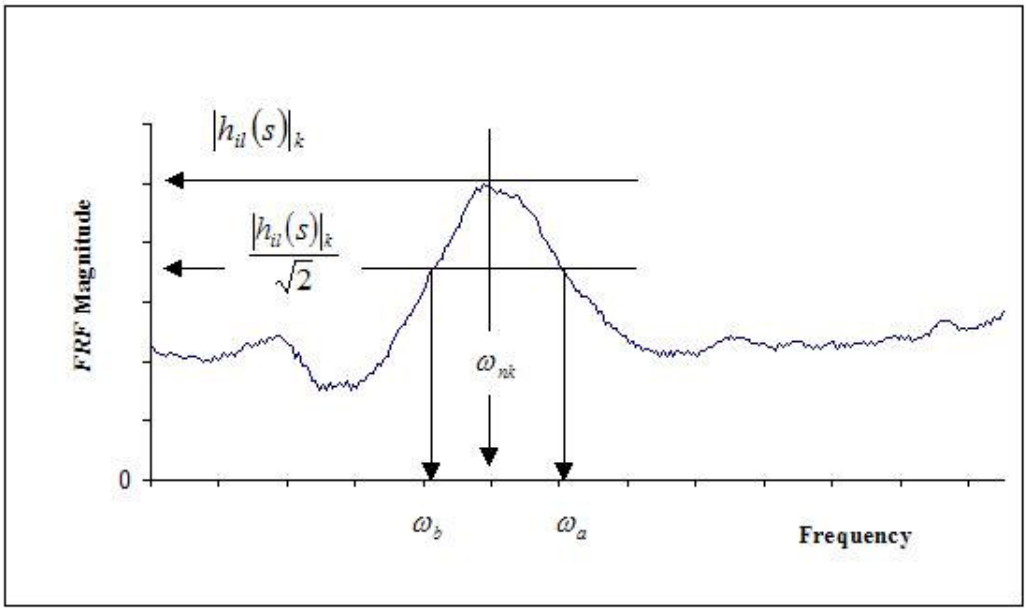

Figure 5-12. Extracting modal parameters from *FRF* peaks.

Figure 5-13 illustrates the method of extracting the modal parameters from the first peak of the *FRF* curve in Figure 5-11.

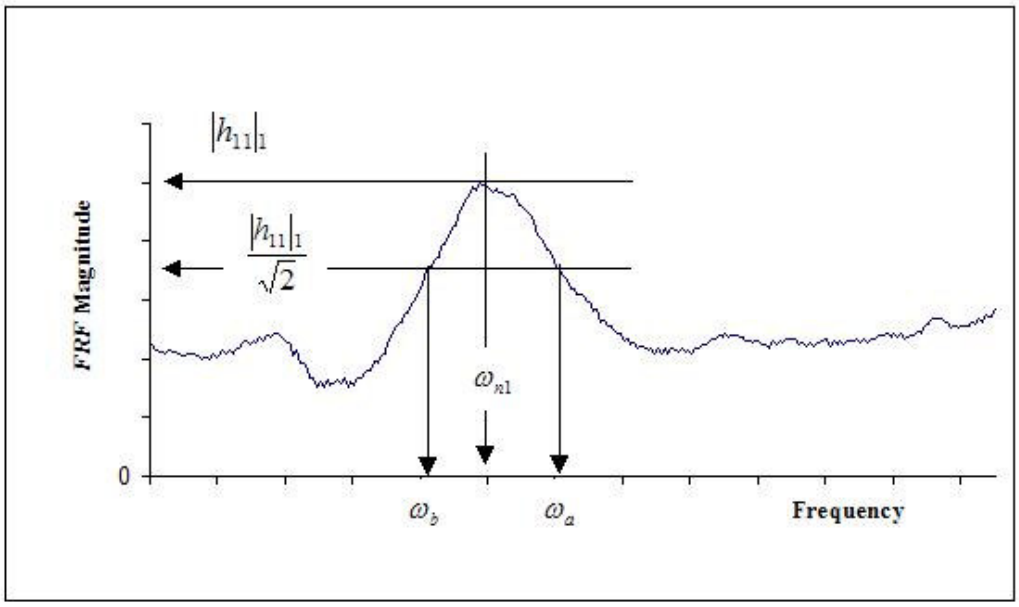

Figure 5-13. Extracting the modal parameters from *FRF* peak for k=1 and h_{11}.

The parameters from Figure 5-13 can be substituted in the above equation as below.

$$u_{11}u_{11} = |h_{11}|_1 \zeta_1 \omega_{n1}^2$$

Where

$$\zeta_1 = \frac{\left(\omega_a^2 - \omega_b^2\right)}{\omega_{n1}^2} \approx \frac{\Delta\omega}{\omega_{n1}}$$

By selecting the other peaks of the *FRF* result in Figure 5-11, u_{11}, u_{12}, u_{13} and u_{14} can be obtained. By changing the location of the accelerometer and the hammer excitation to other possible positions, remaining of the modal parameters can be extracted. This mode shape consists of 4 elements. The corresponding eigenvector of this mode shape is as below.

$$\begin{Bmatrix} u_{1k} \\ u_{2k} \\ u_{3k} \\ u_{4k} \end{Bmatrix} = \begin{Bmatrix} u_1 \\ u_2 \\ u_3 \\ u_4 \end{Bmatrix}_k$$

In this relation, k is the mode number. In this example k=2 that indicates the second natural frequency (ω_{n2}). u_1, u_2, u_3 and u_4 are the deflection of the corresponding points on the beam (Figure 5-10). This mode shape is illustrated in Figure 5-14. Other points of the mode shape are derived by linear interpolation of those four pints (Figure 5-14).

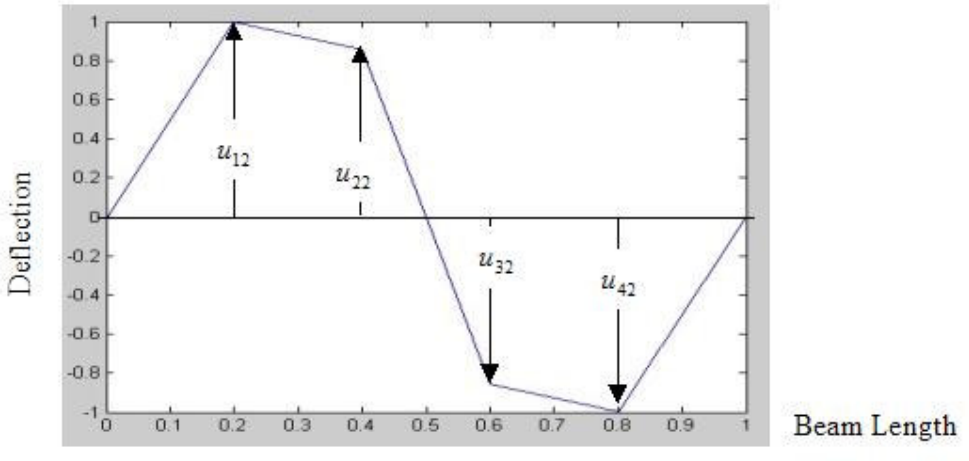

Figure 5-14. A mode shape example of a four-degree of freedom clamped-clamped beam.

Four points in the fuzzy data set are simply replaced by the corresponding four points from the experimental set. In this example the deflection in the fuzzy *MSF* are simply replaced by the corresponding u_1, u_2, u_3 and u_4 values. By doing this, a "spiked" version of the fuzzy curve (fuzzy *MSF*) is created. The spike points are the experimental data points (in this example four points). Figure 5-15 is an example of a spiked version of the curve in Figure 5-8.

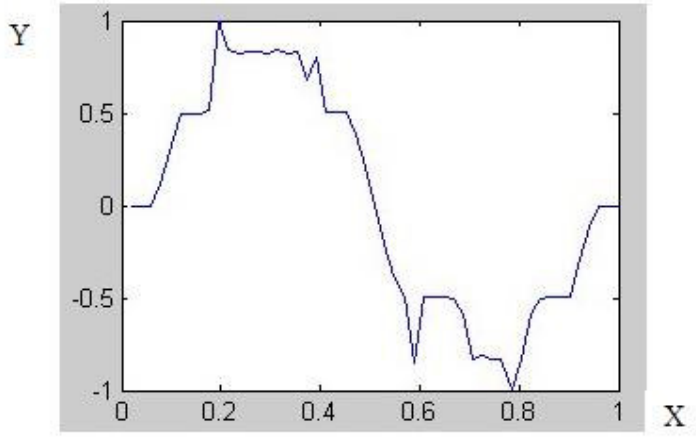

Figure 5-15. Spiked version of the fuzzy *MSF*.

Both the fuzzy *MSF* and the spiked version are illustrated in Figure 5-16. This figure shows the spikes clearly.

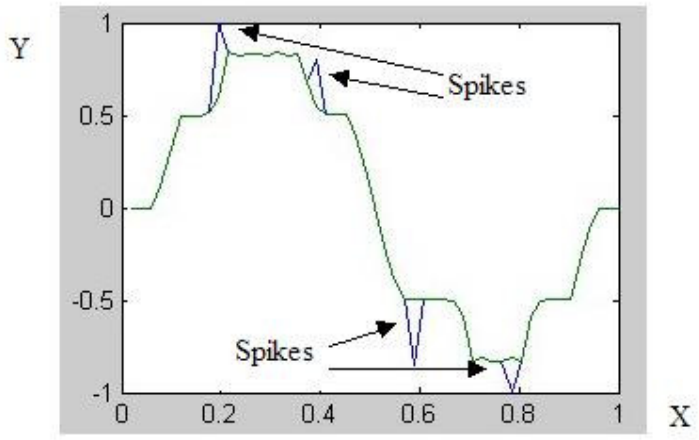

Figure 5-16. The fuzzy *MSF* and the spiked version.

The mode shapes obtained from the fuzzy model might not be the same scale as the experimental model. The mode shapes curve from fuzzy model can be matched to the experimental mode shapes with an appropriate scaling. This is valid because the mode shapes can be multiplied to any arbitrary scaling factor.

The second stage of modification involves using a fuzzy neural network to "smooth" the spiked curve using neural networks.

5.3. Obtaining the mode shapes using neural networks

A fuzzy neural network used here. This network is a single-input-single-output fuzzy neural network. The input training data of the neural network is position on the body (for example the data on the *X* axis in Figure 5-15). The output training data of the neural network is the deflection of the body (for example the data on the *Y* axis in Figure 5-15). Therefore the input of the system is the position on the beam and the deflection of the body (Figure 5-15) is the output or the target of the network. This deflection is the deflections in the updated fuzzy *MSF* (for example the deflection values on the *Y* axis in Figure 5-15). Constructing the *MSFs* using fuzzy sets is

introduced in section 5.1 and the updating procedure in section 5.2. For each *MSF*, one neural network is introduced for each natural frequency (Figure 5-17).

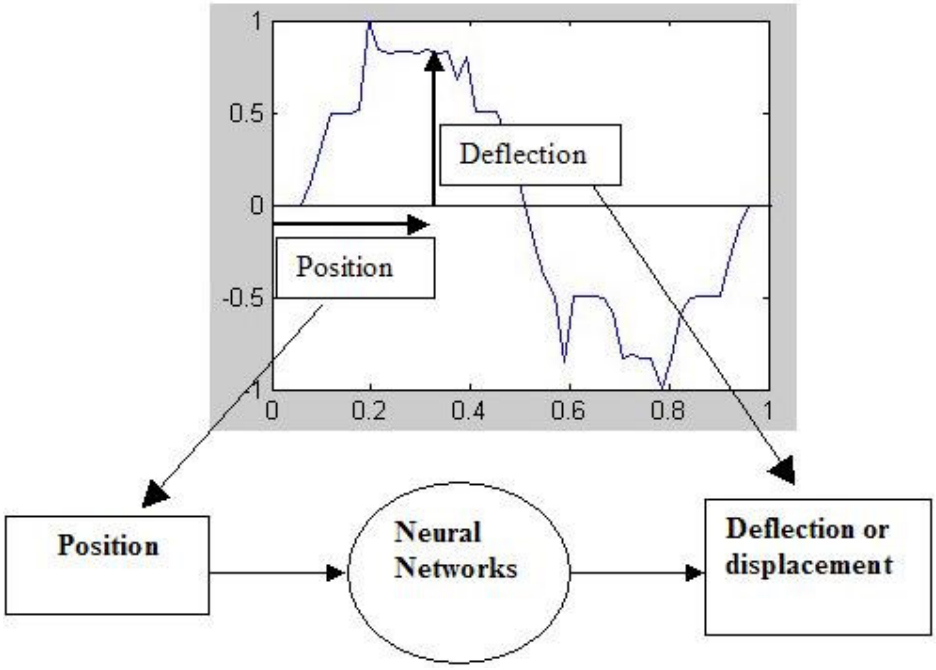

Figure 5-17. Input and output of the neural network

As mentioned in section 5.2, updating the fuzzy *MSF* using experimental data create spikes in the *MSF*. The mode shape from the trained neural networks is different from the updated fuzzy *MSFs*. The neural network is trained by updated fuzzy *MSFs*. The trained neural network gives smooth version of updated fuzzy *MSFs*. In this stage, running the trained neural network generates the final mode shapes. This is illustrated in Figure 5-18 where the position is the input of the network and the deflection is the output. The mode shape is obtained by giving the whole geometry or position of the structure as the input of the network. The corresponding deflection at each position gives the mode shape. There is one neural network for each natural frequency. Therefore each neural network provides only one mode shape for each natural frequency and there are *m* number of neural networks for *m* mode shapes and natural frequencies.

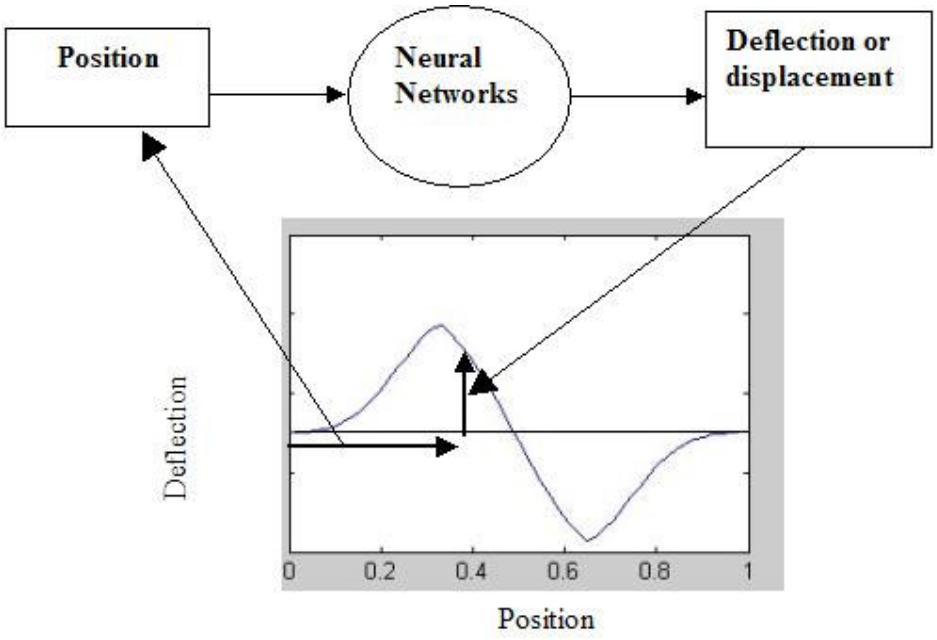

Figure 5-18. Obtaining the mode shape deflections from the neural network.

Figure 5-19 illustrate the application of the method in obtaining the behaviour of the system. The equation in Figure 5-19 is the equation of motion of a mechanical system. In this equation the natural frequency (ω_n) is obtained from a single experimental *FRF* test. Factors c, and constants ψ can be obtained from velocity and displacement initial conditions when the model is to be used in time domain.

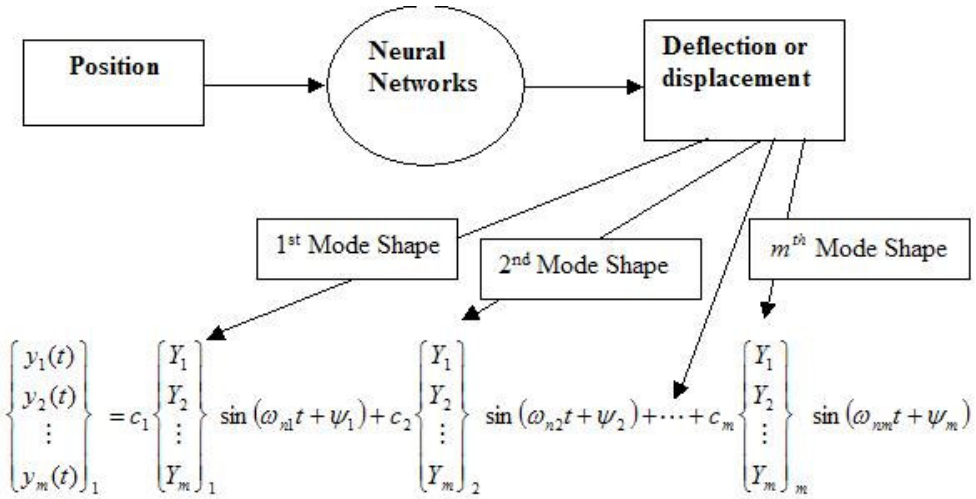

Figure 5-19. Obtaining the response of the system from neural network.

The eigenvectors of the equation of motion in Figure 5-19 are derived from the proposed method in this chapter. The eigenvectors or the mode shapes are derived from the output of the neural network. An example of the output of the neural network is illustrated in Figure 5-20.

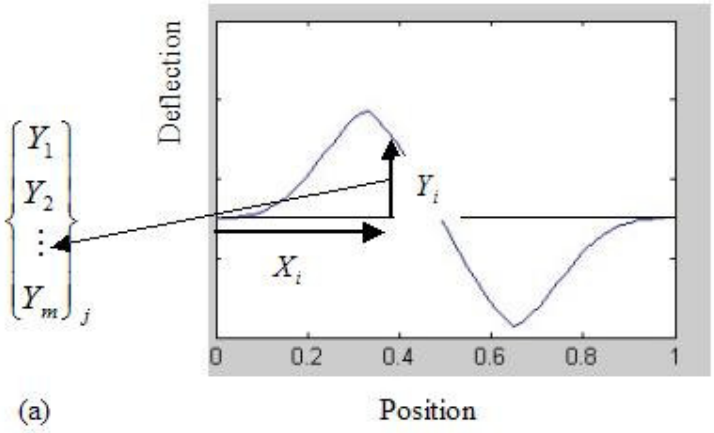

Figure 5-20. Obtaining the j^{th} eigenvector from the j^{th} mode shapes. a) Y_i is one of the elements of the matrix.

The eigenvectors are obtained for each natural frequency. In this stage, the procedure is completed.

The following section discusses the treatment of error in this method.

5.4. Obtaining the error, creating a mode shape where the guess is wrong and/or where there is no guess available for the mode shape

This section includes two parts. The first part introduces the method of calculating the error. To calculate this error, no new experimental data is needed.

The second part proposes a method of obtaining a mode shape where a) The *MSF* is guessed wrongly and the guess for the mode shape belongs to another natural frequency (but in this case the correct *MSF* is also guessed as an alternative and is available among *MSF* guesses and can be found), and where b) The *MSF* is not available the alternative guessed *MSFs* (if there is any) for a particular natural

frequency are wrong. If the available *MSFs* and the alternatives are wrong then an available *MSF* with the minimum error relative to the corresponding experimental model is selected. Then the fuzzy rules that used in constructing of this *MSF* are updated to determine a new *MSF* with less error. This procedure is repeated until the error is acceptable. The following section describes these two parts (a and b).

5.4.1. Obtaining the error

The error of the mode shapes in this method can be calculated relative to the experimental model. The following equation can be used in calculation of the error.

$$e = \sum_{i=1}^{m} \frac{\left|\left(Y_i - Z_i\right)\right|}{\left|Z_i\right|}$$

Where Z_i is the experimental data, Y_i is the data from the proposed mode shape and m is the number of points in the proposed model. If the number of points in the experimental data (for example u_1, u_2, u_3 and u_4 in Figure 5-14) is less than the points in the proposed model, then a linear interpolation of the experimental result is performed (Z_i for $i = 1, 2, \ldots, m$). Therefore any desired number of points can be selected from the linear interpolation of the experimental result. These points can be used for calculating the error between the proposed method and the experimental result. However, linear interpolation of the experimental data itself will have error.

5.4.2. Obtaining a mode shape where a wrong mode shape is guessed and where there is no guess available for the mode shape

Two methods are proposed in this section to deal with two problems, where a) the guess for the mode shape is wrong and where b) there is no guess available for the mode shape.

a) Treatment of error where the guess for the mode shape is wrong

The flowchart in Figure 5-21 describes the treatment of error where the guess for the mode shape is wrong. In this flowchart, first availability of a *MSF* is queried, and if it is available (the answer YES) then the normal method (as described above) is applied to obtain the mode shape (including construction of the mode shape by fuzzy mode shapes, *FRF* updating the mode shape and applying neural networks to update the mode shape). After obtaining the mode shapes, the error between this mode shape and the experimental mode shape is calculated. If the error is acceptable (query about error level) then the procedure ends. If the error is not acceptable then another *MSF* is selected and the procedure is repeated. This procedure is repeated until the "correct" *MSF* is found among available *MSFs*.

b) Creating the mode shape where there is no guess available for the mode shape

In this method a mode shape can be obtained when a heuristic guess is not available. In this case an available *MSF* from the other natural frequencies can be selected. The following flowchart demonstrates the procedure of the proposed method including correction of error in *MSFs*. The procedure in section (a), for the situation where the guess mode shape is wrong, is repeated. The difference between this section and section (a) is that, no *MSF* with acceptable error is found among available *MSFs*.

If none of the *MSFs* satisfy the acceptable error then the *MSF* with the minimum error is selected. Then the flowchart enters correction of fuzzy rules section of the flowchart. This section is an iterative closed loop section and continues until an acceptable rules combination is obtained. The procedure of correction of the fuzzy rules is explained below where the correction is applied to the mode shape to reduce the error.

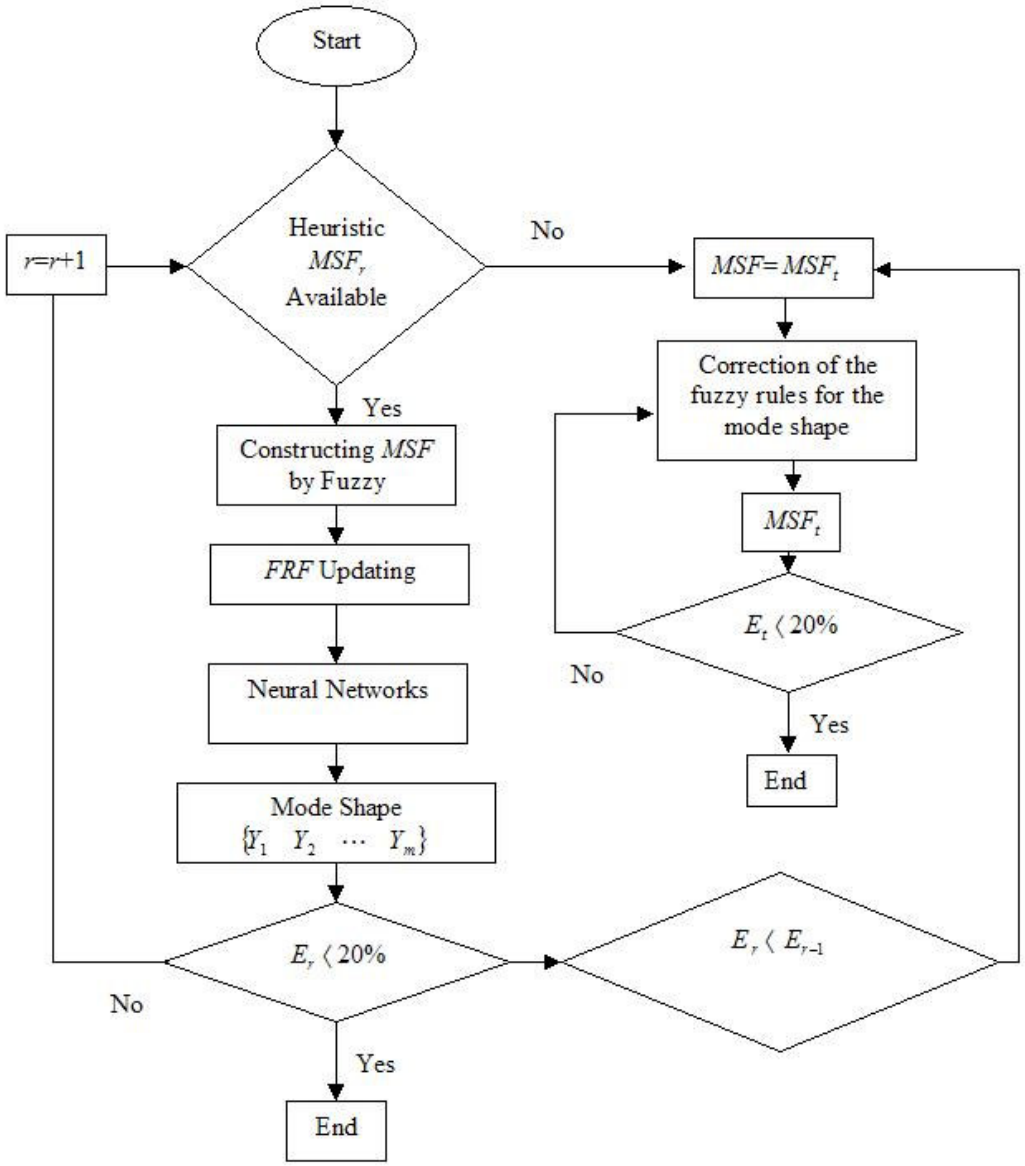

Figure 5-21. Treatment of error flowchart.

To demonstrate the corrective updating of fuzzy rules following example is given with three fuzzy rules. These rules are expressed as below.

Rule 1: If geometry input (input 1) is MF_{i-1} (Membership Function i-1) and $x_{i-1} \in MF_{i-1}$, Frequency input is F_j and the other input (if exist) is I_3 Then the output (Deflection) is y_{i-1}.

Rule 2: If geometry input (input 1) is MF_i (Membership Function i) and $x_i \in MF_i$, Frequency input is F_j and the other input (if exist) is I_3 Then the output (Deflection) is y_i.

Rule 3: If geometry input (input 1) is MF_{i+1} (Membership Function i) and $x_{i+1} \in MF_{i+1}$, Frequency input is F_j and the other input (if exist) is I_3 Then the output (Deflection) is y_{i+1}.

These rules are demonstrated in Figure 5-22 and the mode shape is constructed based on these three rules. Here, in order to carry out updating, the mode shape from experimental modal analysis results have to be interpolated in order to have consistent number of points as the fuzzy mode shape.

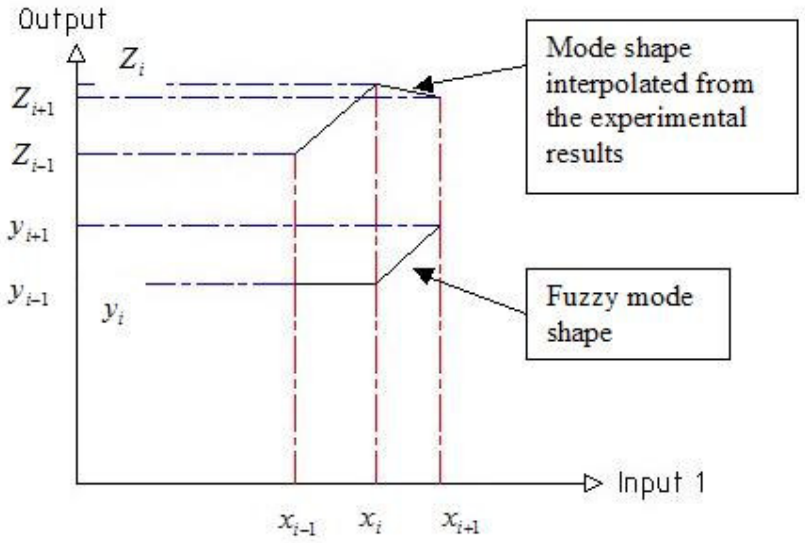

Figure 5-22. Fuzzy representation of a part of a mode shape and the corresponding experimental result.

Having done that, the fuzzy mode shape is ready to be updated using the method described in section 5.2. After updating the fuzzy mode shape with experimental results and using neural network to obtain the final version of the mode shape, then the curve presented in Figure 5-23 is determined. In this figure, $Y(1)$ is the first mode shape result before any correction. The error between the updated fuzzy mode shapes

and the experimental results are calculated according to the scheme shown in Figure 5-23. In this thesis, the vectors that are used to represent the difference between the points of experimental mode shapes and updated fuzzy mode shapes are called Error Vectors.

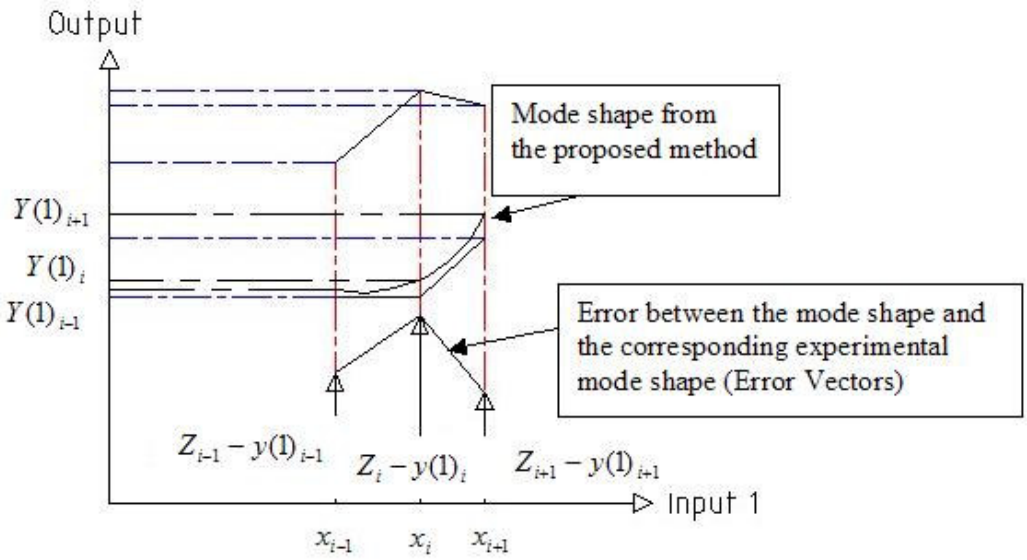

Figure 5-23. Mode shapes after modification and the error between the experimental result and the result from the proposed method (error vectors).

The error for each point is demonstrated in Figure 5-24.

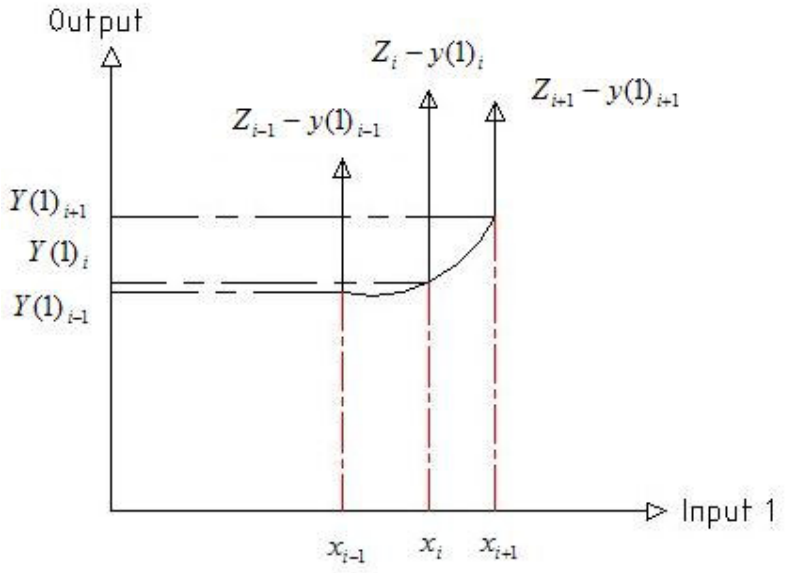

Figure 5-24. Error of each point.

At this stage the following scheme in Figure 5-25 is used to change (correct) the fuzzy rules for each point. For instance, from rule 1, if geometry input (input 1) is MF_{i-1} and Frequency input is F_j, then the output (Deflection) is y_{i-1}. Where y_{i-1} is a fuzzy linguistic term such as medium, large, etc. From Figure 5-24, the error can be calculated as below.

$$E_{i-1} = Z_{i-1} - Y(1)_{i-1}$$

In this case the rule will be changed to the following rule.

If geometry input (input 1) is MF_{i-1} and Frequency input is F_j, then the output (Deflection) is $y_{i-1} + E_{i-1}$.

An example of obtaining the relation between the error magnitudes and the fuzzy linguistic terms is demonstrated in Figure 5-25.

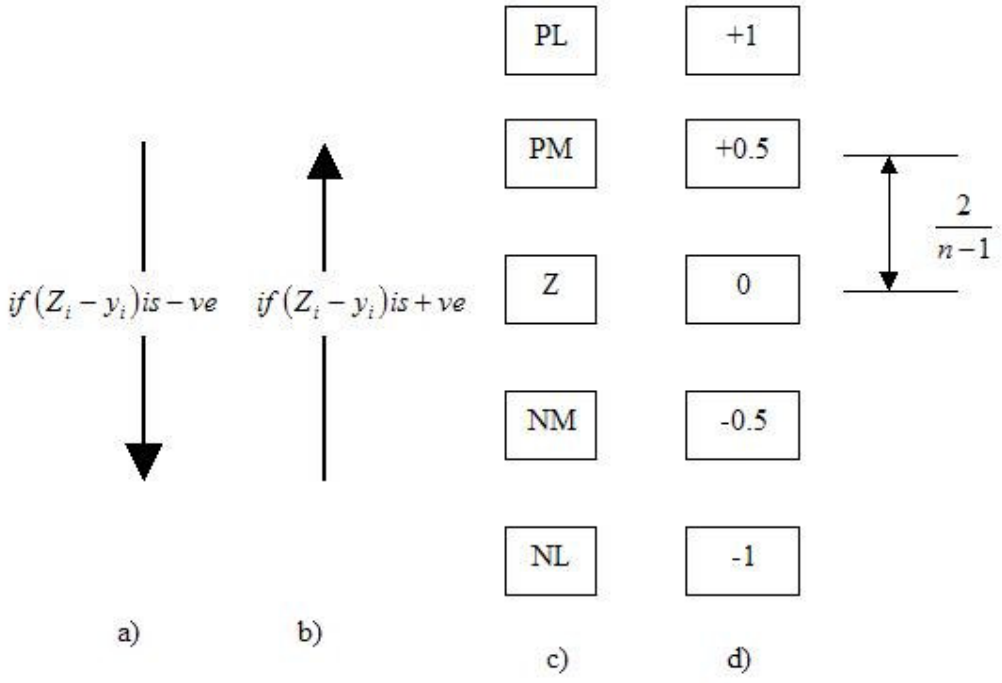

Figure 5-25. An example of relation between error magnitudes and the fuzzy linguistic terms.

The relation between the fuzzy linguistic terms in Figure 5-25(c) and the magnitudes in Figure 5-25(d) can be found from output membership functions. In this case, an example output membership function is presented in Figure 5-26. In this figure, magnitude is given to each fuzzy linguistic term.

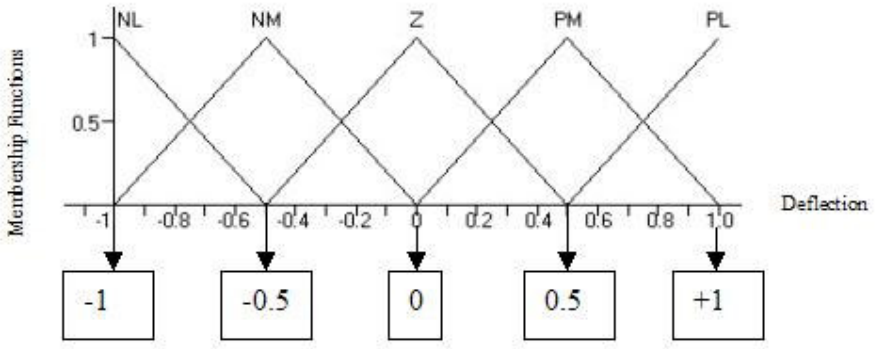

Figure 5-26. Output membership functions.

Assume the output consists of *n* membership functions (as in Figure 5-25 or Figure 5-26 consist of 5 membership functions including *NL, PM, Z, NM* and *NL*) then the magnitude between each fuzzy rule is equal to $\frac{2}{n-1}$ where 2 is the range of output membership functions that is between –1 to 1. Therefore if $\frac{2}{n-1}$ is the distance magnitude between each fuzzy rule then $\frac{E_{i-1}}{(2/n-1)} = \frac{Z_{i-1} - y(1)_{i-1}}{(2/n-1)}$ shows the number of fuzzy rules between the first fuzzy rule and fuzzy rule after correction.

For example if the error is $E_{i-1} = Z_{i-1} - y(1)_{i-1}$=0.4 and the output membership function consist of 5 membership functions (including *NL, PM, Z, NM* and *NL* from Figure 5-25) then $\frac{E_{i-1}}{(2/n-1)} = \frac{0.4}{\frac{2}{5-1}}$=0.8. Rounding up 0.8 to the nearest real number gives 1, which means the method suggests one step correction of fuzzy rules from the initial fuzzy rule (that was used to construct the *MSF*). For example if the first fuzzy rule is *NM* then one step rule changing gives *Z* or for example if the error magnitude was a negative number the rule would change from *NM* to *NL* (Figure 5-25). The error is calculated again for the mode shape with new fuzzy rules. If the error is acceptable then the procedure will end. If the error is not acceptable the procedure is repeated and new fuzzy rules will be created until the error is acceptable.

5.5. Conclusion

The procedure of the proposed method in this thesis is introduced in this chapter. In this method fuzzy sets are used to construct the *MSFs* (to obtain fuzzy *MSFs*), experimental modal analysis is used to update the fuzzy *MSFs* and neural network is used to obtain the final version of the mode shapes. Two methods are also introduced to reduce the error in the mode shapes. The methods are extended to deal with situations where, a) wrong *MSF* is guessed for the corresponding mode shape and natural frequency, and b) There is no *MSF* available for a corresponding natural frequency.

Chapter 6

Experimental Setup

This chapter presents the experimental set up for experimental modal analysis, fuzzy reasoning and neural networks. In modal analysis procedure, instrumented hammer, accelerometer, data acquisition card, PC and *FRF* analysis software are used. In fuzzy and neural networks procedures, MATLAB software [28] with fuzzy, neural network and SIMULINK toolboxes is used.

6.1. Modal analysis

In modal analysis procedure, an instrumented hammer, accelerometers, a charge amplifier, a data acquisition card, a PC and modal analysis software are used. The hammer applies impact forces to the bodies. By applying an impact force to a body, the hammer piezoelectric generates a corresponding voltage. The voltage is calibrated to force. An accelerometer consists of a frame, a mass and a piezoelectric element. Vibrating the mass in the accelerometer generates electrical current in the piezoelectric element. The corresponding voltage of the piezoelectric element is calibrated to acceleration, velocity and displacement. The signals from accelerometers and the impact hammer are translated to a charge amplifier. The charge amplifier is connected to a data acquisition card and a PC. A Frequency

Response Function (*FRF*) analyser is installed on the PC that can be used for modal analysis.

Modal analysis theory is presented in Chapter 3. The experimental procedure used in the proposed method is explained here. The first step in each experiment is calibration. Calibration for experimental modal analysis is presented below.

6.1.1. Calibration

Before measurement, the instruments have to be calibrated. Calibration provides a physical sense of the measured parameters. *FRF* is used to obtain the mode shapes. In this project, a suspended mass is used to calibrate *FRF* signals. The experimental equipment includes a mass with a known magnitude, instrumented hammer and a *FRF* analyser (here, PCI230 card, charge amplifier and Agilent VEE software [29]). The PCI230 card features are, 2-channel, 12 bit digital to analogue conversion with output voltage ranges of 0 to +10. A 28982ENDEVCO instrumented hammer (Figure 6-1) is used here.

Figure 6-1. The instrumented hammer.

An accelerometer (here model AQ40 accelerometer with frequency range of 0.5-8000HZ, supplier Environmental Equipments LTD) is attached to the mass.

Figure 6-2 illustrates the calibration setup with the suspended mass.

The accelerometer and the hammer are connected to a charge amplifier (Figure 6-3). The charge amplifier is a DJB amplifier. The charge amplifier is connected to a data

acquisition card that is assembled in a PC. An *FRF* analyser software is installed on the PC (here AgilentVEE version 5.01).

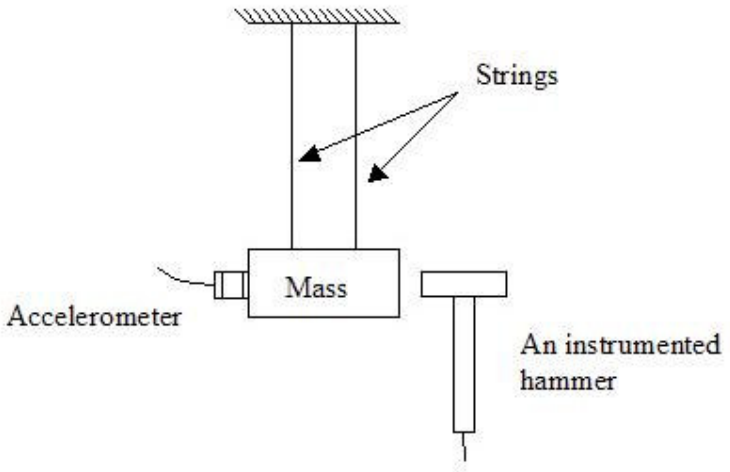

Figure 6-2. *FRF* calibration using an impact hammer and a suspended mass.

Figure 6-3. A charge amplifier

The signal (in the time domain) from the hammer due to exciting the suspended mass is presented in Figure 6-4.

Accelerometer response to the hammer excitation in time domain is presented in Figure 6-5.

FRF can be derived by dividing the displacement by the force. When the hammer hits the mass, the response from the accelerometer is divided by the response of the hammer (in frequency domain).

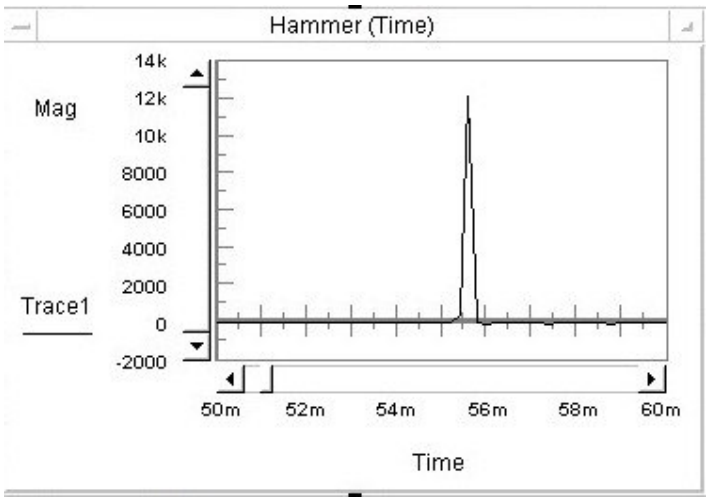

Figure 6-4. Hammer response in time domain.

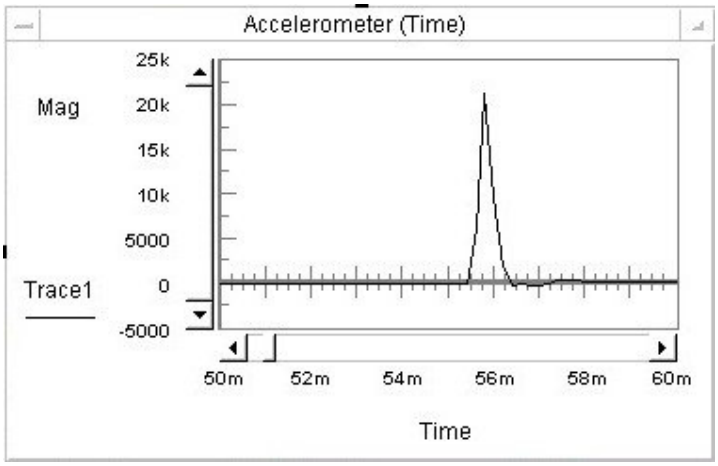

Figure 6-5. Accelerometer response to the hammer excitation in time domain

The software transforms the hammer and accelerometer signals to frequency domain by Fourier transform. Figure 6-6 shows the object (in AgilentVEE software) that is used for transforming time domain to frequency domain by Fourier transform.

Figure 6-6. Fourier transform object in AgilentVEE software

The object presented in Figure 6-7 can obtain division of frequency response of accelerometer by the hammer (AgilentVEE software).

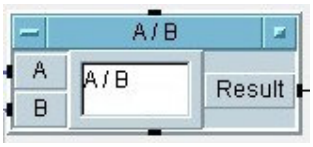

Figure 6-7. Dividing object.

FRF result is presented in Figure 6-8. The average *FRF* magnitude is 3.50. This average is obtained from various *FRF* tests using different impact excitations by the instrumented hammer.

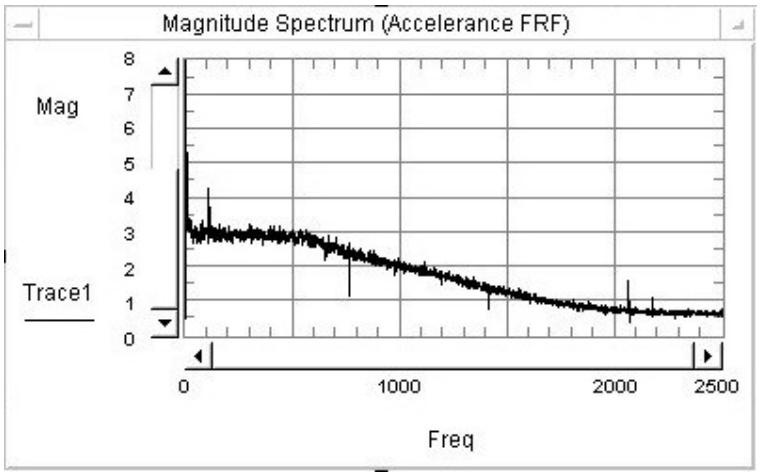

Figure 6-8. *FRF* signal.

In this calibration *FRF*= $\frac{\ddot{X}}{F} = \frac{1}{m}$ (Newton law). The mass magnitude is known and is equal to 0.5 kg. *FRF* magnitude has to be $1/0.5kg = 2$ but the *FRF* result is 3.50. The result magnitude of 3.50 is obtained by averaging various *FRF* results by repeating the calibration test with different levels of impact excitations. 3.50 unit of *FRF* is relative to 2 units of the calibration magnitude. Then the *FRF* calibration value is $3.5/2 = 1.75$. Therefore *FRF* results in modal analysis have to be divided 1.75.

An experimental *FRF* measurement setup using AgilentVEE software is illustrated in Figure 6-9.

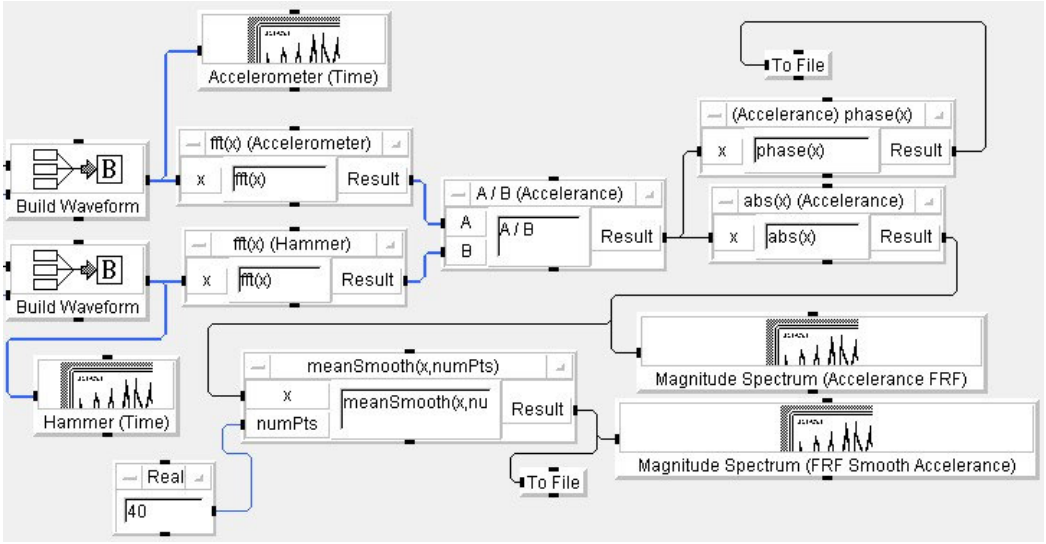

Figure 6-9. AgilentVEE setup for experimental *FRF* measurements.

In Figure 6-9 two Built Waveform objects consist of hammer and accelerometer signals. Fourier transform of these signals are obtained using fft(x). 'A/B' object gives the *FRF* results. 'abs(x)' gives the absolute value of *FRFs* as *FRFs* include imaginary and real numbers. 'phase(x)' gives the phase angles. meansmooth(x,nu) gives the average value of signal. These signals can be plotted using waveform (time) or spectrum (frequency) in time or frequency domain respectively. The result data can also be stored in a file using 'To File' object.

6.2. Fuzzy logic and neural networks

Fuzzy logic and neural networks are used in the proposed method. The methods were introduced in Chapter 5. In this section application of fuzzy logic and neural network toolboxes of MATLAB software are introduced regarding the proposed method.

6.2.1. Fuzzy logic

The application of fuzzy logic toolbox of MATLAB software is introduced here. In the proposed method, the mode shapes are guessed. The guessed mode shapes are called mode shape forms (*MSFs*). *MSF* is introduced based on the approximate deflection values. Fuzzy logic is used to represent these approximate values. The fuzzy representative of *MSFs* consists of input fuzzy membership functions, output membership functions and the corresponding fuzzy rules. The input membership functions consist of dimension (or position) membership function and natural frequency membership function. The number of position membership functions depends on the dimension of the system. For one-dimensional systems there is one position membership function. For two-dimensional structures there are two membership functions. For three-dimensional structures, three membership functions are required. An example of position membership functions, using fuzzy toolbox is illustrated in Figure 6-10.

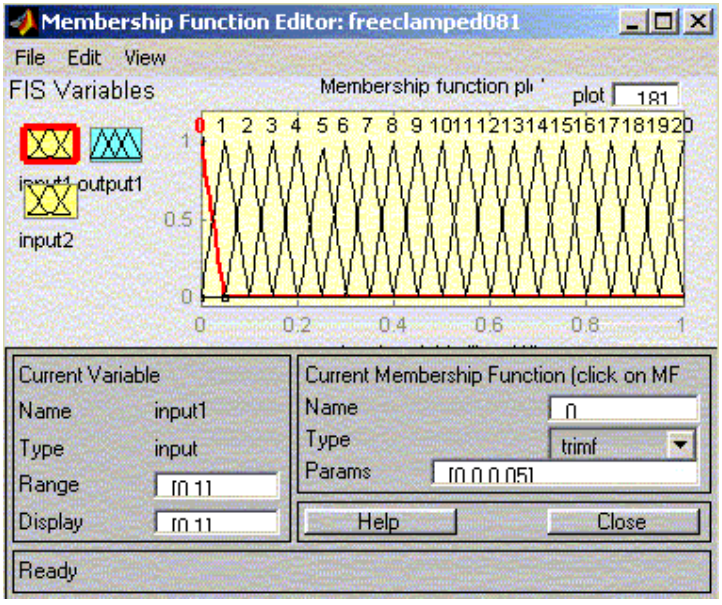

Figure 6-10. Position membership function.

In this figure, numbers from 0 to 20 is assigned to each membership function. Each of these 21 functions corresponds to a position on the body. If the body is two or three-

dimensional, then two or three position membership functions will be required. An example of frequency membership functions is illustrated in Figure 6-11.

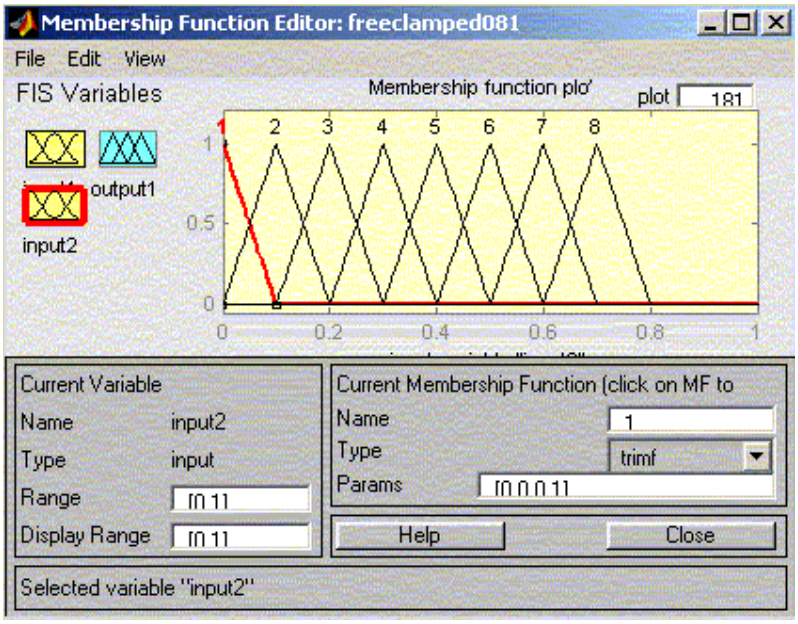

Figure 6-11. Frequency membership functions.

Each function corresponds to a natural frequency. For example membership function number 1 (Figure 6-11) corresponds to the first natural frequency. In this figure the mode shapes of first 8 natural frequencies are of interest. For this reason, there are 8 frequency membership functions.

The output membership functions include deflection properties of the elastic body. An example of the output membership functions is illustrated in Figure 6-12.

In this membership function example, the magnitudes of deflections are introduced by fuzzy terms, *NL, NM, Z, PM* and *PL*. *N* is negative, *P* is positive, *Z* is zero, *M* is medium and *L* is large. After introducing the fuzzy membership functions, the fuzzy rules are required to relate the inputs to the output. The fuzzy rules are constructed based on the *MSFs*. Obtaining the *MSFs* of a system are explained in Chapter 4. For example if a *MSF* is obtained as shown in Figure 6-13, then a set of fuzzy rules for this *MSF* can be expressed as shown in Figure 6-14.

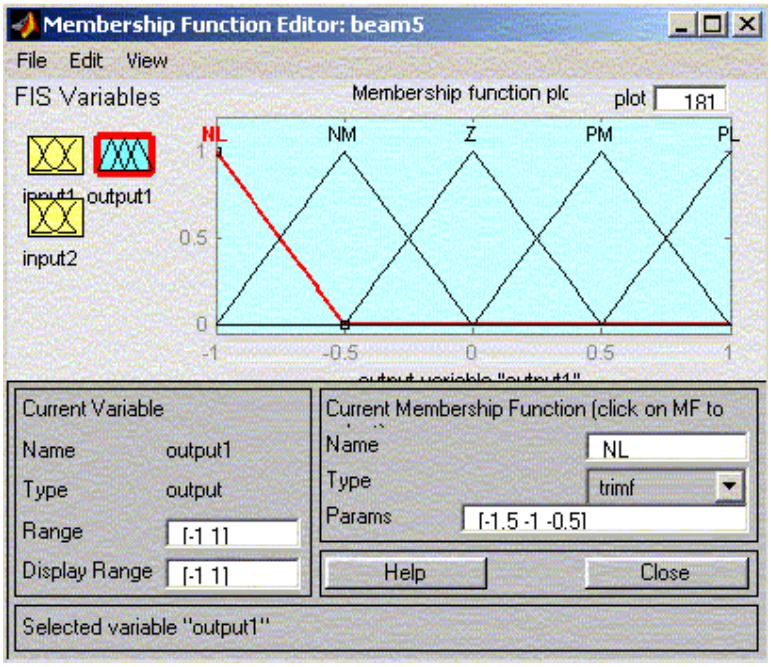

Figure 6-12. Output membership functions (deflection).

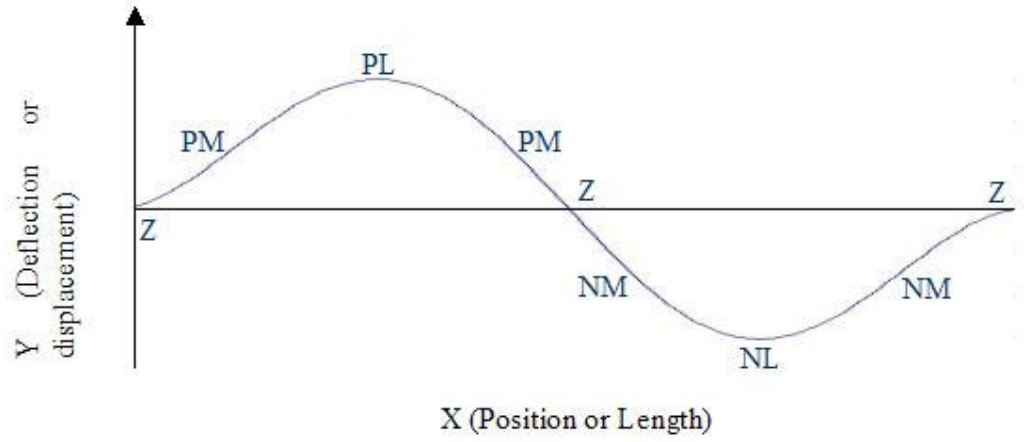

Figure 6-13. A *MSF* sample.

However in this figure only 8 rules are illustrated. The complete number of the rules in this example is more that what is appeared in the following figure. A part of the rules is only shown here.

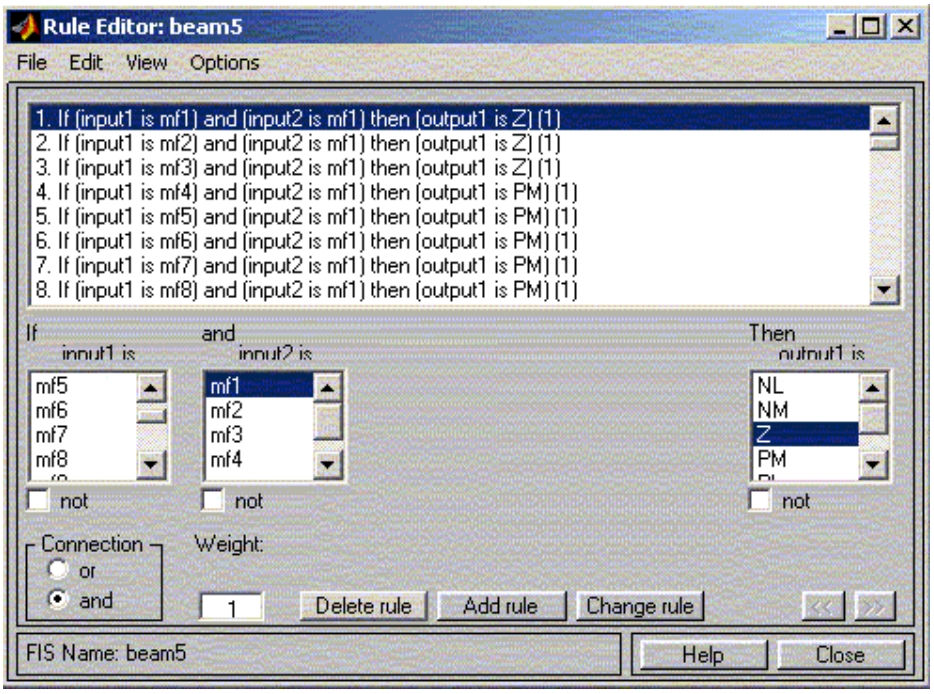

Figure 6-14. Fuzzy Rules.

In the next stage SIMULINK toolbox is used to derive the output from the inputs. Figure 6-15 illustrates an example of SIMULINK setup to obtain the output.

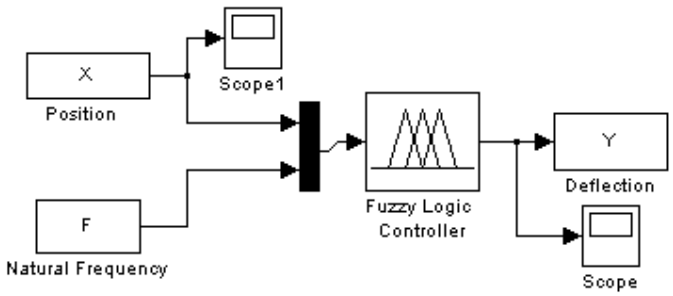

Figure 6-15. SIMULINK fuzzy controller in obtaining deflections (output) from the inputs.

In two-dimensional bodies the SIMULINK model consist of two position inputs (Figure 6-16).

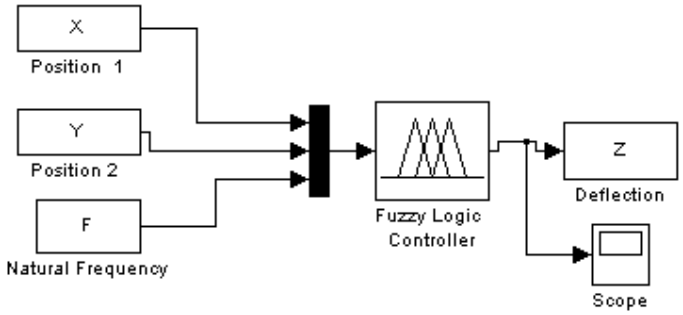

Figure 6-16. SIMULINK setup in two-dimensional modelling.

For three-dimensional modelling another position input is required (Figure 6-17).

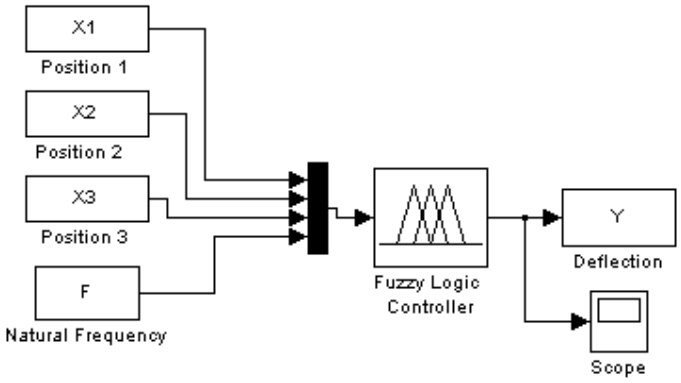

Figure 6-17. SIMULINK setup for three-dimensional modelling

The following setup is used in obtaining the mode shapes using the SIMULINK toolbox.

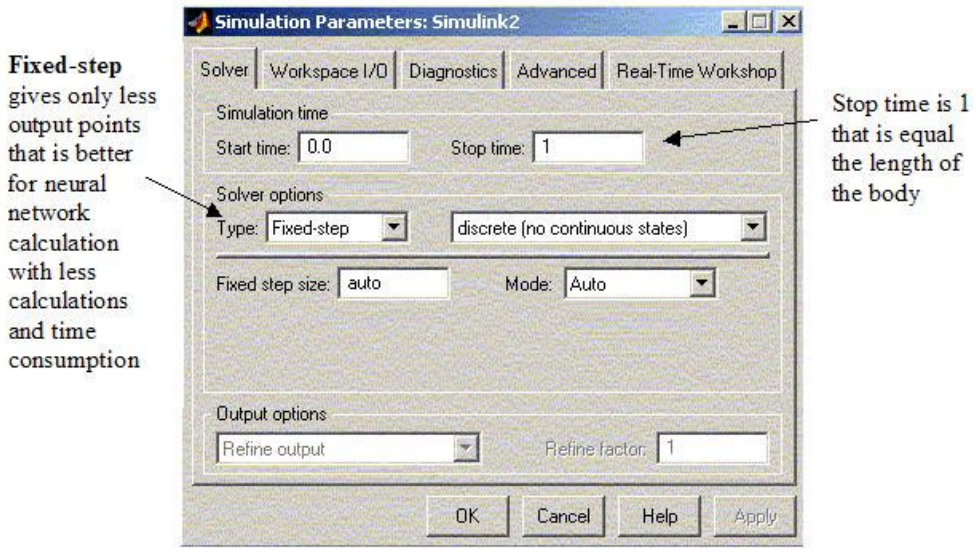

6.2.2. Neural networks

Application of neural network in the proposed method was introduced in Chapter 5. Both Fuzzy Neural Networks and Artificial Neural Networks are used in deriving the mode shapes. Fuzzy Neural Network obtains the results in a shorter time. MATLAB commands in application of Adaptive Neuro-fuzzy Inference System (*ANFIS*) are presented below.

```
trnData = [m ;Ym']';
in_fismat = genfis1(trnData);
out_fismat = anfis(trnData,in_fismat);
```

Where *trnData* is the network training data, *m* is the input training data of the neural network that is the geometry of the body. *Ym* is the deflection output magnitude of *MSFs* from the SIMULINK toolbox that is updated by experimental modal analysis. *Ym* is the output training data of the neural network. *Ym′* is the transpose of *Ym* matrix. *genfis1* initialize the membership function parameters. *anfis* obtain the output of the neural network.

```
evalfis(x,out_fismat));
```

evalfis derives output of the network for any input (here *x* is the input).

Another command can be used to control the epochs. This command has not been discussed here as changing the epochs makes little difference (in the application of *ANFIS* in this thesis) in the results.

For each mode shape one neural network has to be introduced. The input of the networks is the dimension and the output is the deflection. One network is introduced for each mode shape and the corresponding natural frequency.

Chapter 7

Experimental Validation

In this chapter, four examples are provided to validate the proposed method. Example 1 includes the vibration modelling of a clamped-clamped beam. In this example also, the possibility of obtaining the mode shape is presented in two cases, where, a) The mode shapes is guessed wrong, and b) There is no *MSF* available. Example 2 addresses the method to obtain the vibration behaviour of a clamped-free-clamped-free plate. In example 3, the modelling procedure of a 3-beam structure is presented. Example 4 deals with the modelling problem of a clamped-free beam where the updating procedure is performed for only part of the length of the beam. Therefore there is only incomplete experimental data available for updating the fuzzy *MSFs*.

The procedure of guessing mode shapes or obtaining *MSFs* is presented in Chapter 4. The proposed method is introduced in Chapter 5. Experimental setup is presented in Chapter 6.

7.1. One-dimensional elastic bodies

In this section, an example is provided in vibration modelling of a clamped-clamped beam. After the modelling procedure, another example is presented where; a) A

wrong mode shape is guessed for *MSF,* and b) The *MSF* of a particular mode is not available. The method that is presented in Chapter 5 (Method) is used to solve this problem.

7.1.1. Example 1

Vibration modelling of a clamped-clamped beam is considered in this example. The method was presented in Chapter 5. The problem is to obtain the mode shapes of the system up to 4th natural frequency (n=4). The first input of the fuzzy model is the beam length. Figure 7-1 illustrates the membership functions of the first input. The beam length is taken to be normalised to 1.

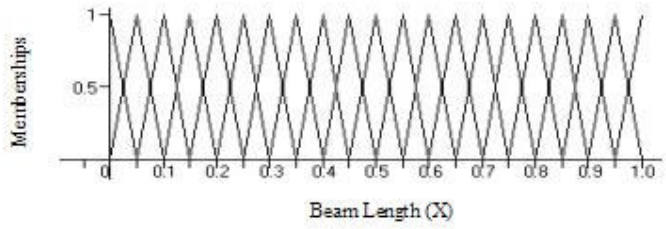

Figure 7-1. Position membership functions (input 1).

The second input of the fuzzy model is frequency. Figure 7-2 shows the membership function of the second input. The region of frequency input is designed for the first to the 4th natural frequency. The magnitude of the natural frequencies are measured by experimental test or *FRF*.

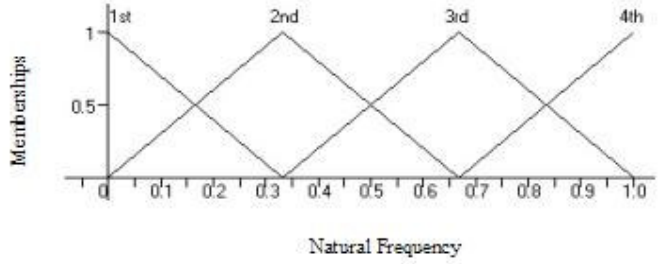

Figure 7-2. Natural frequency membership functions (input 2).

The output of the fuzzy system is deflection or the fuzzy *MSFs*. Figure 7-3 shows the membership function of the output based on the *NL*, *NM*, *Z*, *PM*, and *PL*.

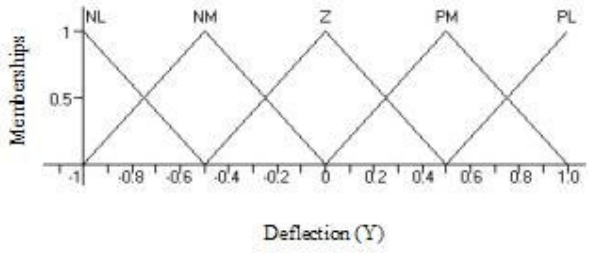

Figure 7-3. Deflection membership functions (output).

Fuzzy rules are defined based on the boundary conditions of the beam and the approximate (guessed) mode shapes of each natural frequency. For example in second natural frequency, the mode shape of the beam is zero (*Z*) and will go up to positive large (*PL*) and this is followed by going down to negative large (*NL*) and again zero (Figure 7-4).

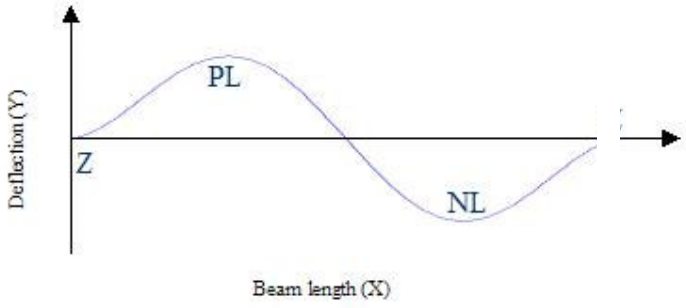

Figure 7-4. Explaining the guessed mode shapes by fuzzy rules.

As the beam is clamped-clamped, then the boundary conditions present zero deflections in both ends. The zero slopes are defined by having two zeros at each end. Zeros at length positions 1 and 2 at the first end, and at length positions 18 and 19 at the other end are shown in Table 7-1.

Table 7-1. Fuzzy rules for the guessed mode shapes (*MSFs*) up to the forth natural frequency.

Frequency / Length ($\times 1/5\times n$)	First natural frequency	Second natural frequency	Third natural frequency	Forth natural frequency
1	*Z*	*Z*	*Z*	*Z*
2	*Z*	*Z*	*Z*	*Z*
3	*PM*	*PM*	*PM*	*PM*
4	*PM*	*PM*	*PL*	*PL*
5	*PM*	*PL*	*PL*	*PM*
6	*PM*	*PL*	*PM*	*Z*
7	*PM*	*PL*	*Z*	*NM*
8	*PM*	*PM*	*NM*	*NL*
9	*PL*	*PM*	*NM*	*NM*
10	*PL*	*Z*	*NL*	*Z*
11	*PL*	*NM*	*NM*	*PM*
12	*PM*	*NM*	*NM*	*PL*
13	*PM*	*NL*	*Z*	*PM*
14	*PM*	*NL*	*PM*	*Z*
15	*PM*	*NL*	*PL*	*NM*
16	*PM*	*NM*	*PL*	*NL*
17	*PM*	*NM*	*PM*	*NM*
18	*Z*	*Z*	*Z*	*Z*
19	*Z*	*Z*	*Z*	*Z*

The fuzzy *MSFs* that are created from membership functions in Figures 1-3 and fuzzy rules in Table 7-1 are illustrated in Figure 7-5.

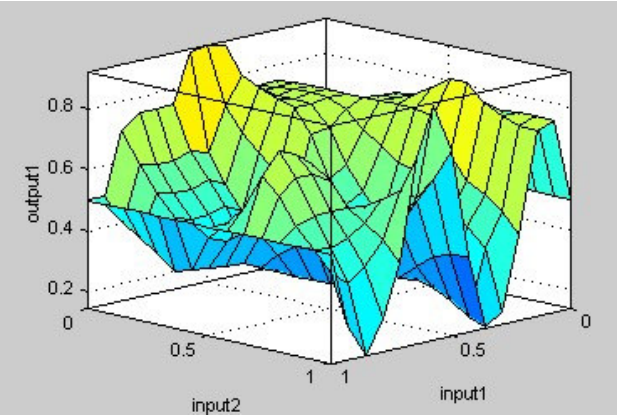

Figure 7-5. The fuzzy *MSFs* from the fuzzy membership functions.

Input 1 is the position on the beam and input 2 is the frequency. The SIMULINK toolbox of MATLAB software is used to generate the fuzzy beam deflections (fuzzy *MSFs*) from fuzzy beam length and fuzzy frequency (inputs). This is illustrated in Figure 7-6.

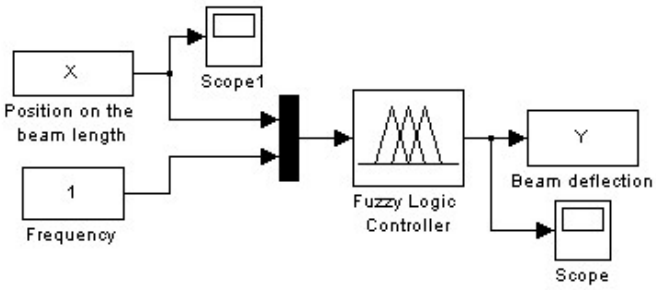

Figure 7-6. SIMULINK fuzzy controller for obtaining the output from the inputs.

To illustrate the output, if the position on the beam is varied between, x=0 to 1 (input 1) and the frequency input is the 4th natural frequency (or number 1 in input2 axis in Figure 7-5), then the output (or Y in Figure 7-6) will be the 4th fuzzy *MSF* of the beam. This output is shown in Figure 7-7(d).

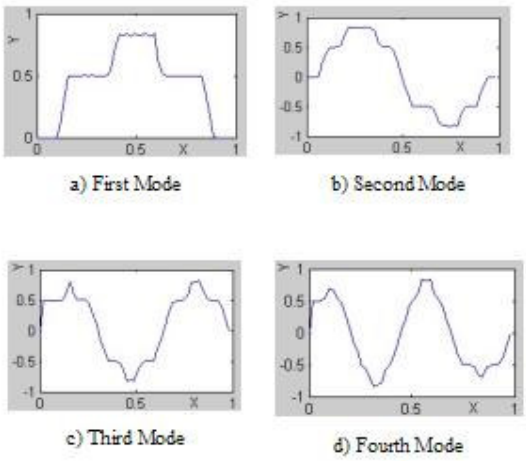

Figure 7-7. Fuzzy *MSFs* from fuzzy model before modification.

After obtaining the fuzzy *MSFs*, these *MSFs* are to be modified by experimental data from a real system. A four-degree of freedom model is derived by modal analysis. The experimental rig is shown in Figure 7-8.

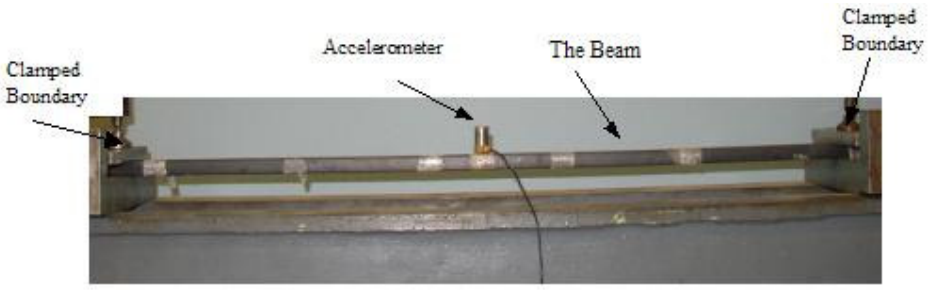

Figure 7-8. A clamped-clamped beam

An accelerometer is attached to the beam to receive the oscillation signals. A charge amplifier is used to amplify and send the signals to the data acquisition card. The data acquisition card (PCI230) is assembled to a Pentium PC. AgilentVEE software is used to obtain the *FRF* curves.

The beam dimension is 500 mm length, 10 mm thickness and 20mm width. The material is steel. Boundary conditions are clamped-clamped.

Before obtaining the eigenvectors (mode shapes) of the beam from *FRF* signals, calibration of *FRF* is performed by using a suspended (488.50gr) mass. An accelerometer is attached to one side of the suspended mass and an instrumented hammer is used to apply an impulse. Fourier transform of both signals (accelerometer and hammer) are obtained by AgilentVEE software. Fourier transform of accelerometer signal from the suspended mass is divided to Fourier transform of hammer signal and the average value result of the division is equalled to one over mass value (1/488.50). The calibration procedure was explained in Chapter 6.

After calibrating *FRF* values, the *FRF* from experimental modal analysis can be used to extract the eigenvectors of the model. The experimental procedure is described below. To find a four-degree of freedom model of the beam, the beam is divided to 5 equal segments. Corresponding four positions to 5 segments are 100mm, 200mm, 300mm, 400mm. An accelerometer is attached on the beam and the instrumented hammer is used to excite the beam. The accelerometer is placed in each of four selected positions. The instrumented hammer is used to excite the beam in each of the four selected points. Sixteen excitations with hammer are applied to the beam corresponding to different combinations of accelerometer and hammer excitation positions. Fast Fourier transform of hammer excitation and accelerometer signals are obtained from AgilentVEE software. Fourier transforms of accelerometer signals are divided by Fourier transform of the signals from the hammer in order to find *FRF* values (for each excitation). A four by four *FRF* matrix is obtained from Sixteen *FRF* data in this experiment. *FRF* curves are presented in Appendix D. Only four *FRF* curves (h_{11}, h_{12}, h_{13} and h_{14}) of 16 *FRFs* are presented in Appendix D. However these four *FRFs* are sufficient to determine the *4DOF* model of the beam. The peak-amplitude (peak-picking) method is performed to extract the modal constants and eigenvectors from the *FRF* matrix. This method is introduced in Chapter 5. The following equation is valid based on this method.

$$\omega = \omega_{n,k} \Rightarrow \left|h_{il}(s)\right|_k = \frac{R_{il,k}}{\zeta_k \omega_{n,k}^2} = \frac{u_{i,k} u_{l,k}}{\zeta_k \omega_{n,k}^2}$$

Where

$$\zeta_k = \frac{\left(\omega_a^2 - \omega_b^2\right)}{\omega_{n,k}^2} \approx \frac{\Delta\omega}{\omega_{n,k}}$$

The experimental results are demonstrated in Table 7-2. Table 7-2 includes first four mode shapes described by 4 positions on the beam (0.2, 0.4, 0.6, 0.8). The position on the beam is normalized, to have the length of the beam equal to 1.

Table 7-2. Mode shapes from experimental modal analysis result.

Position on the beam (normalise)	Mode shape 1	Mode shape 2	Mode shape 3	Mode shape 4
0.2	0.41	1.00	1.00	0.94
0.4	0.98	0.80	-0.41	-1.00
0.6	1.00	-0.85	-0.43	1.00
0.8	0.43	-0.99	1.00	-0.93

Now the experimental mode shapes from Table 7-2 are used to modify the fuzzy *MSFs*. Fuzzy *MSFs* are presented in Figure 7-7. Experimental mode shapes are presented in Figure 7-9.

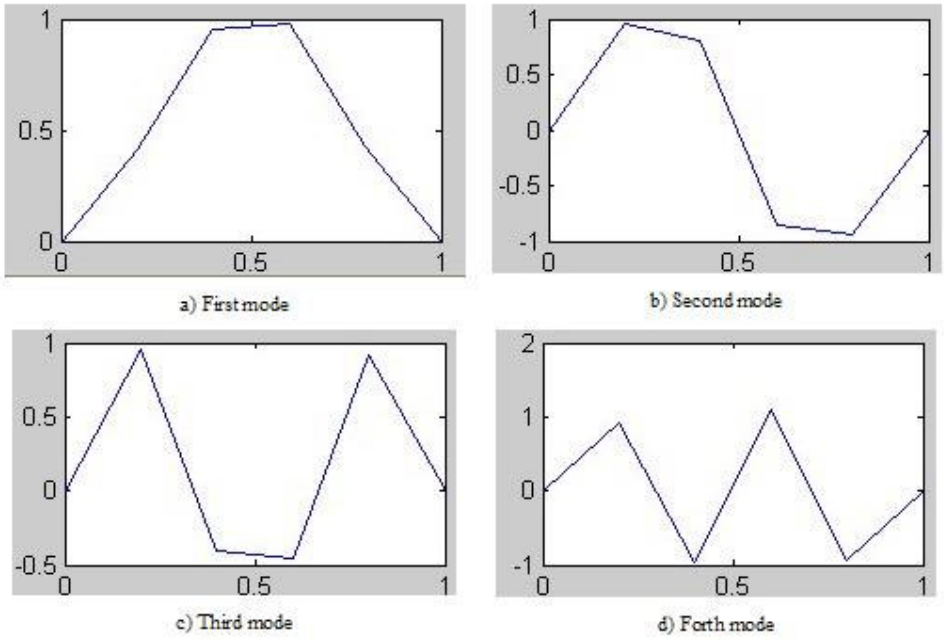

Figure 7-9. Normalized mode shapes from Table 7-2, where the horizontal axis is the position on the beam length and the vertical axis is the deflection of the beam.

Corresponding data from the fuzzy *MSFs* is replaced by the data from experimental mode shapes (in this example, four points). The mode shapes are determined from the updated fuzzy *MSFs*. Experimental measurements were carried out at 4 positions. Updating the fuzzy *MSFs* is performed by simply replacing the points in the fuzzy data set with the corresponding points from the experimental set. The inputs and output fuzzy membership functions are described by 51 points. Therefore each fuzzy *MSF* include 51 numbers of position points and the corresponding 51 numbers of deflection values. Both the fuzzy neural network and back-propagation neural network are used to generate the updated curves (MATLAB software is used). It is found that the fuzzy neural network generates smoother curves compared to back-propagation networks. The neural network is based on a single-input-single-output system. The input of the system is the position on the beam. The deflections from modified fuzzy data determine the output of the network. The following procedure is performed to train the network. The input training data includes the position on the beam for each mode shape (as here, 51 numbers of inputs). Updated fuzzy *MSFs* deflections are the output training data of the network (as here, 51 numbers of outputs). As four degree of freedom modelling is used here, then four neural networks are introduced for each mode shape individually. The same input output and training procedure that is described earlier is used for each neural network. The trained neural networks determine the mode shapes. By giving the position on the beam as the input of the networks, the mode shapes are generated. Figure 7-10 shows the mode shapes from the presented method and experimental data.

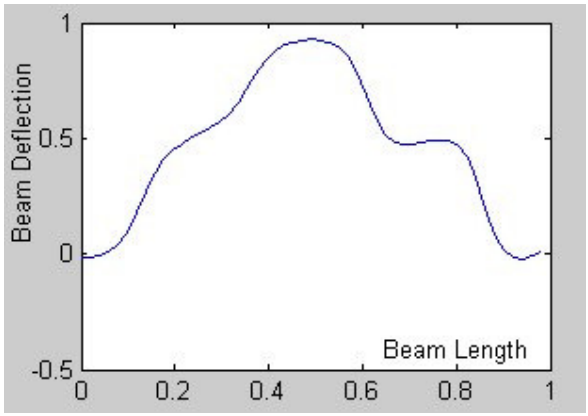

a) The first mode shape.

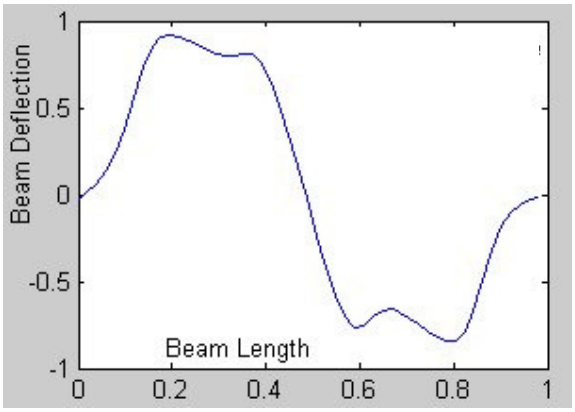

b) The second mode shape.

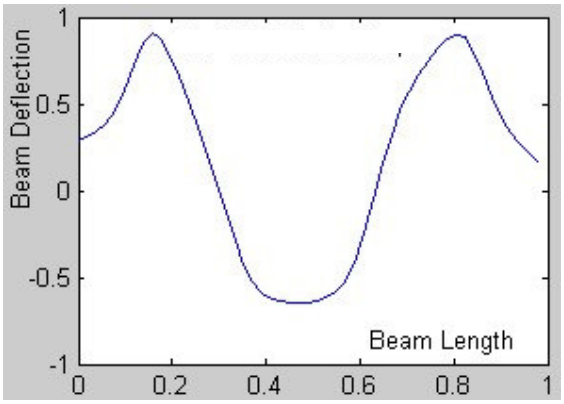

c) The third mode shape.

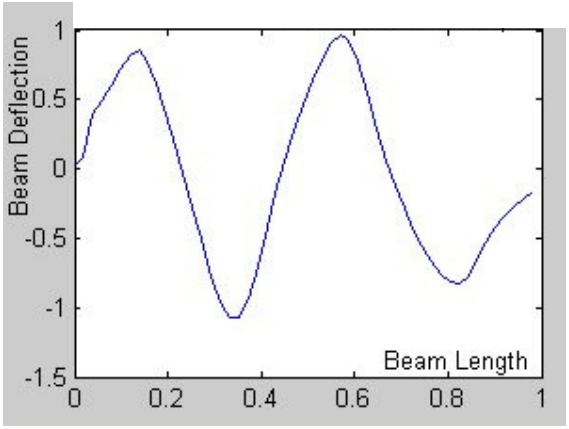

d) The forth mode shape.

Figure 7-10. Mode shape results that is obtained from the proposed method. a) 1st mode b) 2nd mode d) 3rd mode d) 4th mode

The result of this example can be presented in time domain using the following equation.

$$\begin{Bmatrix} y_1(t) \\ y_2(t) \\ y_3(t) \\ y_4(t) \end{Bmatrix} = c_1 \begin{Bmatrix} Y_1 \\ Y_2 \\ Y_3 \\ Y_4 \end{Bmatrix}_1 \sin(\omega_{n1}t + \psi_1) + c_2 \begin{Bmatrix} Y_1 \\ Y_2 \\ Y_3 \\ Y_4 \end{Bmatrix}_2 \sin(\omega_{n2}t + \psi_2) + c_3 \begin{Bmatrix} Y_1 \\ Y_2 \\ Y_3 \\ Y_4 \end{Bmatrix}_3 \sin(\omega_{n3}t + \psi_3) +$$
$$c_4 \begin{Bmatrix} Y_1 \\ Y_2 \\ Y_3 \\ Y_4 \end{Bmatrix}_4 \sin(\omega_{n4}t + \psi_4)$$

Using the eigenvectors obtained from the proposed method and experimental natural frequency values then the equation can be express as below.

$$\begin{Bmatrix} y_1(t) \\ y_2(t) \\ y_3(t) \\ y_4(t) \end{Bmatrix} = c_1 \begin{Bmatrix} 0.41 \\ 0.81 \\ 0.78 \\ 0.55 \end{Bmatrix} \sin(19t + \psi_1) + c_2 \begin{Bmatrix} 0.91 \\ 0.82 \\ -0.78 \\ -0.82 \end{Bmatrix} \sin(53t + \psi_2) + c_3 \begin{Bmatrix} 0.83 \\ -0.68 \\ -0.62 \\ 0.91 \end{Bmatrix} \sin(104t + \psi_3) +$$
$$c_4 \begin{Bmatrix} 0.84 \\ -0.94 \\ 0.91 \\ -0.83 \end{Bmatrix} \sin(174t + \psi_4)$$

Where constants c and ψ can be obtained from displacement and velocity initial conditions.

7.1.2. Comparison of error between the proposed method and the mathematical equation

The mathematical equation of motion of the clamped-clamped beam is used to compare the result that is obtained in this section. Although comparison of the model obtained against further experimental tests was another option. This was declined as

no one specific experimental result can be taken as benchmark. The mathematical equation of motion of a clamped-clamped beam is [41].

$$y = \cosh\left(\frac{\omega x}{L}\right) - \cos\left(\frac{\omega x}{L}\right) - \lambda\left[\sinh\left(\frac{\omega x}{L}\right) - \sin\left(\frac{\omega x}{L}\right)\right] \tag{7-1}$$

$$\omega = {(2i+1)\pi}/{2} \qquad i = 1, 2, 3, \ldots$$

λ is a dimensionless parameter which is the function of the boundary conditions applied to the beam and its magnitudes are presented in Table 7-3 for different natural frequencies.

Table 7-3. λ for mode shape i.

i	**1**	**2**	**3**	**4**	**5, 6, ..**
λ_i	0.982	1.0007	0.9999	1.0000014	1

ω gives very good accuracy for $i > 5$ while for $i < 5$ is less accurate but still a good approximation [41].

The following equation used to calculate the error (e) between the mathematical equation and the proposed method in this example.

$$e = \sum_{i=1}^{51} \frac{\left|\left(X_i - x_i'\right)\right|}{\left|x_i\right|}$$

Where x_i' is the experimental data (deflection) and X_i is the data (deflection) from the proposed method.

The proposed method exhibits a maximum error of 15.57%, relative to the mathematical model in the 4th mode in the mode shapes. Error in the first, second and third mode shapes are 14.3%, 11.2% and 9.8% respectively.

7.1.3. Creating a mode shape where either there is no guess available for mode shape or guessed mode shape is wrong for the clamped-clamped beam

In this method a mode shape can be obtained in two situations as below.

a) A wrong guess is assumed for the mode shape.
b) The heuristic guess is not available.

The method of treating the error in conditions (a) and (b) are introduced in chapter 5.4. The flowchart in Chapter 5, Figure 5-11, demonstrates the procedure of the proposed method. In this flowchart, first a *MSF* is selected, then the method is applied to obtain the mode shape. Obtaining the mode shapes includes construction of the fuzzy *MSFs*, *FRF* updating the mode shape and applying neural network to the updated fuzzy *MSFs*. After obtaining the mode shapes, the error between these mode shapes and the corresponding experimental mode shapes are calculated. If the error is acceptable, then the procedure will end. If the error is not acceptable, then another *MSF* will be used and the procedure will be repeated. If none of the *MSFs* satisfy the acceptable error, then the *MSF* with the minimum error will be selected. In this case alternative guess of mode shapes are available. The alternative mode shapes may be guesses for the other natural frequencies, initially. Then the fuzzy rules of this *MSF* are corrected and the error is calculated. If the error is acceptable then the procedure will end. If the error is not acceptable the correction of fuzzy rules is repeated.

The following example shows the treatment of error when the guess is wrong and when the correct *MSF* (guess) is not available.

a) An example of creating a mode shape when the guess is wrong

Assume the **3rd** mode shape of the clamped-clamped beam (in example 1), to be guessed as Figure 7-11 (the wrong guess). However this mode shape is the **2nd** mode shape.

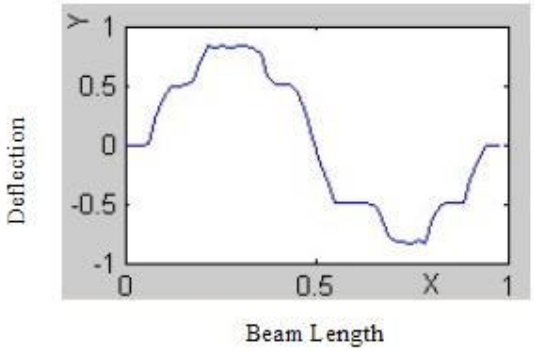

Figure 7-11. Wrong guessed mode shape (*MSF*) for the **3rd** mode.

This mode shape has to be modified after constructing the mode shape by fuzzy membership functions. In the modification stage, this mode shape has to be updated by the 3rd experimental mode shape. A sample of experimental results is presented in Table 7-3.

Table 7-3. Experimental modal analysis data.

Position on the beam (normalise)	Mode shape 1	Mode shape 2	**Mode shape 3**	Mode shape 4
0.2	0.41	1.00	**1.00**	0.94
0.4	0.98	0.80	**-0.41**	-1.00
0.6	1.00	-0.85	**-0.43**	1.00
0.8	0.43	-0.99	**1.00**	-0.93

The experimental results for the 3rd mode shape is illustrated in Figure 7-12.

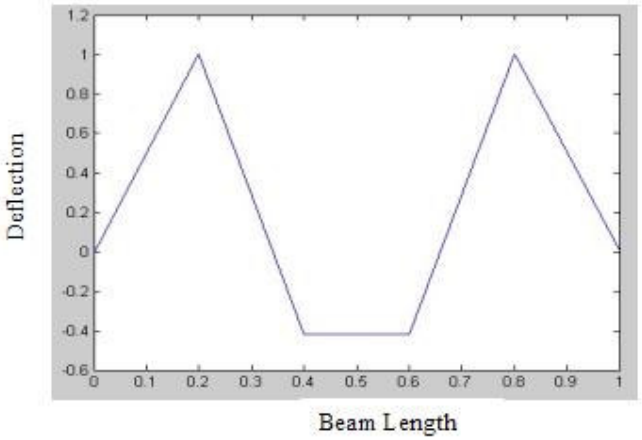

Figure 7-12. Third mode shape from experimental results

The curve in Figure 7-13 is derived after updating procedure (using experimental modal analysis) and after that using neural network for smoothing the mode shape.

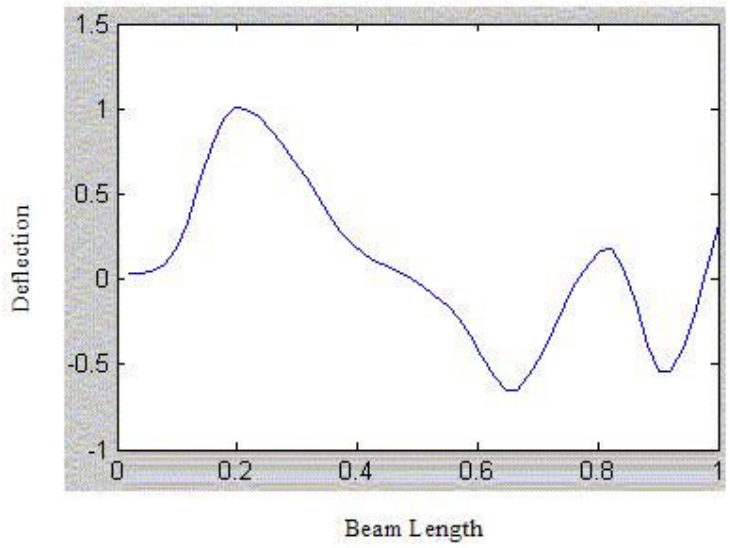

Figure 7-13. Mode shape result from the wrong guessed mode shape.

In this stage the error between the result mode shape in Figure 7-13 is compared with the experimental result (Figure 7-12) that is used in updating the model. These two mode shapes are shown in Figure 7-14 including the difference between each two points in each mode shape using $(x_i - X_i)$ relation. Where x_i is the experimental

data, X_i is the data from the proposed method. 51 points are used for drawing of each curve.

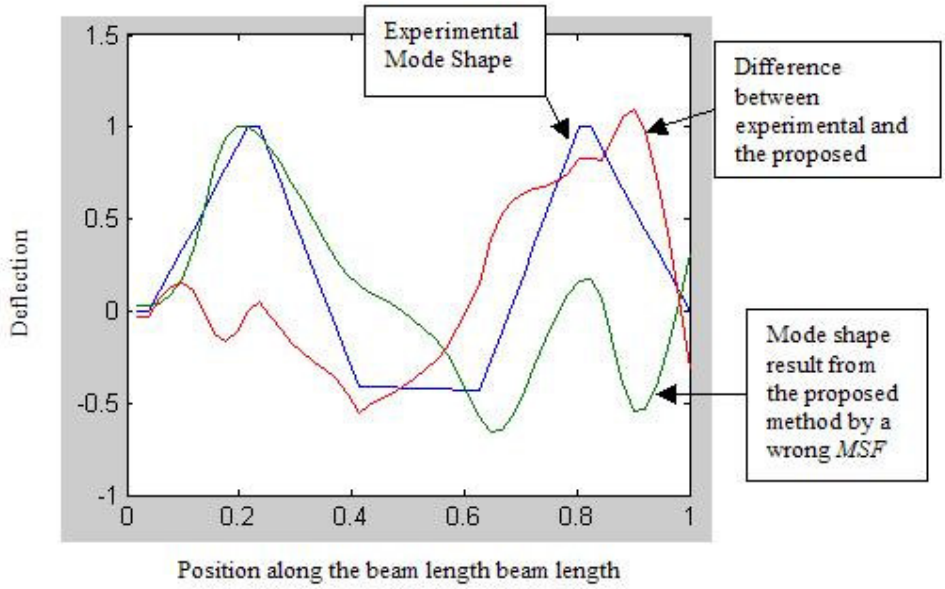

Figure 7-14. Experimental mode shape, the mode shape result from the proposed method (by the wrong guess) and the difference between each point of these two mode shapes (both mode shapes are normalized to 1).

The error between these two mode shapes are calculated using the following equation.

$$e = \sum_{i=1}^{51} \frac{\left|\left(X_i - x_i\right)\right|}{\left|x_i\right|}$$

Where x_i is the experimental data, X_i is the data from the proposed method and 51 is the number of points that are considered for calculating the error. The error is equal to 65.67%. The flowchart suggests that the procedure has to be repeated using another guess of mode shape or *MSF*.

In this example all the available heuristic guesses are presented in Figure 7-15 (up to the forth mode). In this stage the flowchart suggests using another *MSF*, for example the mode shape in Figure 7-15(c). This *MSF* used in example 1. 11.46% error obtained and with this level of error the iteration procedure ends.

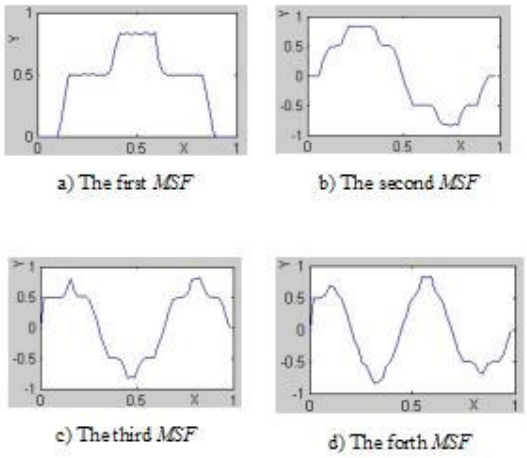

Figure 7-15. The entire available heuristic mode shape guess (*MSFs*) (where X axis is the beam length and the Y axis is the deflection of the beam)

b) An example of creating the mode shape when the guess is not available

If the entire possible heuristic *MSFs* are considered as in Figure 7-16 then the desired *MSF* is not available for the third mode. In this stage the flowchart select the *MSF* with the minimum error relative to the corresponding experimental mode shape data. The error was calculated by the following equation.

$$e = \sum_{i=1}^{51} \frac{\left|\left(X_i - x_i\right)\right|}{\left|x_i\right|}$$

The *MSF* by the minimum error (Error (j)) is selected as MSF_j . Where *j* indicates the corresponding *MSF* number. In this example the *MSF* in Figure 7-16(b) obtained the minimum error. Therefore this *MSF* is used to determine the 3rd mode shape.

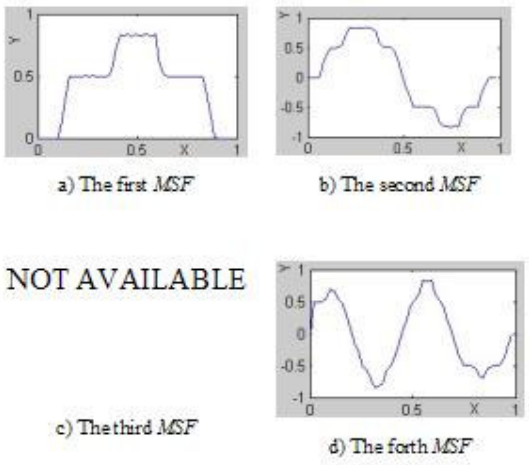

Figure 7-16. The entire available heuristic *MSFs* (where X axis is the beam length and the Y axis is the deflection of the beam)

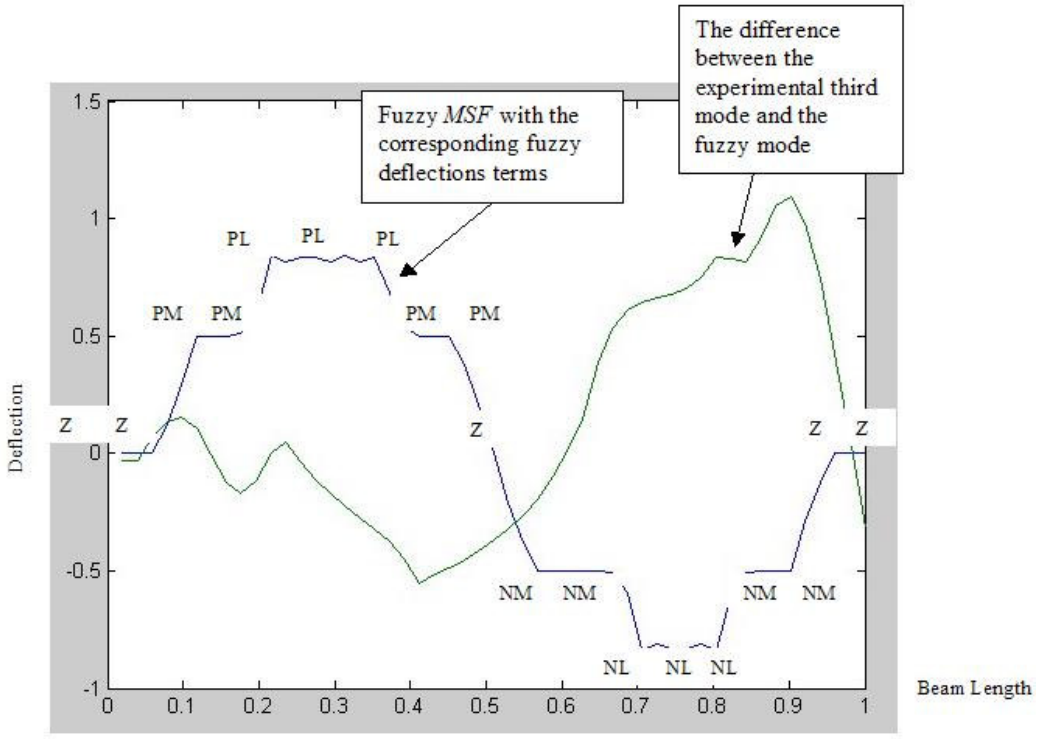

Figure 7-17. Fuzzy second mode shape with the corresponding fuzzy deflection terms (*Z*, *PM*, *PL*, …) and the difference between the second mode shape and the experimental third mode.

Then the fuzzy rules of this *MSF* are corrected and the error is calculated. If the error is acceptable, then the procedure ends. If the error is not acceptable, the correction of

fuzzy rules is repeated. The procedure of the correction of the fuzzy rules is explained below, where the correction is applied to the mode shape to reduce the error. The difference between deflection in the mode shape obtained from the proposed method and the experimental result is illustrated in Figure 7-14. The difference is calculated by $(x_i - X_i)$ where x_i is the experimental beam deflection and X_i is the beam deflection from the proposed method. 51 points are used for this calculation. This difference and the fuzzy second mode shape are illustrated in Figure 7-17.

The fuzzy rules to create this mode shape (Figure 7-16b) is presented in Table 7-1, which is the fuzzy rules of the second mode shape.

The curves in Figure 7-17 are repeated in Figure 7-18. Vectors are used to show the difference magnitudes between the points in the fuzzy *MSF* and the corresponding points in the third experimental mode shape. These are called the Error Vectors in this thesis.

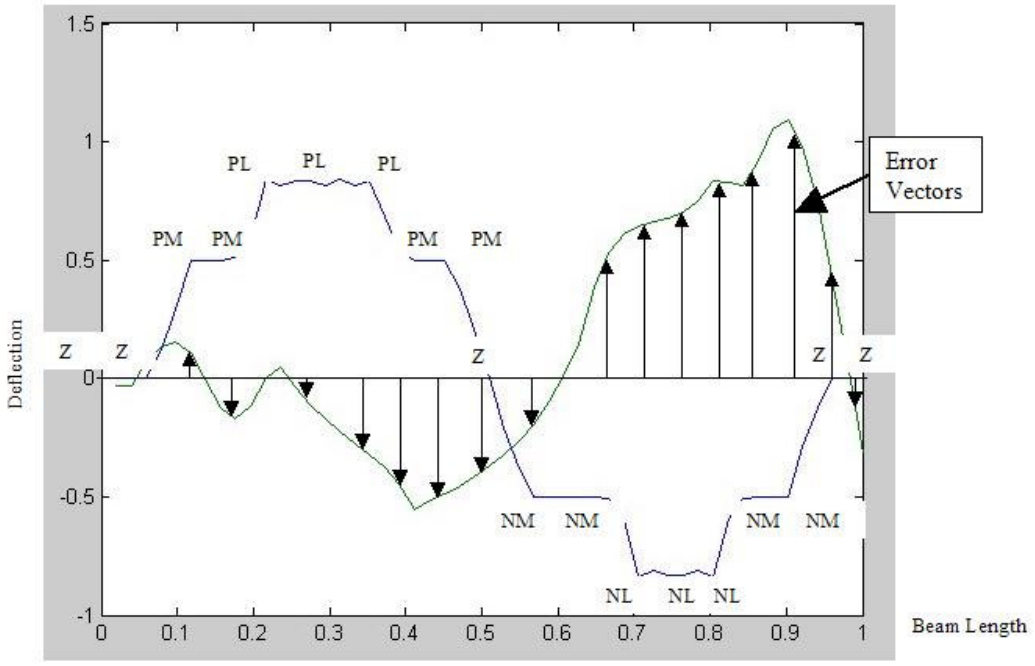

Figure 7-18. The second fuzzy *MSF* with the corresponding fuzzy deflection terms and the difference between the second mode and the experimental third mode the difference is shown with Error Vectors.

The Error Vectors in Figure 7-18 are shifted to the corresponding points on the fuzzy *MSF* (Figure 7-19).

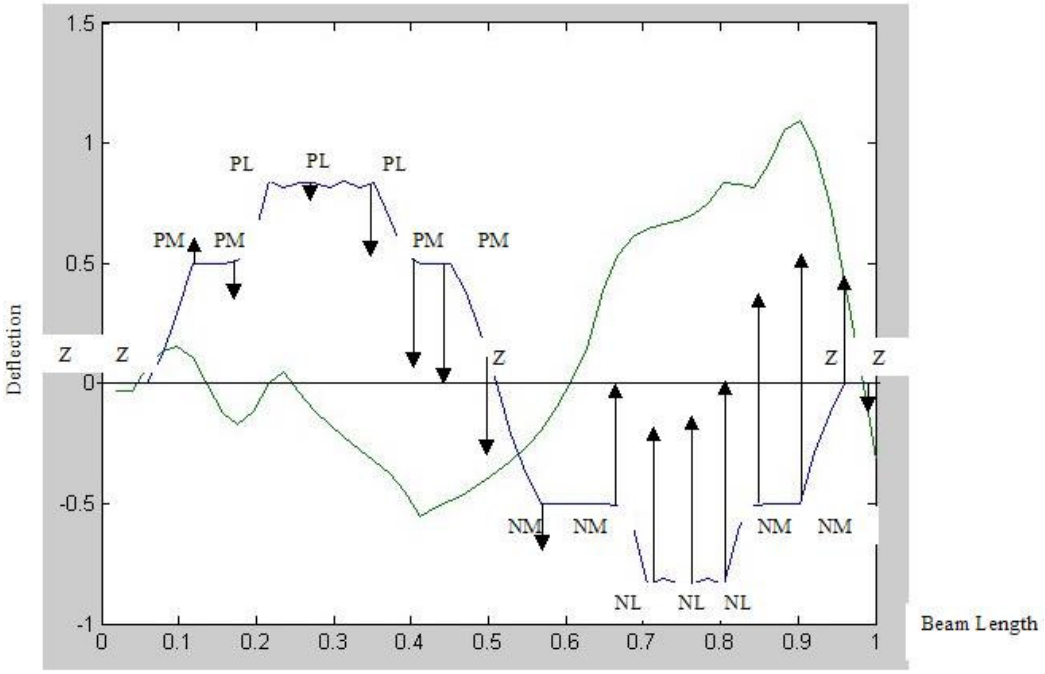

Figure 7-19. Each Error Vector is shifted to the corresponding point on the fuzzy *MSF*.

Now each fuzzy rule in Figure 7-19 has to be changed relative to the corresponding Error Vector. Changing the fuzzy rules is applied based on the process explained in Chapter 5 (Chapter 5, Figures 15 and 16). Each Error Vector magnitude is used to change the fuzzy rules of the fuzzy *MSF*. The relation between the Error Vectors magnitudes and changing the fuzzy rules are presented in Chapter 5. The fuzzy deflections terms are *PL, PM, Z, NM* and *NL*. *P* stands for plus and *N* for minus. The range of fuzzy deflections is between –1 to 1 as in fuzzy output membership functions in this example. The distance between each two fuzzy deflection term is obtained from $\frac{2}{n-1}$. Where 2 is the range (-1 to 1) of output membership functions and *n* is the number of membership functions. There are 5 membership functions here as *PL, PM, Z, NM* and *NL*. Then $\frac{2}{5-1}$=0.5 is the distance between each fuzzy deflection. The fuzzy deflection terms, *PL, PM, Z, NM* and *NL* can be represented by +1, +0.5, 0,

-0.5 (as shown in Chapter 5). Hence the Error Vector can be added to this magnitude. This addition is illustrated in (Figure 5-15, Chapter 5) where the $-|x_i - X_i|$ applies when Error Vector is negative and $|x_i - X_i|$ applies when the Error Vector is positive. For example if the fuzzy deflection is *PM* (+0.5) and the corresponding Error Vector is –1 this fuzzy deflection has to be changed to "+.05-1=-0.5", where the result, –0.5 corresponds to *NM*. Therefore this fuzzy deflection has changed from *PM* to *NM*.

If the magnitude of the result after adding the Error Vector to the fuzzy deflection is out of the fuzzy membership functions range, then the maximum range is applied. For example, if the fuzzy deflection is *PM* (+0.5) and the Error Vector is +1 the result will be "+.05+1=+1.5". But as the maximum range is +1 or *PL*. Therefore this fuzzy deflection can be changed to maximum of +1 or *PL*.

If the Error Vector is not an integer number, then the round-up magnitude is used. For example, if the error is 0.35, then it is considered as 0.5. but if the Error Vector is less than 0.25, it is possible to apply a one step change or rounding up any value between 0 to 0.5, to 0.5. This option is applied here and can be seen in Figure 7-20.

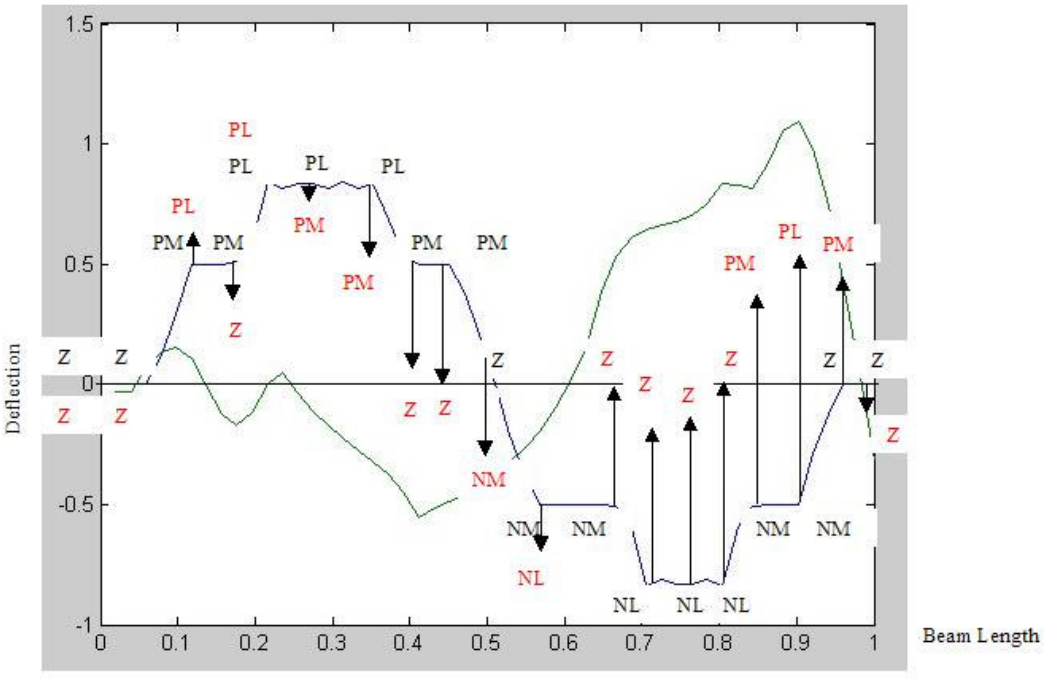

Figure 7-20. Changing fuzzy deflections relative to the corresponding Error Vectors.

Changing the fuzzy deflections in this example relative to Error Vectors is presented in Figure 7-20.

Table 7-4 shows the initial fuzzy rules and the new corrected fuzzy rules that are corrected based on the above discussion.

Table 7-4. Initial fuzzy rules and the new corrected fuzzy rules.

Frequency Length	Fuzzy rules Second natural frequency	New rules I
1	*Z*	*Z*
2	*Z*	*Z*
3	*PM*	*PL*
4	*PM*	*Z*
5	*PL*	*PL*
6	*PL*	*PM*
7	*PL*	*PM*
8	*PM*	*Z*
9	*PM*	*Z*
10	*Z*	*NM*
11	*NM*	*NL*
12	*NM*	*Z*
13	*NL*	*Z*
14	*NL*	*Z*
15	*NL*	*Z*
16	*NM*	*PM*
17	*NM*	*PL*
18	*Z*	*PM*
19	*Z*	*Z*

In this stage the procedure of obtaining the mode shape is repeated and the new fuzzy *MSF* (that is constructed based on the new rules in Table 7-4) is considered in this procedure. This *MSF* is illustrated in Figure 7-21.

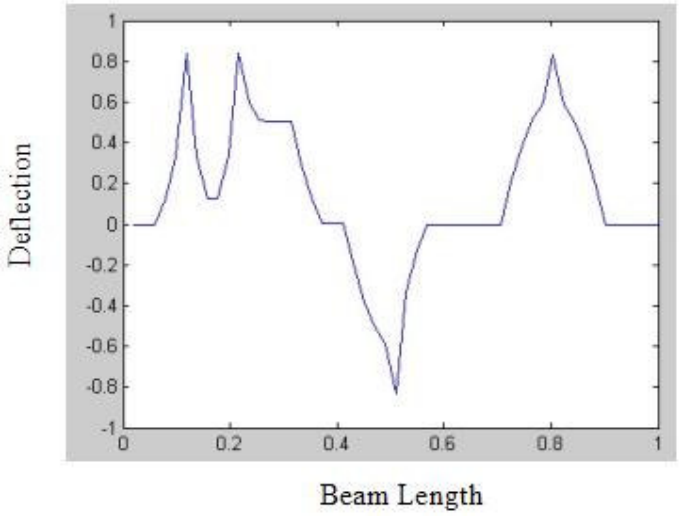

Figure 7-21. The new fuzzy *MSF*.

Now experimental modal analysis is used to update this fuzzy *MSF* and neural network to determine the mode shape (Figure 7-22).

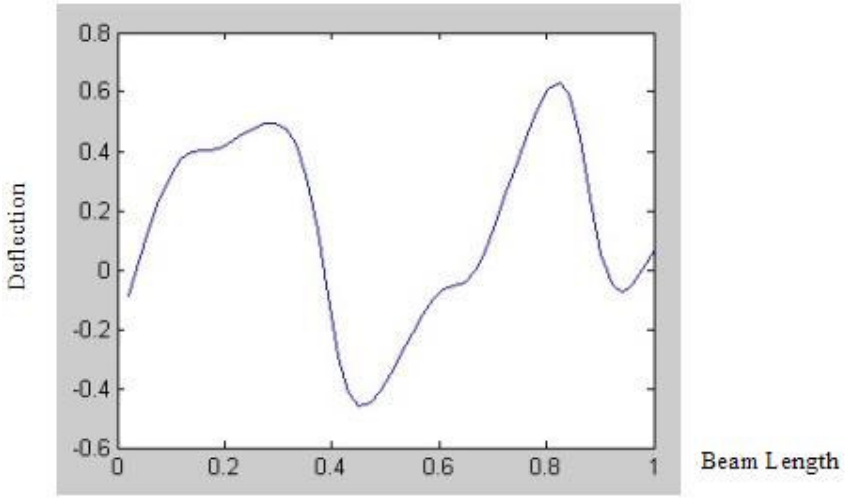

Figure 7-22. The new mode shape constructed based on the new fuzzy rules.

In this stage the procedure is repeated and the difference between the new mode shape (Figure 7-22) and the experimental modal analysis is obtained. The Error Vectors are determined. The fuzzy mode shape and the Error Vectors are illustrated in Figure 7-23.

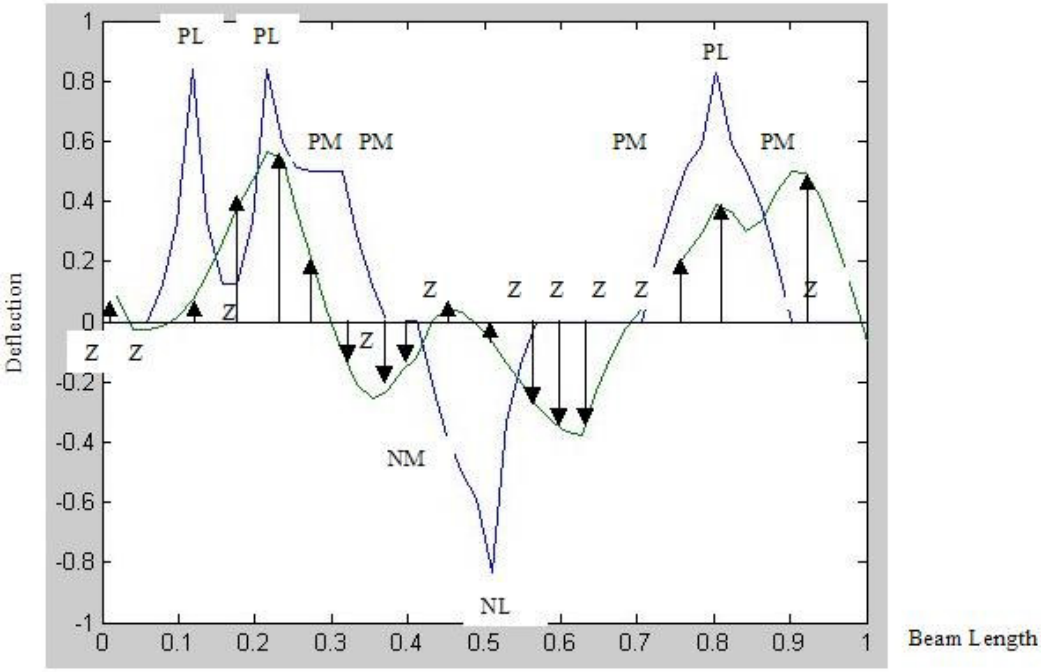

Figure 7-23. Error Vectors and the fuzzy mode shape.

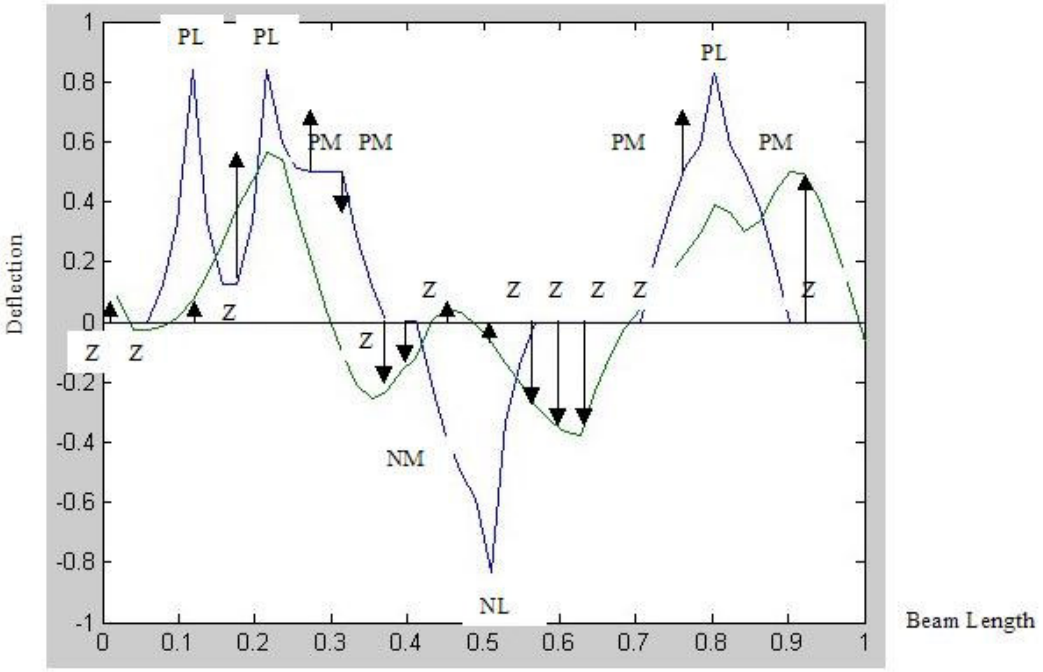

Figure 7-24. Error Vectors are shifted to the corresponding fuzzy rules.

The error vectors are shifted to the corresponding fuzzy deflection in Figure 7-24.

Second new rules are determined based on the Error Vectors (Table 7-5).

Table 7-5. Second new rules.

Frequency	Fuzzy rules	New rules I	New rules II
Length	Second natural frequency		
1	*Z*	*Z*	*Z*
2	*Z*	*Z*	*Z*
3	*PM*	*PL*	*PL*
4	*PM*	*Z*	*PM*
5	*PL*	*PL*	*PL*
6	*PL*	*PM*	*PL*
7	*PL*	*PM*	*PM*
8	*PM*	*Z*	*NM*
9	*PM*	*Z*	*NM*
10	*Z*	*NM*	*NM*
11	*NM*	*NL*	*NL*
12	*NM*	*Z*	*NM*
13	*NL*	*Z*	*NM*
14	*NL*	*Z*	*NM*
15	*NL*	*Z*	*Z*
16	*NM*	*PM*	*PL*
17	*NM*	*PL*	*PL*
18	*Z*	*PM*	*PM*
19	*Z*	*Z*	*Z*

The mode shape is determined after updating and using neural networks as in Figure 7-25.

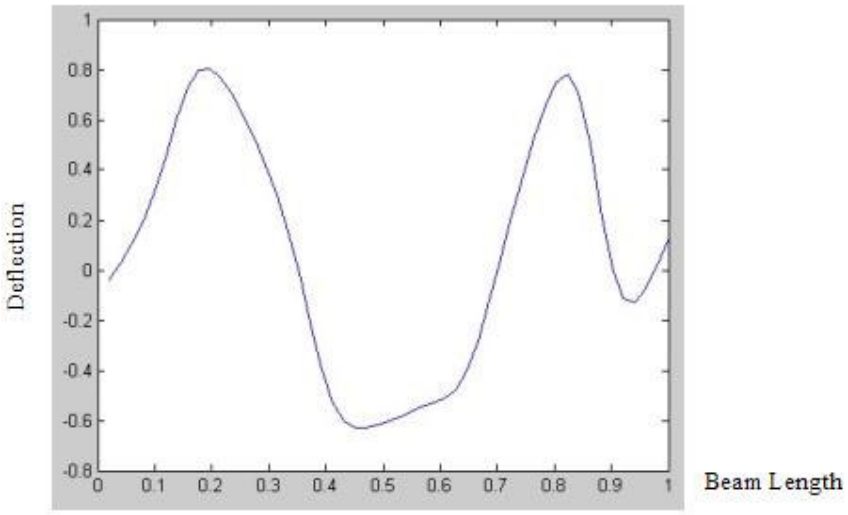

Figure 7-25. Mode shape based on the second new fuzzy rules.

The difference between this mode shape and the experimental modal analysis results are obtained. The error vectors and the fuzzy mode shape are presented in Figure 7-26. The Error vectors are presented for the region that the error is more than 0.25. In this stage if the Error Vector is less than 0.25, there would be no change in the rule.

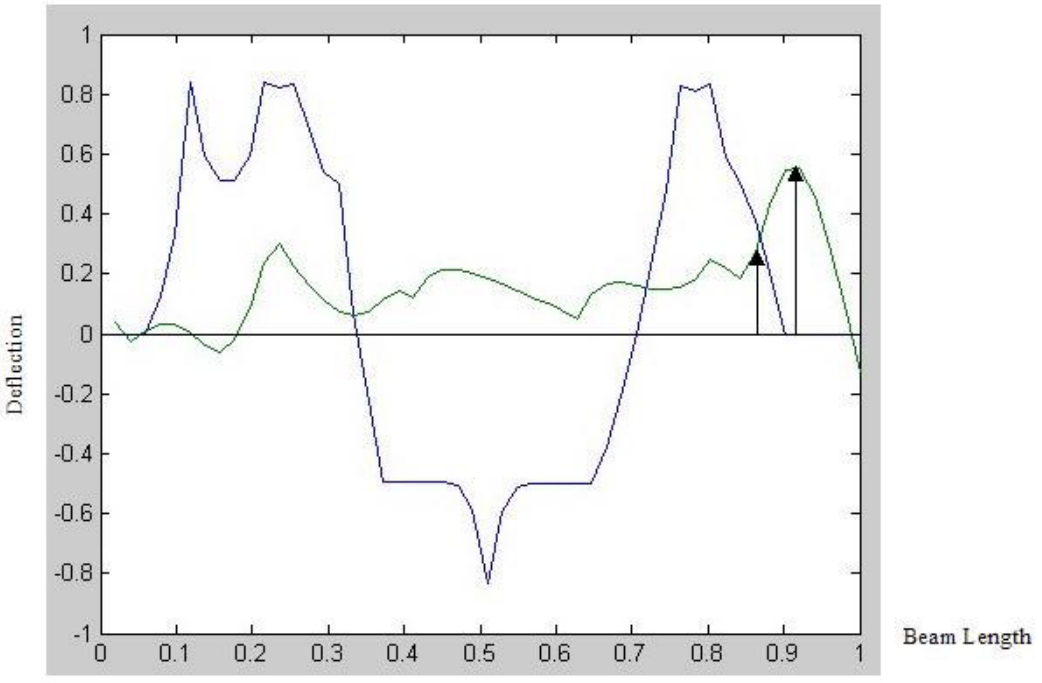

Figure 7-26. Second new fuzzy *MSF* and the difference between the mode shape and the experimental modal analysis, and the Error Vectors.

Third new rule is determined based on the Error Vectors in Figure 7-26. The Error Vectors for the most of the region is less than 0.25 and it is considerable only at the end of the mode shape. Therefore the third new rule can be introduced as in Table 7-6.

Table 7-6. New fuzzy rules.

Frequency	Fuzzy rules	New rules I	New rules II	New rules III
Length ($\times 1/5\times n$)	Second natural frequency			
1	*Z*	*Z*	*Z*	*Z*
2	*Z*	*Z*	*Z*	*Z*
3	*PM*	*PL*	*PL*	*PL*
4	*PM*	*Z*	*PM*	*PM*
5	*PL*	*PL*	*PL*	*PL*
6	*PL*	*PM*	*PL*	*PL*
7	*PL*	*PM*	*PM*	*PM*
8	*PM*	*Z*	*NM*	*NM*
9	*PM*	*Z*	*NM*	*NM*
10	*Z*	*NM*	*NM*	*NM*
11	*NM*	*NL*	*NL*	*NL*
12	*NM*	*Z*	*NM*	*NM*
13	*NL*	*Z*	*NM*	*NM*
14	*NL*	*Z*	*NM*	*NM*
15	*NL*	*Z*	*Z*	*Z*
16	*NM*	*PM*	*PL*	*PL*
17	*NM*	*PL*	*PL*	*PL*
18	*Z*	*PM*	*PM*	*PL*
19	*Z*	*Z*	*Z*	*PM*

After using modal analysis to update the third new fuzzy *MSF* and using neural network to drive the mode shape then the final mode shape can be determined as in Figure 7-27.

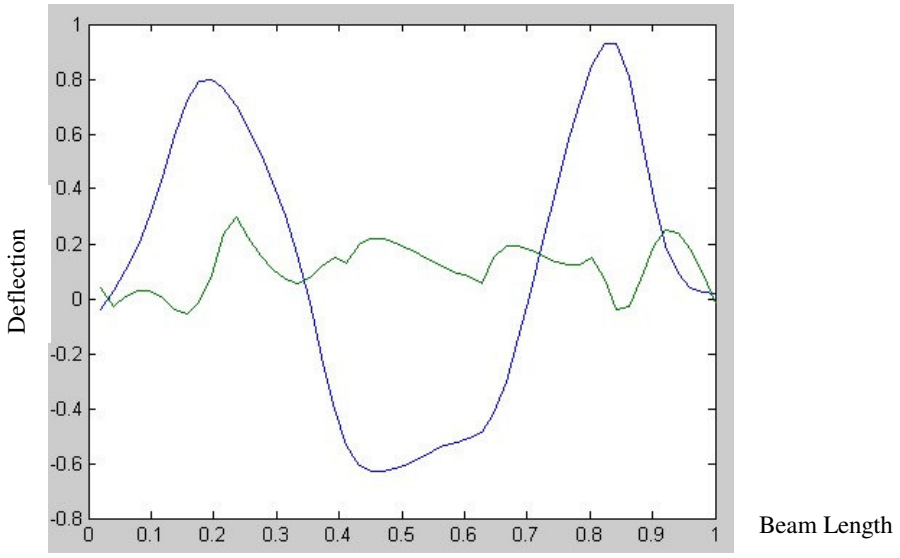

Figure 7-27. Third mode shape after the rule corrections.

In this mode shape the error vectors are less than 0.25. Therefore there are no more changes or corrections in the fuzzy rules. In this stage the overall error between this mode shape and the experimental modal analysis mode shape is calculated. The error magnitude is 17.24%. As this error is less than 20% then this mode shape is considered as an acceptable mode shape for the third mode shape of a clamped-clamped beam. In the above correction procedure the fuzzy rule correction is repeated 3 times to achieve an acceptable mode shape.

7.2. Two-dimensional elastic bodies

An example of a plate is presented in this section. The procedure of the method is the same as the beam example. The differences are explained in the example.

7.2.1. Example 2

A clamped-free-clamped-free plate is considered in this example (Figure 7-28).

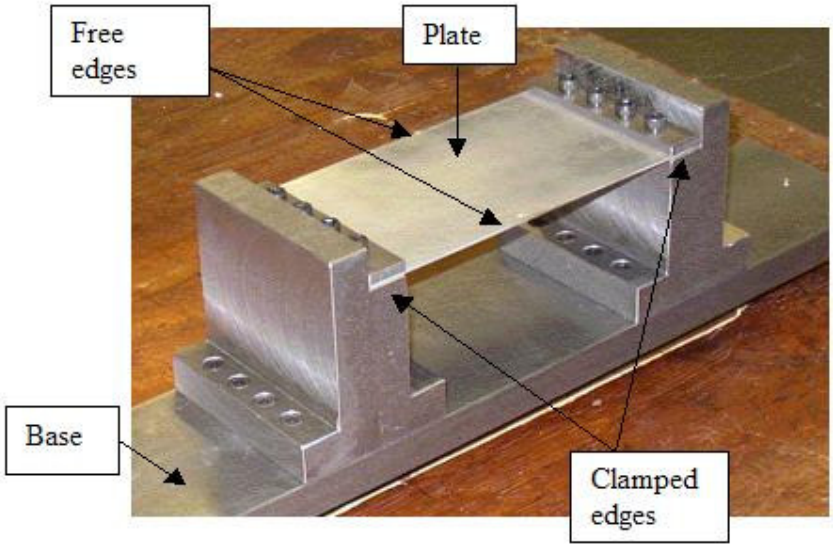

Figure 7-28. A Clamped-free-clamped-free beam.

The differences in this example with one-dimensional bodies are stated below.

1) There are two position inputs along two edges of the plate (X and Y in Figure 7-29).

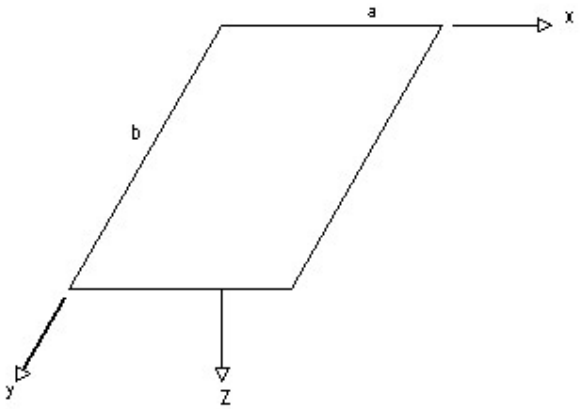

Figure 7-29. X and Y as two position inputs.

Input fuzzy membership functions for X position, Y position and frequency are presented in Figure 7-30-33.

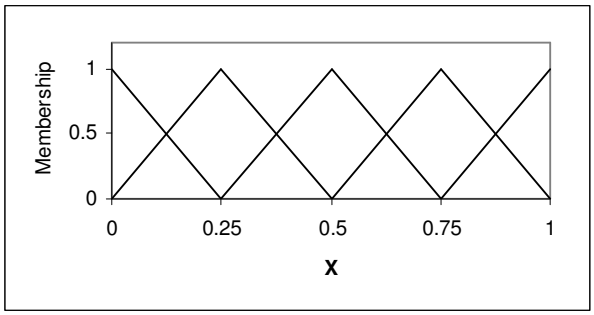

Figure 7-30. Input 1 (X position) membership functions.

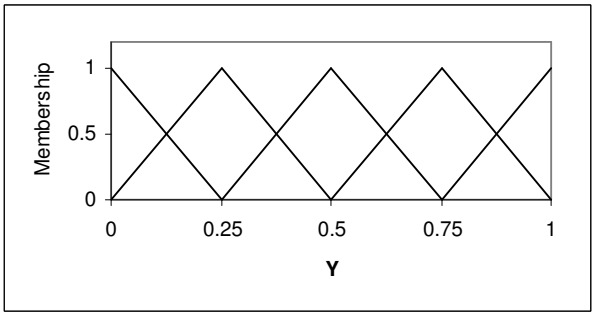

Figure 7-31. Input 2 (Y position) membership functions.

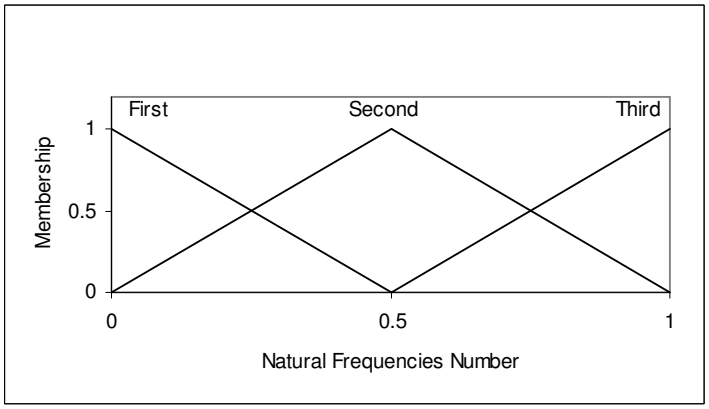

Figure 7-32. Input 3 (frequency) membership functions.

Output or deflection membership function is presented in Figure 7-33.

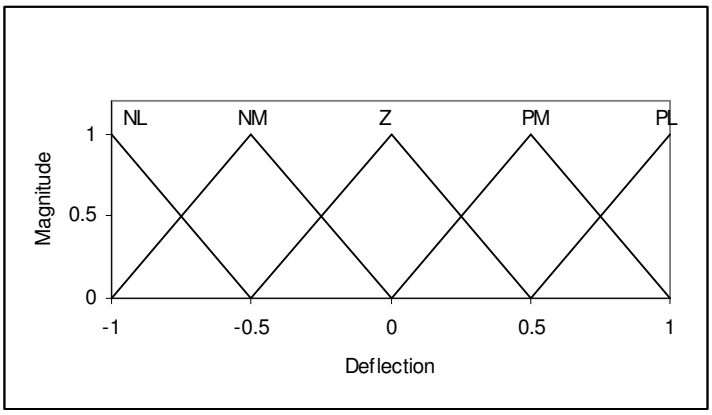

Figure 7-33. Output (deflection) membership functions.

The fuzzy rules to construct the mode shapes of the plate up to the 3rd mode shape are presented in Table 7-7 and 8.

Table 7-7. Fuzzy rules to construct the first fuzzy *MSF* of the plate.

Y	X	0	0.25	0.5	0.75	1
0		Z	PM	PL	PM	Z
0.25		Z	PM	PL	PM	Z
0.5		Z	PM	PL	PM	Z
0.75		Z	PM	PL	PM	Z
1		Z	PM	PL	PM	Z

Table 7-8. Fuzzy rules to construct the second fuzzy *MSF* of the plate.

Y	X	0	0.25	0.5	0.75	1
0		Z	PL	Z	NL	Z
0.25		Z	PL	Z	NL	Z
0.5		Z	PL	Z	NL	Z
0.75		Z	PL	Z	NL	Z
1		Z	PL	Z	NL	Z

Table 7-9. Fuzzy rules to construct the third *MSF* of the plate.

Y	X	0	0.25	0.5	0.75	1
0		Z	PL	NL	PL	Z
0.25		Z	PL	NL	PL	Z
0.5		Z	PL	NL	PL	Z
0.75		Z	PL	NL	PL	Z
1		Z	PL	NL	PL	Z

The fuzzy *MSFs* from above membership functions and rules are presented in Figure 7-34.

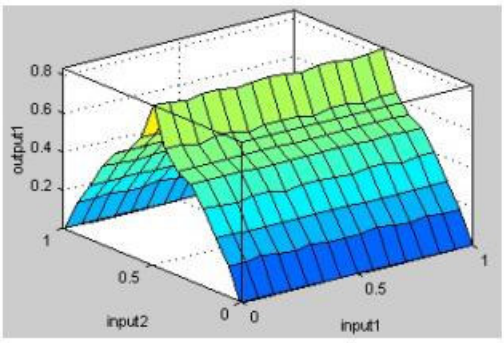

a) The first fuzzy *MSF*.

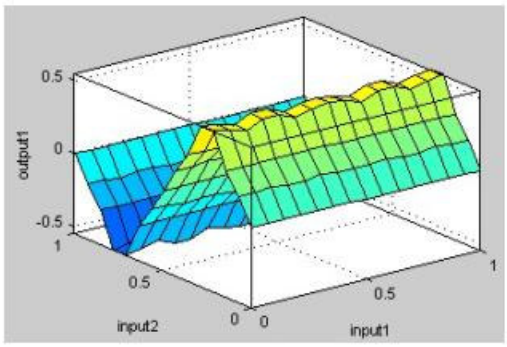

b) The second fuzzy *MSF*.

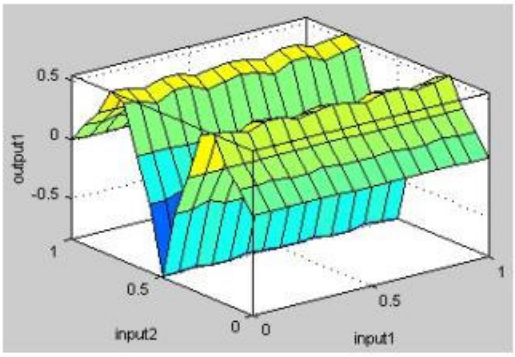

c) The third fuzzy *MSF*.

Figure 7-34. Plate fuzzy *MSFs* that are obtained from the membership functions and the rules presented above.

2) The SIMULINK fuzzy controller consist of three inputs. Two inputs are designed for position and one input for natural frequency (Figure 7-35).

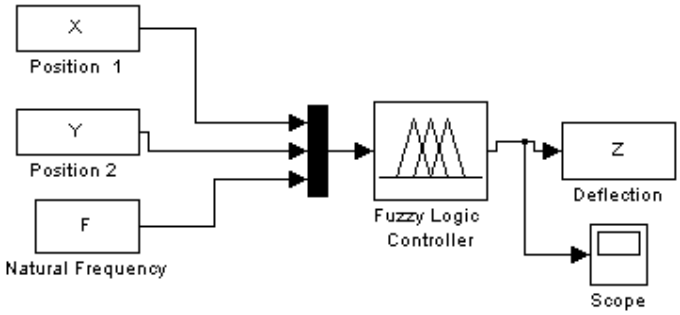

Figure 7-35. SIMULINK fuzzy controller to obtain the output from the inputs.

3) The experimental modal analysis is carried out in two dimensions. The plate is modelled by measuring 6 points on the plate (Figure 7-36).

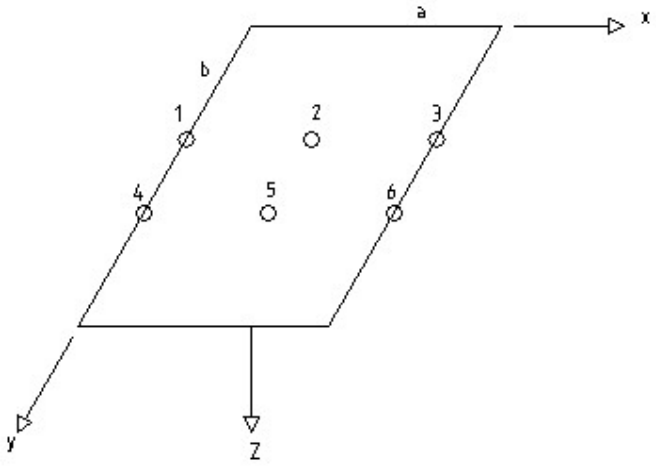

Figure 7-36. Experimental *FRF* measurement points on the plate.

The mode shape can be obtained using the Peak-Picking method. This method is introduced in Chapter 5 and 6. The mode shapes are presented in Table 7-10 (*FRF* results are presented in Appendix D).

The corresponding fuzzy *MSFs* for points 1 to 6 are replaced by the experimental deflection results in Table 7-10. Replacing or updating these data are performed for modes 1 to 3. Updated mode shapes are not smooth surfaces. After updating the fuzzy

data by experimental data the mode shapes are smoothed by interpolating the mode shape surfaces using neural network.

Table 7-10. Deflections of points 1 to 6.

Mode	Point Number	1	2	3	4	5	6
1		0.51	0.52	0.50	0.49	0.54	0.48
2		-1.1	-1.3	-0.99	1.0	1.2	0.98
3		0.99	1.1	1.3	1.2	0.98	1.0

4) Neural networks consist of two inputs and one output where the two inputs include position inputs (Figure 7-37)

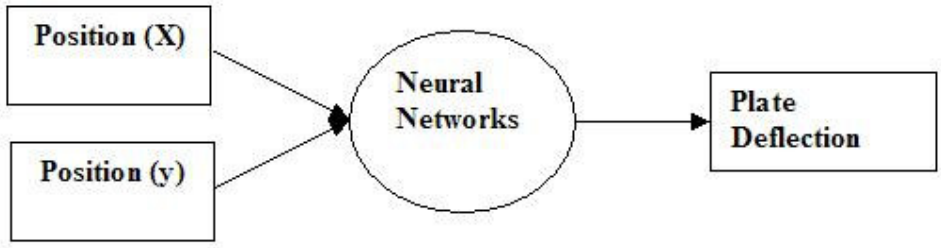

Figure 7-37. Neural networks inputs and output.

Mode shape results are presented in Figure 7-38.

The error in this example is investigated using a corresponding FE model. ANSYS software [42] is used to obtain the vibration model of the clamped-free-clamped-free plate in order to compare the result in this research with FE results. In the FE modelling, the material property of the plate (Figure 7-28) is aluminium with module of elasticity of 71 N/mm² and specific weight of 2.7 Kg/m³. The width of the plate is 100 mm, the length is 180 mm and the thickness is 2 mm. Maximum error of 18.9% occurred in the third mode. Errors of 15.1% and 17.3% occurred in the second and first mode shapes respectively.

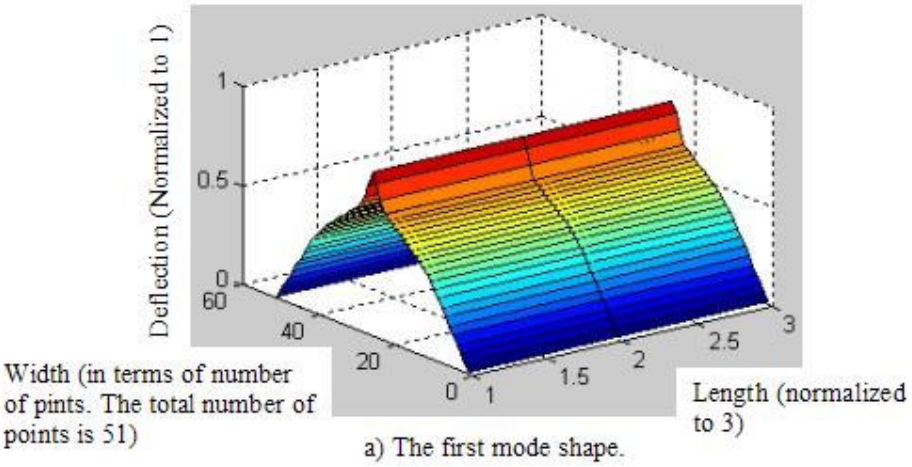

a) The first mode shape.

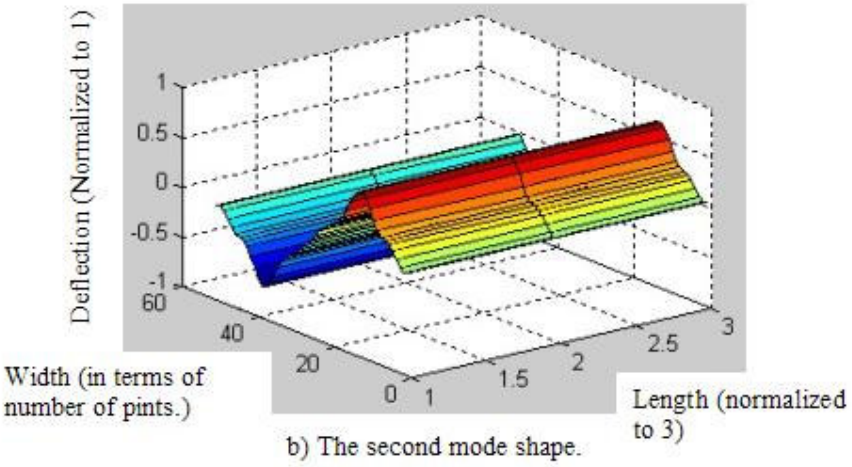

b) The second mode shape.

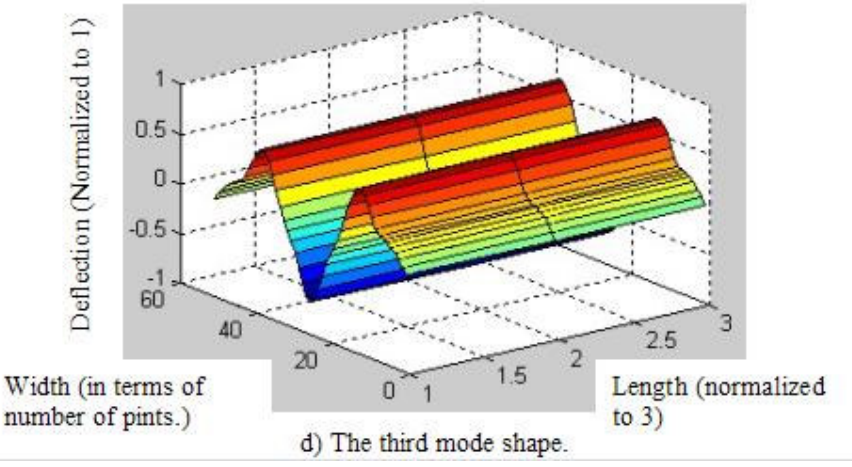

d) The third mode shape.

Figure 7-38. Plate Mode shapes, a) Mode 1, b) Mode 2, and c) Mode 3.

7.3. Structures

A 3-beam structure is presented here as an example. The procedure of the method is the same as Examples 1 and 2. The differences are explained in the example.

7.3.1. Example 3

A 3-beam structure is considered here as an example (Figure 7-39).

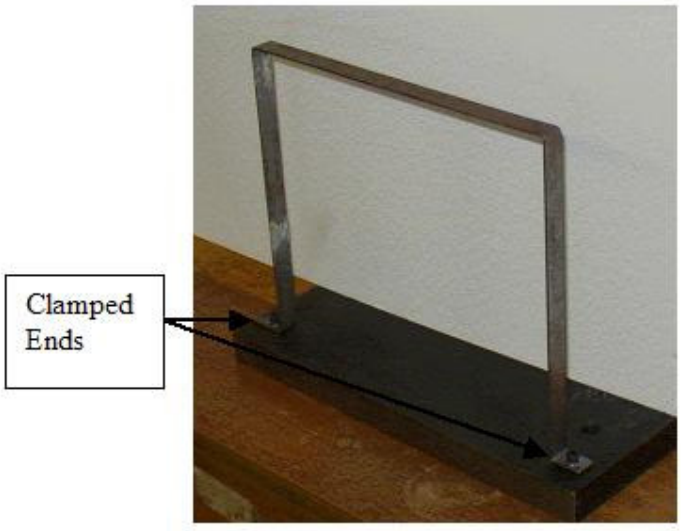

Figure 7-39. A 3-beam structure.

The differences in this example with one-dimensional bodies are stated below.

1) Mode shape forms of the structure for modes 1 and 2 are presented in Figure 7-40 and Figure 7-41. The corresponding fuzzy deflections are presented on each figure. Each fuzzy deflection is introduced for each beam relative to the position of the beam before deflection. *N*, *Z* and *P* notations represent Negative, Zero and Positive fuzzy deflections. However introducing the fuzzy deflection is not a unique approach and any other linguistic terms such as Large, Small and etc. can be introduced. These fuzzy deflections can be introduced for any arbitrary position on the beam too. This is the flexibility of application of fuzzy reasoning in this method. Another advantage of this method is that user described

deflection in local coordinates and question of coordinate transformation does not appear.

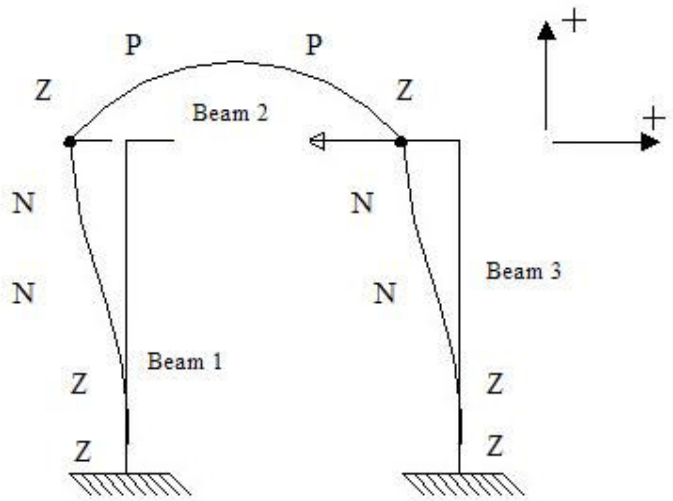

Figure 7-40. Mode Shape Form 1 with the corresponding fuzzy deflections.

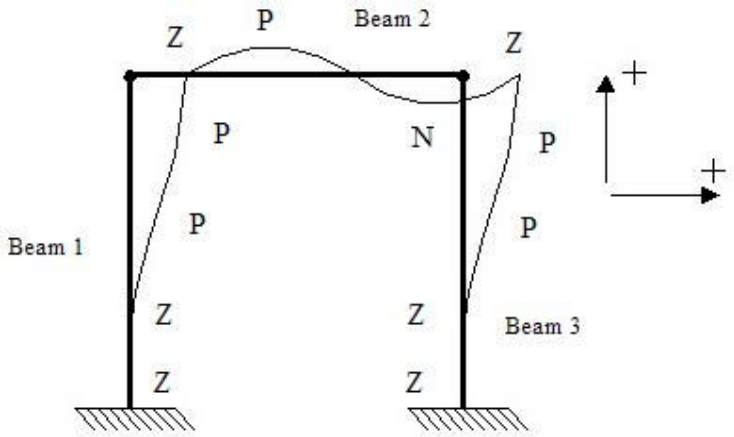

Figure 7-41. Mode Shape Form 2 with the corresponding fuzzy deflections.

Membership functions are presented in Figure 7-42.

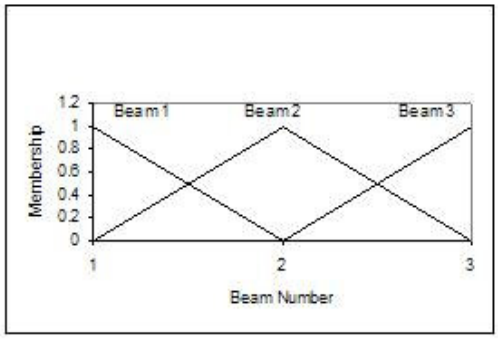

a) Input 1 (beam number) membership functions.

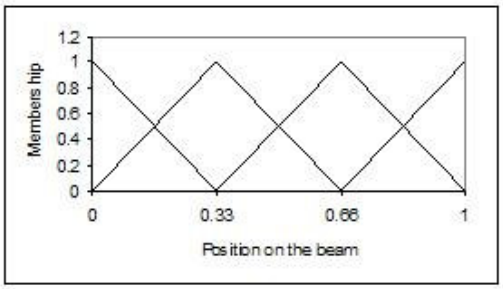

b) Input 2 (position) membership functions.

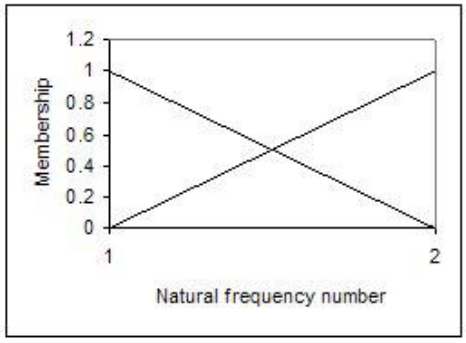

c) Input 3 membership functions.

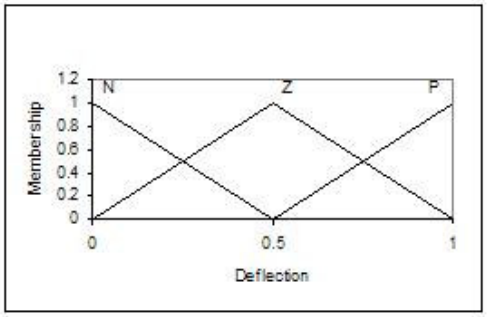

d) Output (deflection) membership functions.

Figure 7-42. Inputs and output membership functions a) Input 1 (Beam Number), b) Input 2 (Position on the beam), c) Input 3 (Natural frequency number), d) Output (Deflection).

The corresponding fuzzy rules for these Mode Shape Forms are presented in Table 7-11 and 12.

Table 7-11. Fuzzy rules for the first *MSF*.

Beam No.	**Position**	**0**	**0.333**	**0.666**	**1**
1		Z	Z	N	N
2		Z	P	P	Z
3		N	N	Z	Z

Table 7-12. Fuzzy rules for the second *MSF*.

Beam No.	Position 0	0.333	0.666	1
1	Z	Z	P	P
2	Z	P	N	Z
3	P	P	Z	Z

2) The SIMULINK fuzzy controller consists of three inputs. Input 1 is considered for the beam number. Input 2 gives the position on the beam. Input 3 is included the interested natural frequency (Figure 7-43). The output is the fuzzy *MSFs*.

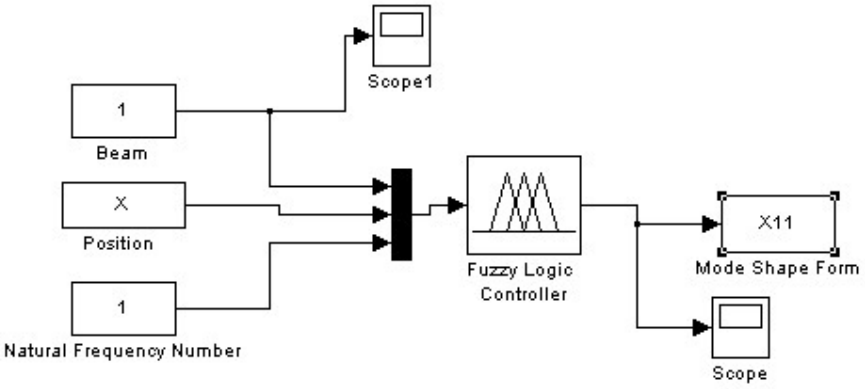

Figure 7-43. SIMULINK fuzzy controller for obtaining the output from inputs. In this figure, beam number 1 is considered for the first natural frequency where the output is the first *MSF* (X11).

Fuzzy mode shape forms are presented in Figure 7-44.

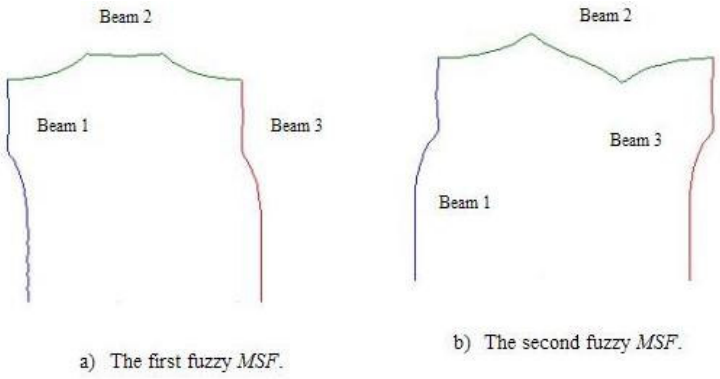

Figure 7-44. Fuzzy Mode Shape Forms derived from SIMULINK.

3) The experimental modal analysis is carried out in two dimensions. Positions of accelerometers are demonstrated in Figure 7-45. Direction of motions of accelerometers is shown with arrows in each position.

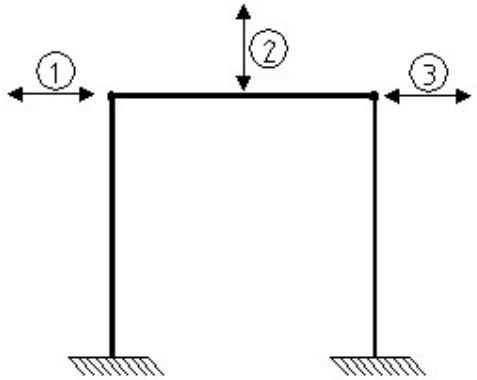

Figure 7-45. Position of accelerometers on the structure and the direction of motion of each accelerometer.

Experimental mode shapes are presented in Table 7-13 (*FRF* results are presented in Appendix D). Positions 1, 2 and 3 are demonstrated in Figure 7-45.

Table 7-13. Experimental mode shapes.

Mode	**Position**	**1**	**2**	**3**
1		-1.1	0.86	-0.94
2		0.97	0.04	1.2

Now the fuzzy *MSFs* are updated by experimental mode shape results. This modification is performed by replacing the fuzzy *MSFs* data by the corresponding experimental data. In the next stage, updated fuzzy *MSFs* are smoothed using neural networks.

4) Neural networks consist of one input and one output (Figure 7-46).

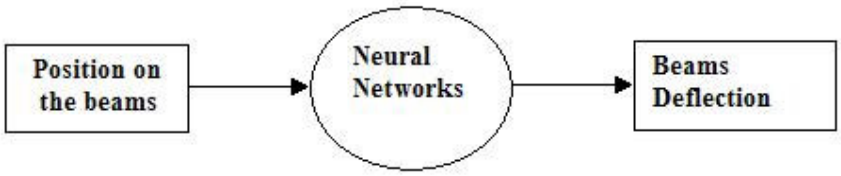

Figure 7-46. Neural networks input and output.

After the neural networks procedure, 3 beams are assembled together. This assembly is performed by placing beams 1, 2 and 3 together in each mode as shown in Figure 7-47.

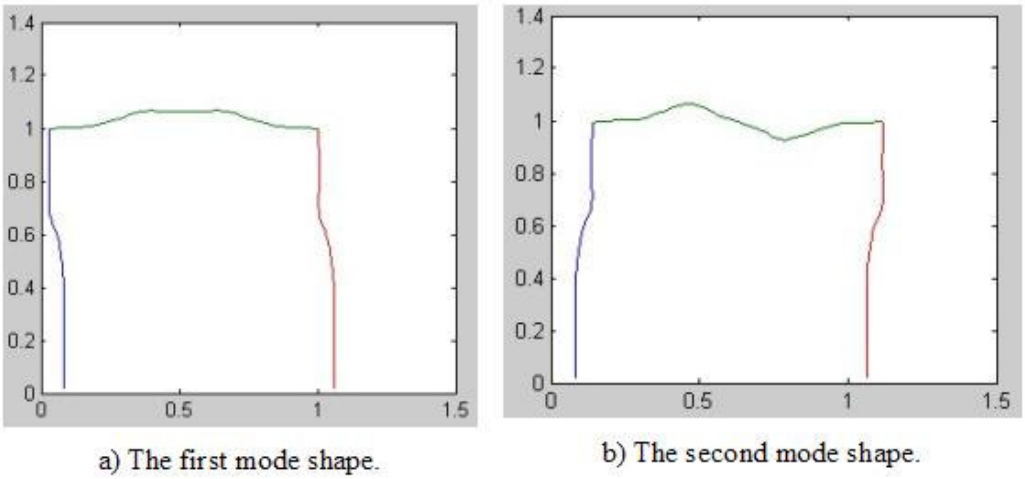

a) The first mode shape. b) The second mode shape.

Figure 7-47. Mode shapes after neural network procedure (beam length is normalized to 1).

A corresponding FE model is used to obtain the error in this example. ANSYS package [42] is used to obtain the vibration model of the frame in order to compare the result in this research with FE results. In the FE modelling, the material property of the frame (Figure 7-39) is steel with module of elasticity of 200 N/mm² and specific weight of 7.9 Kg/m³. The beams of the frame are built from 200 mm length, 15 mm width and 2 mm thickness. An Error of 19.83% occurred in the first mode and 16.41% in the second mode.

7.4. Mode Expansion: Example 4

An example of a clamped-free beam is presented here. There are four differences between this example and example 1.

1) Boundary conditions are different.
2) Experimental *FRF* measurement is not preformed in equal distance positions.
3) The mode shapes are obtained up to 8^{th} natural frequency.
4) Other forms of fuzzy rules are presented to show the flexibility of the fuzzy systems.

The rest of the procedure is the same. The procedure is presented below.

The first input of the fuzzy model is the beam length. Figure 7-48 illustrates the membership functions of the first input. The beam length is taken to be normalised to 1.

The second input of the fuzzy model is frequency. Figure 7-49 shows the membership function of the second input. The region of frequency input is designed to demonstrate first to eighth natural frequency. The magnitude of the natural frequencies is measured by an experimental test or a *FRF* curve. In the frequency membership function the number that represent the first, second and third etc. natural frequency are used to identify the membership functions. For this purpose the natural frequency magnitudes are not used.

The output of the fuzzy model is the deflections of the beam or the mode shapes. Figure 7-50 shows the membership function of the output that is based on the *NL, NLM, NM, ZNM, Z, ZPM, PM, PLM* and *PL.*

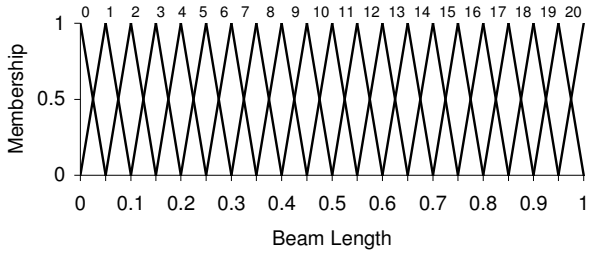

Figure 7-48. The first input (beam length) membership functions.

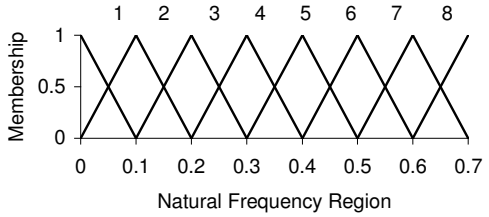

Figure 7-49. The second input (frequency) membership functions up to 8th natural frequency.

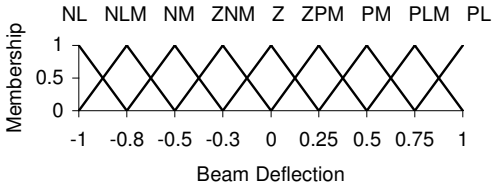

Figure 7-50. Output (deflection) membership functions.

Fuzzy rules are defined based on the boundary conditions of the beam and the approximate mode shapes of each natural frequency.

For example in second natural frequency the mode shape of the beam is, zero (*Z*) and will go up to positive large (*PL*) and this is followed by going down to negative large (*NL*) and again zero (Figure 7-51). However medium regions can be introduced in the middle of large and zero regions (by *ZM*, *M*, and *LM* that can be either positive (*P*) or negative (*N*) too).

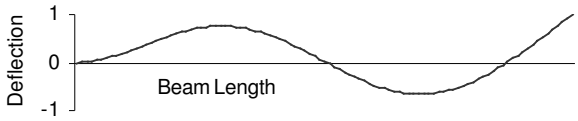

Figure 7-51. A general view of the second mode shape of a Clamped-Free beam without exact deflection magnitudes.

As the beam is Clamped-Free then the boundary conditions present zero deflections at one end. The zero slope is defined by having two zero at the end (zero at length positions 0 and 1 at the first end as shown in Table 7-14). The fuzzy rules based on the approximate mode shapes are presented in Table 7-14. These rules are created for a clamped-free beam up to 8th mode shape.

Table 7-14. Fuzzy rules up to eighth-natural frequency

Natural Frequency								
Beam Length	**1**	**2**	**3**	**4**	**5**	**6**	**7**	**8**
0	*Z*	*Z*	*Z*	*Z*	*Z*	*Z*	*Z*	*Z*
1	*Z*	*Z*	*Z*	*Z*	*Z*	*Z*	*PM*	*Z*
2	*Z*	*Z*	*ZPM*	*PM*	*PM*	*PM*	*PLM*	*PM*
3	*ZPM*	*ZPM*	*PM*	*PL*	*PLM*	*PLM*	*Z*	*PLM*
4	*ZPM*	*ZPM*	*PM*	*PL*	*PM*	*PM*	*NLM*	*PM*
5	*ZPM*	*ZPM*	*PLM*	*PL*	*Z*	*Z*	*NM*	*Z*
6	*ZPM*	*ZPM*	*PLM*	*PM*	*NM*	*NM*	*Z*	*NM*
7	*PM*	*PM*	*PLM*	*Z*	*NLM*	*NLM*	*ZPM*	*NLM*
8	*PM*	*PM*	*PM*	*ZNM*	*NM*	*Z*	*PM*	*Z*
9	*PM*	*PM*	*ZPM*	*NLM*	*Z*	*PLM*	*ZPM*	*PLM*
10	*PM*	*PM*	*Z*	*NLM*	*PM*	*PM*	*Z*	*Z*
11	*PM*	*ZPM*	*ZNM*	*NLM*	*PLM*	*Z*	*ZNM*	*NLM*

12	*PM*	*ZPM*	*NM*	*ZNM*	*PM*	*NM*	*NM*	*Z*
13	*PLM*	*Z*	*NM*	*Z*	*Z*	*NLM*	*Z*	*PLM*
14	*PLM*	*Z*	*NLM*	*PM*	*NM*	*NM*	*PM*	*Z*
15	*PLM*	*ZNM*	*NM*	*PM*	*NLM*	*Z*	*PLM*	*NLM*
16	*PLM*	*ZNM*	*ZNM*	*PLM*	*NLM*	*PM*	*Z*	*Z*
17	*PLM*	*NM*	*Z*	*PM*	*NM*	*PLM*	*NM*	*PLM*
18	*PL*	*NM*	*ZPM*	*Z*	*Z*	*PM*	*NLM*	*PM*
19	*PL*	*NL*	*PM*	*NM*	*PM*	*Z*	*Z*	*Z*
20	*PL*	*NL*	*PL*	*NL*	*PL*	*NM*	*PM*	*NM*

The mode shapes created from the membership functions in Figure 7-48 to 7-50 and fuzzy rules in

Table **7-14** are illustrated in Figure 7-52.

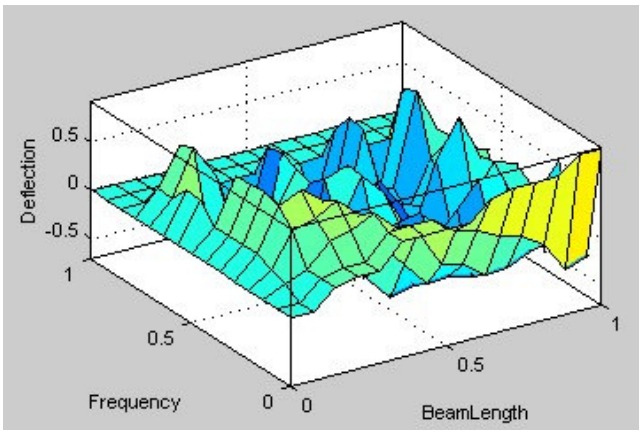

Figure 7-52. The guessed mode shapes created by fuzzy membership functions and rules.

As it is mentioned earlier, input 1 is the position on the beam and input 2 is the natural frequency. The SIMULINK toolbox of MATLAB software is used to generate fuzzy beam deflections (output) from the beam length and frequency (inputs). This is illustrated in Figure 7-53.

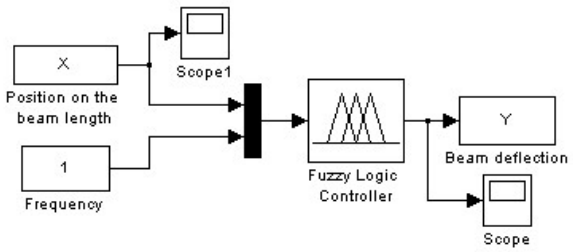

Figure 7-53. MATLAB SIMULINK fuzzy controller for generating the output from inputs.

To illustrate the generation of fuzzy function, if the position on the beam is varied between, x=0 to 1 and the frequency input is the 2nd natural then the output (or Y in Figure 7-53) will be 2nd mode shape of the beam. This output is shown in Figure 7-54(a). By performing this procedure for other natural frequency inputs, deflection (output) for the other mode shapes are derived (Figure 7-54(b) shows the 5th mode as another example).

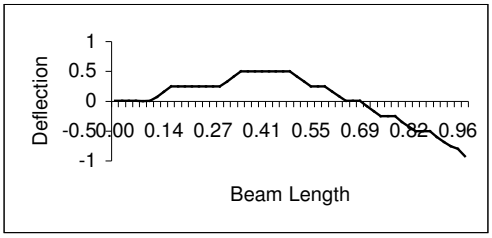

a) Mode 2

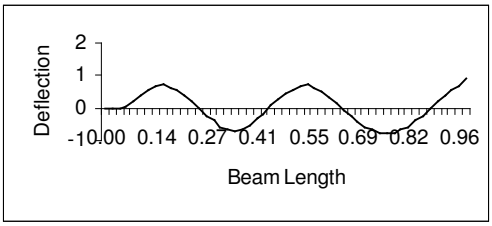

b) Mode 5

Figure 7-54. Mode shapes from fuzzy model before modification, a) The second fuzzy *MSF*, b) The fifth fuzzy *MSF*.

After obtaining the approximate mode shapes (or fuzzy *MSFs*), these *MSFs* are to be modified using experimental data from a real system. Modification of the fuzzy model using experimental modal parameters is discussed below.

In this section an incomplete four-degree of freedom model is derived by modal analysis. Here the complete model refers to a model that the experimental *FRF* measurements are carried out in 8 equal distances points on the beam where beam is divided to 8 points. In this case an incomplete four-degree of freedom model refers to a beam that is divided to 8 segments (and 8 points) but only four points on the beam is measured experimentally in obtaining *FRFs*. These four points are selected from the first four points on the clamped end section of the beam. The experimental rig is shown in Figure 7-55. In this figure the accelerometer is placed in the third point on the beam from the clamped end or left end in the figure.

Figure 7-55. A clamped-Free beam.

An accelerometer is attached to the beam to receive the oscillation signals. A charge amplifier is used to amplify and send the signals to the data acquisition card. The data acquisition card (PCI230) is assembled to a Pentium PC. AgilentVEE software is used to find the *FRF* curves.

The beam dimensions are 500 mm length, 10 mm thickness and 20mm width. The material is steel. The boundary condition is clamped-free.

Before finding the eigenvectors (mode shapes) of the beam from *FRF* signals, calibration of *FRF* is performed by using a suspended (0.5kg) mass. In this calibration Fourier transform of accelerometer signal divided by Fourier transform of the hammer impulse and the peak value result of the division is equalled to one over mass value (1/488.50). Fourier transform of both signals (accelerometer and hammer) are found by AgilentVEE software. The calibration procedure is explained in Chapter 6, experimental setup.

After calibrating *FRF* values, the *FRF* from experimental modal analysis can be used to extract the eigenvectors of the model. The experimental procedure is described below. To obtain an incomplete four-degree of freedom model of the beam, the beam is divided to 8 equal segments, to have 8 points on the beam. Four points are selected to measure experimentally from these eight points (here, first four points from the clamped end). Corresponding four positions are, 62.5mm, 125mm, 187.5mm, 250mm from the clamped end (where the beam length is 500 mm). An accelerometer is attached to the beam and the instrumented hammer is used to excite the beam. The accelerometer is placed in each of four selected positions and the instrumented hammer is used to excite the beam in each four selected points. Sixteen excitations with hammer are applied to the beam corresponding to different combination of accelerometer and hammer excitation positions. Fast Fourier transform of hammer excitation and accelerometer signals are found by AgilentVEE software. Fourier transforms of accelerometer signals are divided by Fourier transform of the signals from hammer in order to obtain *FRF* values. Four by four *FRF* matrix is obtained from sixteen *FRF* data in this experiment. As one row of *FRF* matrix is usually enough to drive the mode shapes so the accelerometer can be placed to one position and hammer excitation can be applied to all four positions. A row of the *FRF* matrix can be constructed by h_{11}, h_{12}, h_{13} and h_{14}. These results are obtained by placing the accelerometer on point 1 and hitting the beam by the hammer on points 1, 2, 3, and 4. Peak-picking method is performed to extract the modal constants and eigenvectors from the *FRF* matrix. This method is presented in Chapter 5 and 6. The experimental results are demonstrated in Table 7-15 (*FRF* curves are presented in Appendix D). Table 7-15 is included first four mode shapes described by 4 measurement positions on the beam. The beam length is normalized to one so the positions on the beam regarding the experimental mode shape measurements include 0.1, 0.2, 0.3 and 0.4.

From Chapter 3, equation (25), we have:

$$u_{ik}u_{lk} = |h_{il}|_k \zeta_k \omega_{nk}^2$$

In this equation i and l are the accelerometer position and excitation position respectively. For example if the accelerometer is placed in 0.1 position and the excitation is applied to position 0.2 then the equation can be presented as below.

$$u_{1k}u_{2k} = |h_{12}|_k \zeta_k \omega_{nk}^2$$

Table 7-15. Normalized mode shapes from experimental modal testing

Position on the beam (normalise)				
Mode shape	**0.1**	**0.2**	**0.3**	**0.4**
1st	0.0259	0.0973	0.2048	0.3395
2nd	0.1379	0.4173	0.6542	0.7137
3rd	0.3254	0.7245	0.6177	0.0197
4th	0.5193	0.6852	-0.1304	-0.7071
5th	0.6733	0.2852	-0.691	0.0009
6th	0.7512	-0.2639	-0.3921	0.7072
7th	0.7325	-0.6502	0.3931	0
8th	0	0.6142	-0.6519	0.6936

The important note in this example is, k that is the number of peaks in the *FRF* curve is not limited to the measurement points. The reason is, each *FRF* curve have any arbitrary number of peaks. More *FRF* peaks are appeared by simply expanding the frequency range of the *FRF* measurement. Therefore in this example, k can be from 1 to any arbitrary number depending on the frequency range of the *FRF* measurement. This frequency range can be adjusted experimentally in order to represent all the sufficient peaks. Consequently, although i and l are limited to the number of *FRF* measurements, but k is not limited. Therefore the experimental mode shapes (u_{ik} or u_{lk}) that are obtained from above equation can be expanded to k number of natural frequency as long as the *FRF* curve includes the k^{th} natural frequency. This allows us to have experimental mode shape up to any arbitrary natural frequency regardless of the limitation of the measurement points. However this mode shape only exhibits in the measured points. This is shown in the following section.

The experimental mode shapes from Table 7-15 are used to modify the fuzzy *MSFs*. Fuzzy *MSFs* are presented in Figure 7-54. Experimental mode shape is derived for an incomplete 4DOF model. Figure 7-56 shows examples of complete and incomplete mode shapes for second, forth and sixth modes. In the presented method, the incomplete set of mode shape data are used to update the models and the complete

8DOF model is presented in the figures for better understanding the difference between complete and incomplete experimental mode shapes.

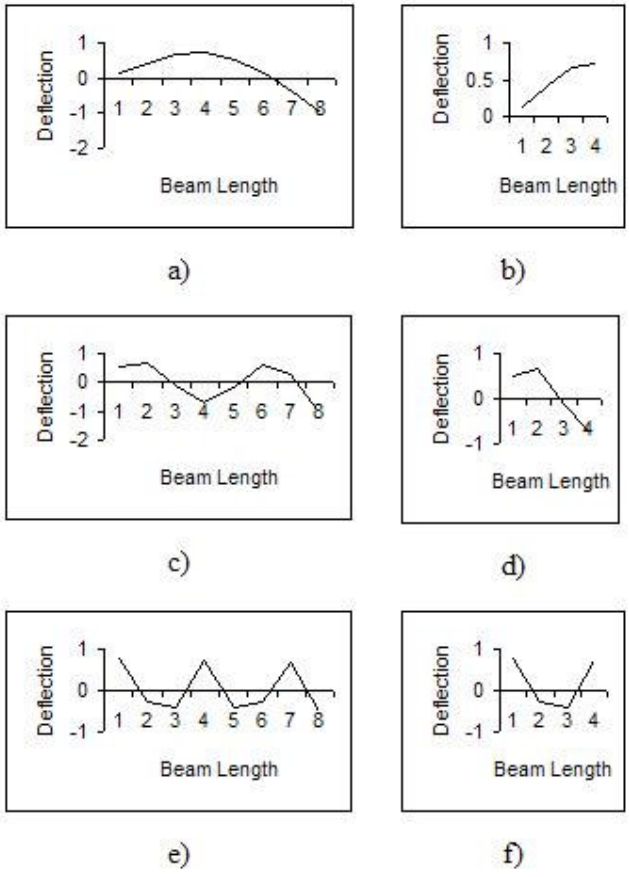

Figure 7-56. Normalized experimental measured mode shapes from table 7-2, a) 2nd Complete mode shape, b) 2nd incomplete mode shape, c) 4th Complete mode shape, d) 4th incomplete mode shape, e) 6th Complete mode shape, f) 6th incomplete mode shape.

A 4DOF experimental modal analysis is performed but the model is capable of having up to eighth mode shape. The reason is that each *FRF* from 4DOF modelling consists of all the natural frequency peaks (as well as eighth for example), so these peaks can be used to find the model up to any frequency range (as explained earlier in this example). The only limitation is that this model shows the mode shapes for four points on the beam or for the points that the experimental measurements are performed. The mode shape for the other points except these four points is not available.

Data from Table 7-15 are used to modify the fuzzy *MSFs* in Figure 7-54. In this stage the modification is performed simply be replacing the fuzzy *MSFs* data with the corresponding experimental data (in this example four points for each mode). Next stage of the modification is to drive smooth curves from these mode shapes, as there are some spikes in the curves generated due to the difference between the experimentally measured points and guessed mode shape.

The mode shapes are derived from the updated fuzzy *MSFs* as explained before. Experimental measurements were carried out at 4 positions by simply replacing the points in the fuzzy *MSF* data with the corresponding points from the experimental set. The inputs and output fuzzy membership functions are described by 51 points. Both fuzzy neural network and back propagation neural network are used to generate the updated curves (MATLAB software is used). As before, it is found that the fuzzy neural network generates smoother curves compared to back propagation networks. The fuzzy neural network is based on a single input-single output system. The input of the system is the position on the beam. The deflections of the mode shapes are the output of the network. The following procedure is performed to train the network. The input training data include, the position on the beam for each mode shape (here, 51 data). Updated fuzzy *MSFs* are included the output training data of the network (here, 51 data). As eight mode shapes are derived then eight neural networks are introduced for each mode shape individually. The same training procedure is used for each neural network. The trained neural networks determine the mode shapes. By giving the position on the beam as the input of the networks, the deflection of the mode shapes are obtained. Figure 7-57 shows the mode shapes from the presented method and the incomplete and complete experimental models.

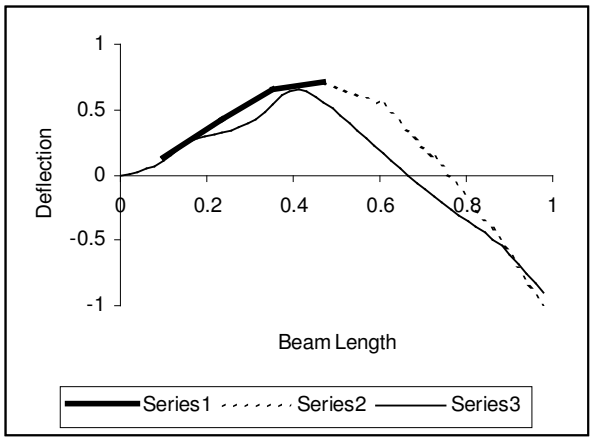

a) The second mode shape.

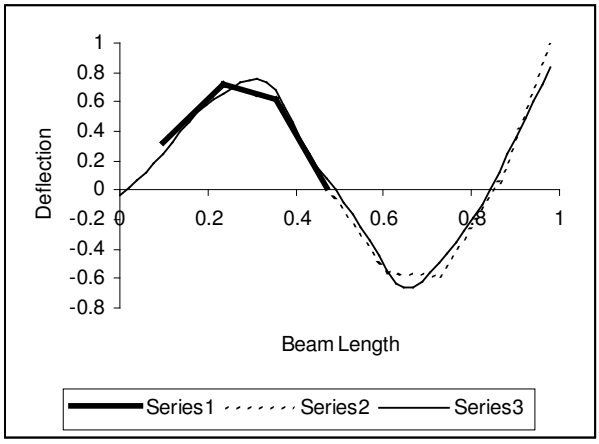

b) The third mode shape.

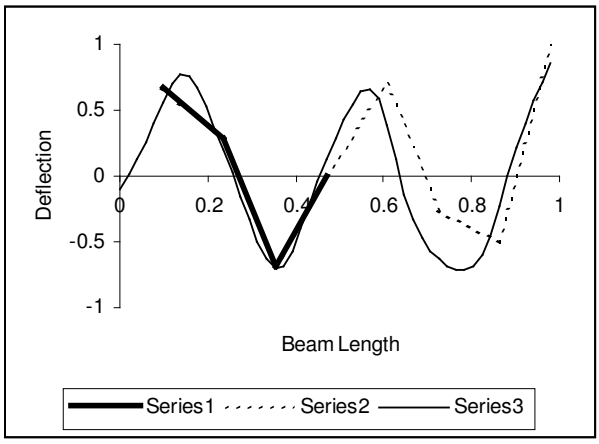

c) The fifth mode shape.

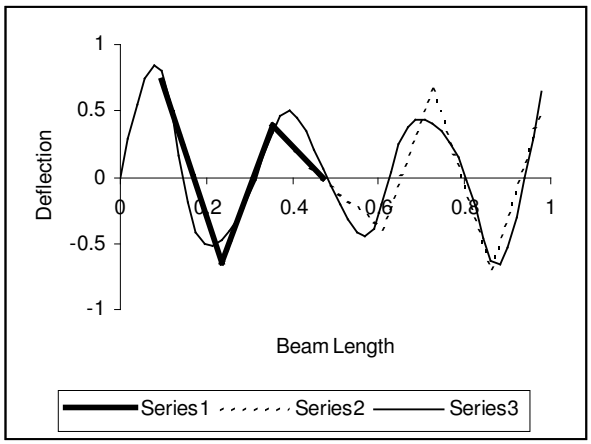

d) The seventh mode shape.

Figure 7-57. The mode shapes, Series1: Incomplete experimental model, Series2: Complete experimental model, Series3: the mode shapes obtained from the proposed method. a) 2nd mode b) 3rd mode d) 5th mode d) 7th mode.

Maximum errors in this example are presented as below. Maximum error of 50% is occurred in seventh mode shape (on position, 0.392, on the beam length) the error is presented in Figure 7-58.

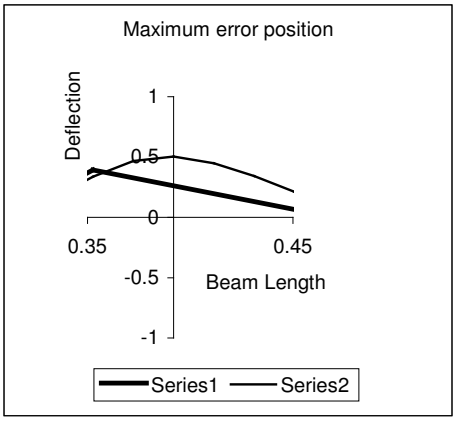

Figure 7-58. The maximum error, Series1: Experimental model, Series 2: proposed model (seventh mode shape)

This error although appears to be rather serious and severe, it is caused between two models with different degrees of freedom. Here a "continuous" model (that is obtained here) is compared with a model with less degree of freedom (incomplete

4DOF modal model) that is only described by linear interpolation with adverse effect on accuracy. The error between continuous model and discrete model must be zero in the positions that the measurement is performed. Then in the proposed model, the maximum error is 41.8% and in most of the other positions it is relatively accurate. This error is demonstrated in Figure 7-59 illustrates the behaviour in the second mode shape between the proposed and experimental models.

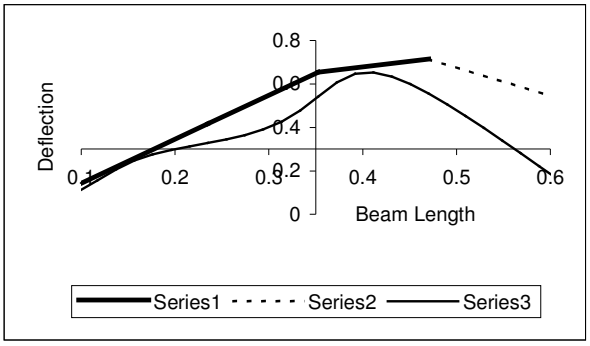

Figure 7-59. Maximum error of the proposed model and experimental model (second mode shape), Series 1: Incomplete experimental model, Series 2: Complete experimental model, Series3: The proposed model.

Here again, the error exists between the proposed model and the complete experimental model where there has been no data to modify the proposed model. In this region the proposed fuzzy model is extrapolated or expanded. Figure 7-60 demonstrates the maximum value of this error that has occurred in second mode shape in position 0.6 along the beam length where no data available to modify the model. This error is 82.8%. However the model is still following the right mode shape trajectory.

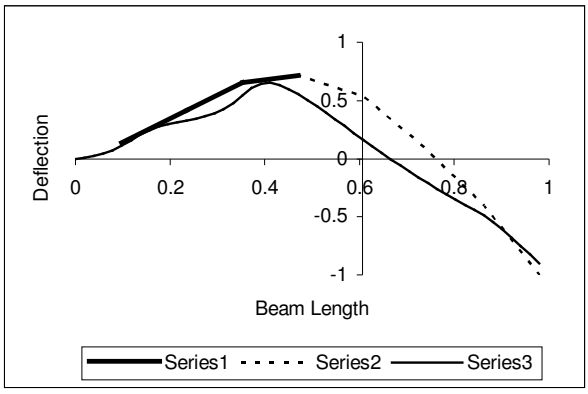

Figure 7-60. The maximum error of the proposed model and experimental model (second mode shape), Series 1: Incomplete experimental model, Series 2: Complete experimental model, Series3: proposed model

As before the result of this example can be presented in time domain using the following equation.

$$\begin{Bmatrix} y_1(t) \\ y_2(t) \\ \vdots \\ y_8(t) \end{Bmatrix}_1 = c_1 \begin{Bmatrix} Y_1 \\ Y_2 \\ \vdots \\ Y_8 \end{Bmatrix}_1 \sin(\omega_{n1} t + \psi_1) + c_2 \begin{Bmatrix} Y_1 \\ Y_2 \\ \vdots \\ Y_8 \end{Bmatrix}_2 \sin(\omega_{n2} t + \psi_2) + \cdots + c_8 \begin{Bmatrix} Y_1 \\ Y_2 \\ \vdots \\ Y_8 \end{Bmatrix}_8 \sin(\omega_{n8} t + \psi_8)$$

Where constants c and ψ can be obtained from displacement and velocity initial conditions.

7.5. Discussion

Example 1 includes a modelling procedure of a clamped-clamped beam. In order to construct the guessed mode shapes (*MSFs*) a fuzzy input is introduced for position on the beam and another input for number of natural frequency. In this example 21 number of membership functions are introduced for position input. Each membership function belongs to a region of the beam. 4 fuzzy membership functions are introduced for natural frequency input to demonstrate the mode shapes up to forth mode. Output membership functions are designed to demonstrate the deflection of

mode shapes. This output consists of 5 memberships including *NL*, *NM*, *Z*, *PM* and *PL*. 76 fuzzy rules introduced to relate the inputs to the output. Alternatively, other kinds of position input and deflection output membership functions can be introduced too. Different number of membership functions and fuzzy rules are used in the other examples to demonstrate the effect of membership functions and rules in the mode shape curves.

Both fuzzy neural network and back-propagation neural network are used to generate the updated curves (MATLAB software used). It is found that the fuzzy neural network generates smoother curves compared to back-propagation networks.
In order to evaluate the error in the proposed method, eigenvectors from the fuzzy model are compared with mathematical mode shape. The proposed method exhibits an error of 15.57%, relative to the mathematical model in the 4^{th} mode. Error in the first, second and third mode shapes are 14.3%, 11.2% and 9.8% respectively.

A discussion is presented in Chapter 7 for the clamped-clamped beam example (example 1) for the situation where a) The guess for the mode shape is wrong and b) There is no guess available for the mode shape. In the first case where the guess for the mode shape is wrong, an initial error of 65.67% is observed. This error is not acceptable. Then the method suggests selecting another mode shape. The error (11.46%) found to be acceptable only when a correct *MSF* is selected. In the second case there is no guess available for the mode shape. Here, fuzzy rules that are used in constructing of fuzzy *MSF* are corrected iteratively to obtain an acceptable version of the *MSF*. First, an available *MSF* with minimum error relative to other available *MSFs* is selected. In this case it was assumed that some guesses are available that correspond to the other natural frequencies and is not the correct mode shape. The method developed describes how fuzzy rules are corrected relative to the experimental modal analysis model. The experimental modal analysis model is the same model that was used for updating procedure. This modal analysis model is a linear interpolation version of the previous modal analysis model. The final version of the *MSF* after correction exhibits a 17.24% error. As this error is less than 20% then this mode shape is considered to be acceptable for the third mode shape of a clamped-clamped beam.

These examples demonstrate the reliability and effectiveness of the methods as they show how wrong *MSFs* can be corrected and new *MSF* can be obtained in the absence of *MSF*s.

Although it was demonstrated that error can be reduced, the methods presented are with certain limitations. The method presented relies on correct guesses of boundary conditions. Therefore the method depends on the possibility to observe of the structure and boundary conditions. Also the method has to be applied with a great care and learning rate has to be controlled to prevent the updated curve from being excessively pulled to the sampling points in the vicinity of sampling points. This is important, especially if the errors between fuzzy curve and measured points are high. This problem somewhat compromises the robustness of the proposed method, however the problem is surmountable and apart from neural network solution other numerical methods for curve smoothing may be devised (although no attempt was made to do this).

Example 2 involves modelling of a two dimensional body. A clamped-free-clamped-free plate was considered in this example. This example, compared to example 1 has another input. This is an extra position input (or geometry input) as the system is of two dimensions. The rest of the procedure is the same as example 1. In this example, different than example 1, 5 membership functions were used in each input. The proposed method result was compared with a FE model. The maximum error of 18.9% occurred in the third mode shape. Errors of 15.1% and 17.3% occurred in the second and first mode shapes respectively.

Example 3 demonstrates the application of the method regarding structural modelling. In this example a 3-beam structure was considered for modelling. Here, compared to example 1, three beams, rather than one beam was used. The position input, frequency input and the deflection output were constructed with the same procedure as the other examples. However, here different membership functions were used. For instant, only 4 membership functions are used for the position input and 2 membership functions for frequency input. Here one more input was required to identify beams. In this example obtained *MSF*s are compared with the corresponding FE model. The

maximum error of 19.83% occurred in the first mode shape and error of 16.41% in the second mode shape.

Example 4 demonstrates a clamped-free beam modelling problem. In this example the experimental updating procedure is applied to only a part of the beam. In this case the proposed method is still applicable. In this example higher errors are exhibited. The reason is, the experimental updating procedure is applied to only a part of the beam and there is not enough experimental data to update the entire fuzzy *MSFs*. However the method still works and presents a trajectory of the mode shapes even in not updated sections.

Chapter 8

Discussion

Deterministic vibration modelling approaches have become very complicated and involve extensive mathematical efforts and the use or development of computational techniques and optimization methods. Further more limitations of deterministic approach have becoming more obvious as dimensionality and complexity of engineering systems continue to grow. Therefore modelling of uncertainty in dynamical behaviour of systems has become an important tool during the last 25 years. This resulted in the development of stochastic methods and provided additional analysis tools to designers. Uncertainty methods enabled engineer to study structures under imprecisely defined excitations such as force and initial conditions, or with other imprecise parameters such as unknown geometry and material properties.

This thesis deals with vibration analysis of mechanical systems with imprecise parameters. Most of structures are imprecisely defined due to lack of information about the parameters of the system, or inaccurate measurements. Parameters of the system are mass, stiffness, damping, geometry and material properties. Lack of information about the system and inaccurate measurements cause uncertainty in the analysis. Some of the sources of inaccuracies in parameters that lead to uncertainties in the analysis are measurement, manufacturing tolerances and time variation of systems properties that are described in Chapter 1 (introduction).

Therefore it is very important to consider these unavoidable uncertainties in order to obtain a realistic model of the structure.

Regarding the literature survey in this thesis, it is found that uncertainty methods developed by previous researchers studied the effect of uncertainty on parameters of systems or uncertain excitations on the system response. However the proposed method in this thesis deals with uncertainty in the behaviour (mode shape) of structures without considering the parameters of the system. This is a novel approach in modelling of vibratory behaviour of structures and has not been done before. This method is significant as it provides an alternative perspective of uncertainty. It proposes that the final behaviour of modes can be described without any reference to system parameters or equations (although the equations of motion are extensively used for comparison purpose). This approach ensures that fuzzy methods can be used. Otherwise it is not possible to start with fuzzy system variables and proceed forward to obtain fuzzy response as many mathematical operations do not have their fuzzy counterparts. However this is a normal procedure in uncertainty analysis using stochastic or statistical methods.

Thus the proposed method in this thesis offers an advantage over other uncertainty analysis methods. Available methods in uncertainty analysis involve solving complicated mathematical equations where the equations consist of imprecise parameters. Solving mathematical equations consisting imprecise parameters provides imprecise and approximate solutions. The proposed method is different from this conventional approach in the sense that the process start with a solution. In other word a solution is guessed and described in terms of fuzzy functions (or fuzzy mode shapes). This initial imprecise and approximate solution of vibratory behaviour of structures is used to start the modelling procedure. As mentioned before, the imprecise and approximate solutions refer to approximate mode shape of structures where the approximate mode shapes of structures are guessed heuristically (Guessing the approximate mode shapes is explained in Chapter 4). Therefore this method avoids complicated and time consuming mathematical computations where other uncertainty methods rely on.

Also the proposed method provides a basis for dealing uncertainty inherently present in all experimental measurements and ensures that the future extension of the method is based on well tested fuzzy formulism.

The method presented in this thesis involves estimating the mode shapes of a structure and describing these shapes in terms of fuzzy membership functions. These initial guesses are based on engineer's experience assisted by end and boundary conditions and the rules introduced in Chapter 4. The second stage of the process is, updating these guessed mode shapes by experimental data. This involves performing experimental modal analysis. The curve updating is not a simple process and poses complications. The main source of complication is related to the fact that, a mode shape derived from experimental *FRFs* collects only a limited number of sampling points. Therefore the main difficulty to be addressed, is, how to update the fuzzy curve with only few sampling points. The method proposes to use neural networks to achieve this. When the fuzzy data is updated by experimental data, the method proposes that the points of the fuzzy data correspond to the sampling points of *FRF* are to be replaced by the experimental data. Doing this creates a new fuzzy curve which is the same as the previous one, except at those points. In another word a "spiked" version of the original fuzzy curve is obtained. In the next stage of this process, neural network is used to "learn" the spiked curve. By controlling the learning process (by preventing it from overtraining) an updated fuzzy curve is generated. The method is similar to ones routinely used in neural network, where noise is added to target curve to enhance network generalisation.

The proposed method relies on informed guess, probably based on experience of operator. In this thesis, it was proposed that to minimise operator dependence a modal shape repertoire may be assembled or mode shapes of analytical solution of some standard structures can be made available to the operator of the proposed method. Never the less the proposed method still heavily rely on the operator. However a method can not be effective and robust unless it is independent of operator. In addressing these two problems relating to concept of guessing, it has to be addressed, what happens if, a) the guessed mode shape is wrong, and b) there is no guess available. In addressing the first problem, mode shape forms are considered for a uniform or regular structure (such as a beam, or simple multi spring mass

system) for the purpose of assisting the guess of the structure under consideration. These *MSFs* may relate to the first, second or other mode shape of the structure. The procedure of fuzzy construction of *MSF*, modal testing for model updating, and neural network learning of data is applied to obtain the mode. The error between this mode shape and modal analysis model is obtained. The modal analysis model is the same model that is used for model updating. If the error is not acceptable then another available *MSF* is considered and the procedure repeated until the correct *MSF* is found. The second obstacle to overcome in order to improve the effectiveness is to deal with the situation where there is no *MSF* available. Either not available in existing repertoire or operator decide not to choose one. In this situation all the method scans all available mode shapes and consider them one by one. The error for each *MSF* is calculated with comparing with the modal test results. The *MSF* with the minimum error is selected. The difference between the deflection points in the experimental modal analysis mode shape and the *MSF* is obtained. The magnitude of this difference is converted to fuzzy deflection terms. Then this new fuzzy deflection that is obtained from the difference between the experimental modal analysis and the proposed model is replaced by the previous fuzzy deflections. This replacement is applied by changing the fuzzy rule for the particular geometry of the structure, where the difference is found. By doing this for the whole geometry and correcting all the fuzzy rules, then the overall error is calculated. If the overall error is acceptable then the procedure will end. If the error is not acceptable then the procedure is repeated by changing the fuzzy rules until the error becomes acceptable.

These two techniques are presented in Chapter 5 and are applied to example 4 in Chapter 7. These techniques found to improve the reliability and robustness of the proposed method.

In Chapter 7, four examples were provided to demonstrate and illustrate the proposed method. The examples were included vibration modelling of a clamped-clamped beam, a clamped-free beam, a clamped-free-clamped-free plate and a 3-beam structure.

As mentioned before, uncertainty in modelling and analysis of structures usually exist due to imprecise excitations such as forces and initial conditions or imprecise

parameters such as masses, material properties, stiffness of the system. In many situations of uncertainty analysis, the error cannot be described in conventional terms. The reasons include; a) It is not possible to find exact solution (for example for complex structures), and b) The deterministic model parameters inevitably contains error. In other word, error of the method of analysis and uncertainty can not be decoupled. Uncertainty modelling methods provide a range of solution for range of uncertain parameters. In this case deterministic methods do not provide information about the solution for a range of parameters, especially if more than one parameter is interested for analysis of the solution. Uncertainty analysis is also used where there is a high error in deterministic methods due to uncertainty in parameters and provides an indication of decreasing or increasing in the solution. Classical uncertainty analysis is described in terms of statistical variables and provides results which inform the level of probability of expecting a certain solution in a given range. Therefore variability of results is neither an error in classical sense or reflection of the effectiveness of the method. The variation of results predicted by the method proposed in this thesis can be interpreted in exactly the same way as the statistical method. The "variation" between the analytical value and fuzzy results, simply reflects the level of uncertainty rather than an error in classical sense. The maximum 20% difference was estimated in the proposed method in comparison against the other results. However this error is calculated relative to experimental modal analysis model that only exists in few points and other points are linearly interpolated and consist of error. In another word the modal analysis model that is used for comparing with the proposed model is not an exact solution. Although the local error in updated positions is found to be around 5%.

Having developed this method, the question is, how these results can be used in an industrial situation. The answer is simple, exactly the same way as how modal analysis used currently. Of course the method proposed here provides additional advantage of uncertainty.

In mathematical terms, fuzzy vector can be used to express the system response function. Just to clarify, fuzzy mode shape forms are equivalent to eigenvectors in classical sense and eigenvalues are the natural frequencies which are crisp and measured during the experiment.

$$\begin{Bmatrix} x_1(t) \\ x_2(t) \\ \vdots \\ x_m(t) \end{Bmatrix} = \sum_{i=1}^{m} c_i \begin{Bmatrix} X_1 \\ X_2 \\ \vdots \\ X_m \end{Bmatrix}_i \sin(\omega_{ni} t + \psi_i)$$

Where in this equation the mode shape matrixes or $\{X_1 \quad X_2 \quad \cdots \quad X_m\}_i^T$ for $i = 1, 2, \cdots, m$ are obtained from the proposed method in this thesis and natural frequencies (ω_{ni}, $i = 1, 2, \cdots, m$) can be obtained from a single *FRF* result. One of the available *FRF* results that was used in modal analysis model updating procedure can be used in this case. Constants c_i and phase angles ψ_i, $i = 1, 2, \cdots, m$ can be obtained form the displacement and velocity initial conditions.

Chapter 9

Conclusion and future work

9.1. Conclusion

A novel method of dealing with uncertainty in vibration modelling was proposed in this thesis. In this respect fuzzy sets were used to deal with the uncertainty in modelling, modal analysis was used for model updating and neural networks simulated the dynamical behaviour of the structure. The procedure of obtaining a vibration model of a structure using the proposed method is listed below.

- Heuristically guessing an approximate version of mode shape functions (*MSF*) and constructing *MSFs* using fuzzy sets (fuzzy *MSFs*) as a tool to deal with the uncertainties.
- Updating the fuzzy *MSFs* using experimental modal analysis.
- Obtaining the mode shapes from fuzzy *MSFs* using neural networks.

Fuzzy membership function found to be a very flexible tool to deal with the uncertainties in the *MSFs* (approximate mode shapes). Experimental modal analysis is an accurate modelling method and found to be suitable for updating of vibratory behaviour of mechanical systems. Neural networks also used successfully in obtaining the final (or mathematical) version of the mode shapes from updated fuzzy *MSFs*.

Therefore this thesis proposes the use of fuzzy sets to describe mode shapes of structures. The method describes a procedure to achieve this. The procedure starts with rough guess of mode shapes (mode shape forms or *MSFs*) and fuzzy membership functions are used to construct the guessed mode shapes. These curves are updated by using experimental *FRF* measurements, obtained at limited number of sampling points. In the last stage of the procedure the updated fuzzy *MSFs* are modified by experimental values at sampling points. This creates a new curve with "spikes". Using fuzzy neural networks to 'learn' the spikes curve produces a smooth and mathematical version of the curve. This method proved to be very effective in generating mode shapes with limited number of sampling points.

The method was demonstrated using a beam, plate and a simple structure (3 beam structure). Fuzzy mode shape forms which were updated and refined by experimental results and neural network using the proposed method are compared against the analytical results.

Achievements in this thesis in modelling of vibration behaviour of structures are listed below.

- *MSFs* (mode shape forms) are introduced and some general rules are obtained for *MSFs* where *MSFs* are approximate mode shapes.
- Guessed mode shapes can be used as the uncertain model of the structure (that can be updated by experimental modal analysis)
- Fuzzy sets found to be a flexible tool in introducing the uncertain vibration model.
- The error observed in models developed by the proposed method is found to be less than 20%, well within levels of uncertainty reported by other researchers [15, 19].
- The proposed method tested and proved to be applicable by four experimental examples for one dimensional and two-dimensional elastic bodies and a three-beam structure.
- In all examples, the levels of uncertainty had not exceeded 20%.
- The method found to be reliable even with cases where initial modal shape has not been guessed accurately.

- The method proposed in this thesis is a novel method and has not been done before.

9.2. Future work

- It is possible to extend the method to study equation of motion where the parameters of the system (such as mass, stiffness, damping dimensions and material properties) can be considered as fuzzy parameters. The effect of changing fuzzy parameters on *MSFs* can be studied. Therefore the *MSFs* can be determined for a range of parameters and can be stored in a library of *MSFs*. This library offers a reference of *MSFs* for a range of structure parameters.
- The second possible further work relates to developing mathematical formalism to support the method proposed in this thesis. One way of achieving this is to study sources of uncertainty and compare it with stochastic methods.
- Developing a package compatible with existing modal testing software and using the proposed method as a new tool.
- Drive a library of *MSFs* with more reliable and general rules based on the method introduced in Chapter 4 in developing *MSF* rules.
- Using the fuzzy presentation of the mode shapes as a fuzzy feedback controller in reducing the error when the *MSFs* are wrong or not available (figure 9-1).

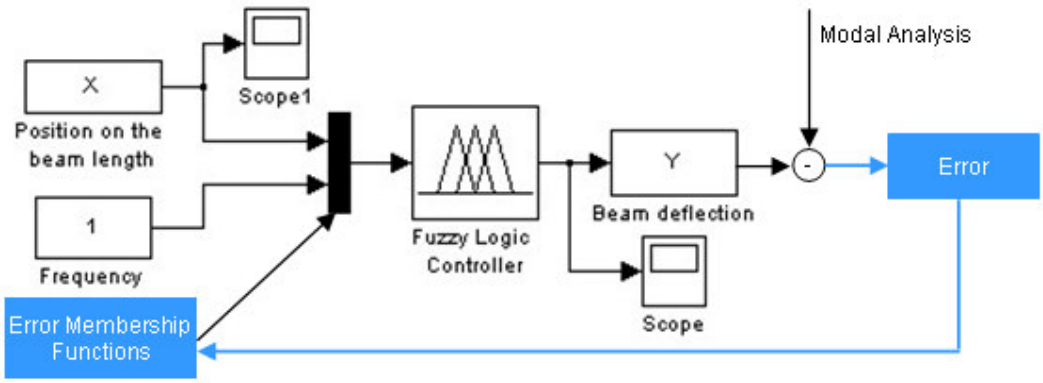

Figure 9-1. Controlling of error.

Appendix A

Orthogonality of modes relative to mass and stiffness matrixes

The vibration behavior of an undamped system can be expressed as below [17, 34].

$$\left([K_x]-\omega^2[M_x]\right)\{x(t)\}=\{0\} \tag{A-1}$$

Where the response can be expressed with the following equation.

$$\{x(t)\}=[P]\{q(t)\}=[P]\begin{bmatrix} Q_1\sin(\omega_{n1}+\psi_1) \\ Q_2\sin(\omega_{n2}+\psi_2)\end{bmatrix} \tag{A-2}$$

To have non zero solutions, Q_1, Q_2, $\sin(\omega_{n1}+\psi_1)$ and $\sin(\omega_{n2}+\psi_2)$ can not be zero or $\{q(t)\}\neq 0$. Then from (A-1) and (A-2):

$$\left([K_x]-\omega^2[M_x]\right)[P]=\{0\}$$

For a particular mode $\omega = \omega_r$ we have:

$$\left([K_x] - \omega_r^2 [M_x]\right)\{P\}_r = \{0\}$$

By Pre multiplying the above equation by $\{P\}_S^T$ then:

$$\{P\}_S^T \left([K_x] - \omega_r^2 [M_x]\right)\{P\}_r = \{0\} \qquad \text{(A-3)}$$

For a particular mode $\omega = \omega_S$ we have:

$$\left([K_x] - \omega_r^2 [M_x]\right)\{P\}_S = \{0\}$$

Transpose of the above equation is as below.

$$\{P\}_S^T \left([K_x]^T - \omega_S^2 [M_x]^T\right) = \{0\}$$

By post multiplying the above equation by $\{P\}_r$, then:

$$\{P\}_S^T \left([K_x]^T - \omega_S^2 [M_x]^T\right)\{P\}_r = \{0\}$$

As mass and stiffness matrices are symmetric, then we have:

$$[K_x]^T = [K_x] \text{ and } [M_x]^T = [M_x]$$

Thus

$$\{P\}_S^T \left([K_x] - \omega_S^2 [M_x]\right)\{P\}_r = \{0\} \qquad \text{(A-4)}$$

Equation (A-4) minus equation (A-3) gives:

$$\{P\}_S^T[K_x]\{P\}_r - \{P\}_S^T[K_x]\{P\}_r + \left(\omega_r^2 - \omega_S^2\right)\{P\}_S^T[M_x]\{P\}_r = \{0\}$$

Or

$$\left(\omega_r^2 - \omega_S^2\right)\{P\}_S^T[M_x]\{P\}_r = \{0\}$$

And for $\omega_r \neq \omega_S$:

$$\{P\}_S^T[M_x]\{P\}_r = \{0\} \qquad \text{(A-5)}$$

That shows orthogonality of the modes relative to the mass matrix.

From (A-5) and (A-3), we have:

$$\{P\}_S^T[K_x]\{P\}_r - \omega_r^2\{P\}_S^T[M_x]\{P\}_r = \{0\} \qquad \text{(A-6)}$$

Or

$$\{P\}_S^T[K_x]\{P\}_r = \{0\}$$

That shows orthogonality of the modes relative to the stiffness matrix.

From (A-6)

$$\{P\}_S^T[K_x]\{P\}_r = \omega_r^2\{P\}_S^T[M_x]\{P\}_r$$

Where

$$\omega_r^2 = \frac{k_r}{m_r}$$

Then

$$\{P\}_S^T[K_x]\{P\}_r = k_r$$

And

$$\{P\}_S^T[M_x]\{P\}_r = m_r$$

The above relations can be expressed with another notation for all the modes as below.

$$[P]^T [K_x][P] = [K_q]$$

And

$$[P]^T [M_x][P] = [M_q]$$

Where $[K_q]$ and $[M_q]$ are diagonal matrixes and $[P] = [\{P\}_1 \quad \{P\}_2 \quad \cdots \quad \{P\}_r \quad \cdots]$.

Appendix B

Plate Vibration

The governing equation of bending vibration of a rectangular plate (Figure B-1) can be written as [38-40].

$$\frac{\partial^4 W(x,y)}{\partial x^4} + 2\frac{\partial^4 W(x,y)}{\partial x^2 \partial y^2} + \frac{\partial^4 W(x,y)}{\partial y^4} = \frac{q(x,y)}{D}$$

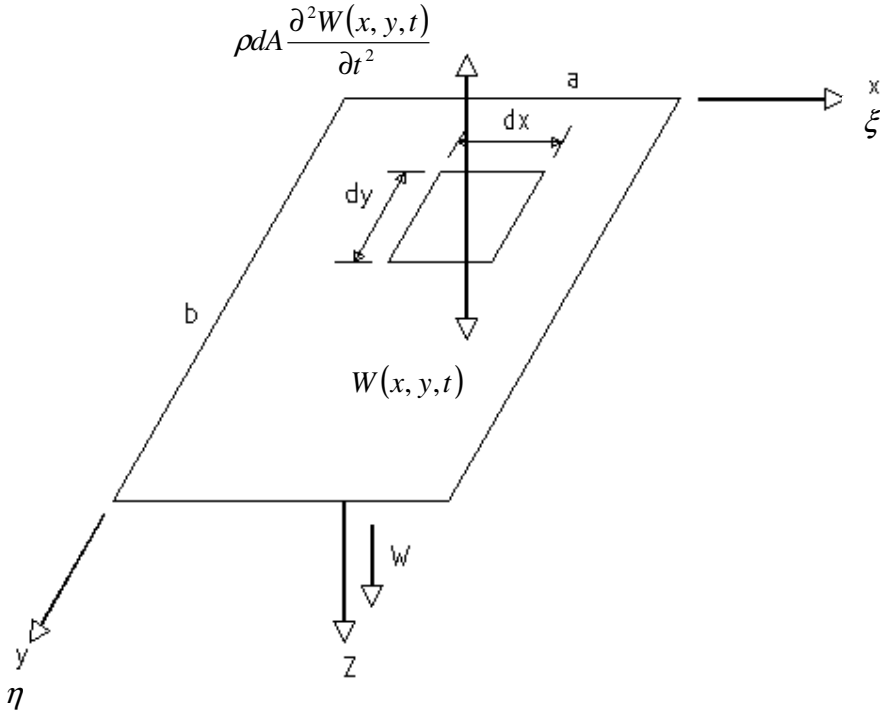

Figure B-1. A rectangular plate and an element of the plate.

Where $q(x, y)$ is the applied static force and W is the displacement (deflection) of the plate.

For the free vibration of the plate the equation in term of geometry and time will be

$$\frac{\partial^4 W(x, y, t)}{\partial x^4} + 2\frac{\partial^4 W(x, y, t)}{\partial x^2 \partial y^2} + \frac{\partial^4 W(x, y, t)}{\partial y^4} + \frac{\rho}{D}\frac{\partial^4 W(x, y, t)}{\partial t^2} = 0 \qquad \text{(B-1)}$$

It is possible to express the solution of the equation as

$$W(x, y, t) = W(x, y)T(t) \qquad \text{(B-2)}$$

By substituting equation (B-2) to (B-1) then

$$T(t)\frac{\rho}{D}\left[\frac{\partial^4 W(x, y)}{\partial x^4} + 2\frac{\partial^4 W(x, y)}{\partial x^2 \partial y^2} + \frac{\partial^4 W(x, y)}{\partial y^4}\right] = -W(x, y)\frac{\partial^2 T(t)}{\partial t}$$

Or

$$\frac{\frac{\rho}{D}\left[\frac{\partial^4 W(x, y)}{\partial x^4} + 2\frac{\partial^4 W(x, y)}{\partial x^2 \partial y^2} + \frac{\partial^4 W(x, y)}{\partial y^4}\right]}{W(x, y)} = -\frac{\frac{\partial^2 T(t)}{\partial t}}{T(t)}$$

As the left hand side of the above equation is a function of x and y and the right hand side is a function of t then the equation is valid when both sides are equal to a constant (here ω^2). The right hand side of the above equation can be obtained as

$$\frac{\partial^2 T(t)}{\partial t} + \omega^2 T(t) = 0$$

Then

$$T(t) = A\sin(\omega t + \alpha)$$

Where A and α can be obtained from initial conditions.

$$\frac{\partial^4 W(x,y)}{\partial x^4}+2\frac{\partial^4 W(x,y)}{\partial x^2\partial y^2}+\frac{\partial^4 W(x,y)}{\partial y^4}-\frac{\omega^2\rho}{D}W(x,y)=0$$

It is useful to express the above equation in terms of dimensionless variables ξ and η. Where $\xi=\frac{x}{a}$ and $\eta=\frac{y}{b}$ and a and b are the dimensions of the plate.

$$\frac{a\frac{\partial^4 W(x,y)}{a}}{a^4\partial\left(\frac{x}{a}\right)^4}+\frac{2a\frac{\partial^4 W(x,y)}{a}}{a^2b^2\partial\left(\frac{x}{a}\right)^2\partial\left(\frac{y}{b}\right)^2}+\frac{a\frac{\partial^4 W(x,y)}{a}}{b^4\partial\left(\frac{y}{b}\right)^4}-\frac{a\omega^2\rho\frac{W(x,y)}{a}}{D}=0$$

Substituting ξ and η then in the equation of motion, we have:

$$\frac{\partial^4 W(\xi,\eta)}{\partial\xi^4}+\frac{2\partial^4 W(\xi,\eta)}{\phi^2\partial\xi^2\partial\eta^2}+\frac{\partial^4 W(\xi,\eta)}{\phi^4\partial\eta^4}-\lambda^4 W(\xi,\eta)=0$$

Where $\lambda^2=\omega a^2\sqrt{\frac{\rho}{D}}$ and $\phi=\frac{b}{a}$ (plate aspect ratio).

By multiplying the above equation by ϕ^4 then we have:

$$\frac{\partial^4 W(\xi,\eta)}{\partial\eta^4}+2\phi^2\frac{\partial^4 W(\xi,\eta)}{\partial\xi^2\partial\eta^2}+\phi^4\frac{\partial^4 W(\xi,\eta)}{\partial\xi^4}-\phi^4\lambda^4 W(\xi,\eta)=0 \qquad \text{(B-3)}$$

To solve the above equation the following assumption is made (Levy-Type solution for free vibration of rectangular plates)

$$\underset{\lim k\to\infty}{W(\xi,\eta)}=\sum_{m=1}^{k}Y_m(\eta)\sin m\pi\xi \qquad \text{(B-4)}$$

By substituting Equation (B-4) into (B-3) then we have:

$$\sum_{m=1}^{\infty}\left\{\frac{d^4Y_m(\eta)}{d\eta^4}-2\phi^2(m\pi)^2\frac{d^2Y_m(\eta)}{d\eta^2}+\phi^4\left[(m\pi)^4-\lambda^4\right]Y_m(\eta)\right\}\sin m\pi\xi=0$$

From above equation:

$$\frac{d^4Y_m(\eta)}{d\eta^4}-2\phi^2(m\pi)^2\frac{d^2Y_m(\eta)}{d\eta^2}+\phi^4\left[(m\pi)^4-\lambda^4\right]Y_m(\eta)=0$$

The solution of the above equation for $(m\pi)^4 \succ or \prec \lambda^4$ can be obtained as:

For $\lambda^2 \succ (m\pi)^2$

$$Y_m(\eta)=A_m\cosh\beta_m\eta+B_m\sinh\beta_m\eta+C_m\sin\gamma_m\eta+D_m\cos\gamma_m\eta \qquad \text{(B-5)}$$

And for $\lambda^2 \prec (m\pi)^2$

$$Y_m(\eta)=A_m\cosh\beta_m\eta+B_m\sinh\beta_m\eta+C_m\sinh\gamma_m\eta+D_m\cosh\gamma_m\eta \qquad \text{(B-6)}$$

Where $\beta_m=\phi\sqrt{\lambda^2+(m\pi)^2}$ and $\gamma_m=\phi\sqrt{\lambda^2+(m\pi)^2}$ *or* $\phi\sqrt{\lambda^2+(m\pi)^2}$

The coefficients A and B can be obtained from boundary conditions where the boundary conditions can be expressed as below

a) Simply supported edges

$$W(x,y)=\frac{\partial^2W(x,y)}{\partial x^2}=0\Big|_{x=a}$$

Or in terms of dimensionless coordinates

$$W(\xi,\eta)=\frac{\partial^2W(\xi,\eta)}{\partial\xi^2}=0\Big|_{\xi=1}$$

b) Clamped edges

$$W(x,y)=\frac{\partial W(x,y)}{\partial x}=0\Big|_{x=a}$$

Or in terms of dimensionless coordinates

$$W(\xi,\eta)=\frac{\partial W(\xi,\eta)}{\partial \xi}=0\Big|_{\xi=1}$$

c) Free edges

Edge $x=a$:

$$\frac{\partial^2 W(x,y)}{\partial x^2}+\upsilon\frac{\partial^2 W(x,y)}{\partial y^2}=0\Big|_{x=a}$$

$$\frac{\partial^3 W(x,y)}{\partial x^3}+\upsilon^*\frac{\partial^3 W(x,y)}{\partial x\partial y^2}=0\Big|_{x=a}$$

Edge $y=b$:

$$\frac{\partial^2 W(x,y)}{\partial y^2}+\upsilon\frac{\partial^2 W(x,y)}{\partial x^2}=0\Big|_{y=b}$$

$$\frac{\partial^3 W(x,y)}{\partial y^3}+\upsilon^*\frac{\partial^3 W(x,y)}{\partial y\partial x^2}=0\Big|_{y=b}$$

And in dimensionless coordinates

Edge $\xi=1$:

$$\frac{\partial^2 W(\xi,\eta)}{\partial \xi^2}+\frac{\upsilon}{\phi^2}\frac{\partial^2 W(\xi,\eta)}{\partial \eta^2}=0\Big|_{\xi=1}$$

$$\frac{\partial^3 W(\xi,\eta)}{\partial \xi^3}+\frac{\upsilon^*}{\phi^2}\frac{\partial^3 W(\xi,\eta)}{\partial \xi\partial \eta^2}=0\Big|_{\xi=1}$$

Edge $\eta=1$:

$$\frac{\partial^2 W(\xi,\eta)}{\partial \eta^2}+\upsilon\phi^2\frac{\partial^2 W(\xi,\eta)}{\partial \xi^2}=0\Big|_{\eta=1}$$

$$\frac{\partial^3 W(\xi,\eta)}{\partial \eta^3}+\upsilon^*\phi^2\frac{\partial^3 W(\xi,\eta)}{\partial \eta\partial \xi^2}=0\Big|_{\eta=1}$$

Appendix C

Structural vibration by finite elements

Figure C-1 shows a 3-beam structure with 3 degrees of freedom (D1, D2 and D3).

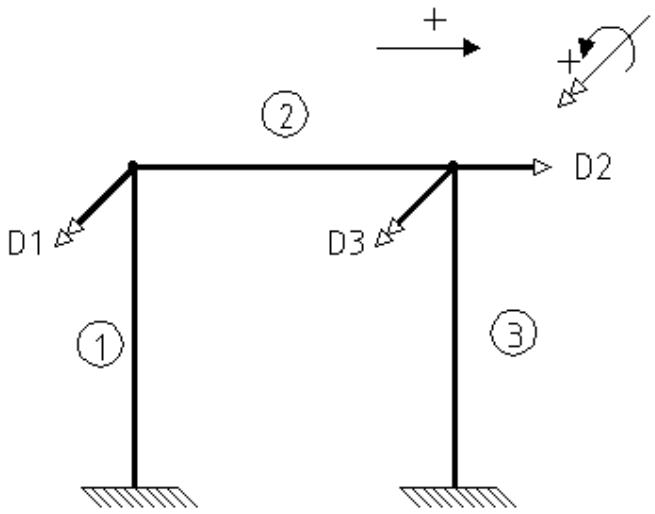

Figure C-1. A three beam structure.

The elements of the structure can be *axial element* (element number 2 with D2 degree of freedom). An axial element is presented in Figure C-2.

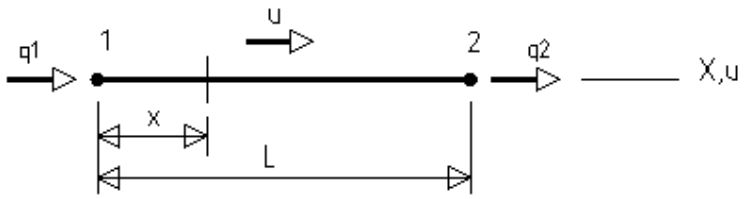

Figure C-2. An axial element

The stiffness (K) and mass (M) matrixes of this element can be obtained as below. If the shape functions can be considered as [35-37]

$$f = [f_1 \quad f_2] = \left[1 - \frac{x}{L} \quad \frac{x}{L}\right]$$

Therefore the differentiation of f relative to x will be:

$$B = d\,f = \frac{df}{dx} = \frac{1}{L}[-1 \quad 1]$$

The element stiffness matrix can be expressed as:

$$K = \int_V B^T E B\, dV = \frac{E}{L^2}\begin{bmatrix}-1\\1\end{bmatrix}[-1 \quad 1]\int_0^L \int_A dA\,dx = \frac{EA}{L}\begin{bmatrix}1 & -1\\-1 & 1\end{bmatrix}$$

And the mass matrix can be obtained as:

$$M = \int_V \rho\, f^T f\, dV = \frac{\rho}{L^2}\int_0^L \int_A \begin{bmatrix}L-x\\x\end{bmatrix}[L-x \quad x]\,dA\,dx = \frac{\rho AL}{6}\begin{bmatrix}2 & 1\\1 & 2\end{bmatrix}$$

The elements of the structure can be *flexural element* (element number 1 and 3 with D1 and D3 degrees of freedom). An axial element is presented in Figure C-3.

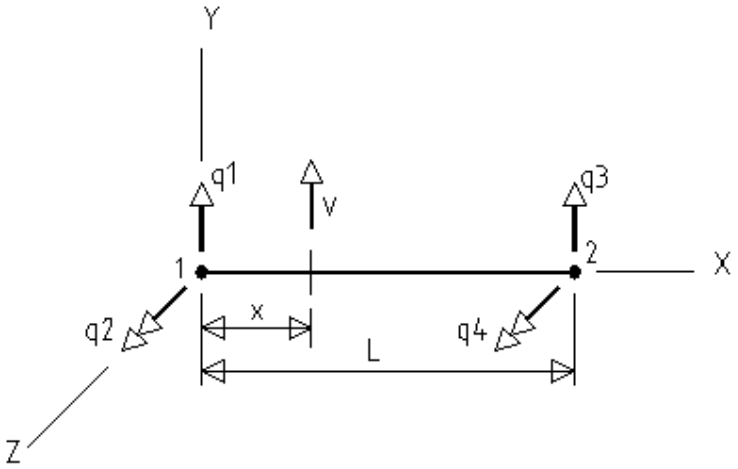

Figure C-3. A flexural element.

The stiffness (K) and mass (M) matrixes of this element can be obtained as below. If the shape functions can be considered as [35-37].

$$f = \begin{bmatrix} f_1 & f_2 & f_3 & f_4 \end{bmatrix}$$
$$= \frac{1}{L^3}\begin{bmatrix} 2x^3 - 3x^2L + L^3 & x^3L - 2x^2L^2 + xL^3 & -2x^3 + 3x^2L & x^3L - x^2L^2 \end{bmatrix}$$

Therefore the differentiation of f relative to x will be:

$$B = d\, f$$
$$= -\frac{y}{L^3}\begin{bmatrix} 12x - 6L & 6xL - 4L^2 & -12x + 6L & 6xL - 2L^2 \end{bmatrix}$$

Where operator d, here is:

$$d = -y\frac{d^2}{dx^2}$$

The element stiffness matrix can be expressed as:

$$K = \int_V B^T E\, B\, dV$$

Then

$$K = \frac{2EI}{L^3}\begin{bmatrix} 6 & 3L & -6 & 3L \\ 3L & 2L^2 & -3L & L^2 \\ -6 & -3L & 6 & -3L \\ 3L & L^2 & -3L & 2L^2 \end{bmatrix}$$

Where

$$I = \int_A y^2 dA$$

And the mass matrix can be obtained as:

$$M_t = \int_V \rho f^T f \, dV$$

Then

$$M_t = \frac{\rho AL}{420}\begin{bmatrix} 156 & 22L & 54 & -13L \\ 22L & 4L^2 & 13L & -3L^2 \\ 54 & 13L & 156 & -22L \\ -13L & -3L^2 & -22L & 4L^2 \end{bmatrix}$$

The mass matrix includes two parts. The translational inertia term that is presented above is much more important. Only this part is usually considered in calculations.

A 6-degrees of freedom element can be obtained by combining the flexural and axial element that is illustrated in Figure C-4.

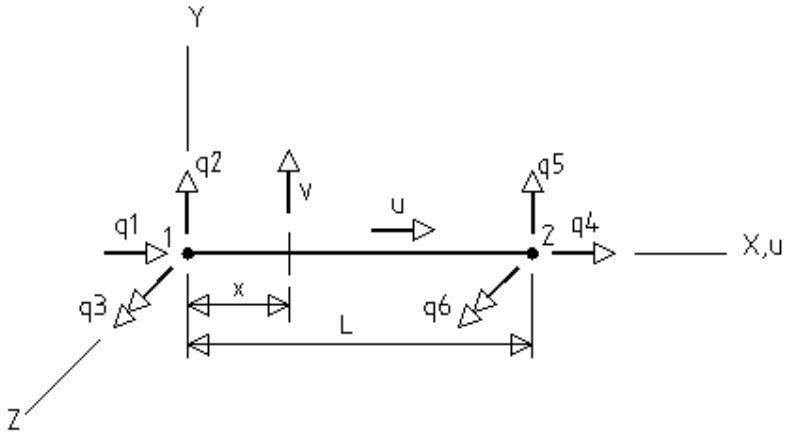

Figure C-4. 6 degree of freedom element.

The stiffness and mass matrix of this element can be presented as below:

$$K = a\begin{bmatrix} b & 0 & 0 & -b & 0 & 0 \\ 0 & 6 & 3L & 0 & -6 & 3L \\ 0 & 3L & 2L^2 & 0 & -3L & L^2 \\ -b & 0 & 0 & b & 0 & 0 \\ 0 & -6 & -3L & 0 & 6 & -3L \\ 0 & 3L & L^2 & 0 & -3L & 2L^2 \end{bmatrix}\begin{matrix}1\\2\\3\\4\\5\\6\end{matrix}$$

$$\begin{matrix}1 & 2 & 3 & 4 & 5 & 6\end{matrix}$$

Where

$$a = \frac{2EI}{L^3} \text{ and } b = \frac{\frac{EA}{L}}{\frac{2EI}{L^3}} = \frac{AL^2}{2I}$$

$$M = c\begin{bmatrix} d & 0 & 0 & -d & 0 & 0 \\ 0 & 156 & 22L & 0 & 54 & -13L \\ 0 & 22L & 4L^2 & 0 & 13L & -3L^2 \\ -d & 0 & 0 & d & 0 & 0 \\ 0 & 54 & 13L & 0 & 156 & -22L \\ 0 & -13L & -3L^2 & 0 & -22L & 4L^2 \end{bmatrix}\begin{matrix}1\\2\\3\\4\\5\\6\end{matrix}$$

$$\begin{matrix}1 & 2 & 3 & 4 & 5 & 6\end{matrix}$$

Where $c = \dfrac{\rho AL}{420}$ and $d = \dfrac{\dfrac{\rho AL}{6}}{\dfrac{\rho AL}{420}} = \dfrac{420}{6} = 70$.

Based on the element introduced in Figure C-4, the elements of the structure in Figure C-1 can be obtained as in Figure C-5. All degrees of freedom are considered for the elements. However the elements only consist of the degrees of the freedom that is shown in Figure C-1 (D1, D2 and D3). Also there is no degree of freedom in nodes 1 and 4 as these nodes are fixed.

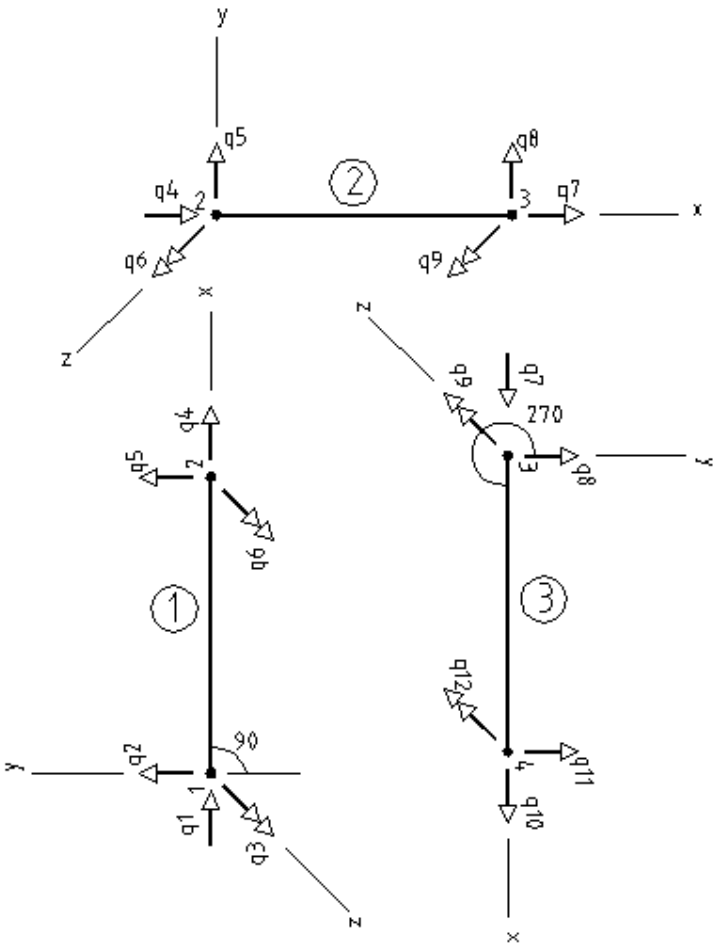

Figure C-5. Elements of the structure with all degrees of freedom.

The elements with the valid degrees of freedom are illustrated in Figure C-6.

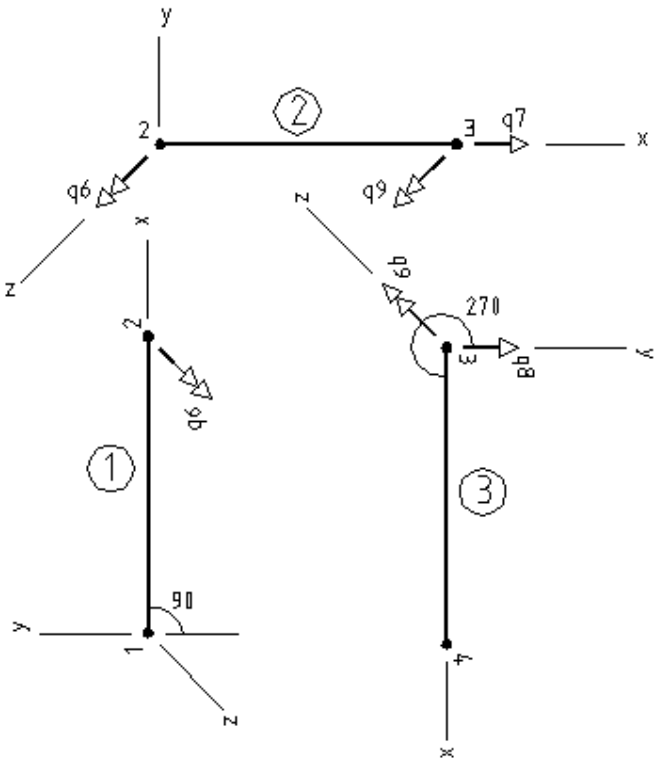

Figure C-6. Elements of the structure.

The structural mass and stiffness matrixes can be obtained as:

$$S_s = \sum_{i=1}^{n_e} K_i$$

And

$$M_s = \sum_{i=1}^{n_e} M_i$$

Where S_s and M_s are the structural stiffness and mass matrixes, n_e is the number of the elements and K_i and M_i are the stiffness and mass matrixes of the elements of the structure. Then the structural matrixes can be expressed as:

$$S_s = K_1 + K_2 + K_3$$

Then based on the matrixes introduced earlier, the stiffness for the elements in Figure C-6 can be presented as

$$S_s = \begin{bmatrix} 0 & 0 & 0 & 0 & 0 & 0 & 0 & 0 & 0 & 0 & 0 & 0 \\ 0 & 0 & 0 & 0 & 0 & 0 & 0 & 0 & 0 & 0 & 0 & 0 \\ 0 & 0 & 0 & 0 & 0 & 0 & 0 & 0 & 0 & 0 & 0 & 0 \\ 0 & 0 & 0 & 0 & 0 & 0 & 0 & 0 & 0 & 0 & 0 & 0 \\ 0 & 0 & 0 & 0 & 0 & 0 & 0 & 0 & 0 & 0 & 0 & 0 \\ 0 & 0 & 0 & 0 & 0 & 2L^2a_1 + 2L^2a_2 & 0 & 0 & L^2a_2 & 0 & 0 & 0 \\ 0 & 0 & 0 & 0 & 0 & 0 & b_2a_2 + 6a_3 & 0 & 3La_3 & 0 & 0 & 0 \\ 0 & 0 & 0 & 0 & 0 & 0 & 0 & 0 & 0 & 0 & 0 & 0 \\ 0 & 0 & 0 & 0 & 0 & L^2a_2 & 3La_3 & 0 & 2L^2a_2 + 2L^2a_3 & 0 & 0 & 0 \\ 0 & 0 & 0 & 0 & 0 & 0 & 0 & 0 & 0 & 0 & 0 & 0 \\ 0 & 0 & 0 & 0 & 0 & 0 & 0 & 0 & 0 & 0 & 0 & 0 \\ 0 & 0 & 0 & 0 & 0 & 0 & 0 & 0 & 0 & 0 & 0 & 0 \end{bmatrix} \begin{matrix} 1 \\ 2 \\ 3 \\ 4 \\ 5 \\ 6 \\ 7 \\ 8 \\ 9 \\ 10 \\ 11 \\ 12 \end{matrix}$$

And $M_s = M_1 + M_2 + M_3$.

Using the same calculation as above for stiffness matrix then the mass matrix will be:

$$M_s = \begin{bmatrix} 0 & 0 & 0 & 0 & 0 & 0 & 0 & 0 & 0 & 0 & 0 & 0 \\ 0 & 0 & 0 & 0 & 0 & 0 & 0 & 0 & 0 & 0 & 0 & 0 \\ 0 & 0 & 0 & 0 & 0 & 0 & 0 & 0 & 0 & 0 & 0 & 0 \\ 0 & 0 & 0 & 0 & 0 & 0 & 0 & 0 & 0 & 0 & 0 & 0 \\ 0 & 0 & 0 & 0 & 0 & 0 & 0 & 0 & 0 & 0 & 0 & 0 \\ 0 & 0 & 0 & 0 & 0 & 4L^2c_1 + 4L^2c_2 & 0 & 0 & -3L^2c_2 & 0 & 0 & 0 \\ 0 & 0 & 0 & 0 & 0 & 0 & d_2c_2 + 156c_3 & 0 & 22Lc_3 & 0 & 0 & 0 \\ 0 & 0 & 0 & 0 & 0 & 0 & 0 & 0 & 0 & 0 & 0 & 0 \\ 0 & 0 & 0 & 0 & 0 & -3L^2c_2 & 22Lc_3 & 0 & 4L^2c_2 + 4L^2c_3 & 0 & 0 & 0 \\ 0 & 0 & 0 & 0 & 0 & 0 & 0 & 0 & 0 & 0 & 0 & 0 \\ 0 & 0 & 0 & 0 & 0 & 0 & 0 & 0 & 0 & 0 & 0 & 0 \\ 0 & 0 & 0 & 0 & 0 & 0 & 0 & 0 & 0 & 0 & 0 & 0 \end{bmatrix} \begin{matrix} 1 \\ 2 \\ 3 \\ 4 \\ 5 \\ 6 \\ 7 \\ 8 \\ 9 \\ 10 \\ 11 \\ 12 \end{matrix}$$

Free vibration equation of motion of the structure can be expressed as:

$$M\,\ddot{D} + S\,D = 0$$

Displacement vector, D can be presented as:

$$D_i = \Phi_i \sin(\omega_i t + \alpha_i)$$

Where $i = 1, 2, \ldots, n$, and n is the number of degrees of freedom. Φ_i is a vector of nodal amplitude or the mode shape for the i^{th} mode of vibration. ω_i is the angular frequency of mode *i*. α_i is the phase angle.

$$\ddot{D}_i = -\omega_i^2 \Phi_i \sin(\omega_i t + \alpha_i)$$

By substituting D and $\ddot{D}$ in the equation of motion then the equation will be:

$$(S - \omega_i^2 M)\Phi_i = 0$$

By substituting stiffness and mass matrixes into the above equation then (zeros in the mass and stiffness matrixes are not entered in the matrix as they have no effect on the equation).

$$\left(\begin{bmatrix} 2L^2a_1 + 2L^2a_2 & 0 & 0 & L^2a_2 \\ 0 & b_2a_2 + 6a_3 & 0 & 3La_3 \\ 0 & 0 & 0 & 0 \\ L^2a_2 & 3La_3 & 0 & 2L^2a_2 + 2L^2a_3 \end{bmatrix} - \omega_i^2 \begin{bmatrix} 4L^2c_1 + 4L^2c_2 & 0 & 0 & -3L^2c_2 \\ 0 & d_2c_2 + 156c_3 & 0 & 22Lc_3 \\ 0 & 0 & 0 & 0 \\ -3L^2c_2 & 22Lc_3 & 0 & 4L^2c_2 + 4L^2c_3 \end{bmatrix} \right) \begin{bmatrix} \Phi_6 \\ \Phi_7 \\ \Phi_8 \\ \Phi_9 \end{bmatrix} = 0$$

Or

$$\begin{bmatrix} 2L^2a_1 + 2L^2a_2 - \omega_i^2\left(4L^2c_1 + 4L^2c_2\right) & 0 \\ 0 & b_2a_2 + 6a_3 - \omega_i^2\left(d_2c_2 + 156c_3\right) \\ 0 & 0 \\ L^2a_2 - \omega_i^2\left(-3L^2c_2\right) & 3La_3 - \omega_i^2\left(22Lc_3\right) \end{bmatrix}$$

$$\begin{bmatrix} 0 & L^2a_2 - \omega_i^2\left(-3L^2c_2\right) \\ 0 & 3La_3 - \omega_i^2\left(22Lc_3\right) \\ 0 & 0 \\ 0 & 2L^2a_2 + 2L^2a_3 - \omega_i^2\left(4L^2c_2 + 4L^2c_3\right) \end{bmatrix} \begin{bmatrix} \Phi_6 \\ \Phi_7 \\ \Phi_8 \\ \Phi_9 \end{bmatrix} = 0$$

Then the system of equation can be expressed as

$$\left[2L^2a_1 + 2L^2a_2 - \omega_i^2\left(4L^2c_1 + 4L^2c_2\right)\right]\Phi_6 + \left[L^2a_2 + \omega_i^2\left(3L^2c_2\right)\right]\Phi_9 = 0 \qquad \text{(C-1)}$$

$$\left[b_2a_2 + 6a_3 - \omega_i^2\left(d_2c_2 + 156c_3\right)\right]\Phi_7 + \left[3La_3 - \omega_i^2\left(22Lc_3\right)\right]\Phi_9 = 0 \qquad \text{(C-2)}$$

$$\left[L^2a_2 + \omega_i^2\left(3L^2c_2\right)\right]\Phi_6 + \left[3La_3 - \omega_i^2\left(22Lc_3\right)\right]\Phi_7 + \left[2L^2a_2 + 2L^2a_3 - \omega_i^2\left(4L^2c_2 + 4L^2c_3\right)\right]\Phi_9 = 0$$

Appendix D

Experimental *FRF* results

FRFs of the ***clamped-clamped beam*** (example 1, Chapter 7) are presented in Figure D-1 when the accelerometer is in point 1 and the excitation force from the hammer is applied to points 1, 2, 3 and 4.

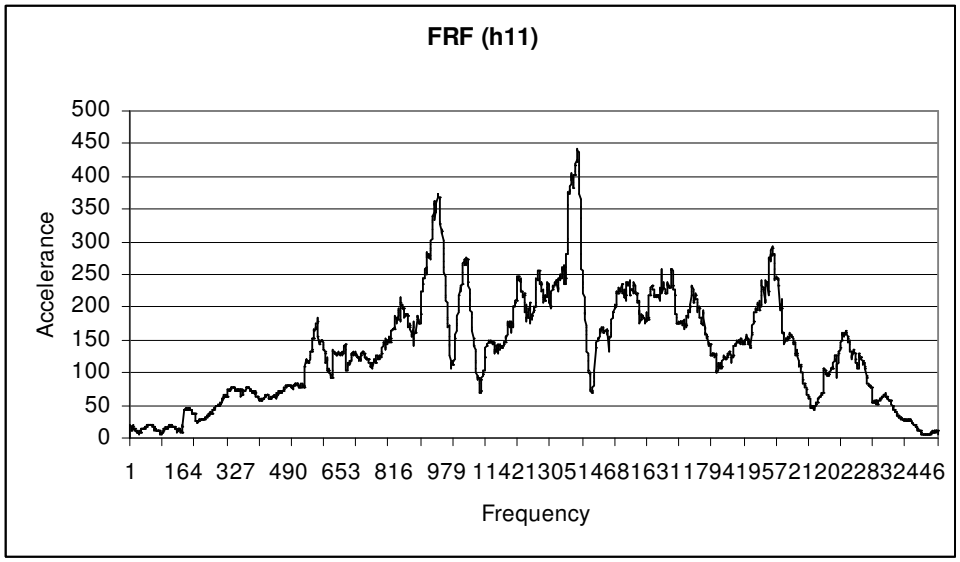

a) h_{11}

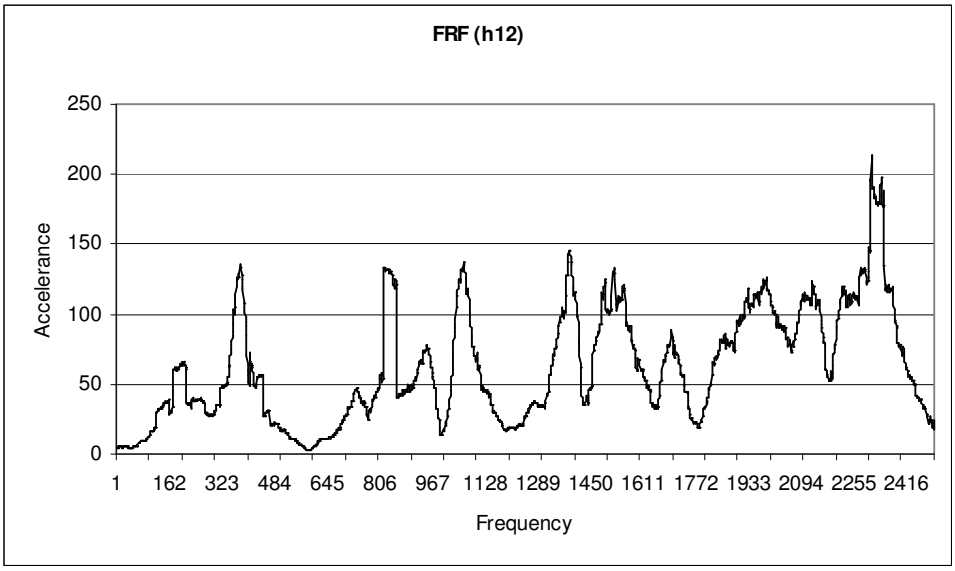

b) h_{12}

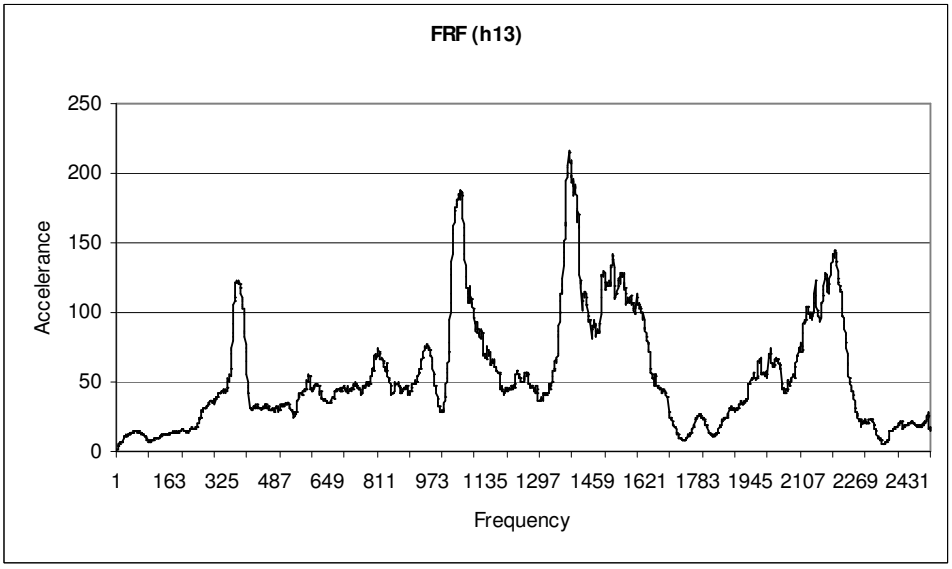

c) h_{13}

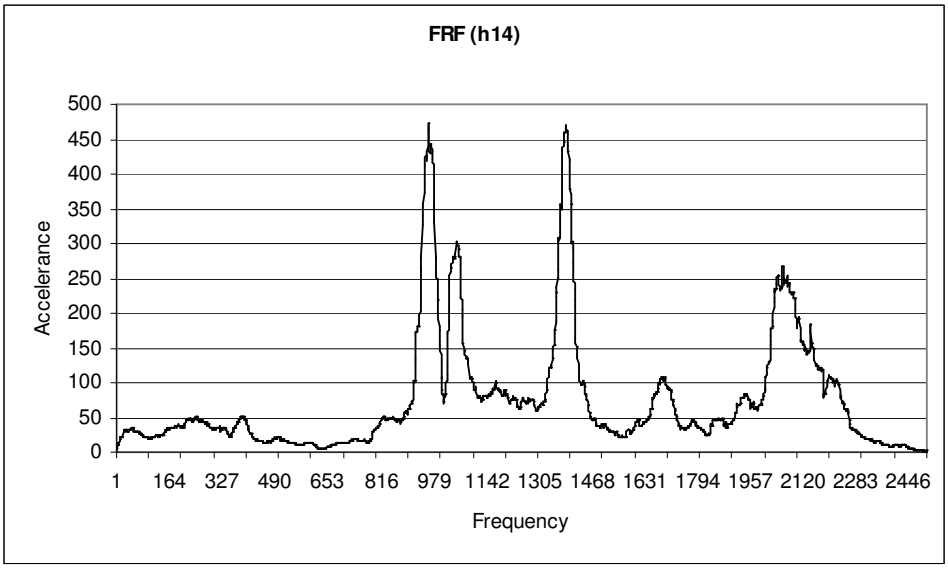

d) h_{14}

Figure D-1. Clamped-clamped *FRF* graphs; a) h_{11}, b) h_{12}, c) h_{13}, d) h_{14}.

FRFs of the ***plate*** (example 2, Chapter 7) are presented in Figure D-2 when the accelerometer is in point 1 and the excitation force from the hammer is applied to points 1, 2, 3, 4, 5 and 6.

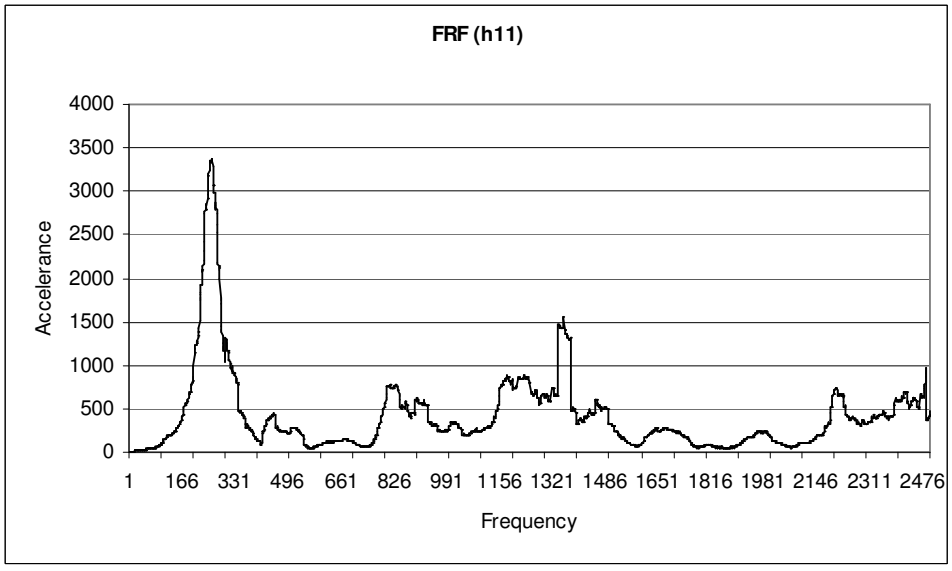

a) h_{11}

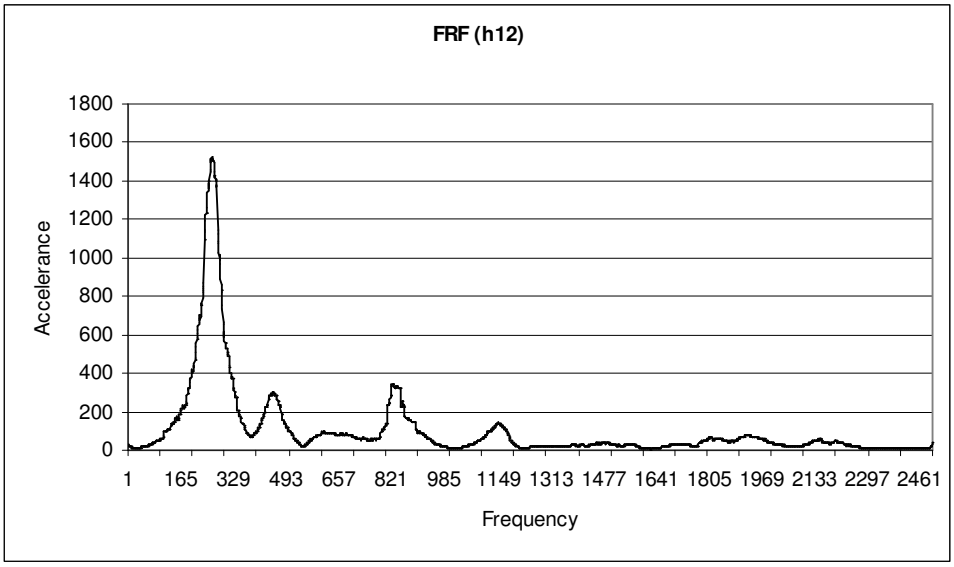

b) h_{12}

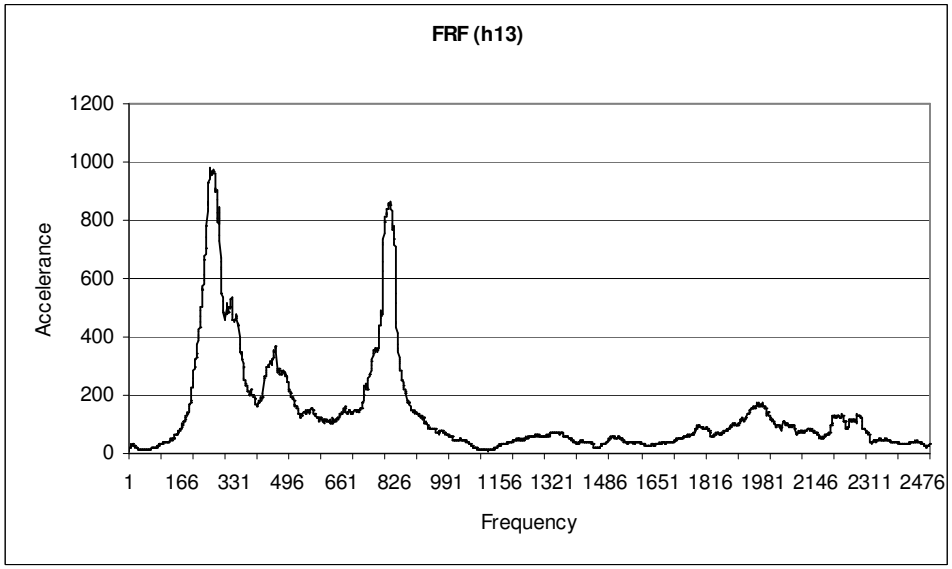

c) h_{13}

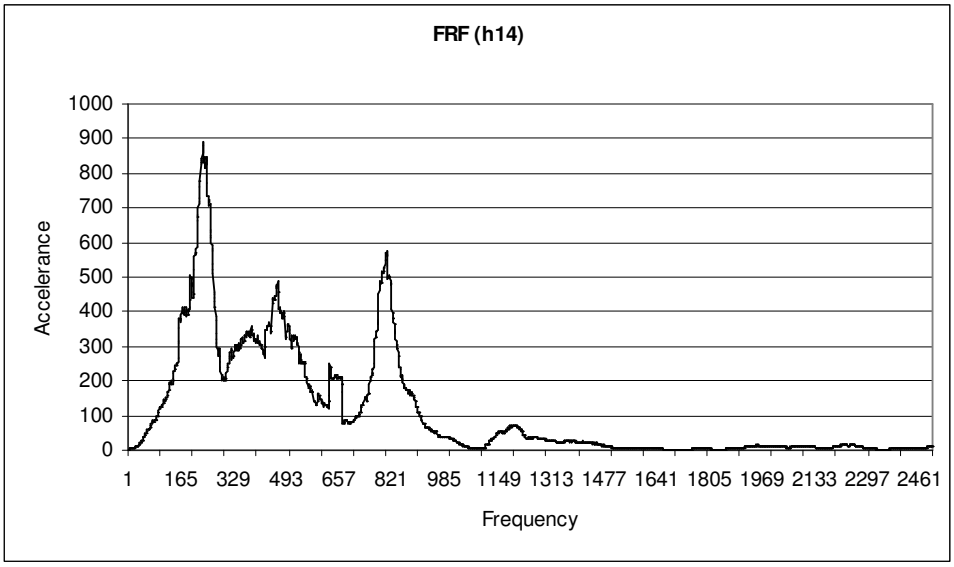

d) h_{14}

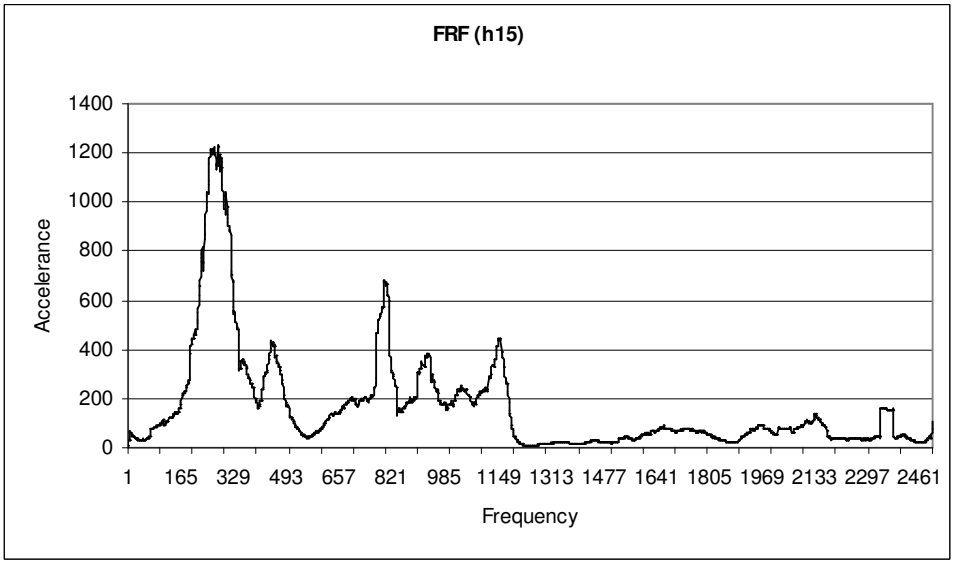

e) h_{15}

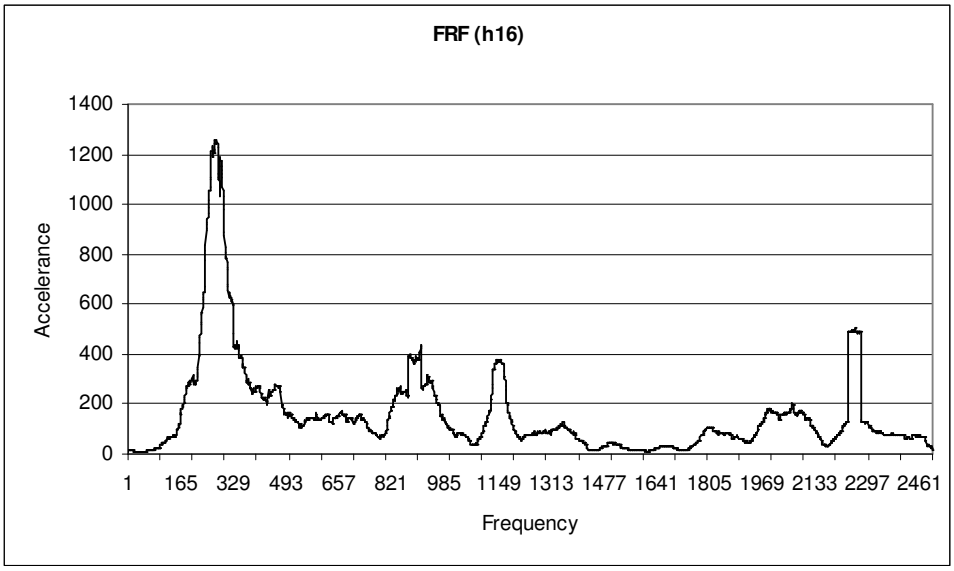

f) h_{16}

Figure D-2. Experimental *FRF* results by placing the accelerometer on point 1 and exciting the plate on points 1 to 6.

FRFs of the ***structure*** (example 3, Chapter 7) are presented in Figure D-3 when the accelerometer is in point 2 and the excitation force from the hammer is applied to points 1, 2 and 3.

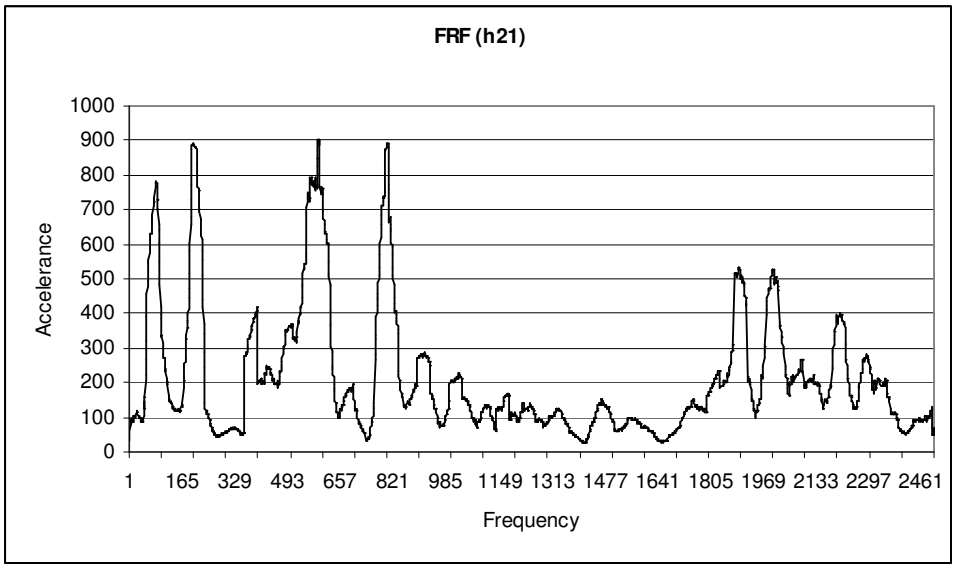

a) h_{21}

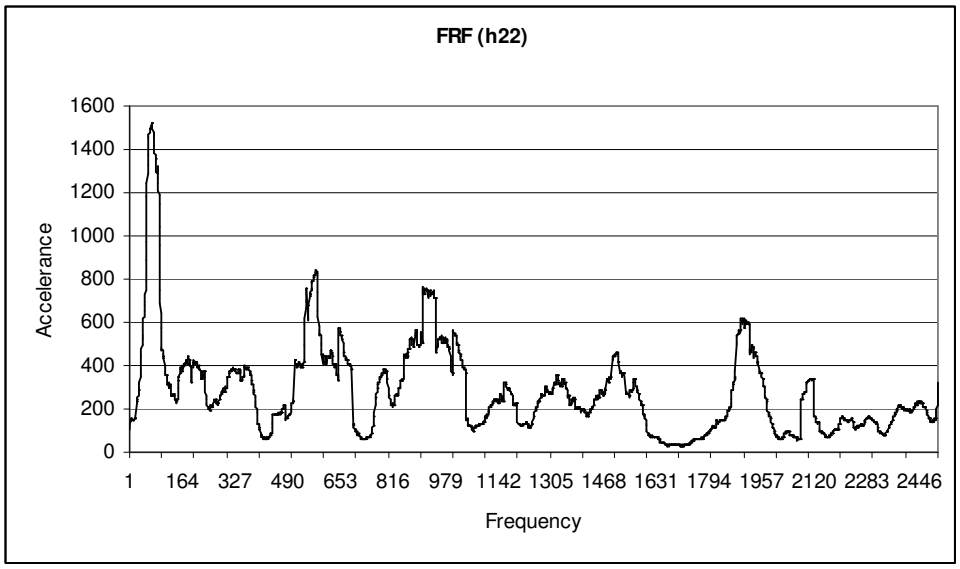

b) h_{22}

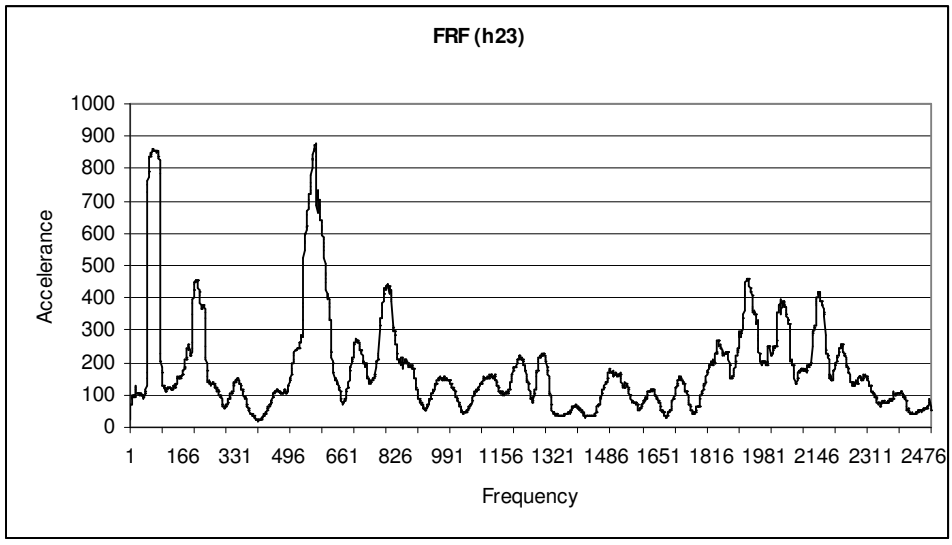

c) h_{23}

Figure D-3. Experimental *FRF* results of the structure.

FRFs of the ***clamped-free beam*** (example 4, Chapter 7) are presented in Figure D-4 when the accelerometer is in point 1 and the excitation force from the hammer is applied to points 1, 2, 3 and 4.

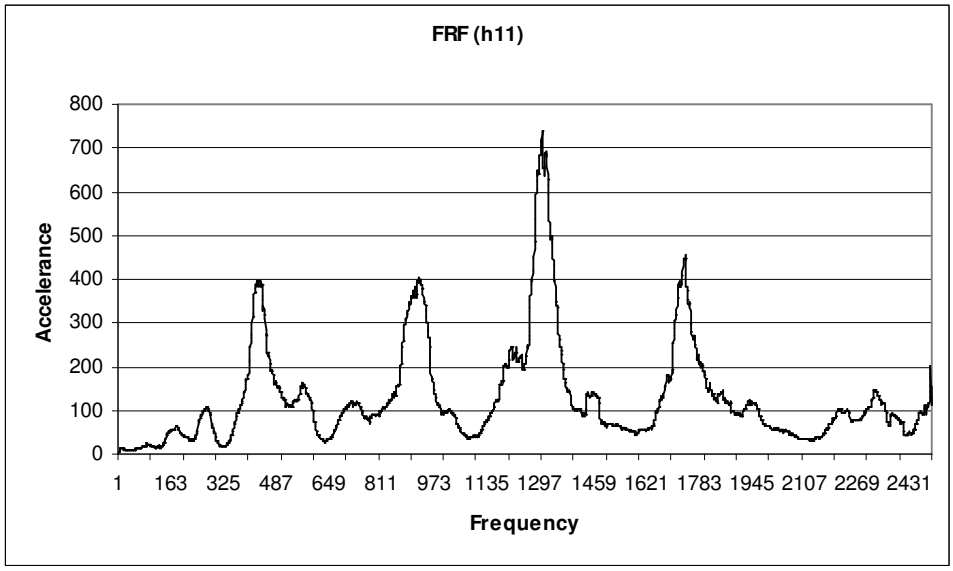

a) h_{11}

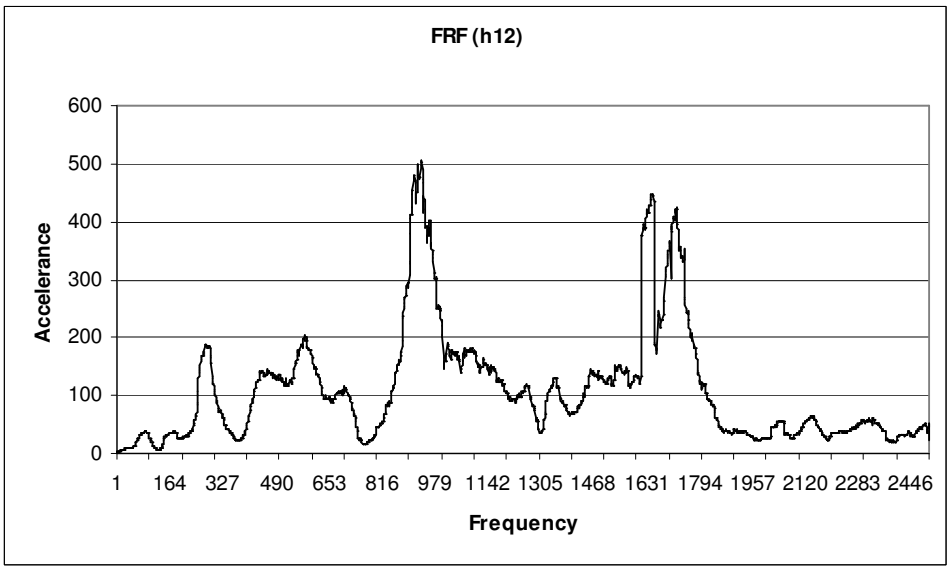

b) h_{12}

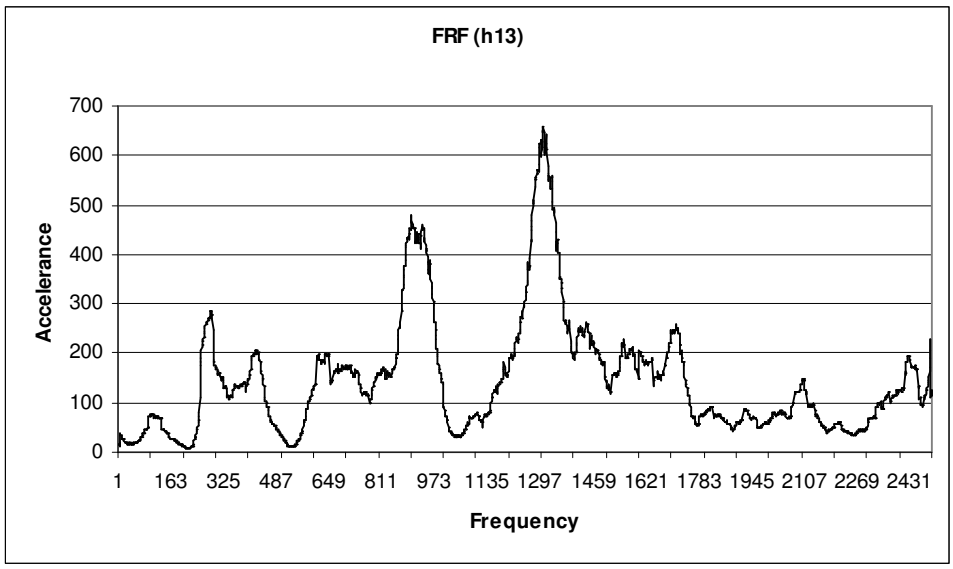

c) h_{13}

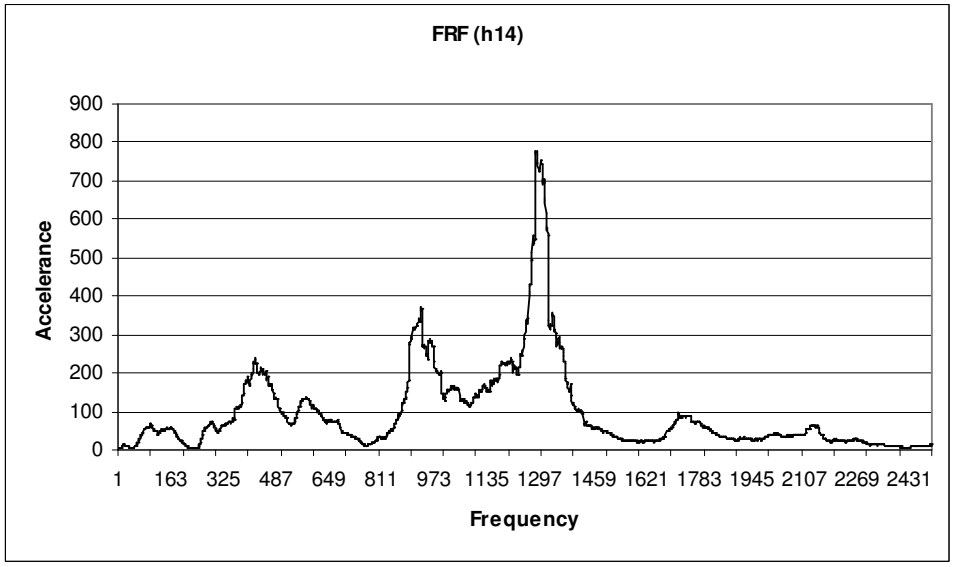

d) h_{14}

Figure D-4. *FRF* results for incomplete (4DOF) clamped-free beam model; a) h_{11}, b) h_{12}, c) h_{13}, d) h_{14}

References:

[1] P. Avitabile and J. O'Callahan, Frequency response function expansion for unmeasured translation and rotation DOFS for impedance modelling application, Mechanical Systems and Signal Processing, Volume 17, Issue 4, July 2003, Pages 723-745.

[2] I. Elishakoff, Essay on uncertainties in elastic and viscoelastic structures: From A.M. Freudenthal's Criticism to modern convex modeling. Comput. Struct. 56 6 (1995), Pages 871–895.

[3] I. Elishakoff and Y. Ren, Finite element methods for structures with large stochastic variations, Oxford University Press, 2003

[4] C. W. de Silva, The role of soft computing in intelligent machines, The royal society, Volume 361, Number 1809, 18 June 2003, pages 1749-1780.

[5] T. M. Wasfy and A. K. Noor, Application of fuzzy sets to transient analysis of space structures, Finite Elements in Analysis and Design, Volume 29, Issues 3-4, 15 June 1998, Pages 153-171.

[6] T. M. Wasfy and A. K. Noor, Finite element analysis of flexible multibody systems with fuzzy parameters, Computer Methods in Applied Mechanics and Engineering, Volume 160, Issues 3-4, 23 July 1998, Pages 223-243.

[7] T. M. Wasfy and A. K. Noor, Multibody dynamic simulation of the next generation space telescope using finite elements and fuzzy sets, Computer Methods in Applied Mechanics and Engineering, Volume 190, Issues 5-7, 10 November 2000, Pages 803-824.

[8] M. J. Leamy, A. K. Noor and T. M. Wasfy, Dynamic simulation of a tethered satellite system using finite elements and fuzzy sets, Computer Methods in Applied Mechanics and Engineering, Volume 190, Issues 37-38, 22 June 2001, Pages 4847-4870.

[9] A. K. Noor, J. H. Starnes and J. M. Peters, Uncertainty analysis of stiffened composite panels, Composite Structures, Volume 51, Issue 2, February 2001, Pages 139-158.

[10] S. S. Rao and J. P. Sawyer, A fuzzy element approach for the analysis of imprecisely-defined systems, AIAA J. 12 (1995), Pages 2364–2370.

[11] S. Valliappan and T. Pham, Fuzzy finite element analysis of a foundation on an elastic soil medium. Int. J. Numer. Anal. Methods Geomech. 17 11 (1993), Pages 771–789.

[12] L. Chen and S. S. Rao, Fuzzy finite-element approach for the vibration analysis of imprecisely-defined systems, Finite Elements in Analysis and Design, Volume 27, Issue 1, 30 September 1997, Pages 69-83.

[13] Y. Qiu and S. S. Rao, A fuzzy approach for the analysis of unbalanced nonlinear rotor systems, Journal of Sound and Vibration, Volume 284, Issues 1-2, 7 June 2005, Pages 299-323.

[14] M. Hanss, S. Hurlebaus and L. Gaul, Fuzzy sensitivity analysis for the identification of material properties of orthotropic plates from natural frequencies, Mechanical Systems and Signal Processing, Volume 16, Issue 5, September 2002, Pages 769-784.

[15] S. Adali, J. C. Bruch, I. S. Sadek and J. M. Sloss, Transient vibrations of cross-ply plates subject to uncertain excitations, Applied Mathematical Modelling, Volume 19, Issue 1, January 1995, Pages 56-63.

[16] P. D. Cha, and W. Gu, Model updating using an incomplete set of experimental modes, Journal of Sound and Vibration, Volume 233, Issue 4, June 2000, Pages 583-596. Issue 5, September 2003, Pages 965-988.

[17] D. J. Ewins, Modal testing: theory and practice, research studies press, 1991.

[18] M. I. Friswell and J. E. Mottershead, Finite element model updating in structural dynamics, Dordrecht ; London : Kluwer Academic Publishers, c1995.

[19] A. Chassiakos and S. Masri, Identification of the internal forces of structural systems by feedforward multilayer networks. Comput. Systems Engrg. (1991), Pages 125–134.

[20] A. Chassiakos and S. Masri, Neural network based identification of structural systems. In: Tzafestas, Borne and Grandinetti, Editors, Proc. Parallel and Distributed Computing in Engineering Systems, North-Holland, Amsterdam (1992).

[21] A. Chassiakos and S. Masri, Modeling unknown structural systems through the use of neural networks. In: Tenth World Congress on Earthquake Engrg. (August 1992).

[22] S. Masri and A. Chassiakos, Some issues on the identification of structural systems through the use of neural networks. In: Internat. Conf. on Safety Evaluation (September 1992).

[23] S. Masri, A. Chassiakos and T. Caughey, Structure-unknown non-linear dynamic systems: identification through neural networks. In: J. Smart Materials and Structures 1, Institute of Physics, (1992), Pages 45–56 (1) .

[24] S. Masri, A. Chassiakos and T. Caughey, Identification of nonlinear dynamic systems using neural networks. Trans. ASME J. Appl. Mech. 60 1 (1993), Pages 123–133.

[25] Y. C. Liang, D. P. Feng and J. E. Cooper, Identification of restoring forces in non-linear vibration systems using fuzzy adaptive neural network, Journal of Sound and Vibration, Volume 242, Issue 1, 19 April 2001, Pages 47-58

[26] P. Bazzurro and C. A. Cornell, Ground-Motion Amplification in Nonlinear Soil Sites with Uncertain Properties, Bulletin of the Seismological Society of America, Volume 94, Number 6B, December 2004, pp. 2090-2109.

[27] F. Khoshnoud, F. Khoshnoud, I. I. Esat, Modal description of vibratory behavior of structures using fuzzy membership functions, Proceedings of the I MECH E Part K Journal of Multi-body Dynamics, Number K4, December 2004, Pages 173-181.

[28] MATLAB, Version 6.1.0.450 Release 12.1 copyright 1984-2001 The MathWorks, Inc.

[29] Agilent VEE, Agilent VEE Pro 7.0x copyright 2000-2005 Agilent Technologies, Inc.

[30] H. T. Nguyen, N. R. Prasad, C. L. Walker, E. A. Walker, A first course in Fuzzy and neural control, Chapman & Hall/CRC, 2003

[31] W. T. Thomson, Vibration theory and applications, Prentice hall, Englewood Cliffs, NJ, 1965.

[32] S. S. Rao, Mechanical Vibrations, Pearson Prentice Hall, 1995

[33] M. Nikkhahbahrami, Theory of vibration and its application in engineering, Tehran University publications, 1992

[34] Y. Altintas, metal cutting mechanics, machine tool vibrations, and CNC design, Cambridge university press, 2000

[35] W. Weaver, P. R. Johnston, Structural dynamics by finite elements, Englewood Cliffs : Prentice-Hall ; London : Prentice-Hall International, c1987.

[36] S. Moaveni, Finite element analysis: theory and application with ANSYS, 2nd ed. Prentice Hall, c2003.

[37] T. R. Chandrupatla, A. D. Belegundu, Introduction to finite elements in engineering, Englewood Cliffs, N.J. : Prentice-Hall, c1991.

[38] D. J. Gorman, Free vibration analysis of rectangular plates, New York ; Oxford : Elsevier, c1982.

[39] A. C. Ugural, Stresses in plates and shells, 2nd ed. Boston, Mass. ; London : McGraw-Hill, c1999.

[40] W. Soedel, Vibrations of shells and plates, New York : M. Dekker, c1981.

[41] R. D. Blevins, formulas for natural frequency and mode shape, Van Nostrand Reinhold, 1990.

[42] ANSYS Release 9.0 copyright © 2004 SAS IP, Inc.